Armitage Nolan, Jennifer Claire (2013) Time of flight mass spectrometry of pharmaceutical systems. PhD thesis, University of Nottingham.

TIME OF FLIGHT MASS SPECTROMETRY OF PHARMACEUTICAL SYSTEMS

Jennifer Armitage Nolan, BSc.

Thesis submitted to the University of Nottingham
for the degree of Doctor of Philosophy

December 2013

Contents

Abstract

Time-of-flight secondary ion mass spectrometry (ToF-SIMS) is a widely used surface chemical analysis technique that is traditionally employed to characterise the first few molecular layers of a material interface. The ability of this technique to accurately reflect the surface chemistry of polymers, biomaterials and many other solid materials is well documented. However, the majority of research that utilises this technique is based upon a qualitative rather than quantitative assessment of the material under investigation.

The qualitative analysis of a range of traditional tablet and bead formulations containing drug and multiple excipients was performed in order to identify key diagnostic ions for all the different components. The lateral distributions of the ions across the surfaces of these formulations were imaged. Two different methods were then used to perform a qualitative analysis of the surfaces and results from these experiments were compared to the bulk composition.

The effect of surface roughness on the ability to produce reproducible quantitative analyses from ToF-SIMS ion yield data was investigated. A range of samples with different topographies were studied including polytetrafluoroethylene (PTFE), glass microscope slides, gold coated abrasive papers and gold coated precision measurement samples. The surface roughness was assessed by Atomic Force Microscopy and Laser Profilometry. Samples were analysed in imaging mode and the variance in ionization across the total image was measured for each sample. Evidence is presented that there is a relationship between ion yield and surface roughness, and that the surface roughness of the analysed surfaces will effect on any quantification approach in the processing of ToF-SIMS data. In addition, the presence of any orientation/directionality in surface features also needs to be evaluated when considering use of a quantitative approach.

To investigate the effect of chemical environment on the ability to derive quantitative data from ToF-SIMS analysis of pharmaceutical materials, drug loaded spun-cast polymer films with low surface roughness were studied. ToF-SIMS data were

obtained for two chemically similar drugs in two different polymer matrices. In the majority of the samples there was no quantitative relationship between drug ion intensity and nominal bulk composition. Due to the large sample set, the multivariate technique, Principal Component Analysis (PCA) was employed to look at variance in secondary ion yields from the different samples. PCA is becoming more prevalent in ToF-SIMS data interrogation as it allows for a mathematically un-biased analysis of sample variables through the identification of the ions that account for the majority of the variance in the sample set. PCA successfully highlighted the impact of the chemical environment, showing secondary ion yields of drugs can be dependent on the surrounding matrix. PCA was also used to look at variance in two of the tablet samples and was successfully able to differentiate between the tablet samples with the lowest and highest concentrations of paracetamol.

This thesis has demonstrated that surface topography and surface chemical environment or matrix will have a significant impact on ion yields in the ToF-SIMS experiments. These findings suggest caution in the use of ToF-SIMS for the quantitative analysis of complex chemically heterogeneous and topographically diverse pharmaceutical formulations.

Acknowledgements

List of Abbreviations

AES   Auger Electron Spectroscopy

AFM   Atomic Force Microscopy

DSIMS   Dynamic Secondary Ion Mass Spectrometry

GC-MS   Gas Chromatography–Mass Spectrometry

MCP   Multi channel plate

m/z   Mass to charge Ratio

PTFE   Polytetrafluoroethylene

PDMS   Polydimethylsiloxane

PCA   Principal Component Analysis

PC1   Principal Component 1

PC2   Principal Component 2

PEG   Polyethylene glycol

PI cm^2 Primary ions per centimetre squared

PMMA   Poly(methyl methacrylate)

RGB   Red Green Blue

ROI   Region of interest

RSF   Relative Sensitivity Factor

SEM   Scanning Electron Microscopy

SF   Sensitivity Factor

SSIMS Static Secondary Ion Mass Spectrometry

ToF-SIMS Time-of-Flight Secondary Ion Mass Spectrometry

UHV Ultra High Vacuum

XPS X-Ray Photoelectron Spectroscopy

List of Figures

List of Tables

Chapter 1.

Introduction

Healthcare innovation is driven by a number of factors including pharmaceutical formulation and development, and the need to characterise these pharmaceutical formulations is of paramount importance. Pharmaceutical formulation is the process in which drugs and excipients are combined. This introduction gives a brief outline of the excipients that are used in these formulations, the use of active pharmaceutical ingredients, and the factors that determine the manufacturing methods that are used to produce formulations.

During the manufacture of a formulation, many interfacial interactions occur. These interactions can take place during the manufacturing process, in the packaging medium, and ultimately within the human body. Consequently, the need for reliable and highly chemically specific methods for surface analysis of formulations is of great importance. Surface analytical techniques are routinely used to in the industry for identification of chemical species at the top few layers of the surface.

The latter part of this introduction describes the use of secondary ion mass spectrometry (SIMS) as an analytical tool for the surface analysis of pharmaceutical compounds. The use of SIMS as a surface analytical technique is also compared to two further well known surface analysis techniques, X-Ray photoelectron spectroscopy (XPS) and Auger electron spectroscopy (AES). The use of Atomic Force Microscopy (AFM) as a technique for analysing surface topography is also discussed.

1.1   Excipients, Active Ingredients and Drug Formulation

Drug formulation is the process in which different ingredients, including the active drug, are combined to produce a final medicinal product. The majority of formulations contain both the active ingredient and one or more excipients [Katdare and Chaubal, 2006].

The number of active pharmaceutical ingredients (APIs) available is vast, and the number of names for drugs is continuously increasing [Mashkovskii, 1993].

Excipients can be defined as inert materials that are used as a diluent or a vehicle for a drug [Katdare and Chaubal, 2006].

1.1.1   Excipients

Excipients can also perform a range of functions in dosage forms and are an integral and essential part of drug development [Aulton, 2002]. Excipients have been engineered to aid therapeutic performance by extending drug release profiles [Villanovea *et al.*, 2011], layered to control drug release rates [Realdon *et al.*, 1997], and used to enhance the efficacy of drugs administered through inhalation [Pilcer and Amighi, 2010]. Excipients can be classified in a number of ways, such as by their type or action. Different types or sources of excipient include animal (e.g. gelatin and beeswax), vegetable (e.g. pectin and starch), mineral (e.g. kaolin and bentonite) and synthetic excipients (e.g. boric acid and calcium stearate) [Guad *et al.*, 2006]. However, excipients are typically classified by their function in a drug formulation. Some of the more common classifications and example excipients are presented in Table 1.2. Other excipients include buffers to control p.H., sweetening agents for taste and preservatives and antioxidants to extend shelf life [Jones, 2006a].

Diluents can also be referred to as fillers or bulking agents. Diluents such as lactose and microcrystalline cellulose are added to make the dosage form a workable size, enabling routine and reliable production and convenient handling by the patient [Aulton, 2002]. The solubility of diluents can affect the dissolution and release of drugs such as spironolactone [Kreutzwald *et al.*, 2007], alter the tensile strength of a formulation [Kachriminas and Malamataris, 2005], and impact the compression and release properties of sustained release tablets [Vaidya and Avachat, 2011].

Classification	Examples of Excipients
Diluents	Lactose, Microcrystalline cellulose, Sucrose, Glucose
Binders	Hydroxypropyl cellulose, Polyvinyl pyrrolidone (PVP)
Disintegrants	Sodium starch glycolate
Glidants	Silica, Magnesium stearate
Lubricants	Talc, Magnesium stearate
Film Coatings	Hydroxypropyl cellulose, Methyl cellulose
Wetting Agents	Sodium laurel sulphate

Table 1.1 Common excipients and their classifications
(adapted from Zheng, 2009 and Aulton, 2002)

Binding agents (binders) can be used to increase cohesion between particles, for example during a compression phase in tablet manufacture to ensure uniformity of drug content throughout a batch of tablets or capsules. In addition, their ability to assist particle binding is often exploited in the wet granulation process. Wet granulation typically involves spraying of a liquid binder; however in recent years novel foam delivery methods have been proposed [Tan and Hapgood, 2011]. Common binding agents include gelatine and polyvinylpyrrolidone (PVP). PVP can also be used as a disintegrant to promote break-up of the formulation in the aqueous environment of the gastrointestinal tract. Further examples of disintegrants include starch and cation exchange resins [Jones, 2006a]. Recently, macromolecular polymer based binders have been developed that have antibacterial properties to treat infections [Bertrand *et al.*, 2011].

Glidants, such as fine silica, can be used to improve the flow properties of a formulation, for example before tableting [York, 1975]. Other materials that are known to improve the flow properties of dry powder mixtures are titanium dioxide, aluminium oxide, and carbon black particles [Meyer and Zimmerman, 2004]. Lubricants are similar in function to glidants, and are used to prevent materials adhering to die surfaces and reducing friction during manufacture. The addition of dry lubricants allows compression at lower pressure and reduces the generation of heat during tablet formulation. Talc is often also used for this purpose, as are calcium and magnesium stearates [Jones, 2006a]. However, there are potentially a number of unwanted effects that the addition of a lubricant can cause. These include a decrease in the binding capability of other components in the tablets which leads to decreased tablet strength, and provision of a hydrophobic layer at the tablet surface resulting in a decrease in disintegration time. Therefore, a balance needs to be achieved between ideal compression factors and inhibiting drug release. This problem is often addressed by the combined addition of both binding agents and disintegrating agents to the formulation [Aulton, 2002].

Film coatings are becoming a popular choice in controlled release systems, where a drug core is enclosed with a polymeric layer. Enteric coatings such as methacrylic acid copolymers, known commercially as Eudragits, are used to control release and absorption of an acid labile drug by remaining intact and impermeable in the acid conditions of the stomach and then dissolving in the more alkaline conditions of the small intestine to release the drug [Belu *et al.*, 2000]. Several different materials have been successfully used to provide targeted drug delivery to the colon, including starch based coatings [Freire *et al.*, 2009], acrylic terpolymers [Arimoto *et al.*, 2004], lauroyldextran and crosslinked galactomannan [Hirsch *et al.*, 1999]. Other materials, such as pectins, have been used in film coatings for liposome delivery [Nguyen *et al.*, 2011]. Cellulose ethers have been used as taste masking films [Milojevic *et al.*, 1996] and for the stabilisation of photosensitive drugs such as nifedipine [Berchard *et al.*, 1992]. The use of film coatings in pharmaceutical formulations is extensive, and there are substantial numbers of review articles published in this field spanning several decades of research, for example [Felton and McGinity, 1999; Siepmann *et al.*, 2008; Mora-Huertas *et al.*, 2010; Simchi *et al.*, 2011].

Wetting agents are also commonly used in pharmaceutical formulation. In liquid dosage forms they provide a homogeneous dispersion of solid particles and improve the wetting and penetration of aqueous solutions into the formulation to allow disruption of the tablet and therefore, dissolution of the drug [Katdare and Chaubal, 2006]. Wetting agents can also affect the release profile of poorly water soluble drugs such as indomethacin, and optimisation of the wetting agent within the formulation can significantly improve drug release [Shokri *et al.*, 2008].

Many of these excipients possess properties that allow them to perform more than one role. For example, magnesium stearate can be used as a glidant, lubricant or anti adherent [Aulton, 2002], and enteric polymers, such as methacrylate copolymers, can also be used as binders [Marvola *et al.*, 1999].

1.1.2 Active Pharmaceutical Ingredients

Active pharmaceutical ingredients (APIs) are typically classified by their therapeutic nature. Therapeutic classifications are concerned with the way in which the drug works, e.g. as an antihistamine or anticoagulant [Moini, 2012]. However, they can also be classified by their chemical structure, for example barbiturates, or by their origin, for example, opiates that originate from plants [Maisto *et al.*, 2011]. The number of drugs available on the market is continually increasing and most drugs are known by several names, for example generic or trade names as in the case of ibuprofen and Nurofen [Jones, 2009].

APIs range from over the counter antipyretics and analgesics [Hersh *et al.*, 2000], to fluorinated anti-cancer agents [Isanbor and O'Hagan, 2006] and anti-malarials [Murambiwa *et al.*, 2011].

The way in which APIs and excipients interact is an important aspect of drug formulation and excipient compatibility studies are an essential part of drug formulation. A range of compatibility tests can be carried out, such as exposing the API, excipients and the complete formulation to different environments [Storey and Ymen, 2011]. Excipient selection often also depends on the chemistry of the active ingredient and the drug delivery route [Katdare and Chaubal, 2006].

1.1.3 Producing Pharmaceutical Formulations

Excipients can be combined with APIs to manufacture dosage forms. The method of manufacture of any dosage form will depend on a number of key criteria. Most commonly, these are production cost, the properties of the ingredients and the target for the active ingredient. Ultimately, they must also satisfy the final aims of any pharmaceutical formulation: an appropriate dose of drug, stability during the specified shelf life and patient safety whilst being clinically effective [Aulton, 2002].

The number and type of pharmaceutical formulations available to the medical field continues to grow at an impressive rate, with these formulations becoming increasingly sophisticated. In recent years there has been an explosion in regards to novel drug delivery vectors, i.e. the manner in which a formulation reaches its target [Aulton, 2002]. However, the "traditional" delivery methods, such as tablets, pills and capsules are still employed in the vast majority of oral drugs. For drugs that can withstand the acid environment of the stomach, the oral route is the most convenient and popular route of administration [Florence and Attwood, 2006]. Alternatively, enteric coatings can be used to protect a formulation against acidity within the stomach so that it is not released until it reaches the intestine [Desai and Lee, 2007].

Pharmaceutical formulations can be manufactured by a number of different methods that are also becoming increasingly sophisticated [Aulton, 2002]. The high number of pharmaceutical applications and the continuous development of pharmaceutical formulations have had a significant effect on the manufacturing process and the use of high-technology equipment for more complex formulations [Sarantopolous, 1995]. However, the "traditional" medications, such as tablets and capsules are still employed in the vast majority of formulations deigned for solid dose drug delivery [Jones, 2006a]. The tableting process is described in Chapter 3. Chapter 3 also describes the process of extrusion and spheronisation to produce spheroids, which are often contained within capsule formulations.

1.2 Secondary Ion Mass Spectrometry Analysis of Pharmaceutical Compounds

Secondary ion mass spectrometry (SIMS) is one of a number of techniques that provide surface chemical information. This technique has been used for several decades to study many different materials from mapping the movement of herbicides into and across leaf cuticles [Perkins *et al.*, 2008] to corrosion of low-lime glass vessels from the Victoria and Albert museum [McPhail, 2006]. A reconstructed 3D plot of the sodium concentration in corroded glass from one of these vessels, using data acquired from SIMS analysis, is presented in Figure 1.1.
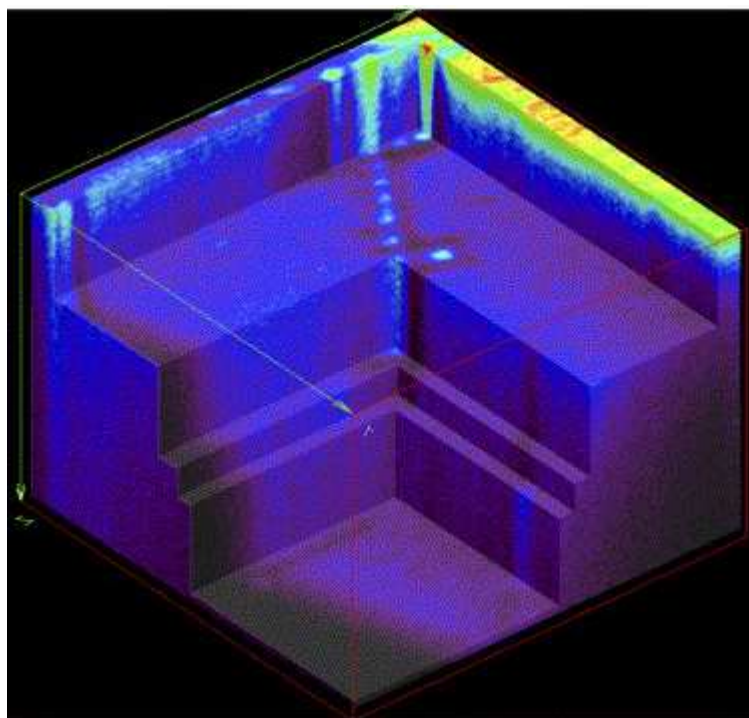
Figure 1.1 A 3D plot of the sodium distribution in corroded glass
(image courtesy of McPhail, 2006)

Principal advantages of SIMS include high detection sensitivity, high depth resolution, isotope specificity and possibilities for three-dimensional imaging of surfaces [Linton and Goldsmith, 1992]. The pharmaceutical industry particularly values this surface chemical information as it is often the interaction between the

very top few molecular layers of a material or substance and the human body that are key to constructing a successful product. Brittain states that the profiling of drugs and excipients and their respective physical and analytical characteristics remains at the core of pharmaceutical development [Brittain, 2009].

There are a substantial number of both books and scientific papers that address the use of SIMS for the analysis of drug formulations and their constituent parts. This section seeks to give a flavour of the vast body of research that has been completed in this field.

A detailed description of SIMS, including the time-of-flight secondary ion mass spectrometry (ToF-SIMS) instrumentation, is provided in Chapter 2. Quantification of SIMS data, the use of relative sensitivity factors (RSFs) and multivariate analysis are discussed in Chapters 4, 5, and 6, respectively.

1.2.1   SIMS Analysis of Active Pharmaceutical Ingredients

The SIMS technique is very applicable to drug product characterisation [Bugay, 2001] and has been extensively used to analyse a large number of drugs, from rapamycin and sirolimus [Mahoney and Fahey, 2008] to theophylline [Belu *et al.*, 2000] and Metoprolol [Belu *et al.*, 2003].

In the late 1970s, Benninghoven and Sichtermann published an article that investigated a range of biologically active compounds, including drugs [Benninghoven and Sichtermann, 1978]. They found that in the majority of cases parent ions were detectable, $[M+H]^+$ in positive ion spectra and $[M-H]^-$ in the negative ion spectra. Large fragment ions characteristic of functional groups were also detected, and they concluded that SIMS was highly effective in the detection and identification of the compounds studied.

ToF-SIMS has been used to identify the presence of antibiotics on spray dried particle surfaces. The use of ToF-SIMS confirmed that hydrophobic and heavier molecules, such as rifampicin, tended to form an outer layer of the final dried particles [Chan *et al.*, 2013]. Imaging of the formed particles also highlighted inconsistent surface coverage that occurred during the manufacturing process and

these findings were supported by dissolution experiments. A ToF-SIMS image of the triple antibiotic formulation is presented in Figure 1.2.
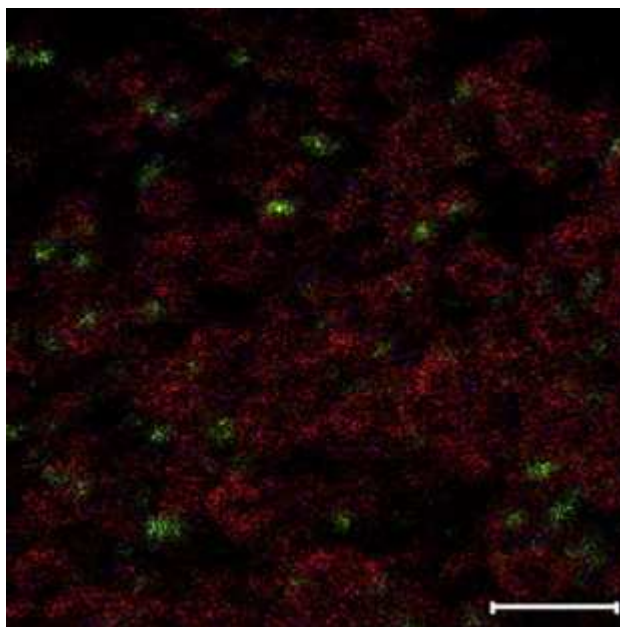
Figure 1.2 (scale bar = 10 µm) TOF-SIMS total ion image
(red = rifampicin, green = isoniazid and blue = pyrazinamide)
(image courtesy of Chan et al., 2013)

Trapp used both SIMS spectroscopy and imaging to determine the distribution of palmitic acid in research on distribution analyses of pharmacologically relevant high molecular compounds. A caesium primary ion source was used and it was concluded that the application of dynamic SIMS was the only SIMS based method that could be used to successfully reveal the distribution profile of palmitic acid in galactose [Trapp and Stahl, 1995]. The use and selection of different primary ion sources and operational modes during a SIMS experiment is discussed in Chapter 2. The use of different primary ion beams and methods to enhance secondary ion generation are discussed in Section 1.2.7.

SIMS has been used to determine the drug surface concentration in a polymer matrix [Lee and Gardella, 2004]. It was concluded that ToF-SIMS can be useful for

evaluating the initial stages of surface reactions such as biodegradability and biocompatibility which are required for biomedical applications.

ToF-SIMS has also been used to characterise foreign materials that enter coated and uncoated tablets, possibly during the manufacturing process [Pajander *et al.*, 2013]. Cross-sectioned tablets were analysed using a polyatomic source and the authors concluded that the use of ToF-SIMS in combination with a number of other techniques, including SEM, allowed for identification of the foreign contaminants. They particularly regarded ToF-SIMS for its sensitivity to compounds which did not contain heteroelements in their structure.

Further examples of the use of SIMS in characterising pharmaceutical formulations are provided in the introduction of Chapter 3.

1.2.2   SIMS Analysis of Drug Delivery Systems

Over the past decade there has been mounting interest in the use of sustained-release systems for drug delivery [Aulton, 2002]. These types of systems have a number of advantages, including decreases in the number of doses required and a more constant level of drug in the body at any one time. Drug release rates are often controlled by diffusion, dissolution, ion exchange or osmotic pressure. Analysis of drug release pellets by ToF-SIMS is discussed in the introduction of Chapter 3.

John *et al.* have investigated the dispersion of the peptide drug leuprolide in a hydroxypropyl cellulose (HPC) polymer matrix [John *et al.*, 1995]. They found that the drug distribution was strongly dependent on the drug to polymer ratio and the drug tended to concentrate at the polymer / air interface. In the HPC control sample spectrum they observed a number of peaks in the mass range 100 –200 separated by 14 mass units and allocated these to loss of methylene fragments (CH_2). The authors used a gallium liquid metal ion source (LMIS) and observed the protonated molecular ion ($[M+H]^+$) of leuprolide at mass 1210 in the positive spectrum. The paper also demonstrated the use of ToF-SIMS in producing ion images. X-ray photoelectron spectroscopy was used as a complimentary technique and the authors assigned discrepancies between the two data sets as differences in sampling depth (10 nm in comparison to atomic monolayers.) They concluded that ToF-SIMS was a sensitive method of determining the distribution of organic molecules.

Drouot *et al.* have also investigated peptides [Drouot *et al.*, 1997]. Their study used ToF-SIMS to characterise different stages of a polymer supported peptide synthesis. They found that by creating spectra at each step of the peptide synthesis they could identify the stages of the growing chains by identifying the characteristic ion peaks. They noted that analysis by ToF-SIMS did not require the time consuming removal and isolation of the peptide from the polymer support as required by conventional spectroscopic methods such as Nuclear Magnetic Resonance (NMR) and Fast Atom Bombardment (FAB).

ToF-SIMS has been used to analyse a porous silicon nanostructured material engineered for the delivery of pharmaceutical ingredients [Kempson *et al.*, 2010]. ToF-SIMS analyses allowed for the detection of organic, inorganic and molecular fragments, which along with complimentary data from Infra-red and XPS enhanced the understanding of the chemical mechanisms of adsorption of the loading elements onto the substrate surface. Further research was to be carried out to enhance signals from the organic substances within the samples.

Static SIMS has been used to aid the characterisation of polystyrene / polyethylene oxide based colloids designed for site specific drug delivery [Brindley *et al.*, 1995]. Changes in the surface composition were observed through analysis of spectra from colloids with varying macromonomer content. Analysis of the data also showed that complete surface coverage of the macromonomer had not been achieved, despite its high ratio in the polymerization reaction. Previous work in 1992 by the same author also used SIMS to investigate the surface of charged and sterically stabilized polymer colloids [Brindley *et al.*, 1992].

Colloidal latex particles can be used in novel therapeutic systems, for example in the delivery of drugs or antibodies [Davies *et al.*, 1993]. In this study, the presence of sugar species at the surface of particles prepared with sugar residues was confirmed, as galactose specific diagnostic ions were evident in the ToF-SIMS spectra.

ToF-SIMS has been used to study both early stage polymer degradation and the surface concentration of water-insoluble additive in a model drug delivery system [Lee and Gardella, 2004]. The authors stated that ToF-SIMS was an effective method

for studying surface reactions involved in the biodegradability and biocompatibility of the system, both key insights required in biomedical applications.

The distribution of siRNA in PLGA nanoparticles have been analysed by ToF-SIMS [Cun *et al.*, 2011]. Following identification of the key ions through analysis of reference samples, the authors were able to successfully map the siRNA distribution from diagnostic ions originating from the nitrogen bases and phosphate backbone. An AFM image of the topography of the siRNA loaded nanoparticle is presented in Figure 1.3.
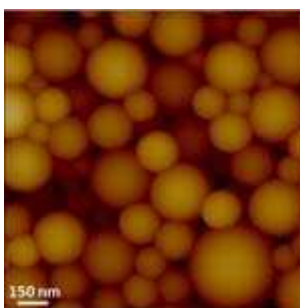
Figure 1.3 AFM topography images of siRNA-loaded nanoparticles (image courtesy of Cun et al., 2011)

More recently, ToF-SIMS has been used to characterise the surface of polymer microspheres designed for controlled release of therapeutic proteins [Rafati *et al.*, 2012]. ToF-SIMS revealed a polyvinyl surfactant at the surface of the microspheres. The internal chemistry was also investigated by analysing cross-sectioned surfaces of the microspheres, which confirmed the presence of protein in large voids and concentrated pores, providing complimentary data to the confocal Raman mapping of this sample.

1.2.3   SIMS Analysis of Excipients in Pharmaceutical Formulations

The overall success of any formulation depends on both the physical and chemical properties of the API and the excipients it contains [Bugay, 2001]. SIMS has been used in several studies to investigate these properties.

SIMS has been used extensively to characterise polymers, including those used as constituent parts of pharmaceutical preparations. For several decades, polymers have provided an important role in tablet and capsule formulations [Uchegbu and Schätzlein, 2006]. The formulation and performance of these pharmaceutical dosage forms, which contain polymeric based materials, is often dependent on their physio-chemical properties [Jones, 2009].

SIMS has been extensively used for the characterisation of polymers contained within formulations [Davies and Lynn, 1990; Mahoney *et al.*, 2006b; Burns and Gardella, 2008]. Ha and Gardella used SIMS as part of a range of techniques to investigate the surface chemistry of biodegradable polymers for drug delivery systems and concluded that surface sensitive techniques had a clear and definitive role in characterising biodegradeable polymers deigned for active applications [Ha and Gardella, 2005].

An excellent review of the use of cluster ion sources for the characterisation of polymeric materials has been written by Mahoney *et al.* [Mahoney, 2010]. The use of different primary ion sources is discussed in Section 1.2.7 and Section 2.2.4.

Davies *et al.* have studied poly(orthoesters) as candidates for controlled release drug delivery systems via ToF-SIMS [Davies *et al.*, 1991]. As well as listing characteristic ion fragmentation patterns and masses for the poly(orthoester) components, the paper speculates on the nature of the fragmentation mechanism of the polymer, i.e. whether it is endocyclic or exocyclic in nature. This work is continued by Leadley *et al.* a number of years later [Leadley *et al.*, 1998a]. ToF-SIMS demonstrated that, following protonation, the cleavage of the alkoxy group followed the exocyclic pathway during acid catalysed hydrolysis.

Many polymers are attractive in the pharmaceutical field due to their biodegradable properties. Leadley *et al.* have studied poly(β-hydroxy acids) [Leadley *et al.*, 1997], these are a subset of polyesters and contain carboxylic acid groups. The paper proposes a model for a biodegradable polymer that's structure allows it to be resorbable due to its functional groups. They found that ToF-SIMS allowed observation of fragmentation patterns that were characteristic of ions of their host polymer.

Copolymers of poly(sebacic anhydride) with ricinoleic acid maleate have also been investigated by Leadley *et al.* [Leadley *et al.*, 1998b]. Again the authors were able to identify characteristic ion fragments. The ToF-SIMS data also gave information about the structure of the copolymer polymer chain in terms of random and/or block sections.

Lang *et al.* have studied the copolymer system Biopol [Lang *et al.*, 1998]. This biodegradable co-polyester represents a promising biocompatible material for controlled drug release. They found that ToF-SIMS provided good quantification results with respect to the standard deviations and comparability between the positive and negative spectra. They also noted that care needs to be taken when quantifying from a specific ion that other ions have not interfered with the m/z value.

ToF-SIMS has been used in the analysis of the composition of sodium starch glycolate products [Edge *et al.*, 2002]. The chemical differences, particularly in sodium chloride concentrations, between sodium starch glycolates obtained from there different sources were successfully identified using data from positive and negative mass spectra. Imaging SIMS provided complimentary information, through mapping the distribution of sodium and chlorine, verifying the results found in the spectra. It was concluded that ToF-SIMS was a valuable tool for investigating sodium starch glycolates, and that ToF-SIMS analyses could be used to confirm observations made by other techniques. ToF-SIMS images of the distribution of chlorine ions on the surface of sodium starch glycolate particles, supplied by two different manufacturers, are presented in Figure 1.4.
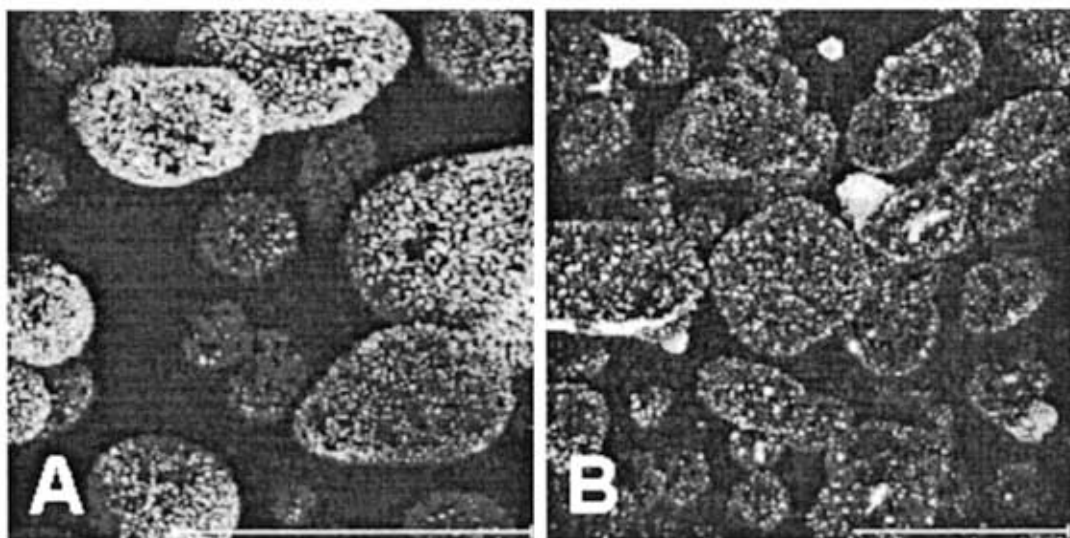
Figure 1.4 ToF-SIMS images of the distribution of chlorine ions on the surface
of sodium starch glycolate particles supplied by two different manufacturers
A = Explotab, B = Vivistar (scale bars, 100 μm)
(image courtesy of Edge, 2002)

1.2.4   SIMS Analysis of Pharmaceuticals in Biological Media

In 1997, Fragu and Kahn published a review on the use of SIMS for pharmacological studies in humans [Fragu and Kahn, 1997]. They stated that this technique had opened new fields in biological investigation due to its ability to map chemical elements in biologically relevant samples and presented element specific SIMS ion images from material obtained in biopsies.

Saldi *et al.* investigated the potential of ToF-SIMS for identifying drugs in biological samples [Saldi *et al.*, 1997]. Varying concentrations of morphine and bromazepam were investigated as solutions spun cast onto silver substrates. They concluded that ToF-SIMS offered a number of advantages including minimal sample preparation, low limits of detection and the ability to analyse more than one drug in any given experiment. Although their conclusions are valid, particularly in the light of work by other researchers, the paper itself is poor with no reference to the preparation of the bromazepam samples and leaving the reader to guess the mass of the protonated bromazepam ion $[M+H]^+$ from the spectra. Although a linear graph showing the

intensity of the protonated morphine ion versus concentration was provided, the respective data for the bromazepam was absent.

John and Odom have studied biological/pharmaceutical compounds and tissue-like matrices [John and Odom, 1997]. They also looked at pure compounds of these materials. Written over 10 years ago, the paper is relatively pessimistic and comments that the molecular sensitivity is poor, particularly with biomolecules in biomaterials, and needs to be improved before the technique can be used for routine trace analysis. However, the paper also comments that the use of large cluster primary ion beams may provide this sensitivity. The need for this improvement has probably promoted the use of materials such as sulphur hexa-fluoride as primary ion sources. The use of different sources to analyse pharmaceutical materials is discussed in the following section. Further information is provided in Chapter 2.

1.2.5 SIMS Imaging of Pharmaceutically Relevant Materials

Surface chemical mapping by ToF-SIMS can be used to determine the distribution of pharmaceutically relevant materials [Barnes *et al.*, 2011]. Once an imaging SIMS experiment has been completed, any peak in the mass spectrum can be used to generate a retrospective ion image [Paul, 2005]. Providing that there are significant ion counts per pixel for any given ion, the ion can be mapped giving a visual representation of its lateral distribution within the sampled area.

Although liquid metal ion guns can cause significant surface damaging limiting lateral resolution to ~1 μm [Jones *et al.*, 2007b], high lateral resolution of 40 nm can now be achieved with modern SIMS instrumentation [Sakamoto *et al.*, 2008].

Clerc *et al*. provide a comprehensive review of the use of SIMS in the fields of *in vivo*. and *in vitro*. mapping of drugs and nuclear medicine compounds [Clerc *et al.*, 1997]. Although the paper is primarily static SIMS based, the authors recognise the importance of ToF-SIMS for imaging of relatively heavy compounds. The paper is also valuable for its extensive dialogue concerning sample preparation.

ToF-SIMS has also been used as an analytical tool to look at the homogeneity of a surface prior to further treatment. Kingshott *et al.* used ToF-SIMS imaging to show

that substrates were chemically uniform after each surface modification step, prior to bacterial adhesion studies [Kingshott *et al.*, 2003].

Rubakhin states that imaging mass spectrometry shows great potential at many stages in the drug delivery process [Rubakhin *et al.*, 2005]. The authors review the fundamentals of mass spectrometry and factors that can determine the specific choice of imaging mass spectrometry techniques, such as spatial resolution and acquisition time. They conclude that imaging mass spectrometry is a useful tool in a number of applications including drug candidate synthesis and screening, and drug detection in cells and tissues.

Passarelli discussed the use of cluster ion sources and sample holders that are compatible with cryogenic samples to successfully image lipids in tissue and cells [Passerelli and Winograd, 2011]. She concluded that new instrumentation with tandem MS capabilities would result in ToF-SIMS being more widely applied to the field of biological samples.

SIMS imaging has also been used to analyse acetaminophen in monolayer and bilayer polymer films [Gillen *et al.*, 2006], commercially available salbutamol coated sugar beads [Kollmer, 2004] and human hair containing traces of arsenic [Audinot *et al.*, 2004].

However, it should be noted that SIMS imaging is not only used in the pharmaceutical industry, but is also widely used in related industries such as medicine (ToF-SIMS imaging of Fabry disease biomarkers [Touboul *et al.*, 2007] and studies of prostate cancer cell lines [Gazi *et al.*, 2004]).

SIMS imaging is also used extensively in other industries. These range widely from its use as a technique to image dopants in optical fibres used in the telecommunications industry [Hellsing *et al.*, 2003] to the analysis of sea salt particles by environmental scientists [Gaspar *et al.*, 2004].

1.2.6 The use of SIMS in Drug Targeting and Distribution Studies

SIMs is routinely used to acquire mass spectroscopy data from surfaces [Chaurand, 2012]. One of the most promising attributes is that that ToF-SIMS can be successfully used for spatial characterisation of an active pharmaceutical ingredient

in a formulated product [Bugay, 2001]. The distribution of ebselen, a pharmaceutical drug containing selenium has been mapped in cellular organelles [Larras-Regard and Mony, 1995]. The authors stated that ion imaging was the only method that could be used to differentiate between the differentiation of the drug in rat kidney proximal and distal tubules, and that imaging of key ions made it possible to determine the (drug) target.

ToF-SIMS was used to detect a model drug (amitriptyline) in ocular tissues [Mains *et al.*, 2011]. The study demonstrated the use of this technique to map the movement of the drug through different tissues in the eye, and identify the predominant tissues where the drug was retained.

Fluorine ions have been used to analyse the distribution of the antimalarial drug, mefloquine in red blood cells [Adovelande *et al.*, 1994]. The authors were able to pinpoint that the drug was accumulating ion the food vacuoles and cytoplasm. One of the key advantages of using SIMS was its ability to map the fluorinated antimalarial drug without the need for radioactive labelling.

1.2.7 The use of Primary Ion Beams and Surface Doping

Bryan *et al* investigated the relative enhancement in ion yield from a gold cluster primary ion gun in comparison to a gallium primary ion source [Bryan *et al.*, 2004]. Pharmaceuticals and polymer additives were studied and it was found that secondary ion yields were enhanced through the use of the gold source, however these varied according to whether atomic, dimer or trimer cluster ions were used. Although the dimer and trimer cluster ions provide greater enhancement in yield in comparison to the atomic gold cluster ion, it was noted that spectra acquisition times were considerably longer.

Appelhans and Delmore compared two primary ions for sampling common organic pharmaceuticals. The secondary ion sputtering efficiency was measured and compared between an atomic primary ion caesium source and a polyatomic primary ion SF_6 source [Appelhans and Delmore, 1989]. They found that the molecular ion peaks of the pharmaceuticals studied were 9 to 24 times higher for the molecular ion beam in comparison to the primary ion beam, and a result of the increase in ion yield, that the minimum detectable mass was also lower when using the molecular beam.

The use of polyatomic ion sources in SIMS has also allowed for robust analysis of poly(lactic acid) films doped with acetaminophenol [Mahoney *et al.*, 2004], materials used in drug eluting stents [Mahoney *et al.*, 2006a] and polymer blends containing protein based drugs [Mahoney *et al.*, 2006b]. The use of different primary ion beams and their ability to increase secondary ion yields is furthered discussed in Section 2.2.4.

In addition to using different primary ion sources, researchers have also discovered that the deliberate additional of certain materials to a surface or bulk sample can result in increased secondary ion yields.

Adriaensen *et al* presented a methodology for using ToF-SIMS to study the distribution of the pharmaceutical risperidone in polyvinylbutyral coatings [Adriaensen *et al.*, 2006]. The coatings were embedded in epoxy resin, and cross-sections of these coatings were analysed before and after gold was deposited on the surface. The authors found that secondary ion signals in the samples that had received the gold coating were more intense. They also used SIMS to successfully produce secondary ion images of the surface components with sub micrometre resolution. Previous work by the same author had also promoted the use of silver and gold deposition for ion yield enhancement in the analysis of pharmaceuticals [Adriaensen *et al.*, 2004]. One of the key findings was that time from deposition to analysis played a role in the level of ion yield signal and that further studies would be required to detect the mechanism responsible for increased ion yield to maximise its use.

1.3   Complimentary Surface Analytical Techniques

Although SIMS is a powerful analytical technique in its own right, it is not always used in isolation, but rather in combination with other techniques. Leadley comments that a multi technique approach is highly important for studying changes in surface chemistry at material interfaces [Leadley *et al.*, 1998a]. For example, SIMS has been used to characterise polymer micro patterns in combination with SEM, AFM and XPS [Hale *et al.*, 2006], Goddard reviewed the use of ToF-SIMS, and other spectral methods such as Fourier transform infra-red spectroscopy and SEM for the analysis of bioactive compounds [Goddard and Hotchkiss, 2007] and Liu cited ToF-SIMS, XPS and AFM as some of the key experimental tools that are used to study nanomaterials [Liu and Webster, 2007]. However, the principle techniques that are traditionally noted as capable of surface chemical analysis are AES, XPS and SIMS [Czichos *et al.*, 2006]. AES and XPS are briefly described in terms of how they work, and the information they impart about the surface in comparison to SIMS based data acquisition. As AFM was also used extensively in this study, a brief review of this technique is presented in Section 1.3.2.

1.3.1   Auger   Electron   Spectroscopy   and   X-Ray   Photoelectron Spectroscopy

AES uses an electron gun to induce radiationless de-excitation of an ionised atom by the Auger emission process [Watts, 1990]. The analysis depth of AES is comparable to ToF-SIMS, with a sampling depth typically within the first few nanometres of the surface. A kinetic energy based spectrum of Auger electrons emitted from the surface is produced and allows the user to identify the chemicals present. Images can also be produced to map the spatial distribution of the Auger peaks observed in the spectra.

XPS measures the binding energies of photoelectrons from a sample surface that has been bombarded with X-rays [Watts, 1990]. As in AES, kinetic based energy spectra are produced. These spectra can be used to determine the elemental composition of the sample, and chemical state information can also be obtained.

The key features of these two techniques, in comparison to SIMS, are presented in Table 1.3.

Studies spanning several decades have used these techniques in combination to provide complimentary information, particularly in the characterisation of metal surfaces [Gettings and Coad, 1975; Teodoro and Moutinho, 2002] and films [Varhegyi *et al.*, 1998; Ahadian *et al.*, 2007].

In 2012, a review article was published for porous silicon (pSi) as a drug delivery candidate [Jarvis *et al.*, 2012]. Both XPS and ToF-SIMS were used to analyse both unmodified and modified pSi. XPS was credited for its ability to characterise pSi through its different oxidation states. The ToF-SIMS experiments allowed for analysis of the distribution of different ions from pSi indicating where surface modification, and hence drug loading could occur.

Gorner *et al*. have studied polymer encapsulated lidocaine controlled release nanoparticles [Gorner *et al.*, 1999]. The ToF-SIMS analyses allowed the authors to understand the form of the encapsulation process. Perhaps more importantly the technique also allowed them to detect lidocaine on the upper most surface of the particles (~1 nm) which was not seen by the XPS data additionally used in this study. Knowledge of the location of the active ingredient was seen as key to understanding how the drug would be metabolised in the body.

	Analytical Technique			
	AES	**XPS**	**SIMS (static)**	**SIMS (imaging)**
Incident Radiation	Electrons	X-Rays	Ions	Ions
Emitted Radiation	Electrons	Electrons	Ions	Ions
Elements Detectable	Li on	He on	All	All
Analysis Depth	3 nm	3 nm	1.5 nm	Dependent on the use of depth profiling
Spatial Resolution	50 nm	10 μm*	1 mm	200 nm
Information Level **E= elemental** **C=chemical**	E (C)	E,C	C (E)	C (E)
Quantification	Good	Good	Poor	Poor
Applicability to inorganics	Reasonable	Good	Good	Reasonable
Applicability to organics	Poor	Good	Good	Reasonable

Table 1.2 Comparison of AES, XPS and SIMS (adapted from Watts, 1990)

* now down to 50 nm – see Chapter 2

1.3.2   Atomic Force Microscopy

AFM can provide topographical and phase information of a sample surface at the submicron level. A tip attached to a flexible cantilever is scanned over a sample surface to measure surface morphology at the atomic scale [Goddard and Hotchkiss, 2007]. The deflection of this tip is recorded and this can be translated into a 3D image [Braga and Ricci, 2004]. A schematic diagram of the key components of the AFM is presented in Figure 1.5.

Figure 1.5 A schematic diagram of the AFM instrument
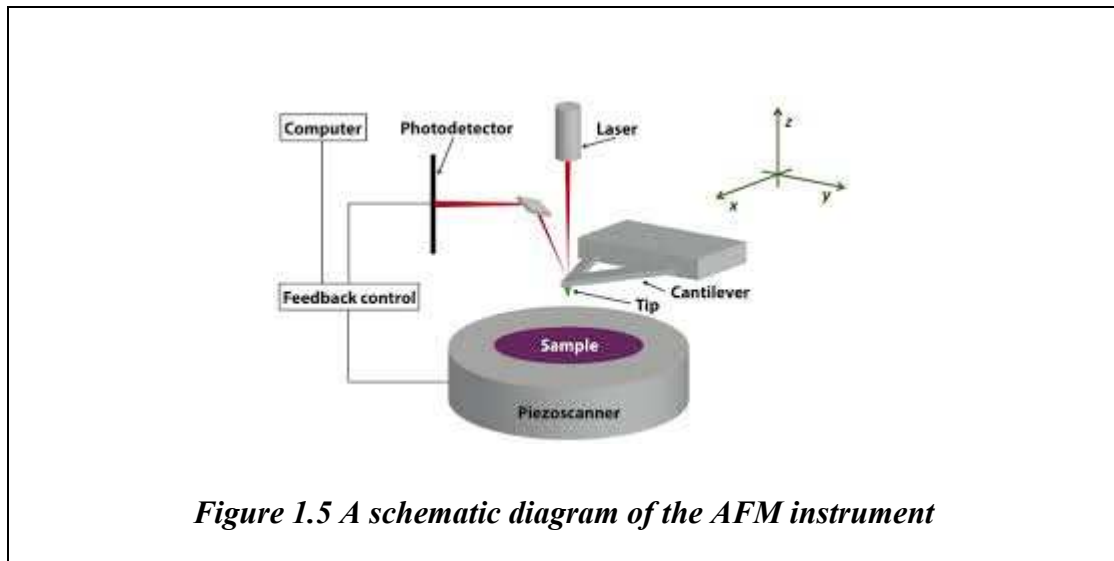
The tip is fixed below a cantilever which can be moved by the use of piezos. A laser is focussed onto the back of this cantilever and as the tip traverses across the surface contours, the deflection is measured through the use of a photodetector. The photodetector consists of four quadrants; left, right, top and bottom. The differences in light intensities between these diodes are converted into voltages. Feedback mechanisms and software control either maintain the tip at a constant height or constant force. In constant height mode the deflection of the tip is measured, and in constant force mode the piezos measure height deviation. The lateral resolution of the AFM is typically 5 nm with a 0.01 nm vertical resolution.

Tapping mode is often used with samples that are easily damaged and hence is particularly useful for imaging soft samples or samples where material may easily be moved from one region to another. The tip is alternatively placed in contact with the surface and then lifted off to avoid this dragging. This is achieved by oscillating the

cantilever at or near its resonant frequency using the piezos. As the tip contacts the surface (around 50,000 times per second) the reduction in oscillation amplitude is measured and converted to a topographical map.

Additionally, the phase difference between the piezos driving oscillation and the cantilever oscillation can be measured. Phase shifts are indicative of changes in the interaction strength between the sample and the tip; hence a phase image provides a map of surface chemistry. Topographical features can also be seen in the phase images of rough samples due to the slow response of the feedback look when the top comes into contact with an edge.

AFM has been used in several studies to provide complimentary data to SIMS analysis. For example, Leadley used SIMS, XPS and in situ AFM to investigate the acid catalysed hydrolysis of poly(orthoesters) and commented that the study demonstrated the complementary nature of these techniques for analysing surface phenomena [Leadley *et al.*, 1998a]. AFM and SIMS have also been used in combination to study nano and microstructured polymer layers [Torrisi *et al.*, 2008], and the lamellar orientation on the surface of poly(bisphenol-A-co-etheroctane) [Lau *et al.*, 2008].

1.4   Aims of the PhD

This thesis aims to assess the use of ToF-SIMS as both a qualitative and quantitative technique through the analysis of pharmaceutical formulations, non-model and model surfaces.

The thesis is divided into four experimental chapters. The first chapter aims to use the ToF-SIMS technique to assess two different drug delivery formulations and the raw materials that were used in their manufacture. Reference spectra will be produced for the raw materials and the interpretation of these spectra will be used to evaluate spectra produced for the key formulations. A secondary aim is to use a number of methods to provide potential quantitative chemical information for each of the samples from the ToF-SIMS data.

The second experimental chapter aims to assess the role of topography on the reproducibility of the ToF-SIMS data for non-model surfaces. Samples that are chemically homogenous and heterogenous will be assessed with the aim of establishing whether changes in surface topography consistently affect ion yields from different materials. The chapter will also investigate whether changes in the primary ion dose density impact data reproducibility.

The penultimate experimental chapter builds on the work from the previous chapter, but used model surfaces with pre-defined roughness profiles.

The final chapter aims to look at the problems of matrix effects in the analysis of complex pharmaceutical formulations. Principal component analysis will be used to assess two different drugs spun cast in two different polymer solutions and two of the formulations produced for the first experimental chapter.

Chapter 2.

Instrumental Methods

2.1   Introduction

The chapter outlines the fundamental aspects of time-of-flight secondary ion mass spectrometry (ToF-SIMS), a surface sensitive technique that utilises a primary ion to bombard a sample surface in high vacuum conditions. The primary ion induces sputtering of secondary ions which are then mass analysed. This technique allows the user to better understand the chemistry and distribution of elements and/or molecular structures on a sample surface [Vickerman and Briggs, 2001]. ToF-SIMS was the primary technique used for the experiments in this thesis; the instrument is based at the Laboratory for Biophysics and Surface Analysis at Nottingham University and is shown below in Figure 2.1.
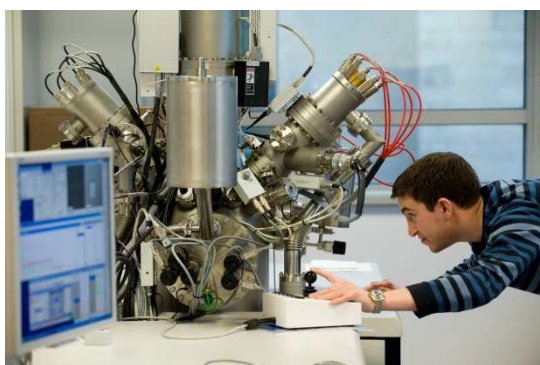
Figure 2.1 The ToF-SIMS instrument at Nottingham University

(image courtesy of the Wellcome Trust)

2.2   Time-of-Flight Secondary Ion Mass Spectrometry

The term SIMS was coined by Alfred Benninghoven in the early seventies apparently to avoid using the over long 'Secondary Ion Mass Spectrometry' in his publications [Vickerman and Briggs, 2001]. Benninghoven relocated from the University of Cologne to the University of Münster (Germany) and continued his work on secondary ion emission. Although the majority of world-wide research at the time was based on dynamic SIMS, Benninghoven and his group concentrated on static SIMS, the pre-cursor to ToF-SIMS. His first ToF-SIMS instrument was completed in 1979. These instruments are now commercially available; the ToF-SIMS instrument used in this thesis was built by ION-TOF, GmbH (Münster, Germany).

2.2.1   Theory

The basic SIMS equation describing ionisation and the formation of secondary ions is given below:

$$I_m = I_p \, Y_m \, \alpha^+ \, \theta_m \, \eta$$

where I_m is the secondary ion current of species *m*, I_p is the primary particle flux, Y_m is the sputter yield, α^+ is the ionisation probability to positive ions, θ_m is the fractional concentration of the chemistry *m* in the surface layer, and η is the transmission of the analysis system [Vickerman and Briggs, 2001]. The instrumental requirements and conditions that are needed for inducing ionisation are discussed in the following sections.

2.2.2   Vacuum Conditions

In order to minimise scattering, a pressure of at least 10^{-5} Torr is required [Briggs, 1998]. However, low pressures in the region of 10^{-9} Torr are more commonly used and the necessity for these ultra-high vacuum conditions is three fold [Hollyhead, 2006]. Primarily, any residual gas in the system can interfere with the primary ion beam causing scattering resulting in loss of spectral intensity. Residual gas can also result in scattering of the secondary ion stream. Finally, residual gas may potentially contaminate a surface; this problem is exacerbated when detection of trace elements is desired.

2.2.3   Sample Entry

The majority of instruments have sample introduction locks to allow for fast sample exchange [Briggs and Seah, 1992]. These are often operated manually and allow for centimetre sized samples or multi-specimen holders to be loaded. Once in the main chamber the sample manipulation stage enables the user to move the sample laterally, in addition to being able to change height and tilt.

2.2.4   The Primary Ion Source

ToF-SIMS can utilise a variety of primary ions as excitation sources. These can be monoatomic e.g. Ga^+, Cs^+, and Xe^+, or polyatomic e.g. C_{60} and SF_5^+ [Grams, 2007; Appelhans and Delmore, 1989]. These sources have characteristic masses and bombardment energies that influence the collision cascade mechanism. The high energy primary beam is typically between 1 and 25 keV. The gallium primary ion source currently exhibits the smallest probe size and highest current density [Pacholski and Winograd, 1999] and was the source that was used for all of the experiments in this thesis. With increasing energy or mass of an atomic primary ion, the secondary ion yield increases (i.e. the number of secondary ions sputtered per primary ion) [Vickerman and Briggs, 2001]. An increase in mass of the primary ion also gives rise to an increased weighting of the higher mass secondary ions. Polyatomic ion sources, such as SF_5^+, fragment on hitting the sample surface, again resulting in an increase of secondary ion yield. The yield enhancement from polyatomic primary ions is also greater in the higher mass region of the spectrum [Wiebel *et al.*, 2003]. Polyatomic sources are also thought to reduce surface and sub-surface damage in comparison to their monoatomic relatives, resulting in the potential for improved detection limits [Kotter and Benninghoven, 1998]. In recent years cluster sources, such as bismuth and C_{60} have been developed that provide new possibilities for analysing molecular compounds [Fletcher *et al.*, 2006; Touboul *et al.*, 2005]. These are particularly relevant in biological systems, through the enhancement of ion yields from higher mass molecular ions.

2.2.5   The Collision Cascade and Sputtering

The energy from the primary ion beam is transferred to the surface layer of a sample with sufficient energy to disrupt inter-atomic attraction and covalent bonds resulting in a collision cascade [Briggs, 1989]. A schematic diagram representing the

interaction of the primary ion beam with the sample surface is presented in Figure 2.2. Initially, on impacting the sample surface the ion will lose energy as it goes through the solid, eventually coming to rest. The region between the surface and where the primary ion comes to rest is known as the excitation volume [Vickerman and Briggs, 2001].

The energy that is lost from the primary ion track translates into atomic motion, and hence causes collisions in the surrounding material. These collisions have a knock-on effect resulting in secondary, and then tertiary collisions and so forth. In a molecular solid this energy may be high enough to cause bond scission. The motion itself initially has some directionality due to the incident angle of the primary beam. However, this memory is quickly lost and the energy distribution becomes more random. Some of this energy is directed back towards the surface, knocking out particles. This is known as sputtering [Vickerman and Briggs, 2001].

Figure 2.2 Schematic diagram to represent the ToF-SIMS sputtering induction process
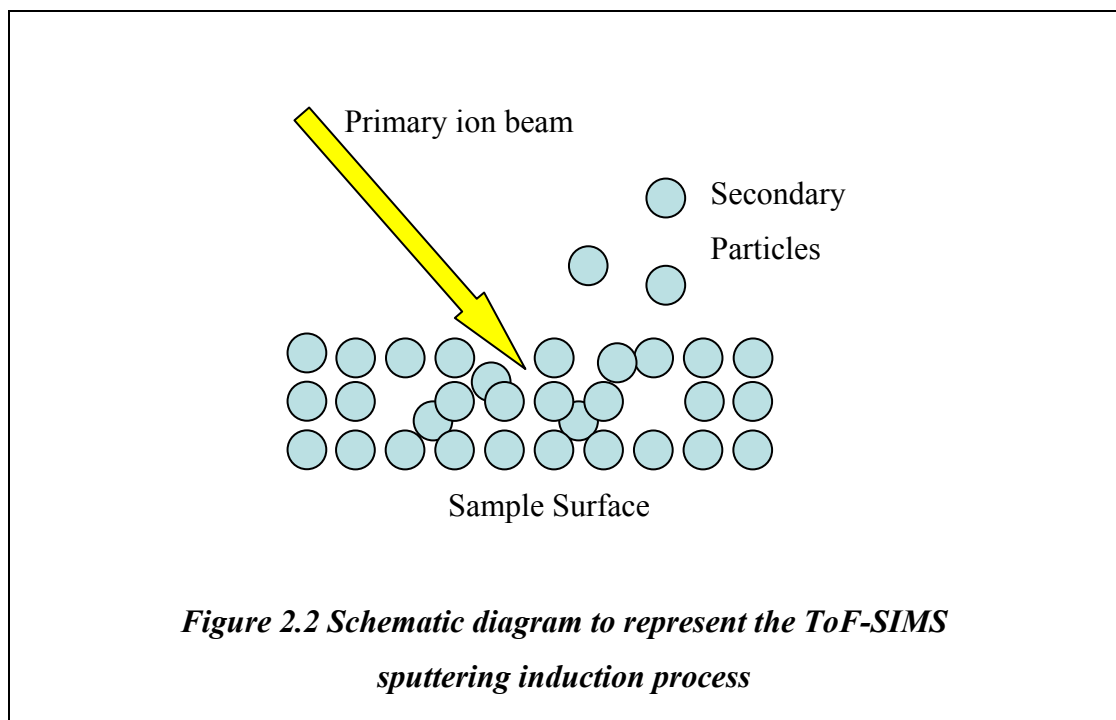
2.2.6 Sputtering and Ionisation Behaviour

The sputter yield represents all sputtered material of species *m*, both neutral and ionic. Sputtering behaviour is difficult to accurately predict or model, particularly in molecular solids as fragmentation can occur in three ways. The primary collision will cause initial fragmentation. Secondary fragmentation can be caused by energy

translation as it returns to the surface [Briggs and Seah, 1992]. Although this energy may not be high enough to cause bond breakage, it may be high enough to "push off" a fragment that has already undergone scission or, indeed, an intact molecule. Further complications in modelling arise as further (tertiary) fragmentation in the form of unimolecular decomposition can also occur in the gas phase, where a charged ion decomposes to form a smaller charged particle and a neutral. Equally, the mechanics of ionisation are not well understood [Vickerman and Briggs, 2001].

The region at the surface in which this sputtering / ionisation is thought to occur, i.e. the transition between the sample bulk and the vacuum, is known as the selvedge region [Vickerman and Briggs, 2001]. There are a number of additional ways in which ions may be produced during the sputtering process. Ionisation of neutral fragments can take place in this region by the attachment of small ions such as H^+, metal ions and halide ions. This is thought to occur by either electron impact or ion-molecule interactions [Briggs, 1998]. Cationisation can also occur, most commonly via the attachment of sodium or potassium ions to a neutral cluster. Low levels of these elements can typically be found in many samples, and are often attributed to contaminants introduced during a manufacturing process such as polymer synthesis. Additionally, the deliberate addition of a cation species to a surface can be used to increase secondary ion yields. Examples of deliberate additions of metal ions to a sample surface for enhancement of ion yield are provided in Section 1.2.7.

2.2.7   The Time-of-Flight Tube

Approximately 1% of material sputtered from a sample surface is charged [Briggs, 1998]. These ions are drawn into the time-of-flight analyser for mass analysis by applying an extraction voltage to the bottom of the tube and keeping the sample at earth [Grams, 2007]. An accelerating voltage of 3 keV is applied to the ions as they enter the field free region of the drift (flight) tube. Therefore, ions enter this tube with velocities (v) according to their mass (m) as shown in the following equation, where E is the kinetic energy of the ion:

$$E = \tfrac{1}{2}\, mV^2$$

As the ions pass through the time of flight tube they are separated as the lower mass (m) ions have higher velocities (V). At the top of the drift tube a reflectron (ion mirror) is employed to compensate for any secondary ion energy distribution which

occurs when ions with the exact same mass arrive at the detector at different times. The reflectron is designed to compensate for differences in velocity and path length by applying an increasing potential in an ion mirror located at the top of the reflectron, prior to the ions reaching the multi-channel plate (MCP). This compensation process is shown in Figure 2.3.

Figure 2.3 Schematic diagram reflecting the ToF-SIMS reflectron configuration (adapted from Vickerman and Briggs, 2001)
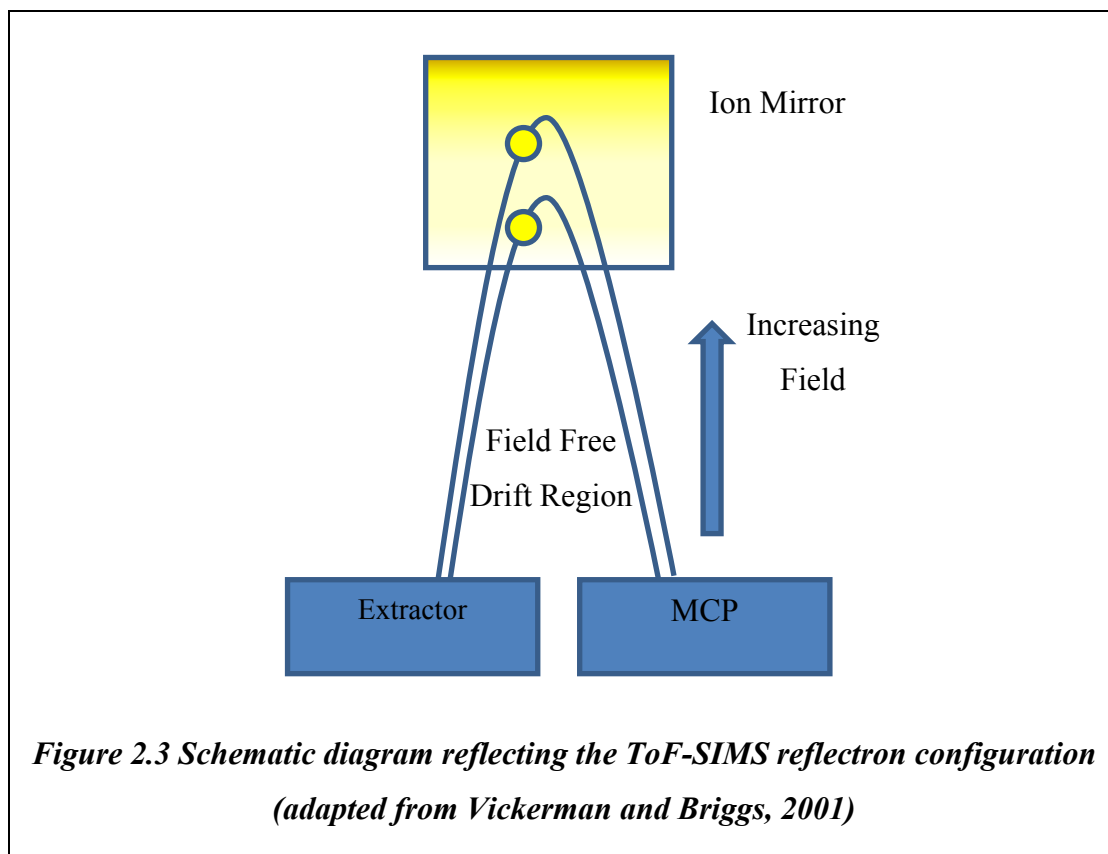
There are a number of factors which give rise to differences in the arrival time of ions with the exact same mass, which can lead to degradation in mass resolution [Briggs, 1998]:

- Time spread due to the width of the primary ion pulse

- Focussing aberrations in the analyser

- Rise time and dead time of the analyser

The width of the primary ion pulse can vary, and longer pulse widths may introduce variations in the start time at which ions leave the surface resulting in loss of mass resolution. The capability of the detector to compensate for differences in kinetic

energies, and finally contributions from the rise time and detector can also further degrade mass resolution. Despite these factors, time-of-flight instruments are becoming more common as they give greater mass resolution than the traditional quadrupole detectors, particularly when an ion mirror (reflectron) is used [Briggs, 1998].

A schematic diagram of the ION TOF ToF-SIMS instrument, which combines the majority of the key elements and mechanisms described above, is presented in Figure 2.4.

2.2.8   **Production of Data**

At the end of their trajectory the ions are detected by a multi-channel plate (see Figure 2.3). By using known hydrocarbon fragments or small atomics the resulting time spectrum can be calibrated to a mass spectrum such as that shown in Figure 2.5. This is achieved by computer software calculating a constant mass proportionality between the arrival time of two masses used for calibration and then using linear regression with further calibration masses to reduce chromatic aberration effects from the reflectron. Time resolution is absolutely key as the accuracy of the system and its detector determine both mass scale exactness and mass resolution [Briggs and Seah, 1992].

Figure 2.4 Schematic diagram of the ION TOF ToF-SIMS instrument

(courtesy of ION-TOF GmbH)

Figure 2.5 Positive ion ToF-SIMS mass spectrum of aluminium foil

(www.surfacespectra.com)
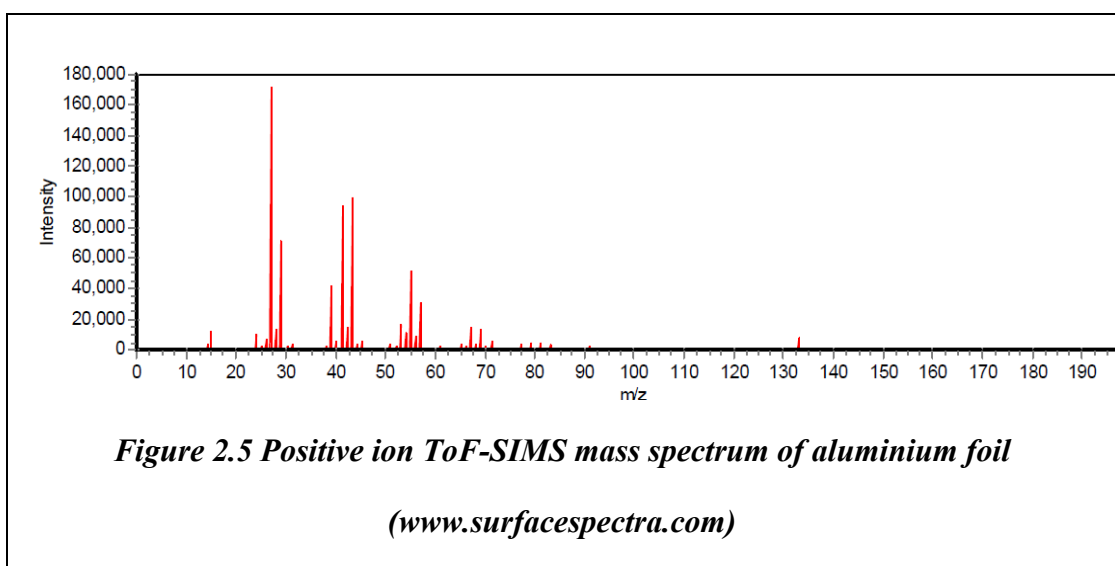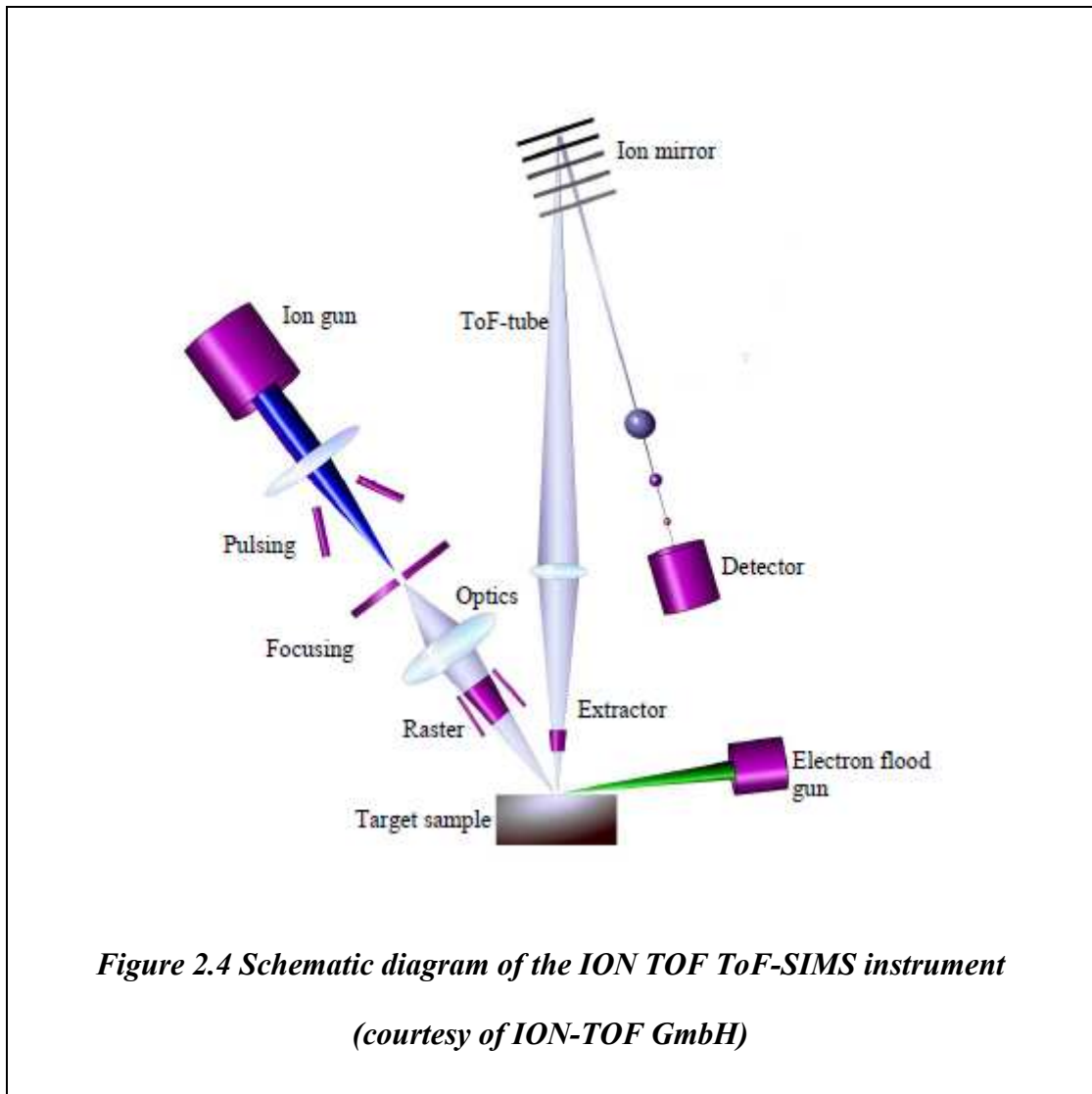
Ion maps can also be produced which show the spatial distribution of ions across the surface. An ion map of $C_2H_3O^+$, indicating the distribution of this ion following micro-contact printing of a PLA-PEG-biotin-NeutrAvidinTM-biotinylated peptide onto a silicon substrate, is presented in Figure 2.6.
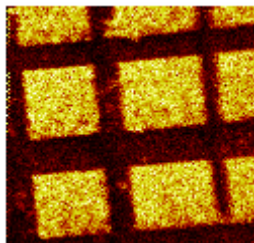
Figure 2.6 500 μm x 500 μm ion image of
PLA-PEG-biotin-NeutrAvidinTM-biotinylated peptide,
[C₂H₃O]⁺ Ion [Hollyhead, 2006]

The ToF-SIMS instrumentation is capable of these two experimental modes of operation (spectroscopy and imaging) because of the unique way in which data is collected. As the primary beam rasters across the surface individual spectra are produced for each ion packet at each pixel within the area. These are then added together by the software to give a total area spectrum. Ion images can be produced from these spectra as advances in computational technology allow users to retrospectively analyse data.

The process of producing spectra and images, and ways in which this data can be processed to gain further information, is shown diagrammatically in Figure 2.7. At the top centre of the diagram a representation of the sample is shown, with the different chemical elements represented by different colours. From this sample, either a total area spectrum or total ion image can be produced. Once the spectrum and/or image have been acquired further processing can be employed. For example, as highlighted by the left hand side of the diagram, an ion peak in the spectrum can be selected and an ion image of the spatial distribution of this ion can be produced. Alternatively, as demonstrated in the right hand side of the diagram, a specific area of the analysis area can be selected and a spectrum of this specific area can be produced.

***Figure 2.7 Schematic diagram detailing this interaction between ion
imaging and spectral acquisition***
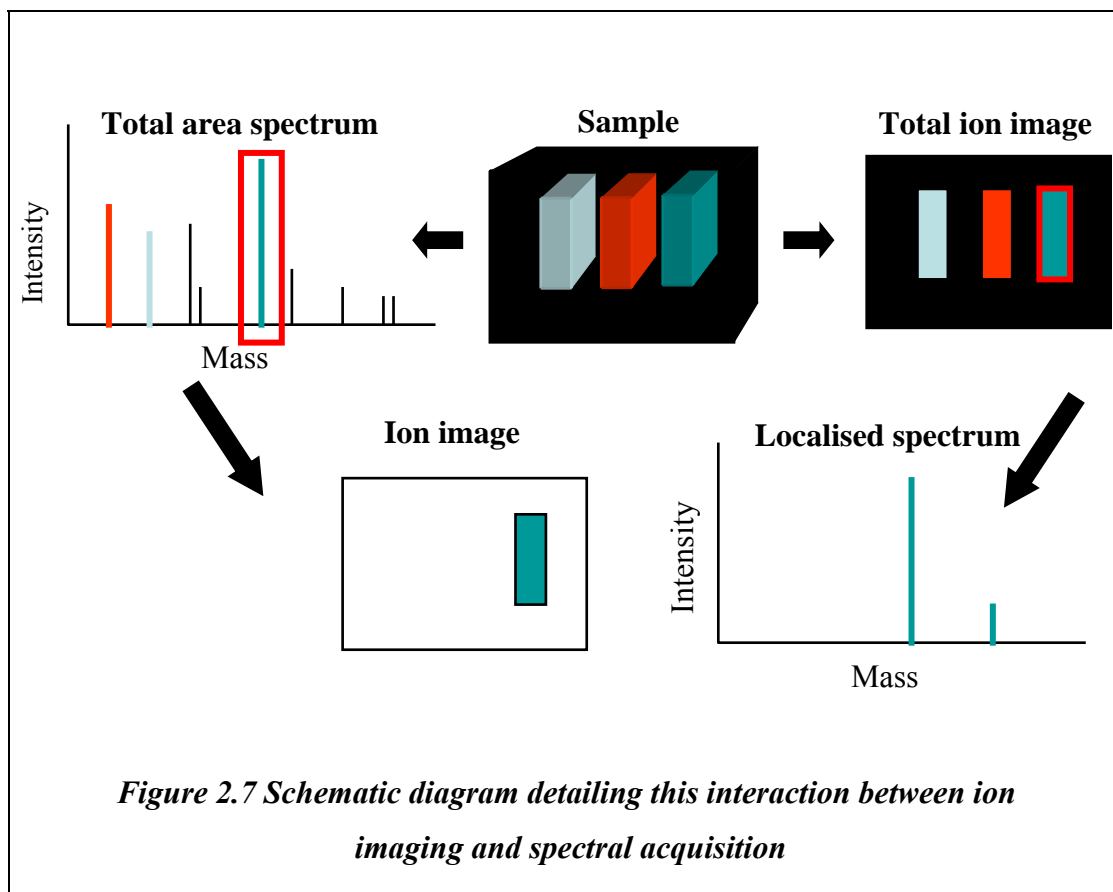
A further experimental mode, known as depth profiling is also available to the user,
where the surface is eroded away by rastering a high primary ion dose (above
10^{17} PI cm^2) across the surface to create a flat bottomed crater [Briggs and Seah,
1992]. Spectra can then be produced as a function of time, and hence depth. Depth
profiling uses dynamic rather than static SIMS and does not keep within the static
limit discussed in Section 2.3.4.

This section has briefly described the three experimental modes in which a
ToF-SIMS instrument can be typically used. The different operational modes are
more fully discussed in the following section.

2.2.9   ToF-SIMS Operational Modes

There are three main experimental modes in which ToF-SIMS can be used
depending on whether the user requires high mass resolution, high image resolution
or depth related information. Unfortunately, with mass and spatial resolution, one
precludes the other. These experimental modes are spectroscopy, imaging and depth

profiling. Spectroscopy and imaging are performed using static regimes, whereas depth profiling utilises dynamic SIMS [Briggs and Seah, 1992]. Within each of these experiments the different operational settings that can be used, which govern both spectra and image resolution, are presented in Table 2.1. The high current bunched (HCB) settings use electrostatically compressed ion pulses and give the best mass resolution but lower spatial resolution, approximately 4-5 μm. The collimated (COL) settings gives the best spatial resolution (typically 50-60 nm) and hence can be used in imaging, but have such an associated poor mass resolution and long acquisition times due to the low current, that in practice these settings are rarely used. Burst alignment (BA) settings are more typically used for imaging and give a spatial resolution of around 200 nm.

Users must decide what information they require and design their experiments in a way to achieve this, for example, in the case where high spatial resolution is required this can be achieved through the use of the burst alignment settings, but will result in lower mass resolution in the spectrum. A trade off could be to run an area in both the burst alignment and high current bunched mode but only using half the maximum static limit dose for each data acquisition. However, the increased signal to noise ratio may prove too expensive to take this route. Time considerations may also play a role; spectroscopy experiments performed with HCB settings are relatively quick whereas imaging experiments typically take much longer. The three settings are summarised in Table 2.1.

Dynamic SIMS or depth profiling allows the user to measure ion intensity as a function of depth, and is achieved by eroding away the surface to form a flat bottomed crater [Briggs and Seah, 1992]. As the primary beam rasters across the surface secondary ions are generated and these ions are drawn into the time-of-flight analyser by applying an extraction voltage to the bottom of the tube. Dynamic and Static SIMS are distinguished by the primary ion dose used during the experiment [Vickerman and Gilmore, 2009]. The static limit is discussed in Section 2.3.4 and refers to the maximum primary ion dose that can be used which will effectively result in a spectrum that is produced from an undamaged surface [Vickerman and Briggs, 2001].

Finally, when selecting a combination of mode and setting the user also needs to consider the selection of the primary ion source. The primary ion source is discussed in Section 2.2.4.

High Current Bunched Settings (HCB)	• Lots of current, hence signal • High mass resolution • Large spot size (around 4-5 μm) • Low spatial resolution • Very quick to acquire
Burst Alignment Settings (BA)	• Good for imaging (around 200 nm resolution is possible) • Small spot size means that species that have a low intensity in high current bunched mode may not be resolved when imaging as they contribute less signal per spot size area • Charge compensation is more critical as the current is deposited in a smaller area
Collimated Settings (COL)	• Increased spatial resolution (around 50-60 nm) • Lower mass resolution than burst alignment (unit mass resolution) • Low current compared to burst alignment mode, hence time consuming

Table 2.1 ToF-SIMS operational settings and their key features

To summarise, users need to decide what information they require from their sample surface and then exploit the capabilities of the ToF-SIMS instrument to achieve this. If both mass and spatial resolution are required, then care needs to be taken not to exceed the static limit. As depth profiling is a destructive technique and results in significant surface damage, any spectroscopy or imaging of a specific analysis area may need to be performed prior to running the instrument in this mode, if information from an undamaged surface is required.

2.3   Understanding ToF-SIMS

ToF-SIMS is a highly sensitive technique, capable of detecting fractions of a monolayer or sub-ppm elemental concentrations at a surface [Passchier and Trouw, 2005]. It offers certain advantages over other techniques in terms of chemical specificity and surface sensitivity as discussed in Chapter 1. These advantages include its excellent chemical sensitivity, the ability to distinguish between two isotopes of the same element and the ability to obtain information in regards to chemical bonding at the surface by analysing molecular ions [O'Connor *et al.*, 2003].

Spectra that are generated from a surface that has few components are relatively easy to interpret using methods outlined in ToF-SIMS reference books such as "ToF-SIMS Surface Analysis by Mass Spectrometry" [Vickerman and Briggs, 2001]. However, more complex spectra, which are often seen in biological materials, are much more difficult to interpret [Vickerman, 2009]. The secondary ion yields that arise from these chemically complex surfaces are often also influenced by the local chemical environment, in a process referred to as matrix effects. Matrix effects can result in the same ion varying by several orders of magnitude depending on the chemical environment from which the ions were sputtered from. Matrix effects are thought to be less severe in organic systems [Kuo, 2007]. Matrix effects are more fully discussed in Section 2.3.1.

The quality of both ToF-SIMS spectra and imaging are governed by resolution. In terms of spectroscopy, mass resolution can be defined as the ability of the instrument to be able to distinguish two peaks of slightly different mass-to-charge ratios [Biemann, 1962]. Spatial resolution describes the ability of the instrument to distinguish between two points as separate and distinct [Westbrook *et al.*, 1998]. The ability to acquire high quality spectra and images from insulating samples can be more challenging, and is often governed by the charge compensation strategy [Briggs, 1998]. Spectra and imaging experiments are typically collected within the static limit, i.e. a primary ion dose that results in less than 1% of the surface receiving an ion impact, and to all intents and purposes results in the data being collected from an undamaged surface [Vickerman and Briggs, 2001]. As ToF-SIMS is an extremely surface sensitive technique, sample handling procedures and sample preparation methods must also be considered prior to analysis.

2.3.1   Spectral Interpretation

Briggs suggests that different principles should be applied to organic and inorganic spectra [Vickerman and Briggs, 2001]. Using the standard mass for carbon at 12.0000, all elements above this have masses at slightly below nominal unit mass (for example, oxygen at 15.9949), whereas organic fragments, which are predominantly carbon and hydrogen based, have masses slightly above the nominal unit mass. It also suggested that polymers can often be identified by their monomer repeat units.

Inorganic ions, such as metal oxides, are usually dominant in the positive ion ToF-SIMS spectrum as M^+ and in the negative ion ToF-SIMS spectrum as $[M-O]^-$ or $[M-OH]^-$. Metal impurities, such as sodium, can also result in positive ions such as $M_xO_yNa^+$. Cationisation can also occur with other alkalis, e.g. $[M+K]^+$ and can often occur with monolayers on metal substrates [Vickerman and Briggs, 2001]. This can often be classed as a matrix effect as it is a result of the surface environment.

Databases, such as The Static SIMS Library (SurfaceSpectra Ltd., Manchester, UK), are a useful resource when identifying peaks. There are also a number of handbooks such as the "Handbook of static secondary ion mass spectrometry (SIMS)" which identify diagnostic ions for materials such as PEG and PMMA [Briggs, 1989].

2.3.1.1   The Formation of Metastable Ions

It is possible for ions to form in the time of flight tubes that have not arisen from the sample surface. These metastable ions occur when a parent ion decays to form daughter ions. This process has been observed in polytetrafluoroethylene (PTFE) through applying changes to the reflectron voltage [Gilmore and Seah, 1999]. Metastable decay only occurs where the emitted secondary ion possesses sufficient internal and kinetic energy to break the atomic bonds that maintain its integrity. This typically results in peak broadening within the spectra.

2.3.1.2   Matrix Effects

Substantial comment is made by Briggs in reference to matrix effects [Briggs, 1998]. Previous studies into matrix effects in the field of dynamic SIMS have shown that the ion yield of a chemical species is dependent on the surrounding material [Vickerman, 2009]. For example, in comparing the ion yield of Si^+ from pure silicon

to silicon dioxide, an increase of about x70 is observed [Briggs, 1998]. It is known that the different chemical environments from which the ions are desorbed and ionised cause these matrix effects. These effects may also play a role in the formation of spectra from complex organic systems acquired within the static limit, and need to be studied.

Matrix effects are also responsible for the difference between a spectrum of a high purity standard in comparison to a spectrum of the same standard on a polymer surface. Molecules in a multi-layer environment are subjected to a different matrix environment from those in a surface monolayer. This effect results in dimer (or higher *n*-mer) ions being desorbed from the surface. This behaviour is particularly common in salts e.g. Na^+X^-, where clusters of $X(NaX)^+_n$ are observed [Briggs, 1998]. $X(NaX)^-_n$ clusters may also be seen in negative spectra, although this is less common.

Mixed surface layers containing more than one type of molecule can also be witness to these changes in ionisation behaviour. For example, a higher yield of $[M+H]^+$ may be observed if another molecule other than M is a source of H^+ ions [Briggs, 1998].

The presence of alkali metals in samples, such as sodium and potassium (possibly as impurities) can lead to the cationisation in the form of $[M+Na]^+$ or $[M+K]^+$. These ions often have higher yields than the protonated analogue $[M+H]^+$. These quasi-molecular ions can also be seen in negative spectra in the form of $[M-Na]^-$ or $[M-K]^-$. Polyethylene glycol containing polymers are particularly susceptible to this form of matrix effect by natural cationisation [Briggs, 1998].

2.3.2 Limits to Resolution

Resolution can be subdivided into two areas – spectral (or mass) resolution for spectroscopy and spatial resolution for imaging. As described in Section 2.2.9 the SIMS instrument can be operated in several modes that utilise different settings that ultimately control these two types of resolution. The mass resolution of ToF-SIMS instruments under optimal conditions is impressive, for example, it is possible to resolve between iron contamination (Fe^+ at m/z 55.935) on a silicon substrate (Si_2^+ at m/z 55.954) [Ohmae *et al.*, 2005]. Pulsed liquid metal ion guns (LMIG), such as gallium, are considered ideal for optimising spatial resolution due to their sub-micron

spot size [Briggs, 1998]. However, cluster ion guns such as gold and bismuth that result in lower spatial resolution are also used in imaging as they can increase the yield and allow mapping of secondary ions in the higher mass ranges [Becker, 2007]. As previously discussed, it is worth noting that if both spectroscopy and imaging are required a trade off may have to be made as an increase in mass resolution results in a decrease in spatial resolution and vice-versa.

2.3.3   Charge Compensation

Sample charging is a problem that is exhibited by many samples, and in particular insulators. Charging mechanisms can result in an accumulation of charge on a sample surface resulting in reduced detection of secondary ions [Leggett and Vickerman, 1995]. The problem of surface charging can often be eliminated by the use of a low energy flood gun. The gun floods the sample surface with low energy electrons between primary ion pulses. It is suggested that the electron dose should be maintained below 6×10^8 electrons m^{-1} for polymeric and organic samples in order to avoid sample damage [Gilmore and Seah, 2002]. However, alternative approaches to sample preparation, where appropriate, have been developed to negate the need for charge compensation. Spin coating is typically used where a powdered solid is dispersed in a solvent and then spun cast onto a rotating sample stub, resulting in an evenly distributed and thin layer to minimise the need for charge compensation. Thin slices of samples can also be mounted onto metal substrates, such as indium or silver, to minimise sample charging effects [Ingram *et al.*, 1999].

2.3.4   Damage and the Static Limit

When conducting a SIMS experiment it is important to remain within the static limit as mass spectral data gained without exceeding this limit are more representative of the undamaged surface [Barner-Kowollik *et al.*, 2011]. This limit, expressed as the number of ions per square cm, ensures that the probability of bombarding a previously damaged area is extremely low. Therefore, if modification has occurred from a primary ion shot this area will not be hit again provided that the static limit is not breached. A simple calculation can be used to approximate the static limit based on a number of assumptions; An approximation is made of the number of atoms in a 1 cm^2 monolayer to be 10^{15}, if it is assumed that a single primary ion impact affects a region of around 10nm, then the surface atoms in the area will be affected by a dose

of 10^{13} ions cm^{-2} [Briggs, 1998]. However, if a large molecule occupies this region then its integrity will be altered by this impact. For an experiment to satisfy the static criterion, an unaffected spectrum must be able to be acquired from the same area more than once. Therefore, a more reasonable value of 10^{12} ions cm^{-2} is more commonly used [Briggs *et al.*, 1984].

2.4   Typical ToF-SIMS Sample Preparation and Analysis Conditions

There are a number of factors, highlighted by the previous sections and Chapter 1 that need to be considered when designing a ToF-SIMS experiment. These are primarily concerned with sample preparation and set up conditions, both of which will influence the ability to obtain accurate information in regards to the sample surface.

2.4.1   Sample Preparation

As discussed in Chapter 1, ToF-SIMS is a highly sensitive technique, typically sampling from the top few nanometres of a sample surface. For this reason, the cleanliness of sample preparation is of extreme importance [Setou, 2008]. Reich suggests that the entire process from storing the sample prior to analysis to mounting the sample prior to insertion into the ToF-SIMS instrument must be considered [Vickerman and Briggs, 2001]. It is therefore of utmost importance that samples are contaminant free (unless it is potential contamination that is to be investigated). Frequently, samples are contaminated with polydimethylsiloxane (PDMS) and phthalates, which are found in most plastic based products [Vickerman and Briggs, 2001]. The characteristic peaks that indicate PDMS contamination are shown in Table 2.2. PDMS is often used as a mould release agent in the manufacture of products such as plastic storage boxes and bags, however contamination that has arisen from samples transported in these types of packaging can often be removed by hexane [Vickerman and Briggs, 2001].

Reich lists the key elements to good sample handling:

- Clean packaging for receiving, sending and storing samples

- Care in the use of pastes and tapes to secure samples, any PDMS in these may migrate to the surface

- Educating clients so that the importance of the above two factors is understood

- Maintenance of clean sample holders

- Maintenance of a clean sample handling area

Aluminium foil is often recommended as a packaging material but some foils are treated with a layer of stearic acid that can transfer to the sample surface and it is recommended that any potential packaging material is itself analysed prior to use [Ratner, 2004].

Contaminants may also result in surface charging; charge compensation is discussed in Section 2.3.3. Samples must also be vacuum compatible, which if necessary can be achieved through dehydration by organic solvents [Ingram *et al.*, 1999].

Positive Ion Spectrum		Negative Ion Spectrum	
Mass (m/z)	**Assignment**	**Mass m/z**	**Assignment**
28	Si^+	59	CH_4OSi^-
43	CH_3Si^+	60	SiO_4^-
45	$SiOH^+$	75	$CH_4O_4Si^-$
59	CH_3OSi^+	119	$CH_4O_4Si_4^-$
73	$(CH_3)_3Si^+$	149	$(CH_4)_4HO_4Si_4^-$
117	$(CH_3)_3OSi_2^+$	223	$(CH_4)_4HO_4Si_4^-$
133	$(CH_3)_4OSi_2^+$		
147	$(CH_3)_5OSi_2^+$		
191	$(CH_3)_5O_2Si_3^+$		
207	$(CH_3)_5O_3Si_3^+$		
221	$(CH_3)_7O_2Si_3^+$		
281	$(CH_3)_7O_4Si_4^+$		
295	$(CH_3)_9O_3Si_4^+$		
325	$(CH_3)_4O_4Si_4^+$		
355	$(CH_4)_4O_4Si_4^+$		

Table 2.2 Ions in the positive and negative ToF-SIMS spectra that are indicative of contamination, (adapted from Briggs, Brown and Vickerman, 1989.

2.4.2 ToF-SIMS Analysis Conditions

During this work static ToF-SIMS measurements were performed on an ION-TOF ToF-SIMS IV instrument (ION-TOF GmbH, Münster, Germany). Where necessary, the flood gun was operated at 3 keV, 30 µA to compensate for sample charging. Specific analysis conditions such as mode, dose and analysis area are discussed in the appropriate chapters as they were sample dependent. However, in all cases the analysis dose was kept below the static limit of 1 x 10^{13} ions cm^{-1}.

Chapter 3.

The Role of ToF-SIMS in the Characterisation and Quantification of Drugs and Excipients in Pharmaceutical Formulations

---

3.1 Introduction

There are a number of vectors used in solid dose drug delivery, three of which are summarised in Table 3.1.

Method 1: Tablets	*Method 2: Powders*	*Method 3: Capsules*
Easy to package, transport and dispense; convenient for self medication	Often used for high doses of drugs that have low toxicity	Largely devoid of taste and odour, can be used for unpalatable drugs

Table 3.1 Vectors used in solid dose drug delivery systems
(adapted from Durgin and Hanan, 2005)

Tablets and capsules are recognised as two of the main types of pharmaceutical formulation used for solid dose drug delivery [Jones, 2006a]. Capsules can contain powders, liquids and spheroids. For the purpose of this thesis, both tablet and spheroidal bead formulations were manufactured for study, using a range of excipients and a single API.

3.1.1 Selection of Materials for Analysis

Paracetamol was selected as the active ingredient in both of the formulations. Paracetamol, also known as acetaminophen, is an aromatic amide introduced by Von Mering in 1893 as an analgesic and antipyretic [Bosch *et al.*, 2006]. It is one of the most widely used analgesics and commonly used in several over the counter, and

prescription analgesics. Paracetamol is also often incorporated into cold/flu formulations.

The tablet formulations used spray dried lactose and a low concentration of magnesium stearate as excipients. Spray dried lactose was selected as a bulking agent/diluent to make the formulation of sufficient size. Magnesium stearate was selected as a glidant to prevent the API/excipient mixture adhering to the die surfaces during tablet manufacture. The use of excipients in pharmaceutical formulations is more fully described in Chapter 1.

The second formulation, spheronised beads, also contained two excipients. As in the tablet manufacture, spray dried lactose was selected as a bulking agent. Again, spray dried lactose was used rather than "traditional" lactose as its greater spheroidal morphology gives the final mixture better flow characteristics and results in a more homogeneous mix. Microcrystalline cellulose was selected as the second excipient. This material is a widely used filler in solid dose drug delivery systems as it is biocompatible and chemically inert [Aulton, 2002].

3.1.2 Manufacturing Tablets and Spheronised Beads

The tablets and spheronised beads used in this chapter were made using small scale versions of the manufacturing processes outlined in this section.

As with many drugs and excipients, the raw materials used in the tablet formulations were supplied in powder form. These powders need to be mixed and then granulated or, if the mixing process provides sufficient homogeneity, they can be directly compressed without using a granulation step. The main aim was to get a homogenous formulation where there is a consistent drug dose within each tablet, and the distribution of the drug within the tablet is uniform.

Tablet manufacture typically composes of three key stages following preparation of the powder mix or granules [Aulton, 2002]:

> ➤ Die Filling
>> ➤ The hopper moves into position and the powder flows into the die under gravitational force. The end of the die is stoppered by the lower punch.

➢ Tablet Formation

    ➢ The upper punch is lowered into the die with appropriate force, compressing the powder to form the tablet.

➢ Tablet ejection

    ➢ The lower punch rises till it is level with the bottom of the die. A pushing device then removes the tablet.

Figure 3.1 details the machinery that is used for this process.

Figure 3.1 Schematic diagram representing the tableting manufacturing process (adapted from Aulton, 2002)
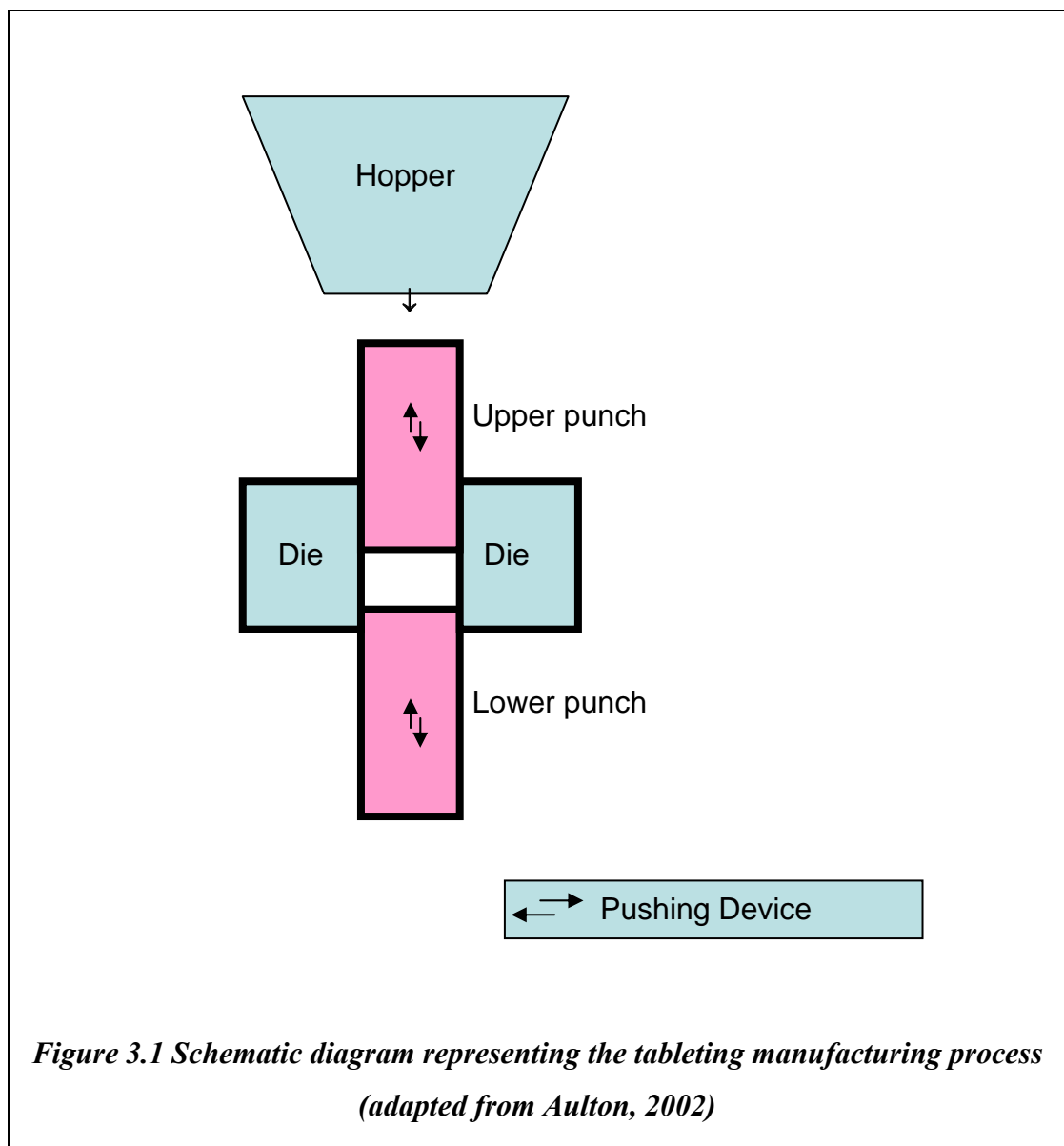
Spheroids are typically manufactured using extrusion and spheronisation. This is a well-known and established method to make solid dose formulations, and a comprehensive literature review of this process was published in the mid-1990s [Vervaet *et al.*, 1995]. The process involves producing small spherical agglomerates, called spheroids, of a controlled size distribution which is determined by the manufacturing conditions. Extrusion is typically used to incorporate the active ingredient within the formulation. However, spheronisation can take place without extrusion, when sugar or starch particles that have been coated with the active ingredient, are used.

Extrusion and spheronisation typically composes of five key stages [Aulton, 2002]:

- Mixing of dry ingredients
  - ➢ To establish homogeneity within the batch
- Wet massing
  - ➢ To establish an appropriately plastic wet mass
- Extrusion
  - ➢ To form rod-shaped masses of a pre-defined diameter
- Spheronisation
  - ➢ To round the extruded masses into spheroids
- Drying
  - ➢ To a pre-defined moisture content

During the drying phase the beads may also be coated. Many manufacturers will also perform a final screening stage to ensure that the size distribution of the spheroids is within set parameters.

The extrusion and spheronisation process is shown diagrammatically in Figure 3.2.

Figure 3.2 The extrusion and spheronisation process
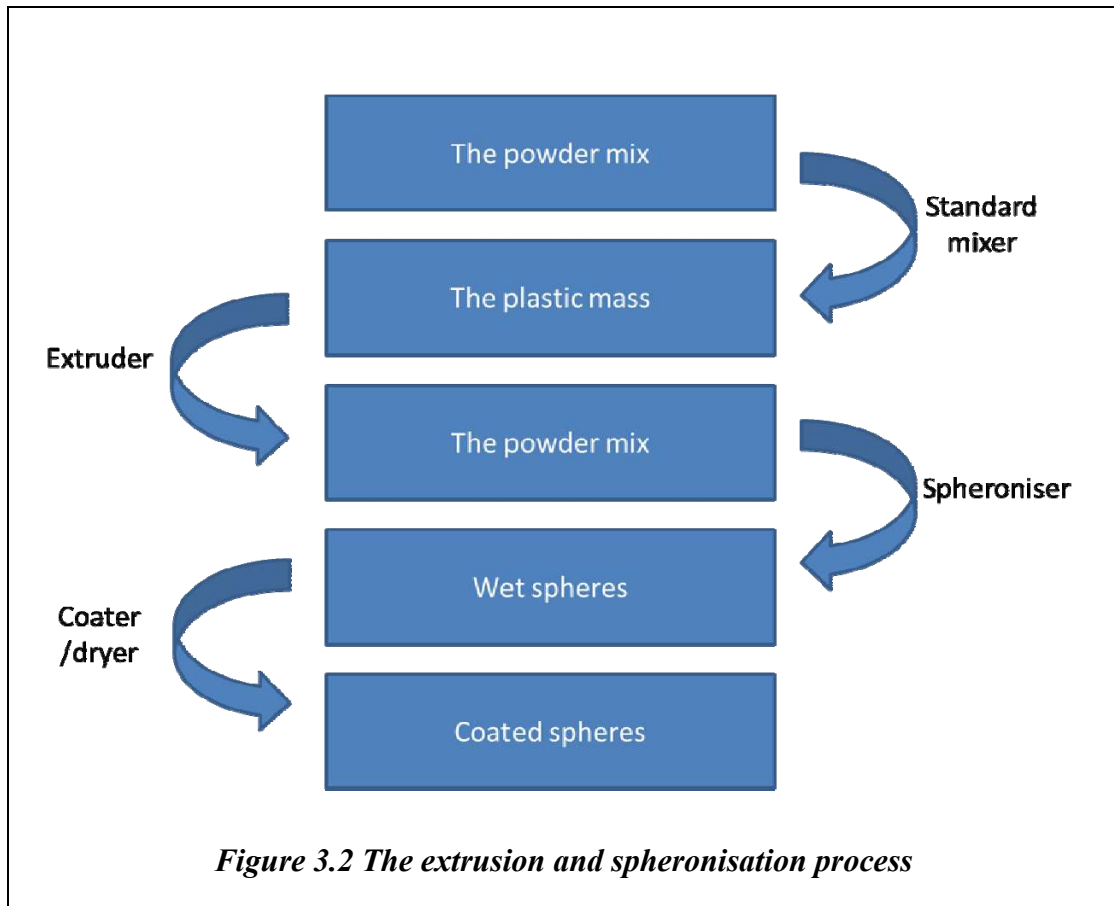
The spheroidal material within capsules can be referred to as pellets, beads or microspheres. The process of manufacturing spheroids has now evolved into a cost effective and rapid method of producing a unique solid dosage form that offers several advantages [Dukic´-Ott *et al.*, 2009]. The pellets are, in effect, individual drug units and therefore reduce the risk of irritating the stomach lining with high localised drug concentrations that would be more likely to occur with a single unit formulation. Pellets can be manufactured with several different components containing different active ingredients that may not be compatible in a single formulation. In addition, dosage forms with different concentrations can be produced within the same batch by altering the fill weight of the pellets.

Pellets can easily be coated (e.g. with an enteric coating) due to their smooth surface morphology, spheroidal shape and narrow size distribution. As each pellet has its own coating, if this coating fails, only a small amount of drug would be released. In comparison, if the coating of a single unit dose (such as a tablet) failed then the entire dose could be released.

The properties cited above are usually recognised as the main advantages of this method of manufacture in respect of the active ingredients. However, there are more advantages of this method, particularly in regards to the process itself [www.caleva.co.uk]:

- The spheroidal morphology gives good flow characteristics, allowing ease of capsule filling

- The process eliminates dust, resulting in a dust free packaging environment and potential reductions in toxic, environmental and explosive hazards

- Product settlement is reduced by spheronisation of powder products

- Product consistency is improved by using a free flowing "ready mixed" product

There is a wide range of spheroidal products on the market, from cold preparations to analgesics to vitamin supplements. These all utilise this unique method of manufacture to provide viable and effective drug formulations.

3.1.3   ToF-SIMS Analysis of Tablets and Bead Systems

Belu *et al*. have studied three multi-layered drug beads, comprising a drug core enclosed by one or more polymeric layers [Belu *et al.*, 2000]. Three beads were studied, containing different active ingredients in each one, paracetamol, theophylline and prednisolone, and commercially available polymeric coatings. In addition to acquiring spectra from the bead systems, spectra for each of the pure materials were produced, providing ToF-SIMS reference spectra of these materials for the first time. The experimental design used by Belu to acquire spectra from different areas of the sample is presented in Figure 3.3.

Heterogeneous Sample Surface
(Bead Cross-section)

Total Analysis Area

Bead Coat
Bead Core

A. SIMS spectrum
from summation of each
spectrum at each pixel point

A. Total Ion Image

B. SIMS spectra
extracted from
specific areas of
the sample

B. Plots of location
of selected ions

Figure 3.3 Schematic diagram showing the experimental design for
ToF-SIMS analysis of a cross sectioned drug bead
(image courtesy of Belu, 2000)

The paper provided positive ion spectra identifying the drugs, excipients and polymers within the beads. The authors were unable to specify a parent molecule for a small proportion of the peaks assigned a chemical composition. However, parent molecules were assigned for all three of the active ingredients, in the positive ion spectra. The study emphasised the benefit of sub-micrometre spatial resolution and the ease of producing chemical ion maps of different components. It was also noted that providing a fingerprint spectra of a pharmaceutical system is useful both in reference purposes and for defending against patent infringement and counterfeiting.

SIMS has been used to provide reference spectra for sodium chloride and sodium chloride – magnesium stearate mixes in tablets [Hussain *et al.*, 1990]. A method based on using ratios of the sodium and atomic ions was successfully used to establish the concentration of each material at the tablet surface. The use of SIMS spectroscopy and complimentary SIMS imaging gave information on the effect of varying mixing time on the distribution of magnesium stearate and sodium chloride at the tablet surface.

Belu has previously reported on ToF-SIMS spectra of Avicel, a form of microcrystalline cellulose. She concluded that both positive and negative spectra are dominated by hydrocarbon fragments from the cellulose [Belu *et al.*, 2000].

Prestidge *et al.* have also used ToF-SIMS to study solid-state pharmaceuticals and highlight specific case studies concerning the distribution and stability of pharmaceutical actives within drug pellets [Prestidge *et al.*, 2007].

A more comprehensive review of the use of SIMS in the analysis of pharmaceutical formulations is provided in Chapter 1.

3.1.4   Aims of the Chapter

This initial experimental chapter focuses on using ToF-SIMS to analyse two formulations and the raw materials that were used in these formulations. Both tablets and spheroidal beads were manufactured containing varying concentrations of paracetamol as an active pharmaceutical ingredient (API). The tablets contained spray dried lactose and magnesium stearate in addition to the API, whereas the beads contained spray dried lactose and microcrystalline cellulose as excipients.

The main aims of this chapter are to two fold. In the first instance, they are to assess the ability of ToF-SIMS to evaluate the raw materials through generation of reference spectra, and the multi-component systems through generation of both spectra and chemical ion maps. Secondly, the chapter aims to evaluate the use of ToF-SIMS for detecting and differentiating between the components that are used to make the two formulations.

SEM is also used to provide complimentary information.

3.2 Materials and Methods

3.2.1 Raw Materials

A number of typical excipients and materials were utilised as detailed in Table 3.2.

Excipient Material	*Chemical Formula*	*Type*	*Manufacturer*
Lactose	$C_{12}H_{22}O_{11}$	Bulking Agent	Sigma
Spray Dried Lactose	$C_{12}H_{22}O_{11}$	Bulking Agent	Sigma
Magnesium stearate	$C_{36}H_{70}MgO_4$	Lubricant	Sigma
Microcrystalline Cellulose	$C_6H_{10}O_5$	Bulking agent	Fluka
Hexane	$CH_3(CH_2)_4CH_3$	Solvent	Sigma
Chloroform	$CHCl_3$	Solvent	Sigma

Table 3.2 Details of excipient materials used to manufacture
the tablet and beads studied

In addition, paracetamol $C_8H_9NO_2$ (NBS Biologicals Ltd., Huntingdon, UK) was used as the active ingredient in both the tablet and spheroidal bead formulations.

3.2.1.1   ToF-SIMS Sample Preparation and Analysis Conditions

Figure 3.4 details the typical construction of a powder sample prepared for SIMS analysis using a double adhesive layer method.

                 ☐ = powder

                 ☐ = sellotape

                 ☐ = double sided tape

Figure 3.4 Schematic diagram representing ToF-SIMS sample construction for powder materials
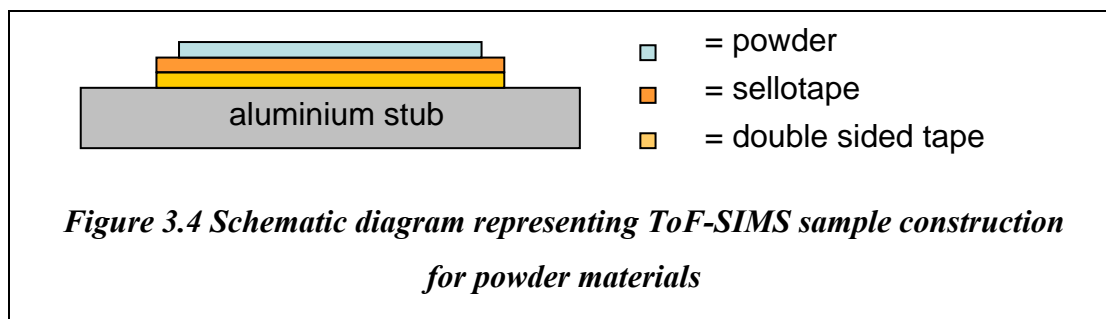
This method was used as preliminary analyses of the double sided tape (3M, Bracknell, UK) highlighted silicone contamination and hence unsuitability for direct powder mounting. However, conventional sellotape (3M, Bracknell, UK) was found to be free from silicone contamination so was selected as an intermediate layer between the double sided tape and the powder. 10 mm diameter aluminium stubs were used for several reasons, most significantly due to aluminium's non-magnetic properties. In addition, samples were "back mounted" into the sample holder and therefore a flat surface was required for the mounting blocks to brace against. Before use, the aluminium discs were cleaned in an ultrasonic bath using a two solvent cleaning process of high purity hexane followed by high purity chloroform. The double sided tape and sellotape layers were then adhered in turn to the disk surface and the powder materials were sprinkled onto these layers. Excess powder was removed by gently tapping the disk on a hard surface. The powder application procedure was repeated twice to ensure an even and full coverage. The samples were then back mounted into the sample holder, minimising the effect of any tilt that may be present in the discs.

Static ToF-SIMS measurements were performed on an ION-TOF ToF-SIMS IV instrument (ION TOF GmbH, Münster, Germany). In all experiments gallium was used as the primary ion. The flood gun was operated at 3 keV, 30 μA to compensate for sample charging. Random sampling areas of 100 μm x 100 μm were analysed using spectroscopy (high current bunched) mode in order to obtain high mass

resolution spectra. In all cases the analysis dose was kept below the static limit of 1 x 10^{13} ions cm^{-1}.

3.2.1.2   SEM Sample Preparation and Analysis Conditions

The powder samples were mounted onto standard SEM stubs with double sided carbon tabs (both items Agar Scientific Ltd., Essex, UK) using the same method of powder application as detailed in the ToF-SIMS sample preparation process detailed above.

These samples were then gold coated for 4 minutes using an Emscope 500 coater (Emscope, Ashford, UK) operated at 15 µA. The samples were analysed in a Philips XL30 SEM utilising a lanthanum hexaboride filament operated at 10 keV and with a working distance of 10 mm. Figure 3.5 details the typical construction of a powder sample prepared for SEM analysis using a double adhesive layer and gold coat method.

□ = gold
□ = powder
■ = carbon tab

SEM stub

Figure 3.5 Schematic diagram representing SEM sample construction for powder materials
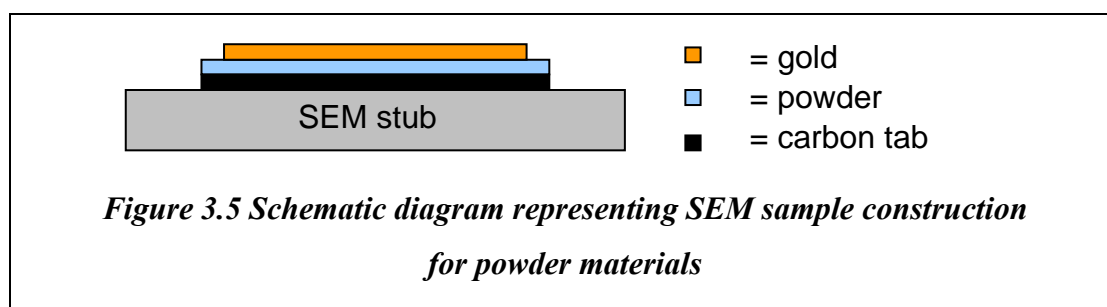
3.2.2   Tablets

Tablet formulations were prepared using the active ingredient, paracetamol, with spray dried lactose and magnesium stearate as excipients. Four different concentrations of the active ingredient were studied using a range of 20-80 wt% paracetamol. 20 g batches of each sample type were prepared. The raw ingredients were mixed in a Y-cone blender (Normand Electrical Co. Ltd., Neco. Works, London, UK) for 5 minutes and this mixture was transferred to a die press manufacturing 8 mm diameter tablets with a 2-3 mm depth. The hardness values of the tablets were measured using a Holland C50 Hardness Tester to confirm the die press settings were appropriate. The four different tablet types with relative concentrations and samples IDs are detailed in Table 3.3.

Sample ID:	Concentration (wt%)		
	Paracetamol	*Spray Dried Lactose*	*Magnesium stearate*
20P	20	79.5	0.5
40P	40	59.5	0.5
60P	60	39.5	0.5
80P	80	19.5	0.5

Table 3.3 Tablet identification table displaying sample ID and wt% of ingredients

The finished tablets were analysed using both SEM and ToF-SIMS.

3.2.2.1 ToF-SIMS sample Preparation and Analysis Conditions

The tablet samples were mounted onto 10 mm aluminium stubs with double sided carbon tabs as shown in Figure 3.6.

Figure 3.6 Schematic diagram representing ToF-SIMS sample construction for tablet samples
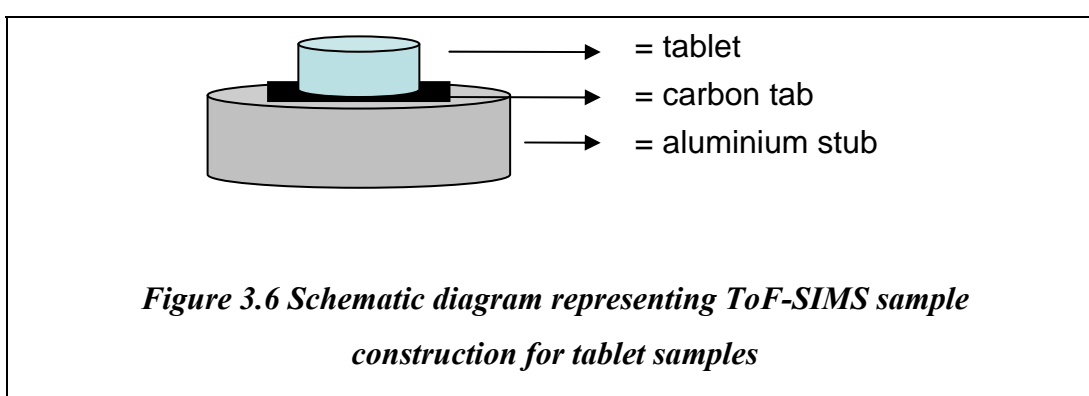
This method was preferred to the double adhesive layer method described above as the carbon tabs were sufficiently far enough away from the tablets upper surface for potential contamination not to be a concern and a single adhesive layer made the

mounting process simpler. Care was taken when setting up the experiment to ensure the upper tablet surface did not come into contact with the analyzer as the tablet sat proud of the sample holder surface.

Static ToF-SIMS measurements were performed using the same conditions used for analysing the excipients described in Section 3.2.1.1. Larger areas of 249 μm x 249 μm were also analysed to produce ion images utilising the gallium gun in burst alignment mode to maximise spatial resolution. Again, in all cases the analysis dose was kept below the static limit of 1 x 10^{13} ions cm^{-1}.

3.2.2.2   SEM Sample Preparation and Analysis Conditions

As detailed in Section 3.2.1.2., the sample (an entire tablet) was mounted onto an aluminium stub using a double-sided carbon tab. Analysis conditions were identical to those specified in Section 3.2.1.2.

3.2.3   Micro-spheronised Beads

The beads were prepared using the active ingredient, paracetamol, with spray dried lactose and microcrystalline cellulose as excipients. These raw materials were mixed in a metal mixing bowl cleaned in high purity hexane in order to minimise any potential contamination. The beads were manufactured using the wet granulation method as described in the introduction of this chapter. Water was used as the wetting agent. Extrusion and spheronisation were carried out using a G.B. Caleva Ltd., Dorset, England EXT 10 extruder and Model 120 spheroniser. As the surface of the extruder had a plastic surface it was covered with aluminium foil to minimise contamination. Following extrusion and spheronisation metal sieves were used to retain beads with a diameter of 850 – 1000 μm. The three different bead types, relative concentrations and samples IDs are shown in Table 3.4.

Sample ID:	Concentration (wt%)		
	Paracetamol	*Spray Dried Lactose*	*Microcrystalline Cellulose*
P40	40	10	50
P25	25	25	50
P10	10	40	50

Table 3.4 Bead identification table displaying sample ID and wt% of ingredients

3.2.3.1 ToF-SIMS Sample Preparation and Analysis Conditions

The beads were mounted onto an aluminium stub using a two part epoxy purchased from RS Components, Nottingham, UK. These samples were sectioned using an RMC ultramicrotome (source) to produce a planar flat surface. This involved performing a manual cut at or near the centre with a razor blade, followed by 5 automatic cuts at 5 µm and 10 automatic cuts at 0.5 µm. The sample was maintained at a 6° downwards tilt. A schematic diagram of the final cross-sectioned samples prior to analysis is presented in Figure 3.7.

= sectioned bead

= two part epoxy

= aluminium stub

Figure 3.7 Schematic diagram representing ToF-SIMS sample construction for cross sectioned beads
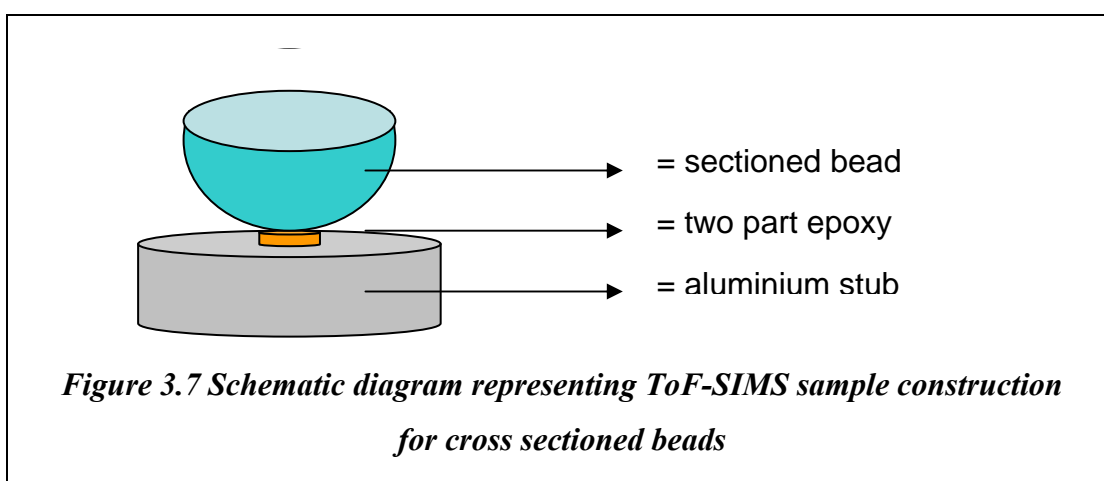
ToF-SIMS data from the first batch of samples produced showed that surfaces were contaminated by the epoxy, which may have been dragged across the surface by the blade of the ultramicrotome. Therefore, extreme care was taken with subsequent batches to ensure that the glue did not ride further than half way up the bead.

Static ToF-SIMS measurements were performed using the same conditions used for analysing the excipients described in Section 3.2.1.1. Larger areas of 249 µm x 249 µm were analysed to produce ion images utilising the gallium gun in burst alignment mode to maximise spatial resolution. Again, in all cases the analysis dose was kept below the static limit of 1 x 10^{13} ions cm^{-1}.

3.2.3.2   SEM Sample Preparation and Analysis Conditions

As detailed in Section 3.2.3.1., the sample (a cross sectioned bead) was mounted onto an aluminium stub using a two part epoxy. Analysis conditions were as described in Section 3.2.1.2.

3.3 Results and Discussion

3.3.1   Raw Materials

Three separate raw excipient materials were used in the manufacture of the tablets and beads; the tablets contained spray dried lactose as a bulking agent and magnesium stearate as a lubricant, whereas the beads contained spray dried lactose and microcrystalline cellulose as bulking agents. Both contained paracetamol as the active ingredient. All reference materials were examined by SEM and ToF-SIMS, in both their raw state and as part of a complete tablet or bead system.

3.3.1.1   SEM Results

Micrographs were taken of all the raw materials at three different magnifications. The magnifications selected were determined by the particle size and distribution of each raw material, in order to adequately show the topographical features. The raw material micrographs were used as comparators against the SEM and SIMS images of the tablet and bead surfaces. SEM micrographs of paracetamol crystals at three different magnifications are presented in Figure 3.8. These micrographs showed that the structures were predominantly "needle" like, with a large number of finer structures attached to the larger crystals. A wide distribution of crystal size was observed with larger crystals of up to 200 μm and smaller crystal structures of several microns.
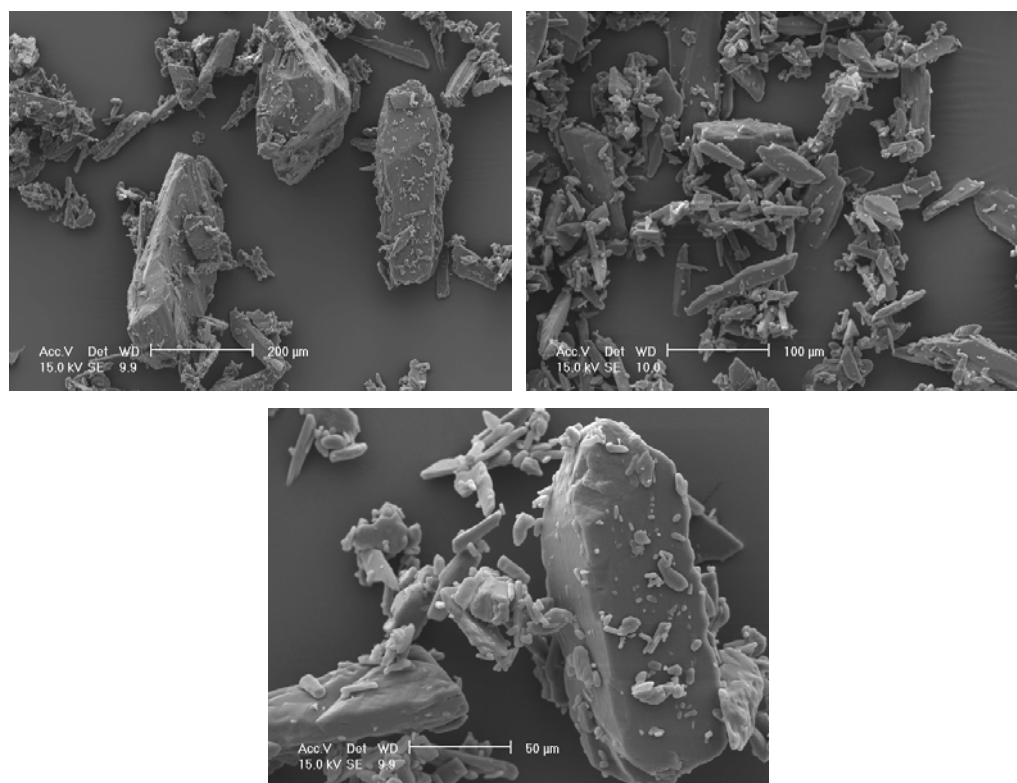
Figure 3.8 SEM micrographs of paracetamol
at three different magnifications

SEM micrographs of magnesium stearate at three different magnifications are presented in Figure 3.9. The micrographs showed fine plate like structures ranging from around 5 to 20 μm in diameter. Some evidence of agglomeration was apparent; this was expected as magnesium stearate is a lubricant and hence 'sticks' to surfaces. The material was generally symmetrical and isotropic in nature, with no apparent elongation in any plane.
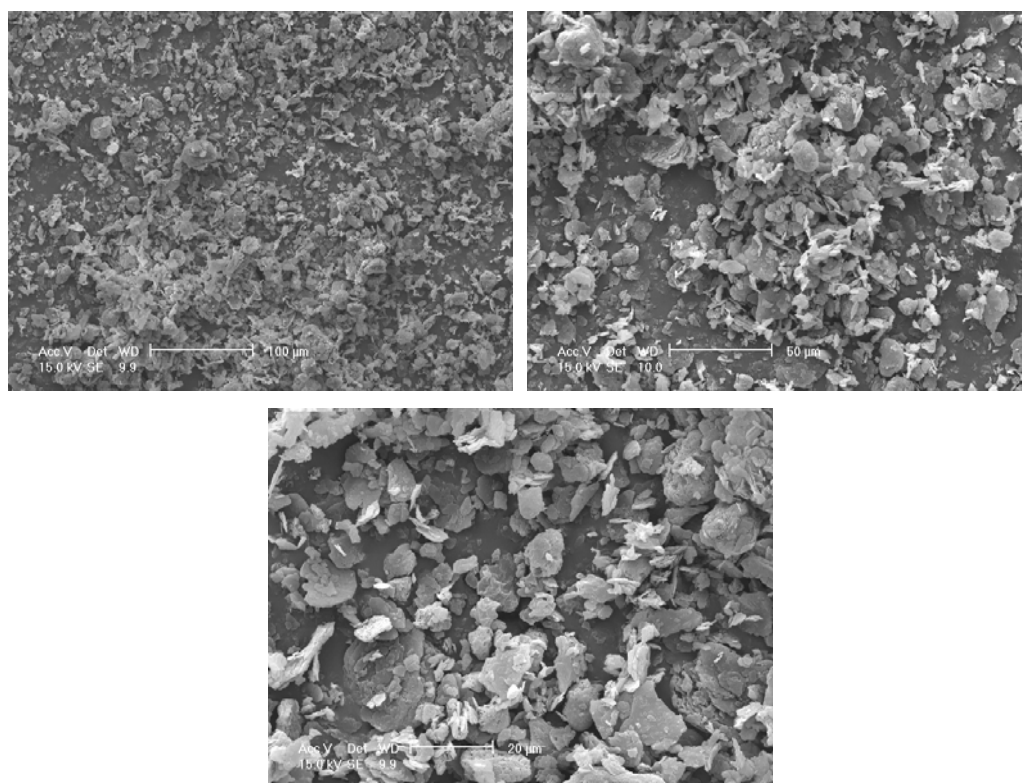
Figure 3.9 SEM micrographs of magnesium stearate
at three different magnifications

SEM micrographs of lactose at three different magnifications and spray dried lactose used in the bead manufacture (right hand side) are presented in Figure 3.10. The upper set of micrographs highlighted a large distribution in particle size. Particles ranged from sub-micron up to 100 μm in a single plane. The lower set of spray dried lactose micrographs showed that a number of the particles had formed spheroidal agglomerates. These structures are typical of spray dried lactose where the manufacturing process is specifically designed to encourage these types of formations as they provide improved flow characteristics as previously discussed. The spray dried lactose micrographs also showed a much narrower size distribution, with the agglomerates forming ranging in size from around 50 to 200 μm.

SEM micrographs of microcrystalline cellulose particles at three different magnifications are presented in Figure 3.11. These particles were typically elongated

and there was some evidence of agglomeration with multiple particles forming rafts of around 100 μm in length. The size distribution was similar to that seen in spray dried lactose, with particles/agglomerates typically ranging in size from 50 to 200 μm.

Figure 3.10 SEM micrographs of lactose (left hand side) and spray dried lactose (right hand side)at three different magnifications
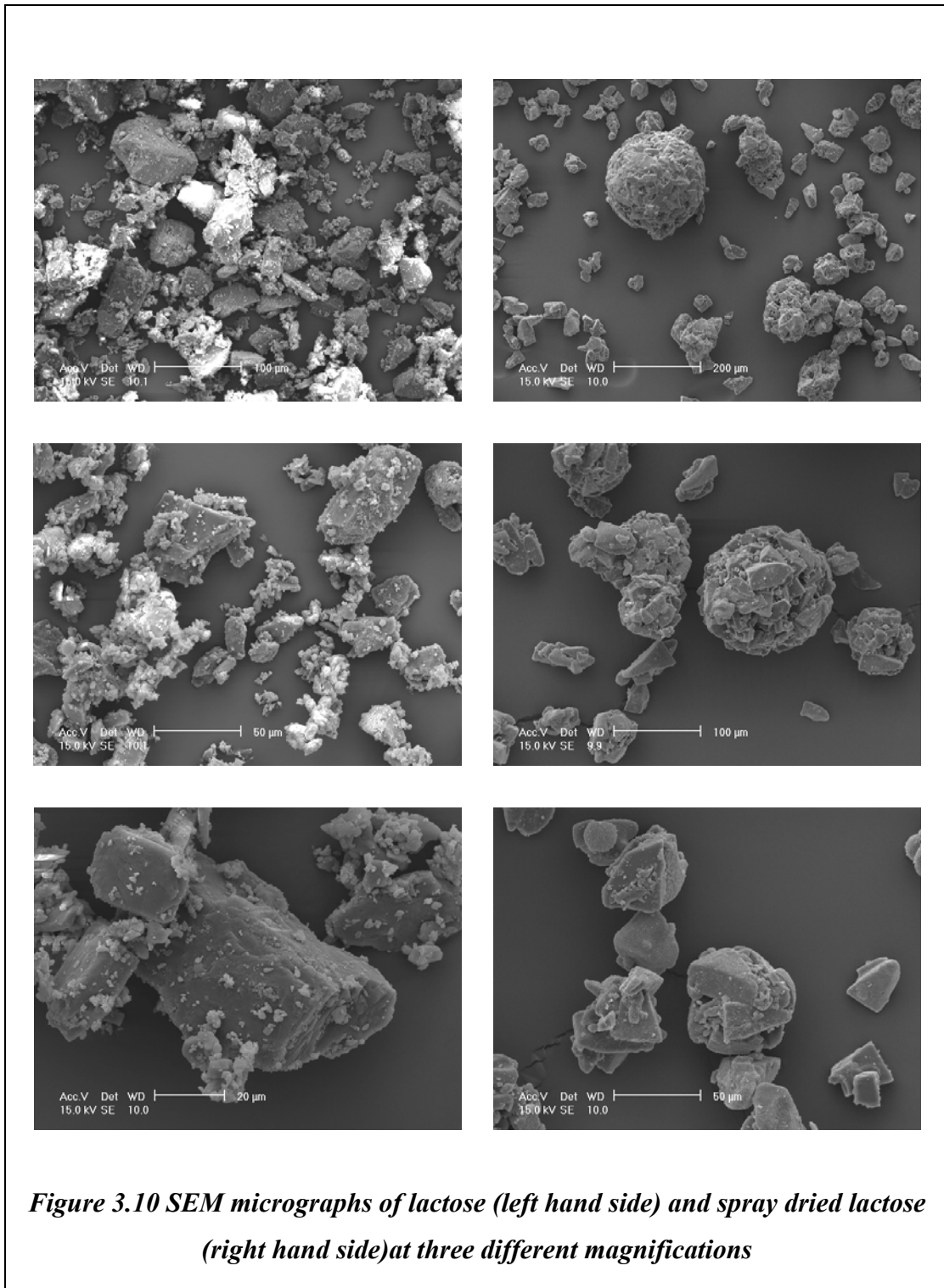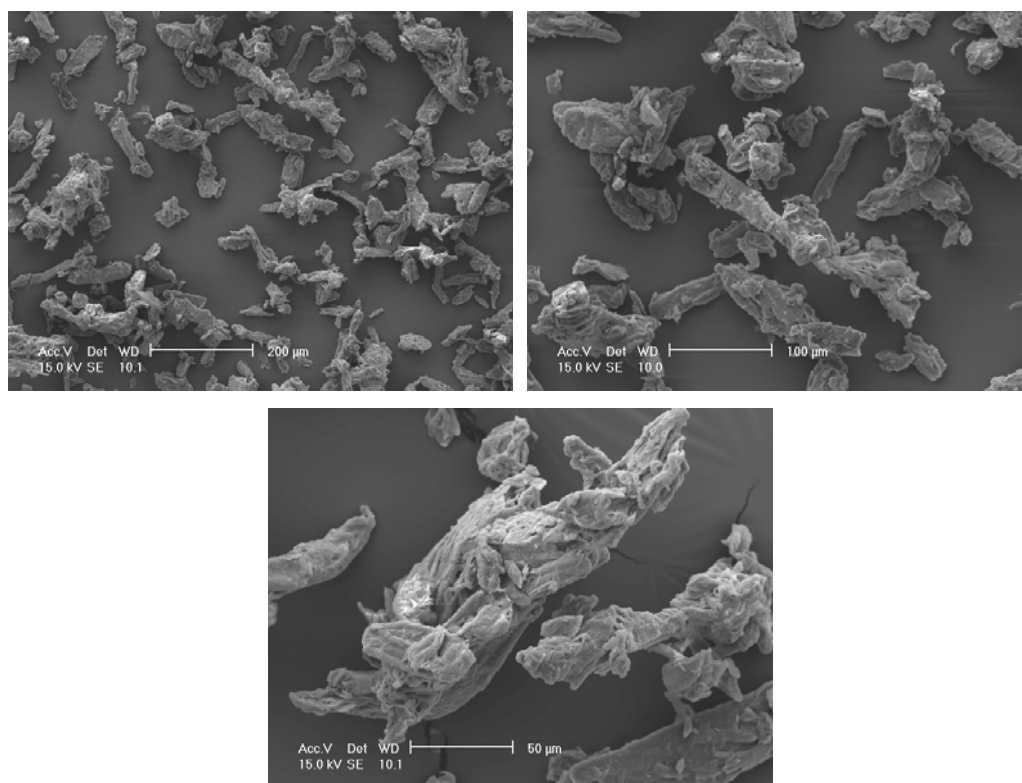
Figure 3.11 SEM micrographs of microcrystalline cellulose at 3 different magnifications

3.3.1.2 ToF-SIMS Analysis of Paracetamol and Excipient Powders

ToF-SIMS spectra were generated for the raw materials used in both the tablet and bead manufacture. Positive and negative ToF-SIMS spectra are presented for paracetamol (Figure 3.12 and Figure 3.13, respectively), magnesium stearate (Figure 3.14 and Figure 3.15, respectively), spray dried lactose (Figure 3.16 and Figure 3.17, respectively), and microcrystalline cellulose (Figure 3.18 and Figure 3.19, respectively).
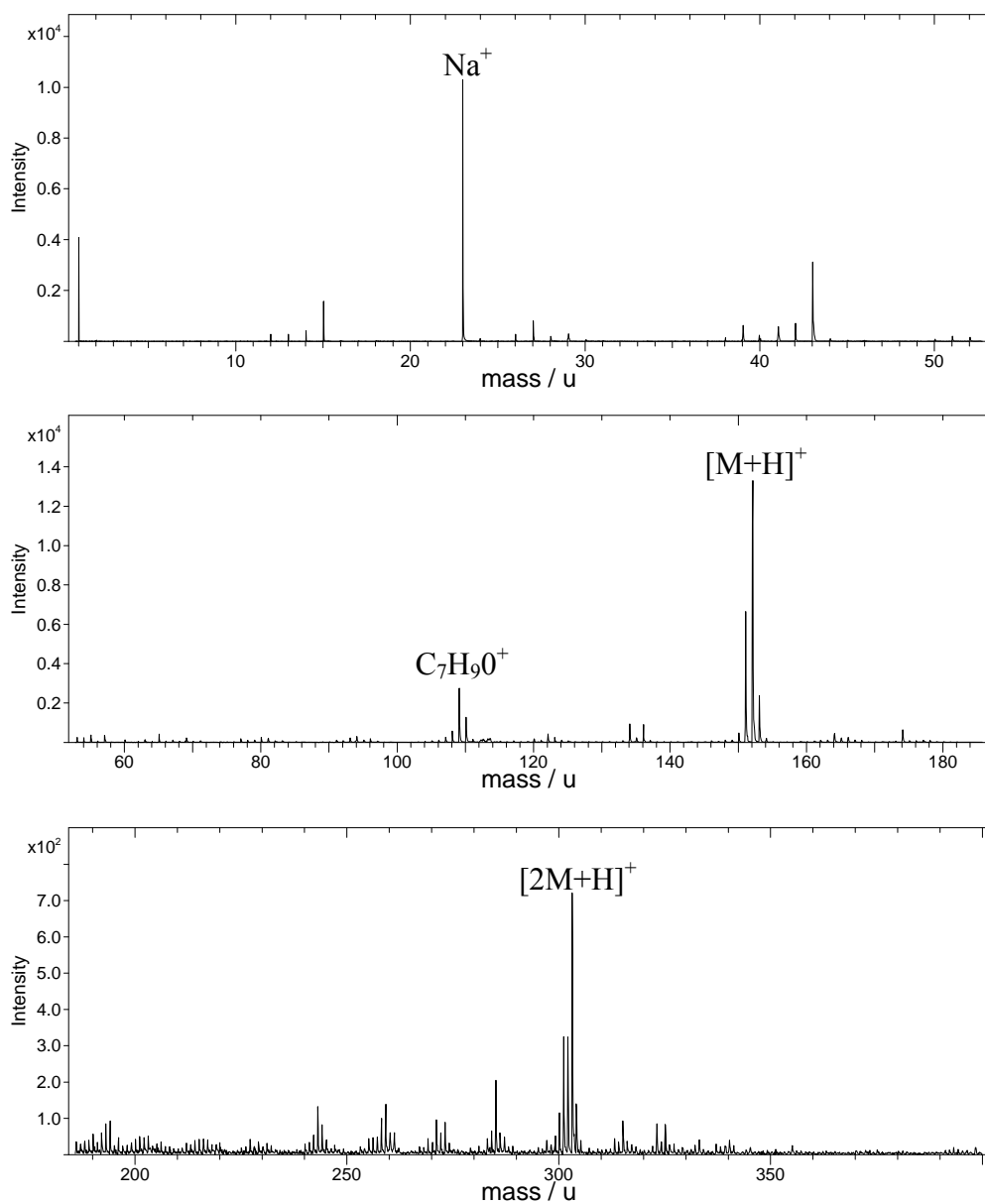
Figure 3.12 Positive ion ToF-SIMS spectrum of paracetamol
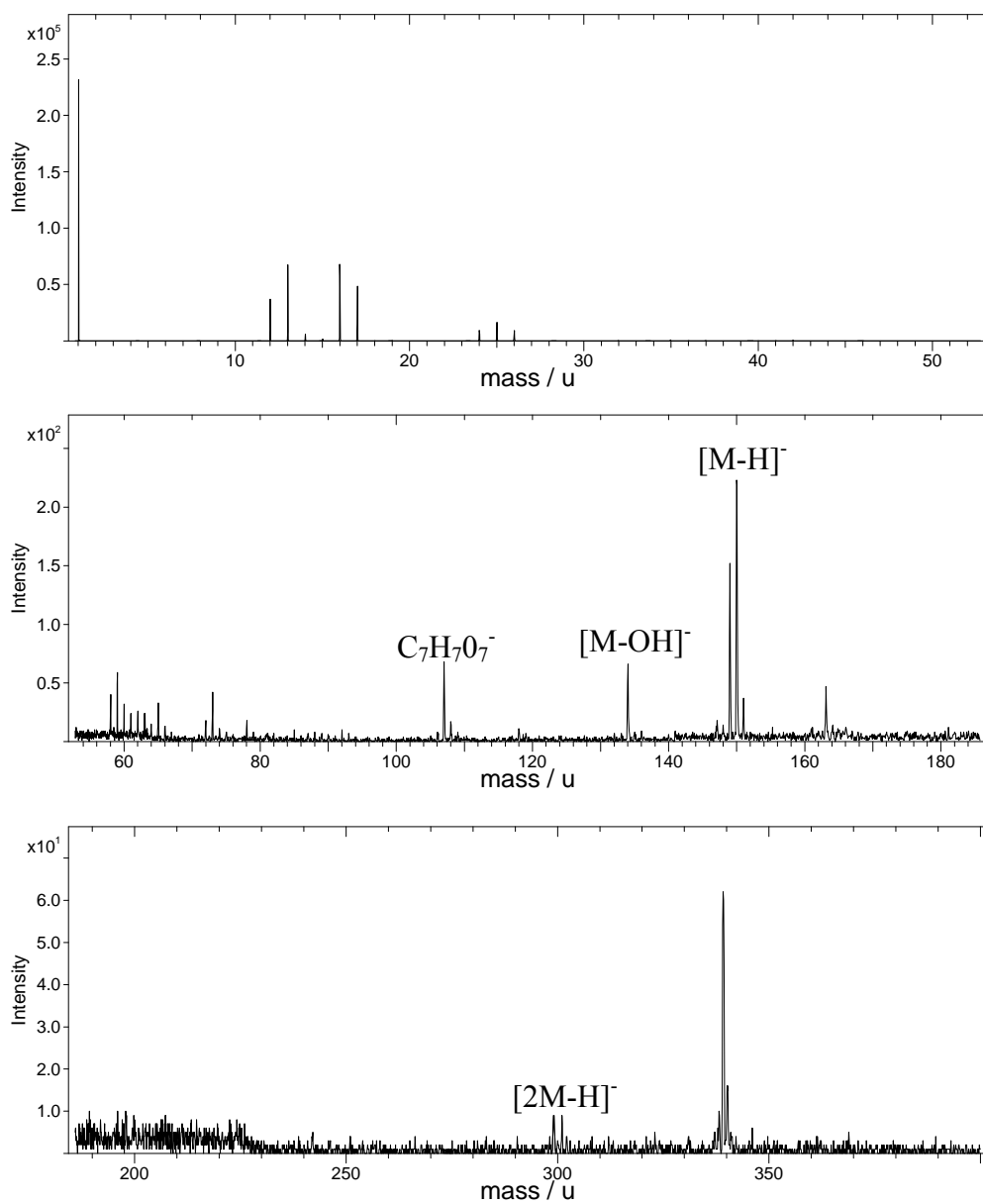
Figure 3.13 Negative ion ToF-SIMS spectrum of paracetamol
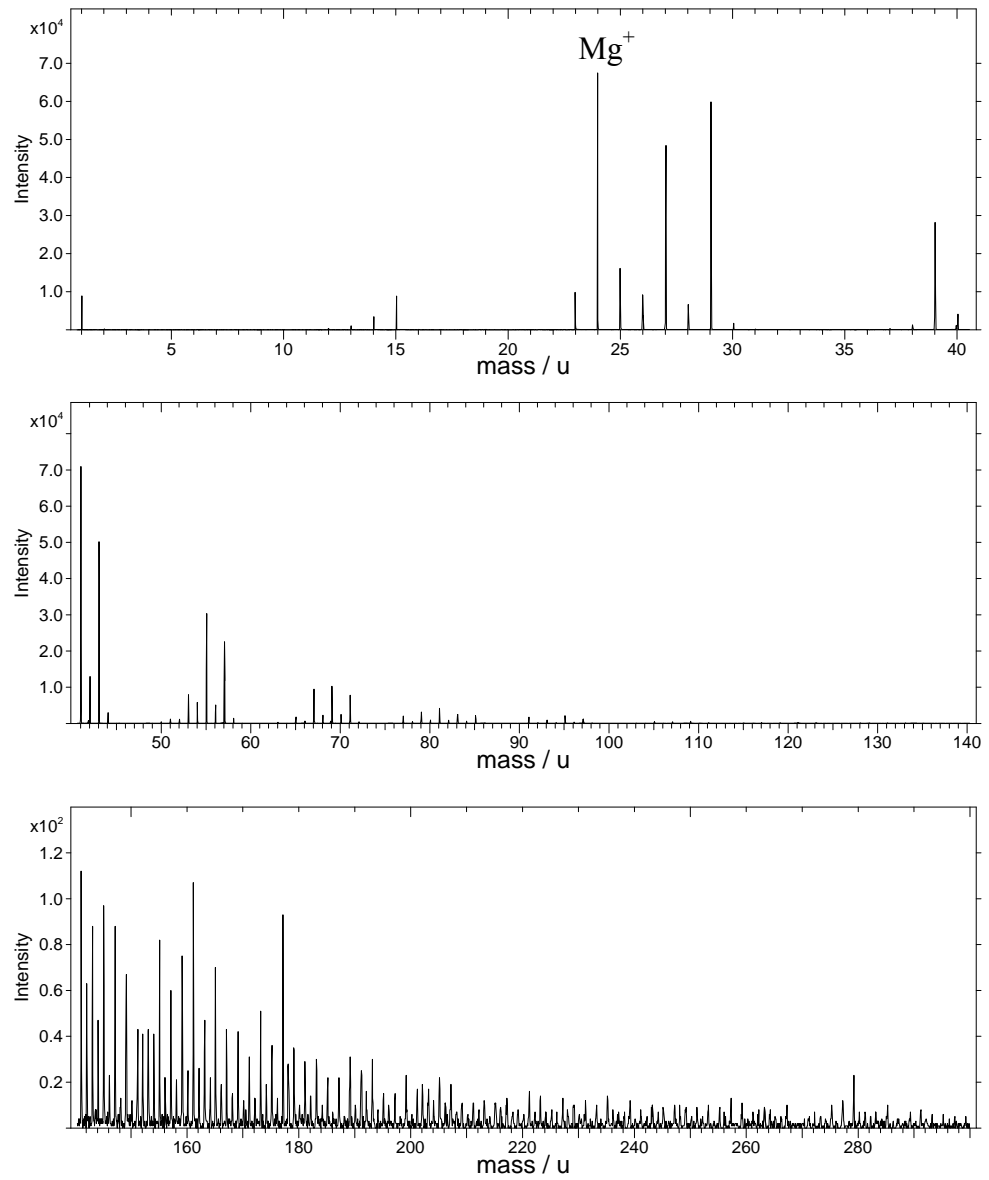
Figure 3.14 Positive ion ToF-SIMS spectrum of magnesium stearate
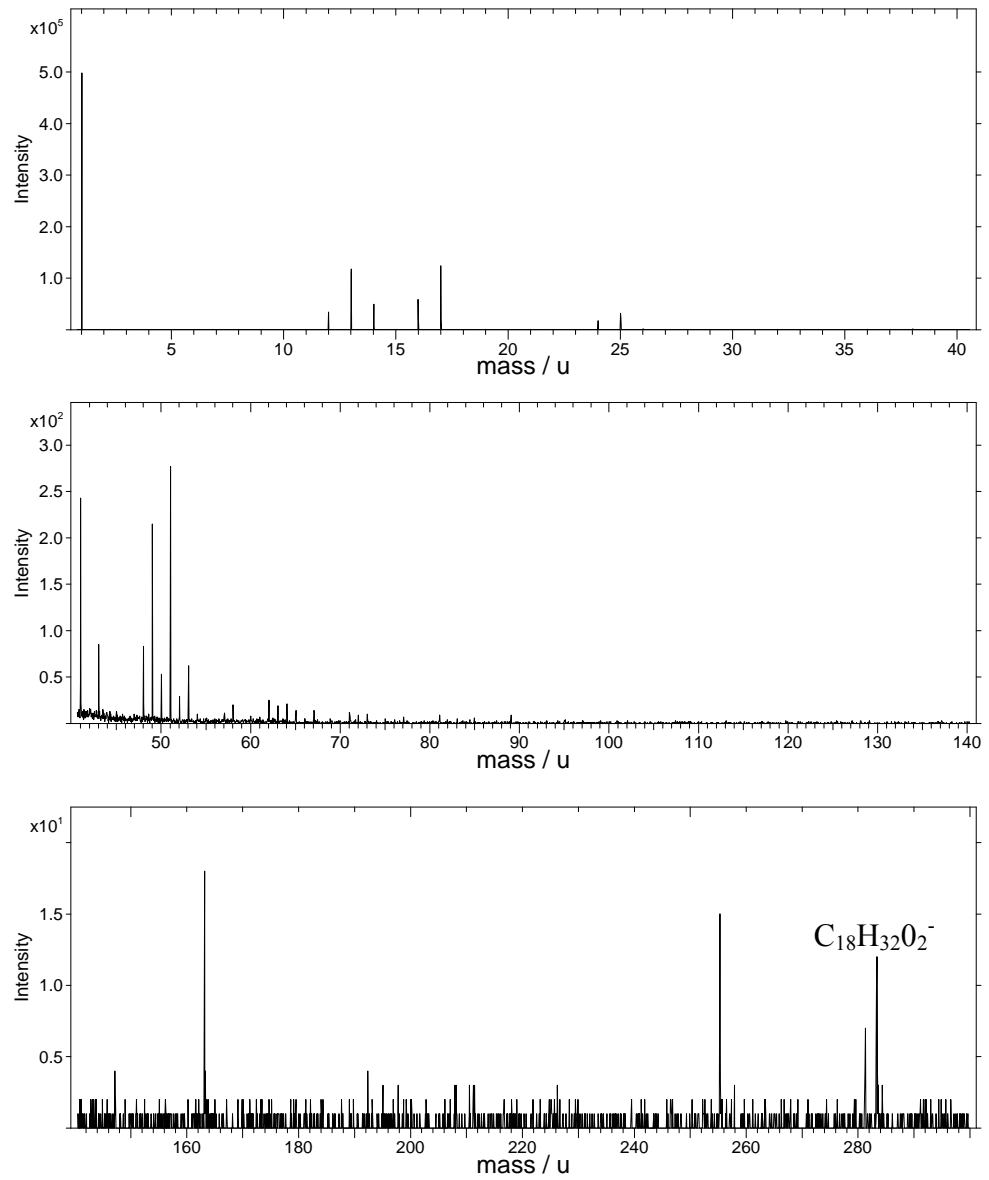
Figure 3.15 Negative ion ToF-SIMS spectrum of magnesium stearate
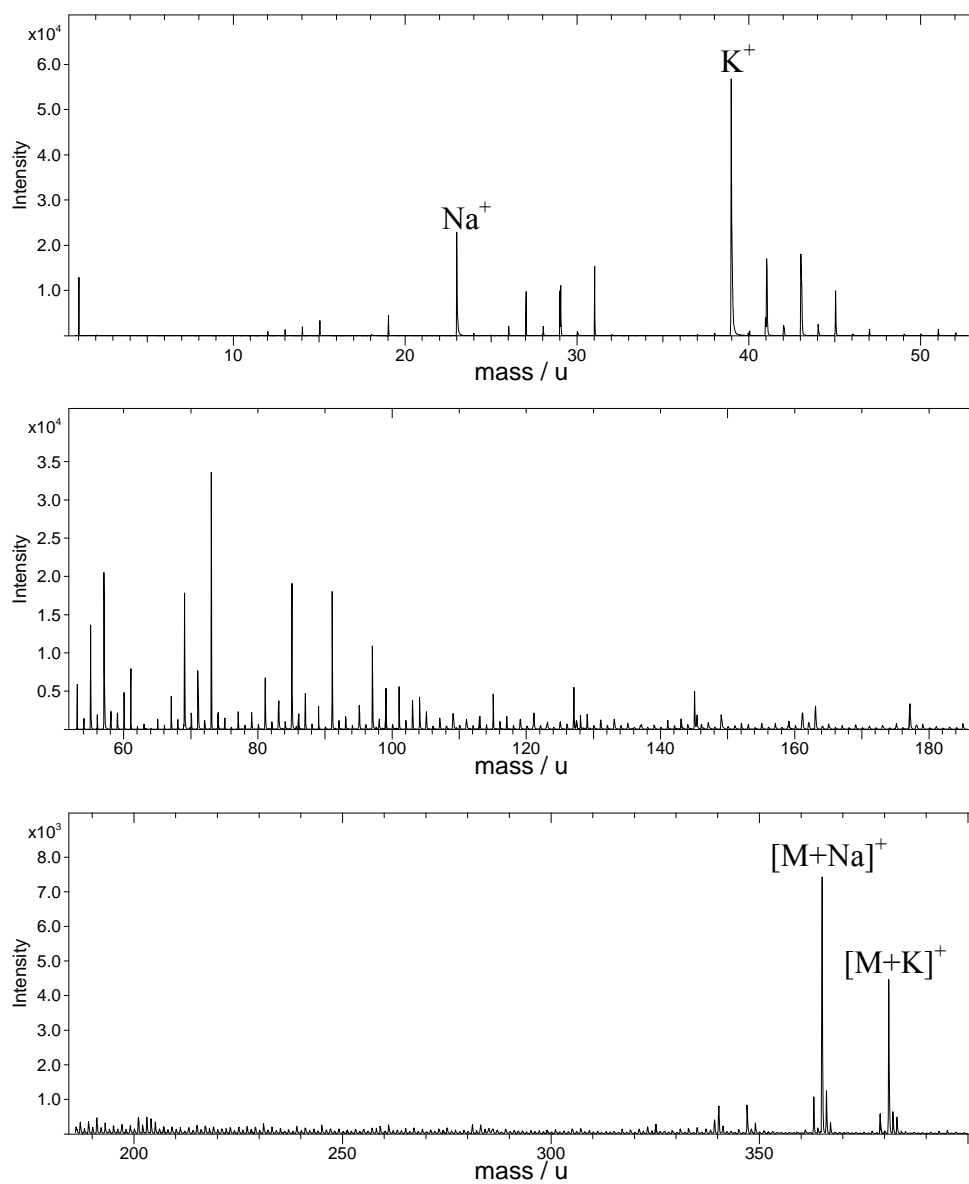
Figure 3.16 Positive ion ToF-SIMS spectrum of spray dried lactose
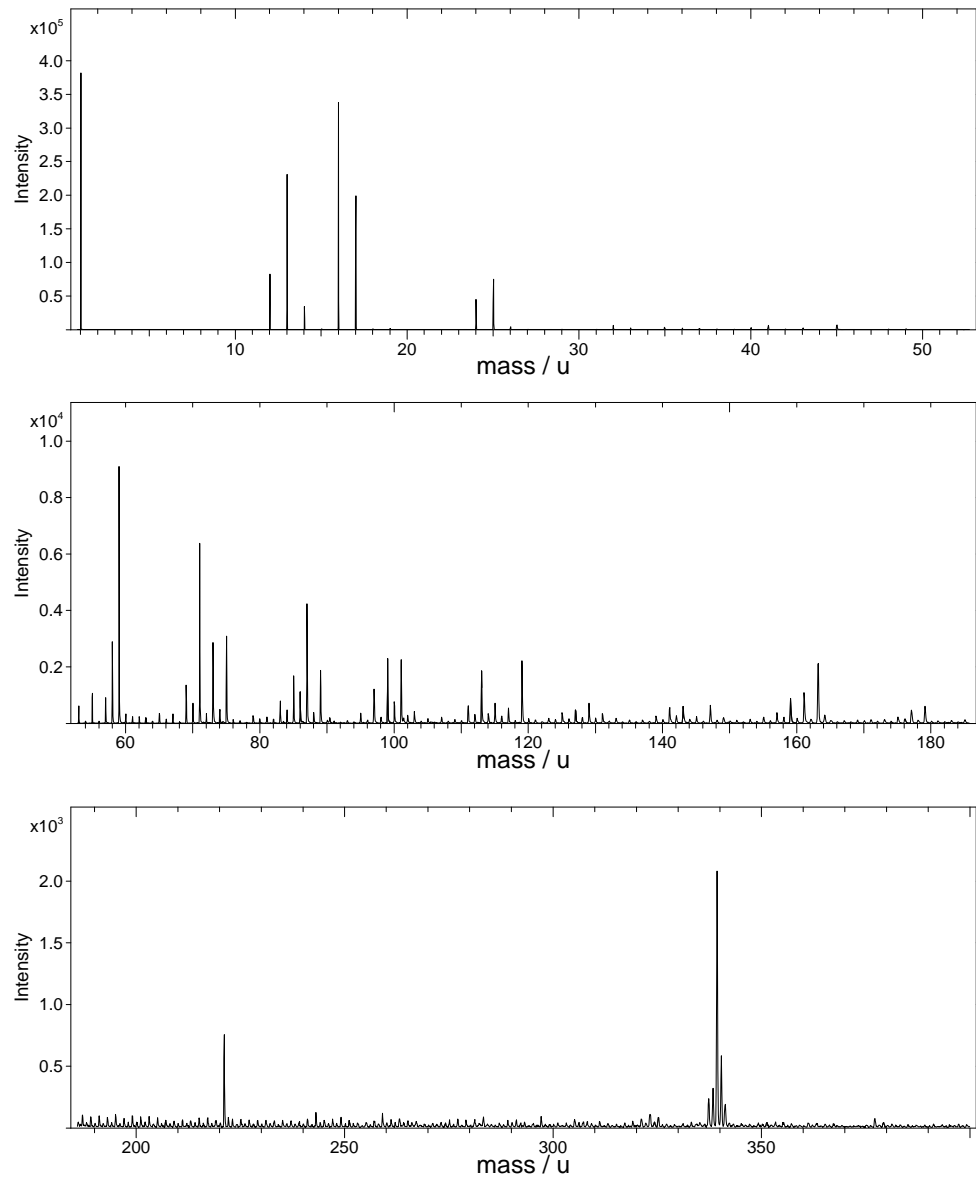
Figure 3.17 Negative ion ToF-SIMS spectrum of spray dried lactose
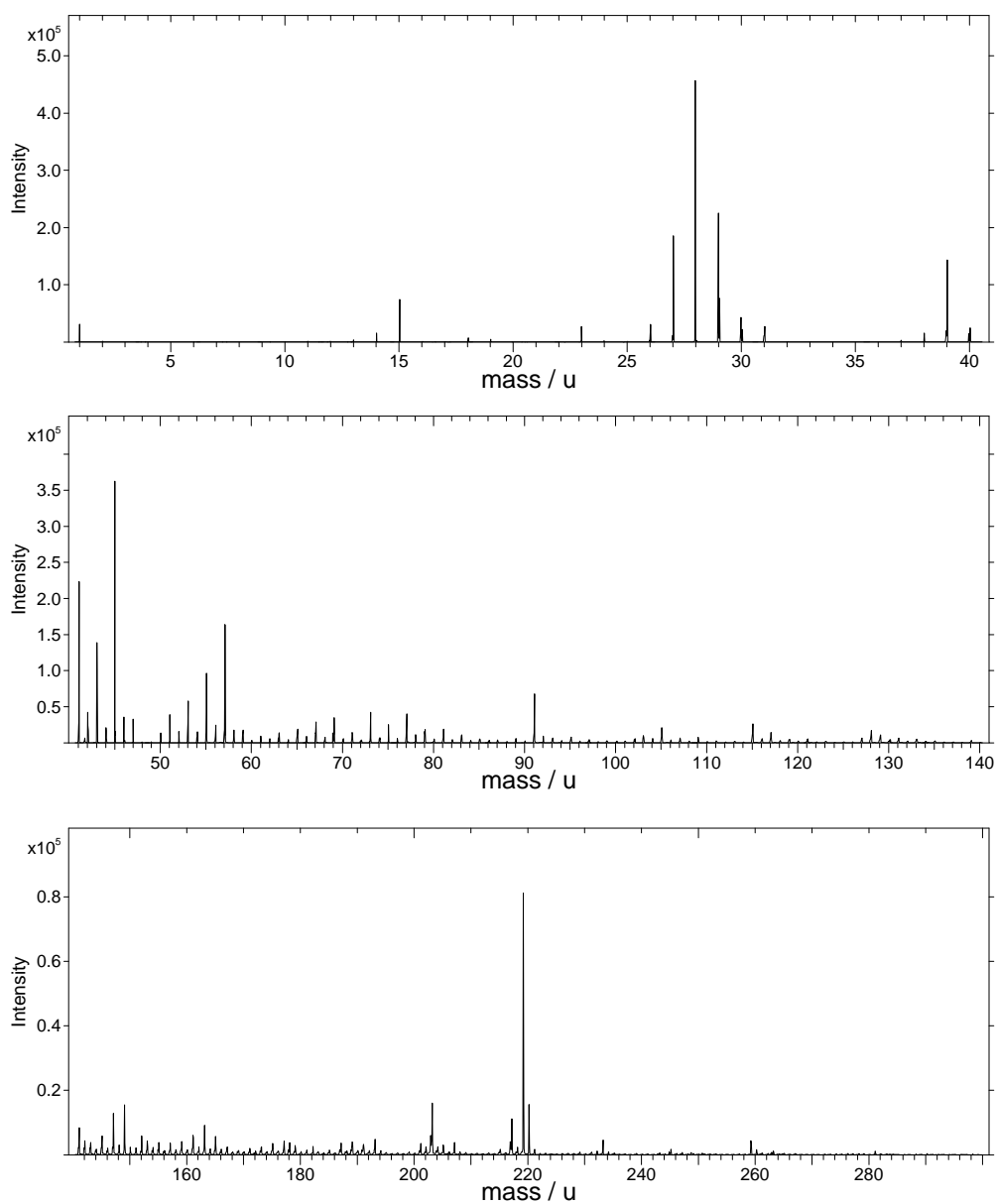
Figure 3.18 Positive ion ToF-SIMS spectrum of microcrystalline cellulose
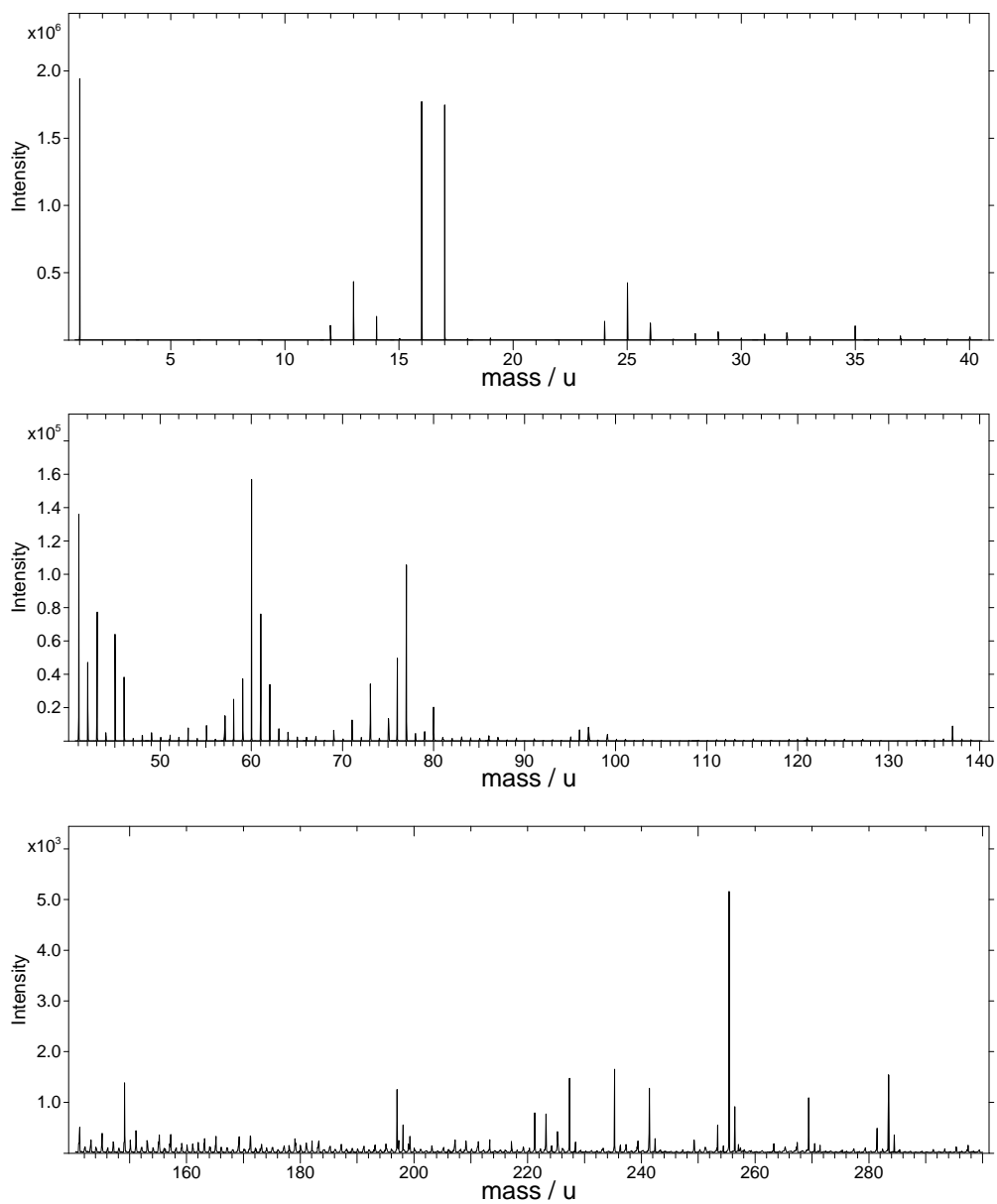
Figure 3.19 Negative ion ToF-SIMS spectrum of microcrystalline cellulose

The positive and negative ion ToF-SIMS spectra of paracetamol are presented in Figure 3.12 and Figure 3.13, respectively. Both these spectra showed no evidence of sample contamination as described in Section 2.4.1. Paracetamol has a relative molecular mass (RMM) of 151 with the empirical formula $C_8H_9NO_2$. A number of peaks previously identified by Belu as paracetamol were observed in both the positive and negative ion ToF-SIMS spectra [Belu *et al.*, 2000]. In the positive ion ToF-SIMS spectrum a paracetamol fragment was observed at m/z 109^+ $C_7H_9O^+$; Belu attributed this to an intact molecule minus CONH. In addition, a protonated molecular ion $[M+H]^+$ was observed at m/z 152^+. A further diagnostic peak was observed in the positive ion ToF-SIMS spectrum at m/z 303^+, representing $[2M+H]^+$. Additional peaks prevalent in the positive spectra included a sodium cation at m/z 23^+, and a number of low mass hydrocarbon fragments in the m/z 20 to 50 range.

In the negative ion ToF-SIMS spectrum a diagnostic peak was observed at m/z 150^- attributable to $[M-H]^-$. Peaks were also observed at m/z 107^- and 134^- which were attributed to $C_7H_7O_7^-$ and $[M-OH]^-$, respectively. In the higher mass region the peak at m/z 301 was diagnostic of $[2M-H]^-$.

The positive and negative ion ToF-SIMS spectra of magnesium stearate are presented in Figure 3.14 and Figure 3.15, respectively. Magnesium stearate has an RMM of 591. The magnesium ion Mg^+ can clearly be identified in the positive ion ToF-SIMS spectrum at m/z 24^+. Sutcliffe reported a low intensity stearate (C18) anion peak at m/z 283^+ which correlates with the peak observed at m/z 283^+ in the positive ion ToF-SIMS spectrum [Sutcliffe *et al.*, 2003]. Pignataro also supports the presence of a stearate anion at this mass, and attributes this ion to $C_{18}H_{35}O_2^-$ [Pignataro *et al.*, 1999]. However, despite the presence of these higher mass diagnostic ions, the magnesium ion is so strong in intensity it is often used as a diagnostic [Zhou *et al.*, 2011].

The positive and negative ion ToF-SIMS spectra of spray dried lactose are presented in Figure 3.16 and Figure 3.17, respectively. Lactose has an RMM of 342 with the empirical formula $C_{12}H_{22}O_{11}$. In the positive ion ToF-SIMS spectrum cationised molecular ions can be observed at both m/z 365^+ and m/z 381^+ corresponding to $[M+Na]^+$ and $[M+K]^+$, respectively. These cations have also observed by Belu [Belu *et al.*, 2000]. Sodium and potassium cations were clearly defined in the positive ion

ToF-SIMS spectrum at m/z 23^+ and 39^+, respectively. In the negative ion ToF-SIMS spectrum a number of peaks can be observed in the m/z 50 to 100 region. Belu attributed a number of these to lactose fragments, but did not identify them as diagnostic peaks [Belu *et al.*, 2000]. However, the negative ion ToF-SIMS spectrum presented in this thesis clearly showed two diagnostic peaks in the high mass region at m/z 221^- and m/z 339^-. It is speculated that these represent an intact parent molecule with a loss of side chain groups.

The positive and negative ion ToF-SIMS spectra of microcrystalline cellulose are presented in Figure 3.18 and Figure 3.19, respectively In the positive ion ToF-SIMS spectrum hydrocarbon fragments were observed at m/z 15^+, representing CH_3, and an intact molecule with the loss of a methylene group, $[M-CH_2]^+$ was observed at m/z 148^+ (the mass of an intact unit being 162, empirical formula $C_6H_{10}O_5$). The positive ion ToF-SIMS spectrum also highlighted a repeat pattern of 14 unit masses which was clearly seen in the higher mass regions. These peaks represented the loss of CH_2 from higher *n*-mer units. As seen in previous studies, both the positive and negative ion ToF-SIMS spectra were dominated by peaks from cellulose fragments that are common in many types of cellulose [Belu *et al.*, 2000]. The presence of the peaks made it difficult to assign a clear and intense diagnostic peak for microcrystalline cellulose.

Although high grade raw materials were purchased a number of initial samples were run from the laboratory stock which were found to be highly contaminated. The contamination arose from silicones with linear structures evident from the peaks at m/z 73^+, 147^+ and 221^+, masses representing $(CH_3)_3Si$, $(CH_3)_3Si-O-Si(CH_3)_2$ and $(CH_3)_3Si-O-Si(CH_3)_2-O-Si(CH_3)_2$ respectively . Cyclic silicone structures were also observed at m/z 207^+ and 281^+ [Vickerman and Briggs, 2001]. Silicone contamination and its effects are discussed in Section 2.4.1.

The source of the silicones was not investigated, but probably arose from the manufacturing process. Silicone contamination demonstrates problems that occur when running "real world" samples as opposed to model systems as created in this thesis using high purity raw materials. The peaks dominate the spectra often dwarfing the underlying peaks that arise from the excipients and APIs. This

observation may compromise recommending the use of ToF-SIMS for non-model samples.

Clear diagnostic peaks and their assignments are summarised in Table 3.5. This preliminary work with the raw materials clearly highlighted that the diagnostic peaks were more easily identified and recognizable in the positive ion ToF-SIMS spectra. Therefore, for future experiments positive ion ToF-SIMS spectra and images have been gathered and analysed using some of the key ions described in in Table 3.5.
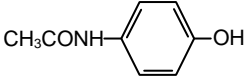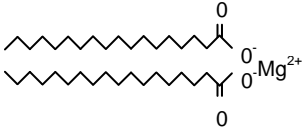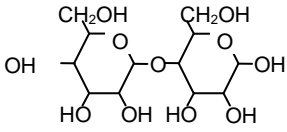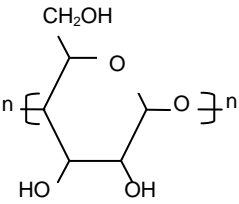
Material	+ve ions	Assignment	-ve ions	Assignment
Paracetamol CH₃CONH—⟨benzene ring⟩—OH	109 152 303	$C_7H_9O^+$ $[M+H]^+$ $[2M+H]$	134 150 301	$[M-OH]^-$ $[M-H]^-$ $[2M-H]^-$
Magnesium stearate (stearate structure with Mg^{2+})	24	Mg^+	283	$[C_{18}H_{35}O_2]^-$
Spray Dried Lactose (lactose structure)	365 381	$[M+Na]^+$ $[M+K]^+$	221 339	unassigned unassigned
Microcrystalline Cellulose (cellulose structure)	148	$[M-CH_2]^+$	No diagnostic peaks	-

Table 3.5 Table summarising the characteristic ToF-SIMS ions identified in the raw materials used for tablet and bead manufacture

3.3.2   Tablets

3.3.2.1   SEM Results

SEM micrographs of each of the four tablet types taken at comparative magnifications are presented in Figure 3.20. From left to right they represent 20%, 40%, 60% and 80% paracetamol wt. %, respectively. As the concentration of the active ingredient increased, a clear change was seen in surface morphology. The previously reported needle like structure of the paracetamol (Figure 3.8) became more apparent and the surface structure also became more "open" with increasing drug concentration. This was probably due to the increasing proportion of the highly brittle paracetamol structures contained within the tablet. Differentiation between the magnesium stearate and spray dried lactose components cannot easily be observed. Components within the tablets underwent compaction, and this was particularly noticeable in the lower drug concentration tablets. Magnesium stearate is a fine particulate that acts as a boundary lubricant and tends to adhere to larger particle surfaces [Aulton, 2002]. It has a low resistance to shearing, which causes it to spread. In addition, the spray dried lactose had deformed under compaction and therefore there was little evidence in the micrographs of any of the spray dried lactose spheroids that were observed in the raw material (Figure 3.10). The smoothness of these surfaces can be attributed to these shearing and compaction phenomena. The SIMS ion images presented later in this chapter more clearly highlighted the distribution of the raw materials.
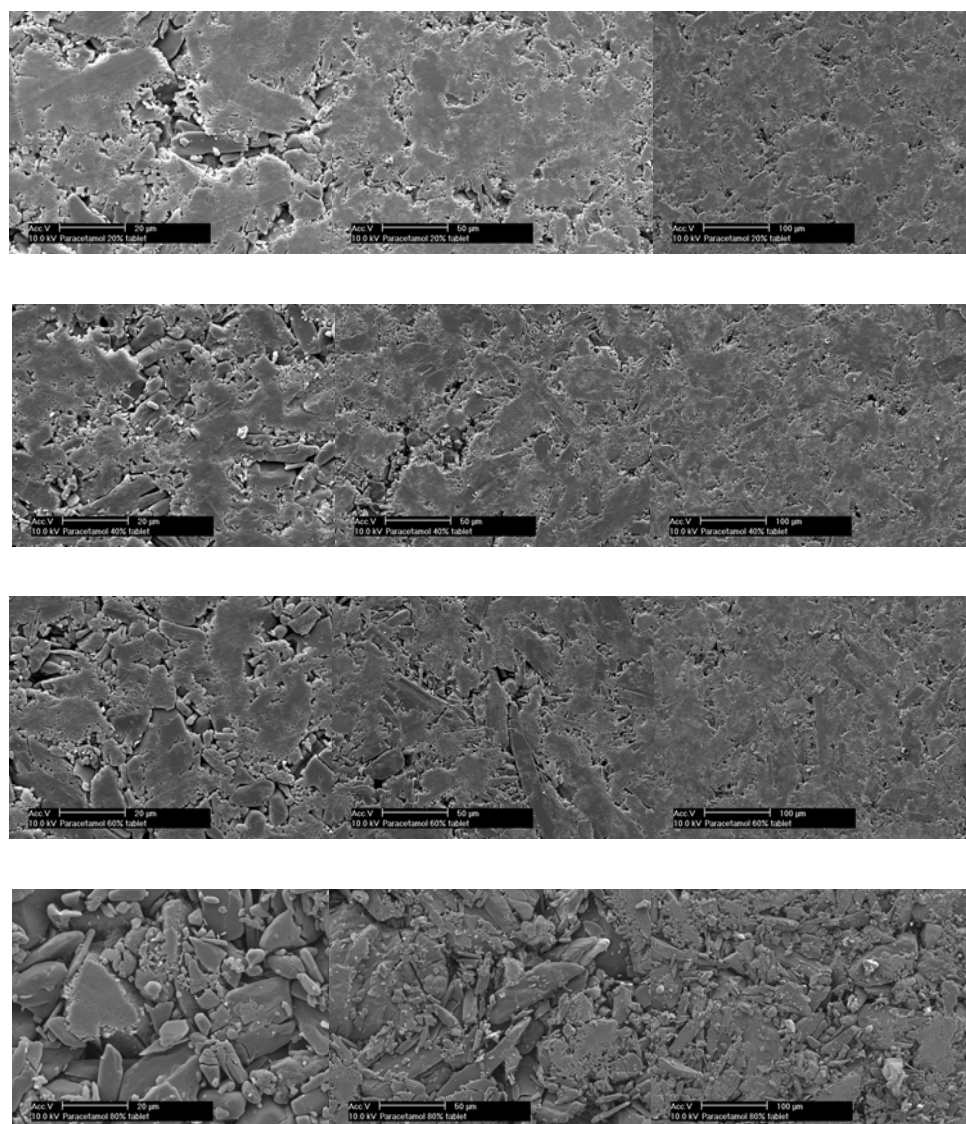
Figure 3.20 SEM micrographs of 20P, 40P, 60P and 80P paracetamol tablets
(see Table 3.3)

3.3.2.2 ToF-SIMS Analysis of Tablet Spectra

ToF-SIMS spectra were acquired in order to evaluate the ability of the technique to distinguish between samples with varying concentrations of a material and to establish whether the raw materials can still be readily identified in a mixed material spectrum. The interpretation of the following set of positive and negative spectra represent the tablets containing the greatest (80%) and lowest (20%) quantities of

paracetamol. These were chosen as they represent the two extremes of the paracetamol wt% concentrations in the manufactured tablets. These spectra are taken over a 100 x 100 μm area and acquired in high current bunched mode.

The positive and negative ion ToF-SIMS spectra of the 80 wt/wt% paracetamol tablet are presented in Figure 3.21 and Figure 3.22, respectively. Diagnostic peaks indicative of paracetamol can be observed at m/z 109^+, 152^+ and 303^+ which correspond to $C_7H_9O^+$, $[M+H]^+$ and $[2M+H]^+$ respectively. A magnesium peak can be observed at m/z 24^+. A low intensity peak can be observed at m/z 365^+, representing spray dried lactose. The negative ion ToF-SIMS spectrum of the 80 wt/wt% paracetamol tablet is presented in Figure 3.22. Paracetamol diagnostic peaks were highly prevalent at m/z 107 ($C_7H_7O^-$), 150 ($[M-H]^-$) and 301 ($[2M-H]^-$). These were in agreement with diagnostic ions reported for the paracetamol raw material discussed in Section 3.3.1.2.

The positive and negative ion ToF-SIMS spectra of the 20 wt/wt% paracetamol tablets are presented in Figure 3.23 and Figure 3.24, respectively. In the positive ion ToF-SIMS spectrum diagnostic paracetamol peaks can be observed at m/z 109^+, 152^+ and 303^+ but at a much lower intensity than those observed for the higher concentration paracetamol tablet detailed above. The spray dried lactose ions at m/z 365^+ ($[M+Na]^+$) and m/z 381^+ ($[M+K]^+$) can be observed at a much higher intensity due to their increased bulk concentration in the formulation. Again a peak arising from the magnesium ion can be observed at m/z 24^+, and is present at a similar intensity to that in the 80 wt/wt% paracetamol tablet positive ion ToF-SIMS spectrum. The positive ion ToF-SIMS spectrum also exhibited the lower mass region hydrocarbon fragments as observed in the pure spray dried lactose reference material. Paracetamol and spray dried lactose peaks could also be identified in the negative ion ToF-SIMS spectra. Paracetamol diagnostic peaks were observed at m/z 107 ($C_7H_7O^-$), 150 ($[M-H]^-$) and 301 ($[2M-H]^-$).The peak at m/z 221^- can be attributed to a spray dried lactose fragment, as previously identified in the reference spectra.
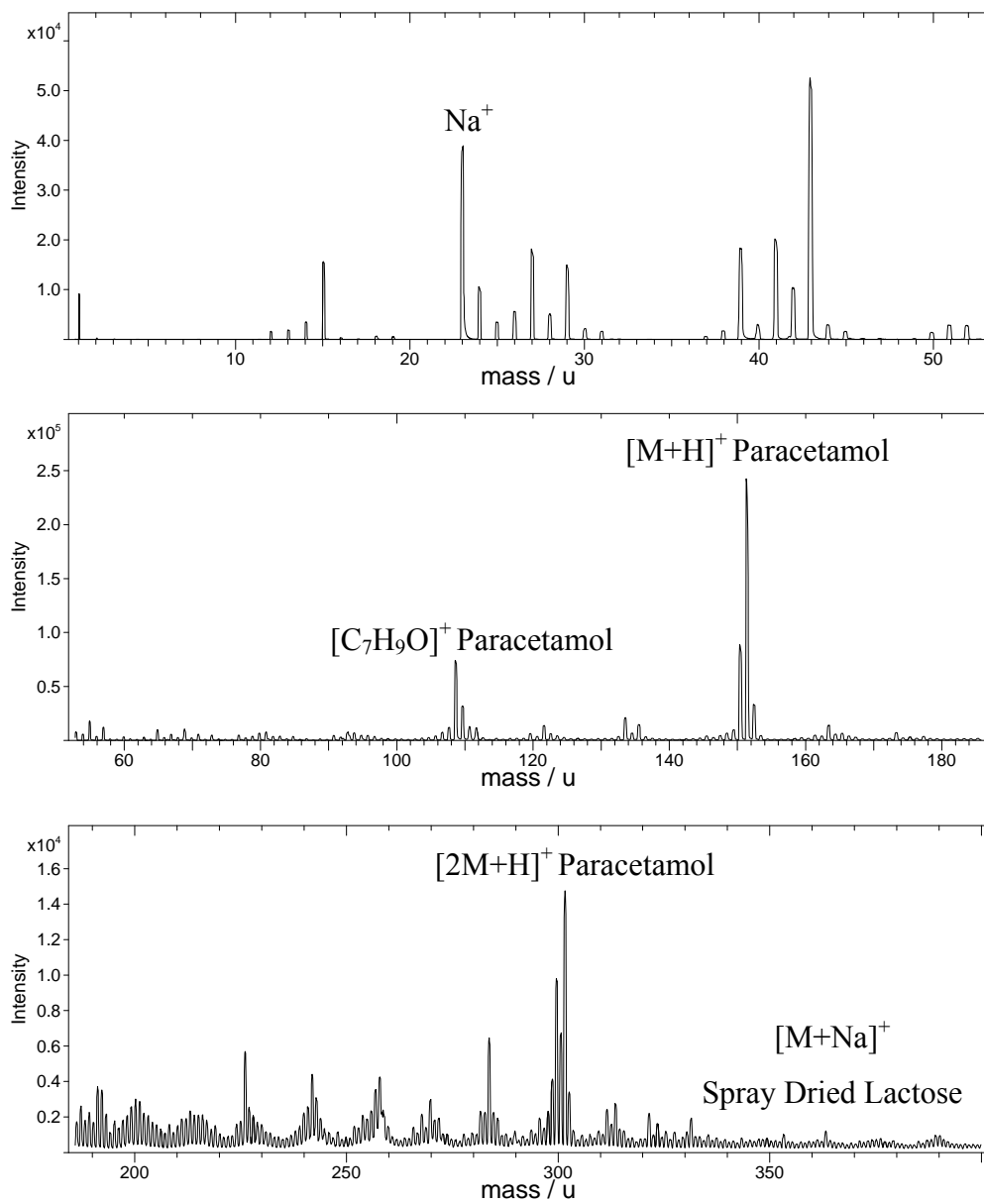
Figure 3.21 Positive ion ToF-SIMS spectrum of 80% paracetamol tablet
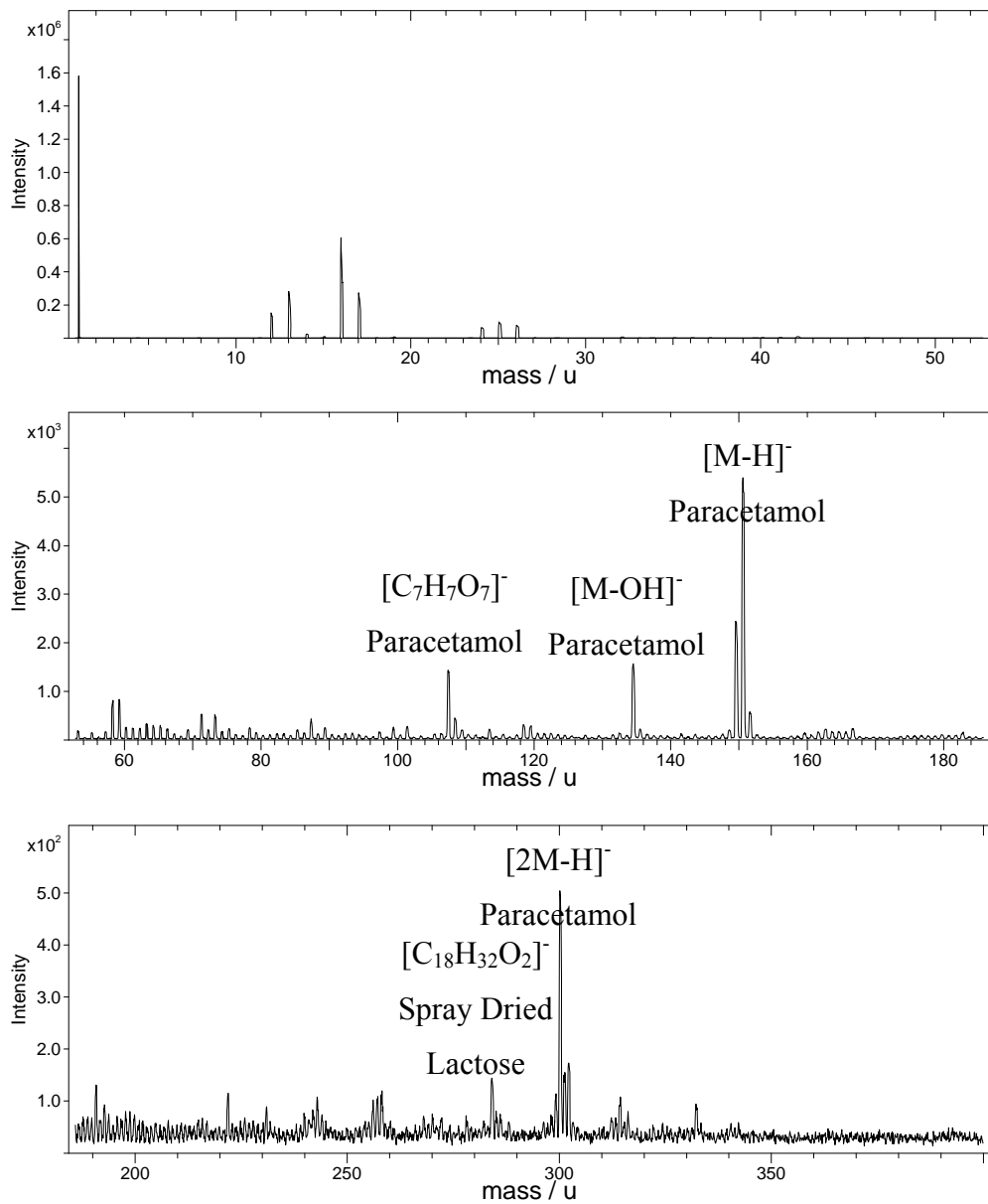
Figure 3.22 Negative ion ToF-SIMS spectrum of 80% paracetamol tablet
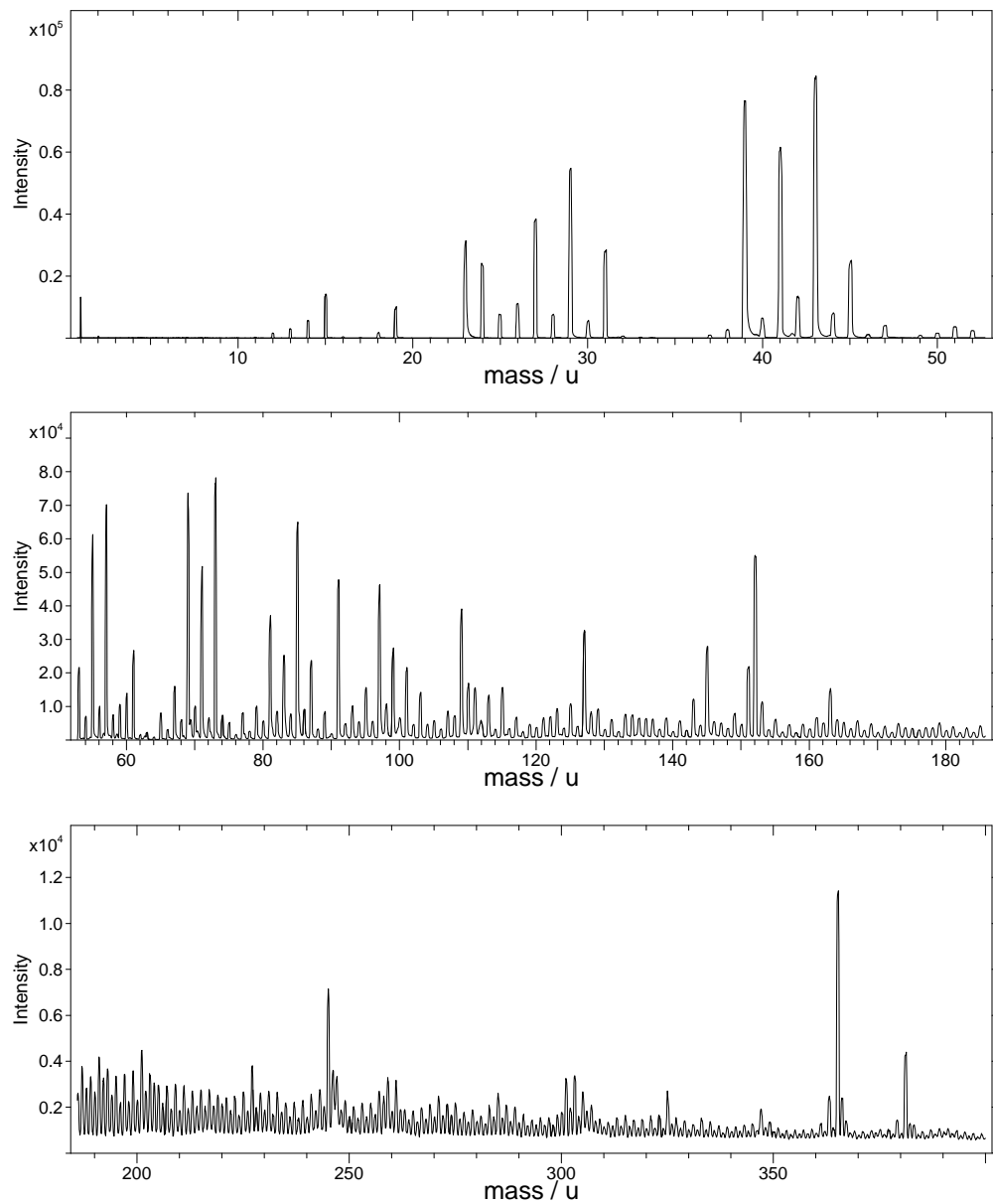
Figure 3.23 Positive ion ToF-SIMS spectrum of 20% paracetamol tablet

(peak assignments as per 80% paracetamol tablet)
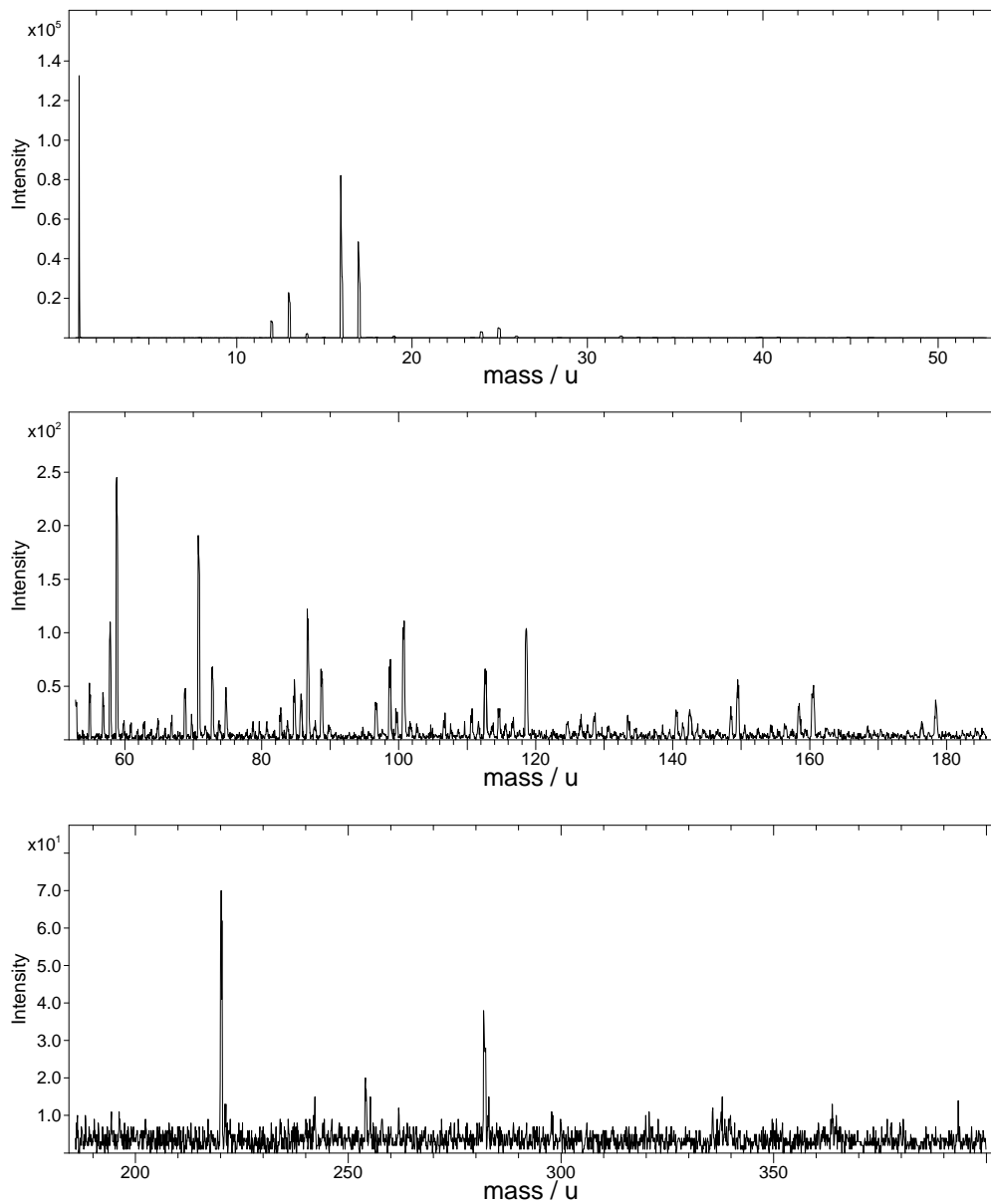
Figure 3.24 Negative ion ToF-SIMS spectrum of 20% paracetamol tablet

(peak assignments as per 80% paracetamol tablet)

3.3.2.3   SIMS Ion Image Results

ToF-SIMS positive ion images were generated using the diagnostic ions of the different components in the tablet formulations. The distribution of the positive ions discussed in Section 3.3.1.2 was mapped by running a positive ion image reconstruction of the selected peaks from the positive ion ToF-SIMS spectrum. ToF-image is a program built into the ION-TOF software that allows the user to assign the colours red, blue and green to individual or sets of ions. The spatial distribution of these ions can then be mapped (this can be achieved as the software effectively collects a spectrum per pixel and then sums these to produce a total area spectrum). Red, green and blue were assigned to three ions, used to produce the positive ion ToF-SIMS images, as follows:

Red: m/z 24^+ Magnesium Stearate $[Mg]^+$

Green: m/z 152^+ Paracetamol $[M+H]^+$

Blue: m/z 365^+ Spray Dried Lactose $[M+Na]^+$

Individual ion images were produced for each ion and then a composite overlay was produced from these. The following set of figures represent high resolution 249 μm x 249 μm positive ion images and overlays taken using burst alignment mode, the lowest wt% paracetamol tablet is shown in the initial figure, with increasing quantities of paracetamol in the subsequent figures. The size of the ion image selected was dictated by instrument time and the size of the components. Therefore, the area selected did not represent an entire tablet surface. Image acquisition time was kept below the static limit discussed in Chapter 2.

The positive ion images and overlay representing the 20 wt/wt% paracetamol tablet are presented in Figure 3.25. The distinct larger paracetamol crystals of up to 200 μm that were readily apparent in the equivalent tablet SEM images presented in Figure 3.20 cannot be observed. The distribution of the pixels indicated that the material may have been changed by the compaction process, with smaller and finer structures. As paracetamol is a brittle material this is not unexpected [Ganderton *et al.*, 1995]. In comparison, the size and distribution of the spray dried lactose was much more consistent with the comparative SEM image. What appear to be agglomerates can be

clearly seen, particularly in the 50 to 100 μm range, this indicated that the spray dried lactose seemed to have been less physically effected by the compaction process. Spray dried lactose appeared to be the dominant feature of the image. Although, the wt % of magnesium stearate was low at 0.5%, the apparent quantity of this material at the surface appeared to be high. This may have been due to its properties as a slip agent effectively attaching to and deforming at the drug and other excipient surfaces. It was predominantly present in larger agglomerates. The overlay image also highlighted that the distribution of magnesium stearate appeared to be within the region associated with the paracetamol.

The positive ion images and overlay representing the 40 wt/wt% paracetamol tablet are presented in Figure 3.26. The concentration of paracetamol at the surface appeared to be similar to that of the 20% tablet but the spray dried lactose concentration appeared to have decreased and was present in clusters that were larger than those observed in the previous image. Like the paracetamol, the proportion of magnesium stearate appeared to be similar to that of the 20% tablet, and again was present in larger clusters. The surface appeared to be comparable to the SEM image of this surface.

The positive ion images and overlay representing the 60 wt/wt% paracetamol tablet are presented in Figure 3.27. The changes that could be observed in this tablet surface were significantly greater than those observed when moving between the two images from the lowest concentrations of the drug. The paracetamol was far more dominant and greater roughness was observed in this material, giving the whole image a greater topographical profile. The quantity of spray dried lactose had decreased and there appeared to be further changes in its distribution, with smaller clusters formed. The largest change was observed in the magnesium stearate ion image. There was significantly less present than what could be observed in the previous images, and in a similar pattern to the spray dried lactose, it appeared to be present in smaller agglomerated clusters. In the SEM images the largest change between the images occurred between the 60% and 80% samples, whereas in the SIMS images the most significant jump appeared between the 40% and 60% samples. This may be due to the fact that it was not possible to clearly visualise the magnesium stearate on the SEM images, or differentiate between this material and

the spray dried lactose. The SIMS ion images gave better information about the chemical components at the surface and their distribution, in addition to displaying a considerable amount of topographical information.

The positive ion images and overlay representing the 80 wt/wt% paracetamol tablet are presented in Figure 3.28. In this image of the surface, the clearest correlation between the topographical features and ion distribution can be observed. The overlay was highly comparable to the SEM image shown in Figure 3.18, the substructure within the paracetamol crystals can clearly be seen, the surface is rougher; containing a greater number of pits and voids. The quantity of spray dried lactose has again decreased and was present in small clusters. The quantity of magnesium stearate was also reduced, again forming in smaller agglomerates than observed in the previous image. As previously commented, although the SEM images clearly highlighted the location and distribution of the paracetamol structures, the SIMS images gave better information in regards to the spray dried lactose and magnesium stearate distribution. In Section 3.3.2.4 these images are discussed in relation to both spectral ion intensity information and computational calculations of the ion images in regards to component distribution.

In summary, throughout the images (Figure 3.25 to Figure 3.28) as the drug concentration increased, a corresponding increase in the quantity of paracetamol was observed (shown in green). There was a correlating decrease in the spray dried lactose (shown in blue) and this material continued to sit in isolation from the other two materials. It also formed tighter agglomerates as the drug concentration was increased. This change in the surface concentration mirrored the data obtained from the ToF-SIMS spectroscopy of the different tablet surfaces. A different pattern was observed with the magnesium stearate. Although all tablets contained the same amount of magnesium stearate (0.5 wt%) and the ToF-SIMS spectroscopy appeared to indicate a stable level of Mg ions within the spectra as drug concentration was increased, the ToF-SIMS ion images appeared to suggest that the distribution of this material seemed to decrease and change in its distribution across the surface, forming smaller agglomerated clusters as drug concentration was increased. This was surprising and unexpected due to the ability of the colloidal lubricant to coat over the surface of the drug and excipient particles, a process necessary for its function in

reducing friction. One explanation could be that in the real world sample of the tablet surface, there are differences in the lubricant coverage across the surface particularly at high drug concentrations where poorer mixing of the drug and excipients may occur. Clearly the distributions of the two excipients appeared to change as a function of drug concentration. This data highlighted the value of ToF-SIMS in not only identifying the presence of a material at a surface, but also its distribution across the surface of a complex formulation, and the relationship of this distribution with other components within the sample.
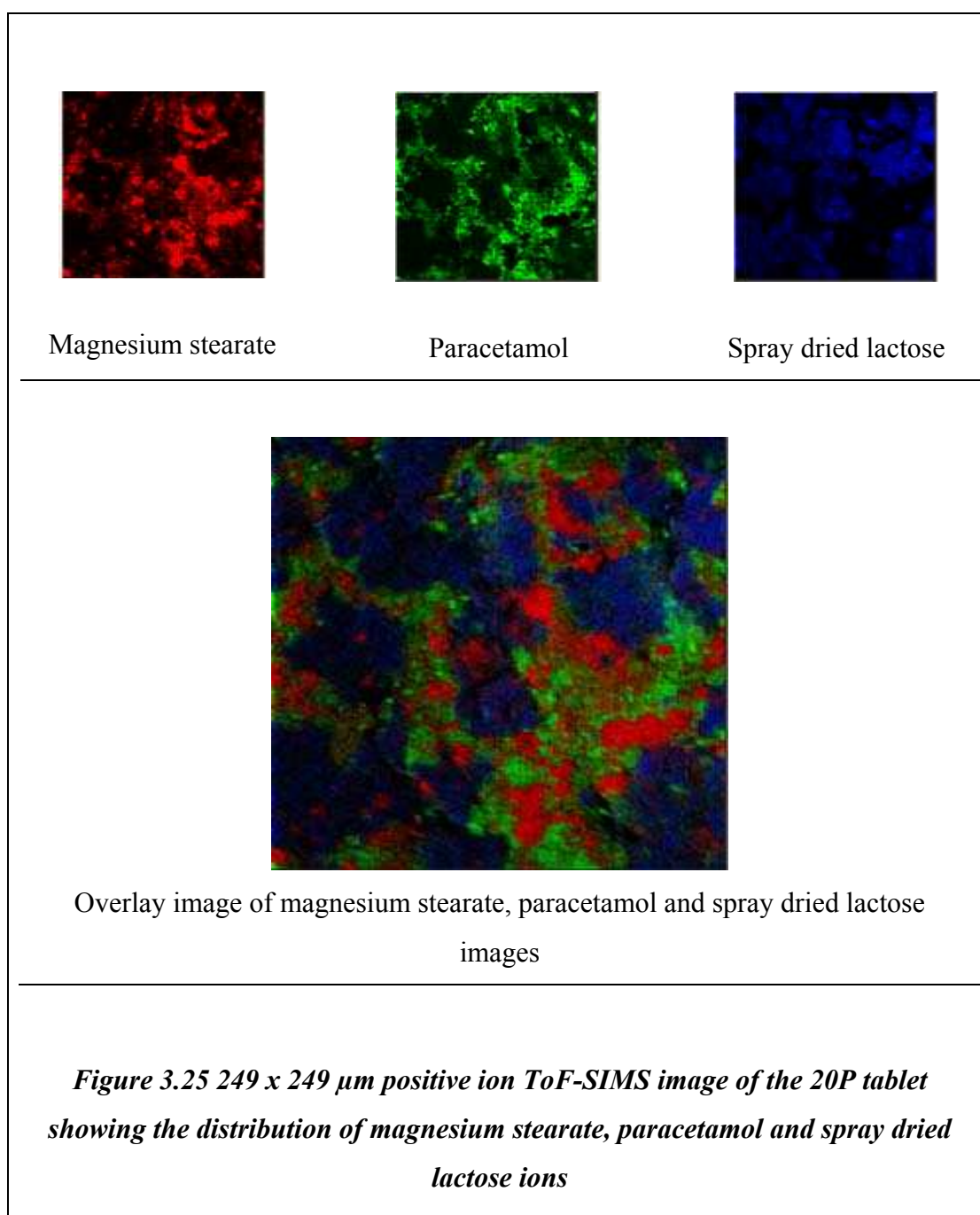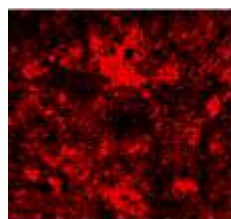
Magnesium stearate   Paracetamol   Spray dried lactose
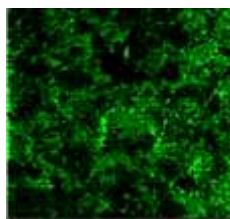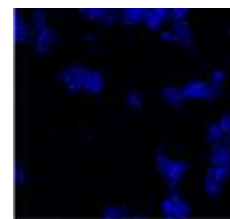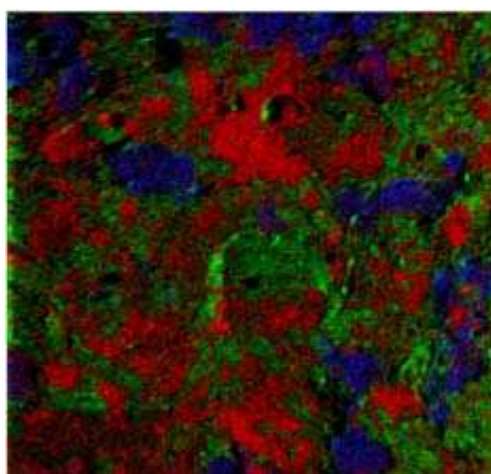
Overlay image of magnesium stearate, paracetamol and spray dried lactose images

Figure 3.25 249 x 249 μm positive ion ToF-SIMS image of the 20P tablet showing the distribution of magnesium stearate, paracetamol and spray dried lactose ions

Magnesium stearate   Paracetamol   Spray dried lactose

Overlay image of magnesium stearate, paracetamol and spray dried lactose images

Figure 3.26 249 x 249 µm positive ion ToF-SIMS image of the 40P tablet showing the distribution of magnesium stearate, paracetamol and spray dried lactose ions
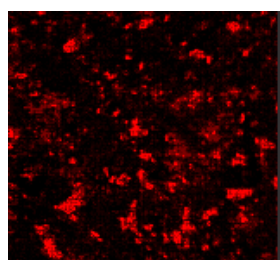
Magnesium stearate   Paracetamol   Spray dried lactose
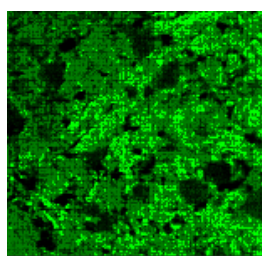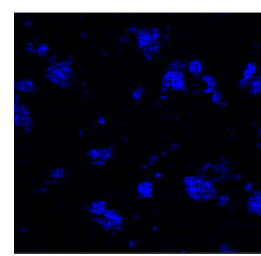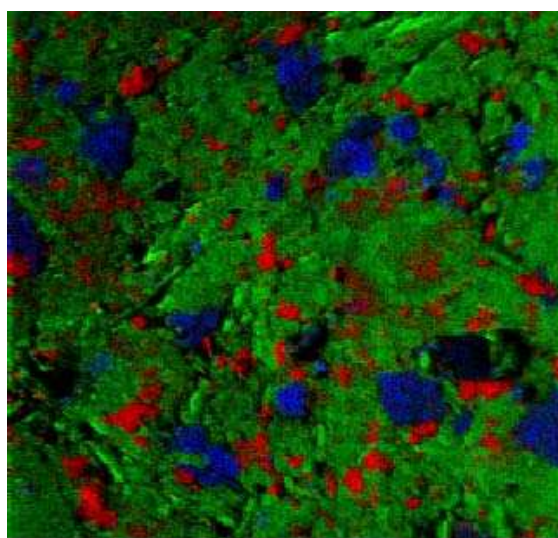
Overlay image of magnesium stearate, paracetamol and spray dried lactose images

Figure 3.27 249 x 249 µm positive ion ToF-SIMS image of the 60P tablet showing the distribution of magnesium stearate, paracetamol and spray dried lactose ions
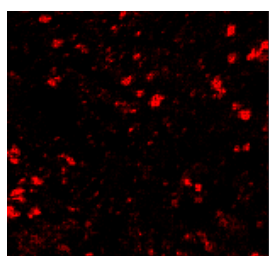
| Magnesium stearate | Paracetamol | Spray dried lactose |
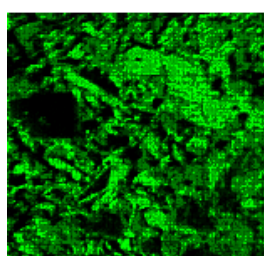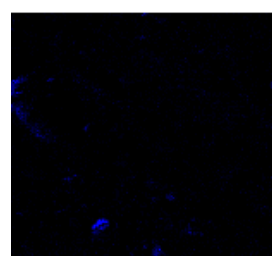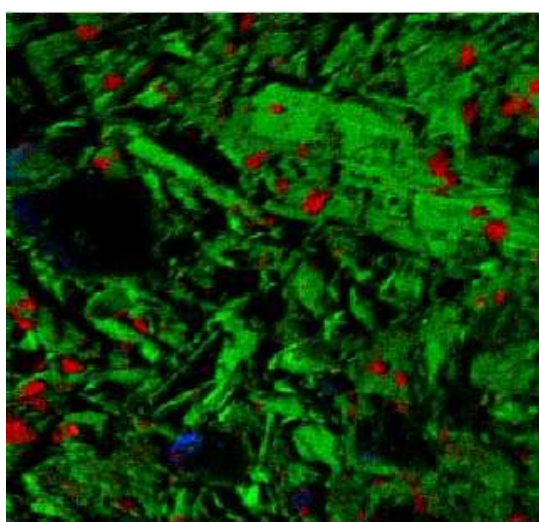
Overlay image of magnesium stearate, paracetamol and spray dried lactose images

Figure 3.28 249 x 249 µm positive ion ToF-SIMS image of the 80P tablet showing the distribution of magnesium stearate, paracetamol and spray dried lactose ions

3.3.2.4   **Further Analysis of Tablet Data**

As previously discussed in the introduction, ToF-SIMS is traditionally seen as a qualitative technique and the quantification of ToF-SIMS spectra can be difficult due to factors such as magnitude changes in ionisation efficiencies, ion yield variation, and chemical environment. The volume of analysis can also raise questions to whether results are truly representative of the actual sample due to the sensitivity to only the first few monolayers [Barnes *et al.*, 2011]. The use of ToF-SIMS to provide reliable quantitative data is further investigated in Chapter 4 and Chapter 5.

In this Chapter a number of different methods have been used to extract quantitative information from the data. In the first instance, three positive ion ToF-SIMS spectra were produced for each of the four different tablet concentrations. These spectra were acquired from three areas of the sample surface 100 μm apart, and for 249 μm x 249 μm sampling areas. The raw counts from the diagnostic peaks identified in Section 3.3.1.2 were then plotted for each tablet concentration as a percentage of the total counts for the three ions. This data is shown in Figure 3.29. The three ions were, as previously, magnesium stearate at m/z 24^+, paracetamol at m/z 152^+ and spray dried lactose at m/z 365^+. These three components were represented as a percentage of the sum of the three raw ion count values.

Figure 3.29 Graph showing percentage ion counts by peak area for the four tablets for paracetamol, magnesium stearate and spray dried lactose
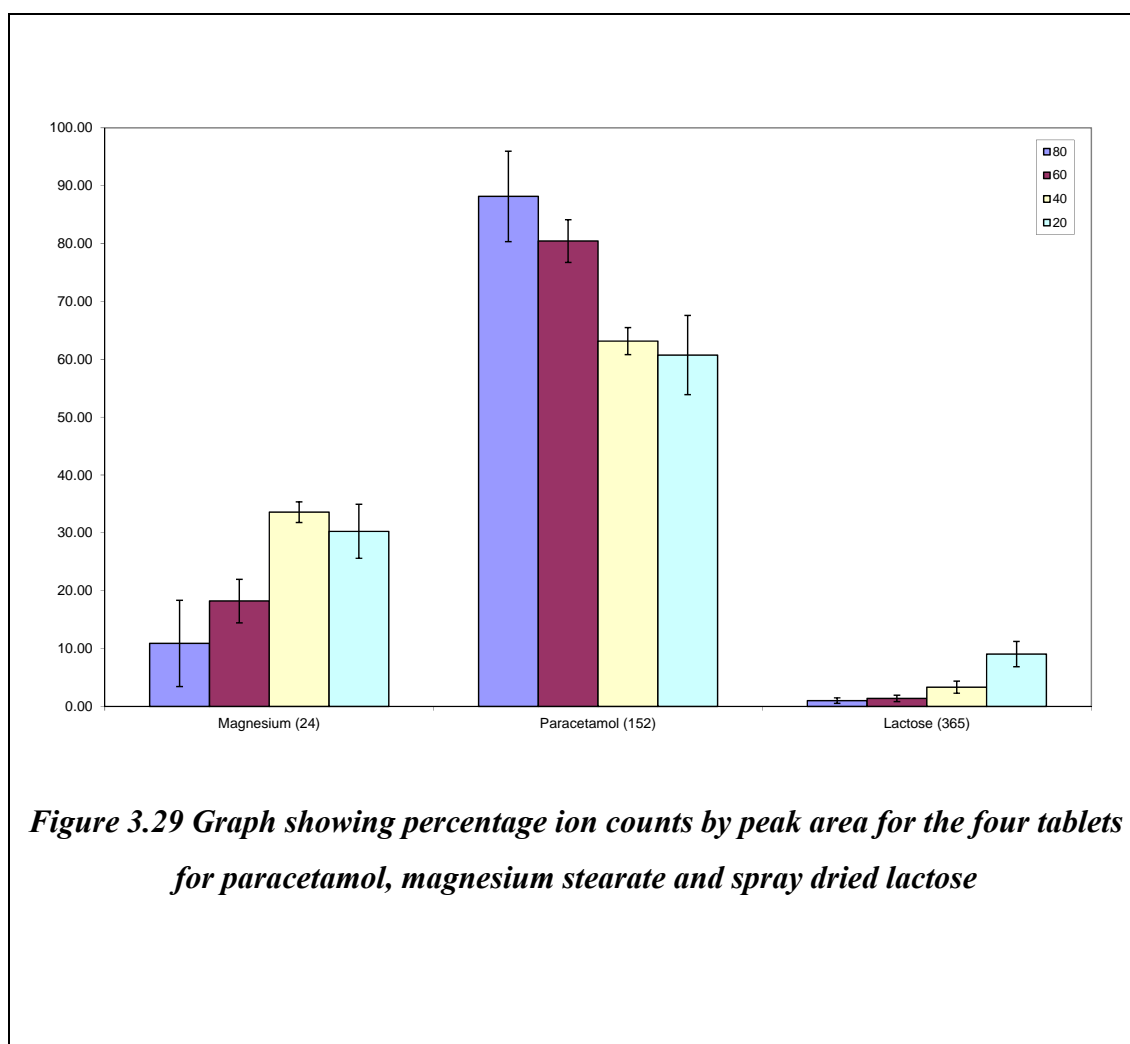
The paracetamol and spray dried lactose percentages showed a respective decrease and corresponding increase as they moved through from the highest to the lowest drug concentration levels in the actual tablets. The magnesium stearate levels were highest in the 40% tablet and lowest in the 80% tablet. The % values from these three components are further discussed in greater detail below in conjunction with the data derived from the ion images.

Figure 3.30 compares two different methods for assessing the surface chemistry of the tablet. The actual bulk composition is shown along with the percentages for each tablet from the "peak areas" graph above in Figure 3.29 and the percentages derived from the ToF-SIMS positive ion images. Percentage data from the ion images was produced by a custom designed RGB image analysis program. It was specifically written to interrogate the levels of red, green and blue (RGB) in ToF-SIMS ion

113

overlay images. The program analyses all the RGB data from each overlay image; assigning a value between 0 and 255 for each channel of red, green, and blue for each pixel. These values are totalled to find the maximum value. The individual channel totals are then divided by the maximum value and the figure multiplied by 100 to find the percentage. For example, in a single pixel:

R = 150; G = 100; B = 10; Total = 260,

(R/T)*100 = 57.69%,
(G/T)*100 = 38.46%, and
(B/T)*100 = 3.85% respectively.

		% by peak area		
		Magnesium Stearate 24[+]	**Paracetamol 152[+]**	**Spray Dried Lactose 365[+]**
Tablet ID	**80P**	10.87	88.14	0.98
	60P	18.21	80.42	1.37
	40P	33.57	63.13	3.31
	20P	30.25	60.72	9.03

		% by RGB image analysis		
		Magnesium Stearate 24[+]	**Paracetamol 152[+]**	**Spray Dried Lactose 365[+]**
Tablet ID	**80P**	15.15	81.85	2.99
	60P	23.17	66.46	10.37
	40P	49.53	40.87	9.59
	20P	38.55	34.93	26.51

		% by actual bulk composition		
		Magnesium Stearate	**Paracetamol**	**Spray Dried Lactose**
Tablet ID	**80P**	0.50	80.00	19.50
	60P	0.50	60.00	39.50
	40P	0.50	40.00	59.50
	20P	0.50	20.00	79.50

Figure 3.30 Comparative percentages of tablet samples by peak area, ToF-image and actual make up (bulk composition)

In both methods the level of magnesium stearate was higher than that of the bulk composition. This was reflected visually in the ion images presented in Figure 3.25 to Figure 3.28. Both methods showed the highest concentration of magnesium stearate in the 40P tablet and the lowest concentration in the 80P tablet. With the exception of the 40P tablet, both data sets showed that as the drug concentration increased less magnesium stearate was observed at the surface. The ion images also highlighted the uneven distribution and heterogeneity of the three components at the surface, which may have accounted for the 40P data point anomaly. Although, the image data percentages were from a single typical positive ion ToF-SIMS ion image of the surface, the data from the spectra was averaged over three runs, yet still showed a higher level of magnesium stearate in the 40P tablet than the trend suggested would be anticipated. An alternative, but lengthy approach, would to be to significantly increase the number of analysis areas to improve the reliability of the data. Whether magnesium stearate levels in the 40P tablet were still out of step in comparison to the other tablet concentrations over a greater sampling range could then be ascertained. Both methods showed an increase in paracetamol levels from the lowest to the highest tablet concentrations, and demonstrated higher levels of surface drug within the formulation than would have been anticipated from bulk levels. The output from the RGB analysis program produced data that were more in line with the actual bulk composition, with figures of 81.85%, 66.46%, 40.87% and 34.93%, in comparison to the respective bulk composition values of 80%, 60%, 40% and 20%. Drug concentration levels that were higher than the bulk composition and RGB analysis method were observed when the peak area method was used, with values of 88.14%, 80.42%, 63.13% and 60.72%.

Higher values were observed when using the RGB analysis method in comparison to the peak area method in respect of the spray dried lactose levels, with figures of 2.99%, 10.37%, 9.59% and 26.5% compared with 0.98%, 1.37%, 3.31% and 9.03% (bulk composition 19.5%, 39.5%, 59.5% and 79.5%). The peak area data showed the spray dried lactose levels steadily increased as the drug concentration reduced, with a value range of 0.98% to 9.03%. However, although the spray dried lactose levels from the overlay showed the lowest level in line with the bulk composition in the highest drug concentration, and the highest levels also in line with the lowest drug concentration, the levels in 40P tablet were again inconsistent with those from the

bulk composition. The image reflected this, where this lower value was apparent from the lack of blue areas within the overlay. Again, this could have been a result of the observed chemical heterogeneity of the sample surface. As with the magnesium stearate, the RGB analysis program gave higher values for spray dried lactose, which were more representative of the bulk composition, than the peak area method for the spray dried lactose concentrations.

As a whole, the figure highlighted the large discrepancy between the actual bulk composition of the tablets and the "raw" results from the both the SIMS spectra and images, particularly in relation to the excipients. In conclusion, the data from the RGB analysis program appeared to provide better quantitative information than the raw peak area method.

A further method was employed to look at the data through the use of ratios. The RGB analysis data was used, as this had been established as showing greater coherence with the bulk composition than the peak area data. In each case, the individual element values were ratioed against themselves and the paracetamol values in an A / A + B format. These results are shown in Figure 3.31. This method showed some interesting results as in all cases, the 40P data that was out of synch in both the peak area and RGB method was brought into line with the other concentrations. Both the M/M+P and L/L+P data showed a steady increase from the 20P to 80P tablet concentrations. This indicated that the surface concentrations of both of the excipients in the formulation were directly related to the paracetamol concentration. This relationship would be anticipated with the spray dried lactose as the concentration increased with decreasing drug concentration was reflected in the bulk composition. However, although the magnesium stearate had a fixed bulk composition, the concentration of this material at the surface appeared to be governed by the other two materials, with tablets containing a lower drug concentrations / higher spray dried lactose concentrations having a greater proportion of magnesium stearate at the surface. This may have been due to the way in which the compression forces acted on the materials during tablet manufacture. The P/P+L ratio values showed an increase from the 20P to the 80P tablet. This was in line with the bulk composition, where the proportion of spray dried lactose decreased in line with increasing paracetamol levels. The values were higher than expected from the

bulk composition, i.e., if bulk compositions were used in the ratio for the 80P tablet a value of 0.804 would be obtained (0.8 / 0.8+0.195). This apparently high value using the P/P+L ration can be attributed to the previously discussed higher levels of magnesium stearate (and hence lower levels of spray dried lactose) at the surface.

Sample	M/M+P	L/L+P	P/ L+P
80P	0.16	0.04	0.96
60P	0.24	0.13	0.87
40P	0.44	0.19	0.81
20P	0.52	0.43	0.57

Figure 3.31 Ratios of key diagnostic elements in the paracetamol tablets, where M = Magnesium stearate, P = Paracetamol and L = Spray dried lactose

The peak area and imaging measurements were purely based on average raw counts / pixel colour level information of the three diagnostic peaks and did not take into account how readily an ion can be produced from the surface. This highlighted that it is absolutely imperative that raw SIMS data are not used for quantitative purposes unless there is a clear understanding of the relative ability of any individual ion to form both from the pure material and a matrix environment. These factors will be discussed further in later chapters. As the ToF-SIMS experiment effectively produces a spectrum per pixel, the ToF-image program is limited in comparison as it only uses data from the allocated species.

All the factors above are predominantly concerned with the limitations of the SIMS data and the way in which it is processed. However, Hussain *et al*. discovered that mixing time during tablet preparation can also have an effect on the detection level of different species [Hussain *et al.*, 1990]. Therefore, it is of paramount importance to ensure that any samples submitted for analysis have been manufactured in the same manner. In effect, two samples with the same levels of components could

otherwise give differing results. If differences are inevitable, these must be accounted for when presenting results.

3.3.3.   **Micro-spheronised Beads**

3.3.3.1   **The Effect of Curvature on Time-of-Flight**

Initial ToF-SIMS studies of paracetamol in a multi-layer drug bead have been undertaken previously [Belu *et al.*, 2000]. In this work, three beads systems containing drug levels ranging from 10 to 40% were prepared for ToF-SIMS analysis by using a similar cross-sectioning method to that used by Belu.

The instrumental methods section of this thesis covers the mechanics of the ToF-SIMS process. A fundamental part of the ToF-SIMS process, as the name suggests, is time-of-flight. Therefore, the geometry of the sample will play a role in the analysis. If we imagine a totally flat homogenous surface, then the time-of-flight of identical ions from a surface should remain constant across its area. However, if we modify the surface to introduce Z plane changes then the time-of-flight of these identical ions would differ slightly depending on the distance of the point that the ion arose from in relation to the mass analyzer. A "perfect" sample surface would need to be totally flat in order to eliminate the influence of Z value variations on time-of-flight. Bead samples analysed in this work have been cross sectioned in order to achieve a flat surface as possible. The impact of analyzing a bead in its raw state (i.e. a spheroid) would potentially result in ions arising from a range of different "heights" dependent on the curvature of the bead and the area of analysis. This variance in Z over analysis area is presented for a 1000 μm diameter bead in Figure 3.32. The x-axis represents the x, y analysis area dimensions and the y-axis represents change in Z from the centre of this analysis area to the edge, assuming that the centre point is at the "top" of the bead. From the figure it can be observed that there would be a 5 μm change in Z across a 100 μm analysis area. All surface morphology is in effect a result of Z value variations. The following two chapters will more thoroughly analyse and address the impact this has on the user's ability to produce reliable and repeatable quantitative data from ToF-SIMS, by looking at roughness effects on non-model and model surfaces. Belu has previously analysed bead systems, producing spectra for the excipients (in powder form), the coating (on the curved bead surface) and the internal structure (cross – sectioned bead) [Belu *et al.*, 2000]. Although she did not specifically cite any problems with analysing the

curved surface, the spectra produced contained significantly less counts than those of the raw materials and the cross sectioned surface.
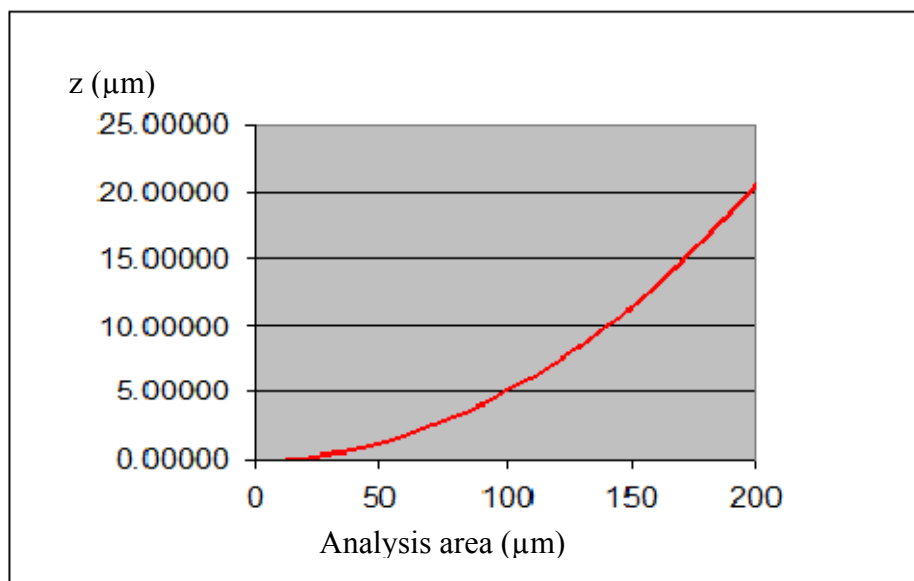
Figure 3.32 Graph to show the Z change over a given area for a
1000 μm diameter spheroidal bead

3.3.3.2   Analysis of ToF-SIMS Cross Sectioned Bead Spectra

The positive and negative ion ToF-SIMS spectra of a 100 μm area of the sectioned face from the 25 wt/wt% paracetamol bead (sample ID P25) are presented in Figure 3.33 and Figure 3.34, respectively. Clearly identifiable peaks at m/z 109^+ and 152^+ were observed in the positive ion ToF-SIMS spectrum, which had previously been assigned to the paracetamol fragment $C_7H_9O^+$ and the protonated molecular ion $[M+H]^+$. In addition, the $[2M+H]^+$ ion was also observed at m/z 303^+. The low intensity peak observed at m/z 365^+ represented the cationised spray dried lactose molecular ion $[M+Na]^+$.

In the negative ion ToF-SIMS spectrum, paracetamol diagnostic peaks were observed at m/z 107^- ($C_7H_7O^-$), 150^- ($[M-H]^-$) and 301^- ($[2M-H]^-$). The previously observed spray dried lactose peak at m/z 221 was also noted in the reference spectrum.

Positive and negative ion ToF-SIMS spectra were not presented for the other two bead samples (P10 and P40). Despite the differences in paracetamol and spray dried

lactose concentrations, no significant differences were observed within these spectra. This may have been due to the relatively small analysis area (100 μm) that was used in high resolution spectroscopy; as the physical size of the paracetamol structures was large (up to 200 μm), they could have easily dominated this sampling area. This was not an issue in the tablet work reported earlier in this chapter, where it was speculated that the manufacturing process had significantly reduced the size of the paracetamol particulates. However, the range in concentration for the active ingredient in the beads was also significantly less than that of the tablets, varying from 10 to 40 wt/wt% of paracetamol, in comparison to the 20 to 80 wt/wt% paracetamol concentration in the tablet samples. Beads with higher concentrations of paracetamol could not be produced by the spheronisation methods, as sufficient quantities of spray dried lactose and microcrystalline cellulose were required to facilitate the exudate to spheronise process.
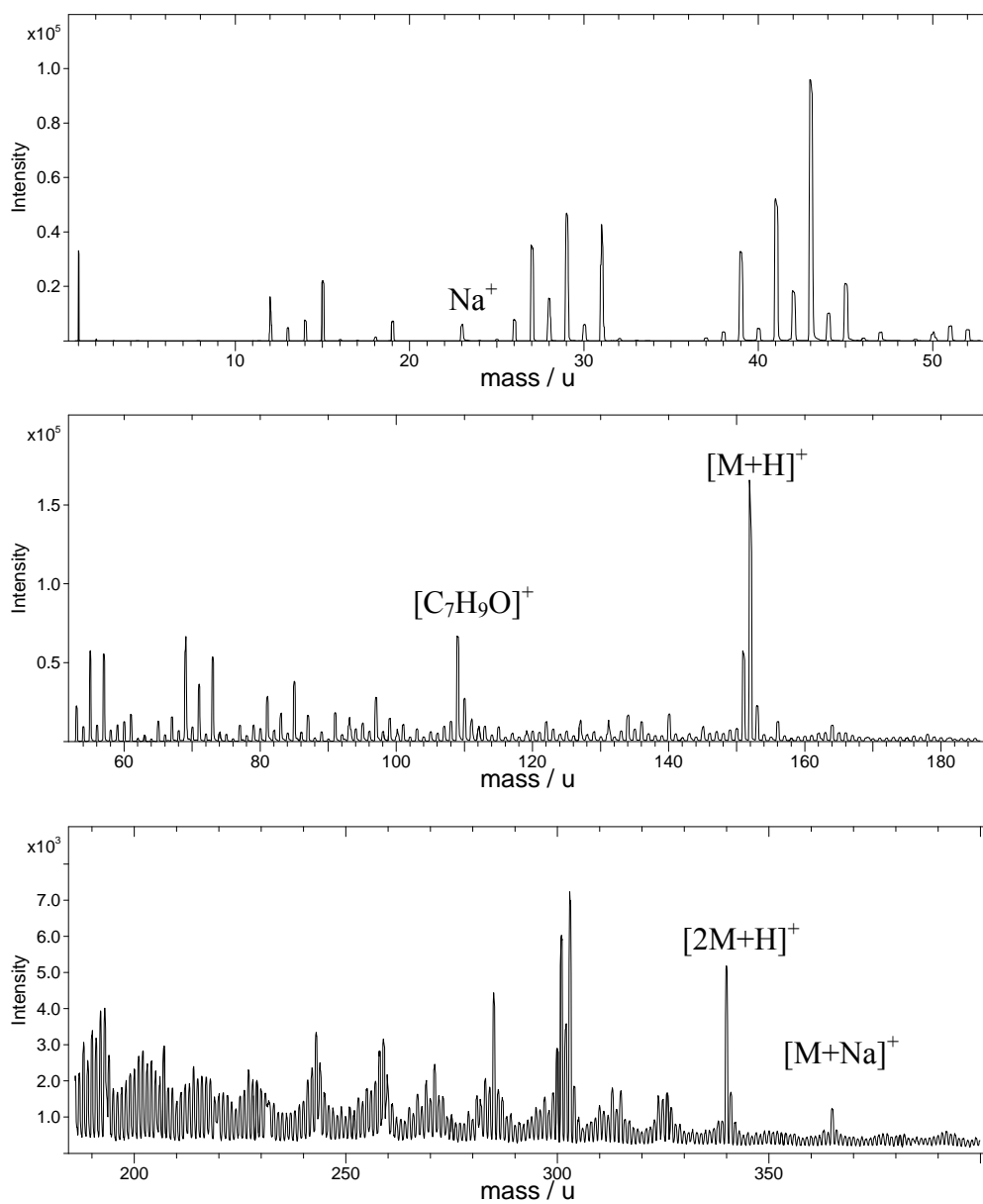
Figure 3.33 Positive ion ToF-SIMS spectrum of P25 cross-sectioned bead
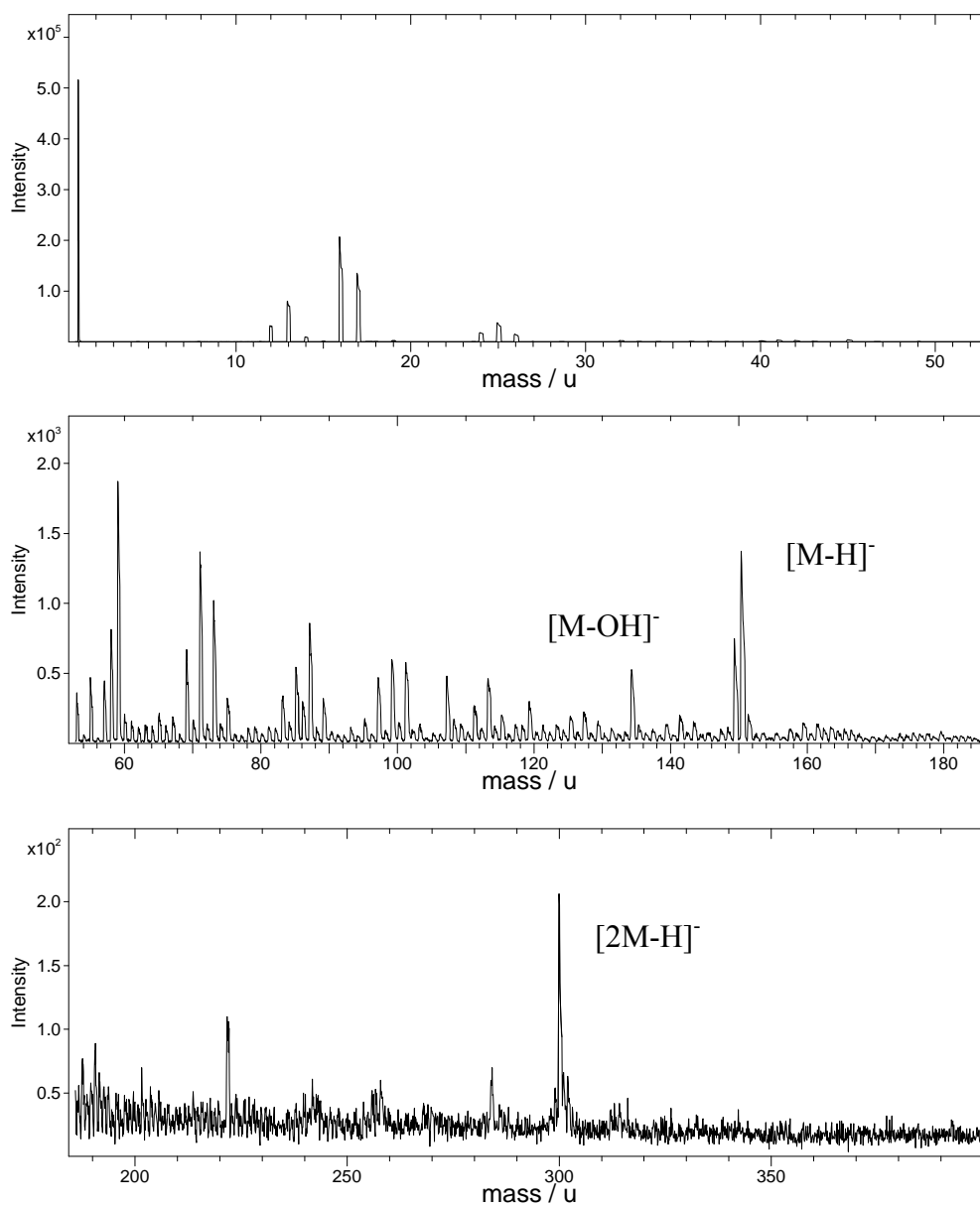
Figure 3.34 Negative ion ToF-SIMS spectrum of P25 cross-sectioned bead

125

3.3.3.3 Analysis of ToF-SIMS Imaging Results

ToF-SIMS positive ion images from the cross-sectioned beads over 249 μm x 249 μm areas are presented in Figure 3.35. The method in which the image overlay was produced is described in Section 3.3.2.3.

As there was no easily identifiable diagnostic ion in the microcrystalline cellulose positive ion ToF-SIMS spectrum an alternate approach was taken to map the distribution of this material across the sample surface. ToF-image was used to generate positive ion image overlays using combinations of ions. (The method in which this program functions is also described in Section 3.3.2.3). To produce the images the following assignments were made:

Red: m/z 152^+ Paracetamol $[M+H]^+$

Green: sum of m/z 365^+ Spray dried lactose $[M+Na]^+$
and m/z 381^+ Spray dried lactose $[M+K]^+$

Blue: sum of all ions Representative of microcrystalline cellulose

This procedure allowed for the mapping of spray dried lactose (blue / green areas (cyan)), paracetamol (magenta areas) and microcrystalline cellulose (blue areas). As blue mapped the sum of all ions, it was concluded that any black areas in the images represented holes in the sample surface. A number of peak combinations were attempted and the RBG settings listed above resulted in the best contrast image to visualise the spatial distribution of the three raw materials. In all images the paracetamol appeared "magenta" in colour rather than the clear red colour observed in the tablet images. This was due to the blue channel mapping the sum of all ions so in pixels where paracetamol was present in the red channel, the "sum of all ions" was also present, producing magenta from the two colour combinations. This mechanism also highlighted the spray dried lactose distribution by adding the blue and green channel information to produce cyan. Microcrystalline cellulose distribution can be observed in the pure blue pixels, where there were no contributions from the red (paracetamol) or green (spray dried lactose) channels.

The RGB analysis information for the three images is presented in Figure 3.36. The highest level of paracetamol was observed in the P40 sample. In the P40 positive ion image, a large crystal can be observed to the left hand side of the image. Both the P25 and P10 positive ion images showed a finer distribution of the paracetamol throughout the sample in terms of crystal size. The RGB analysis confirmed visual observations of the images; that over the areas mapped the percentage of paracetamol was greater in the P10 than the P25 sample. As has been previously commented, larger sampling areas or larger sample runs may confirm whether this was an actual trend or a result of the specific sampling area analysed.

The spray dried lactose levels appeared to be reasonably consistent across the sample surface, both visually and from the positive ion images at a figure of approximately 10% of the sample surface. However, this material appeared to show greater dispersal in the beads with the two higher paracetamol concentrations. This mirrored results from the tablet samples, where the spray dried lactose also appeared to be more finely dispersed as the drug concentration increased. In both cases, this indicated that the compaction process was causing the material to deform and break up under compression. The levels of microcrystalline cellulose appeared to follow the same trend as the spray dried lactose distribution, as highlighted by the RGB analysis results. However, it is important to cite that the way in which the RGB program calculates percentages (as detailed in Section 3.3.2.4) would result in these values being artificially high, as the information from all the ions was summed together. This highlighted that the lack of a diagnostic peak not only affects the user's ability to produce images with clearly defined areas of material, such as were produced with the paracetamol tablets, but also that the RGB information is compromised when a diagnostic ion cannot be identified.

Differences were also observed in the cross-sectioned spheroids positive ion images in comparison to the compacted mass powder tablet ion images. The positive ion bead images exhibited a much smoother surface morphology than their tablet image counterparts, which was relatively consistent across the concentration range. However, the tablet samples showed increasing surface topography as the drug concentration increased. These differences can be attributed to the variations in

preparation method; where the tablets were compressed into form and the beads were cross-sectioned using a sharp blade effectively cutting a smooth planar surface.

The ToF-SIMS program can perform retrospective imaging and spectroscopy experiments if the data is saved in its raw format. (The mechanisms for data collection and storage are more fully discussed in Chapter 2). Users can select one or more "regions of interest" (ROI) from an image and then produce a spectrum in the same polarity from these selected areas. The positive ion ToF-SIMS spectrum presented in Figure 3.37 was produced by selecting the paracetamol crystal as the ROI. The positive ion ToF-SIMS spectrum from the P25 sample where several areas away from the paracetamol regions were selected to produce the spectrum is presented in Figure 3.38. The two key diagnostic paracetamol ions at m/z 109^{+} and m/z 152^{+} can clearly be seen in the first spectrum but are absent in the second spectrum, where the spectrum is dominated, particularly in the lower mass region by hydrocarbon fragments. These post acquisition spectra highlight the versatility of the ION-TOF ToF-SIMS instrument in allowing the user to gain greater insight from the data post experiment.
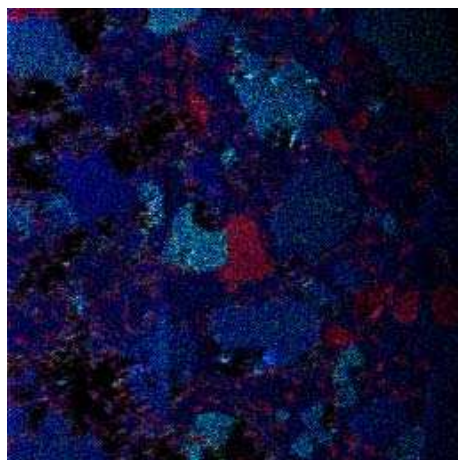
P10 bead
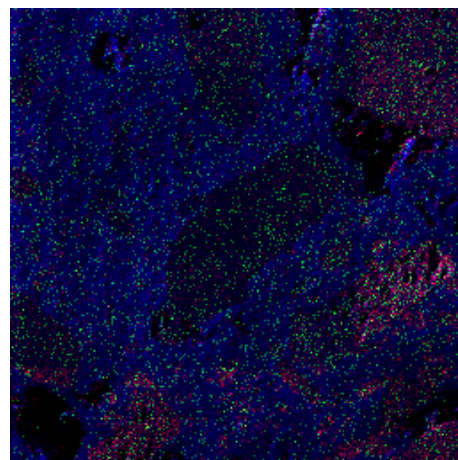
P25 bead
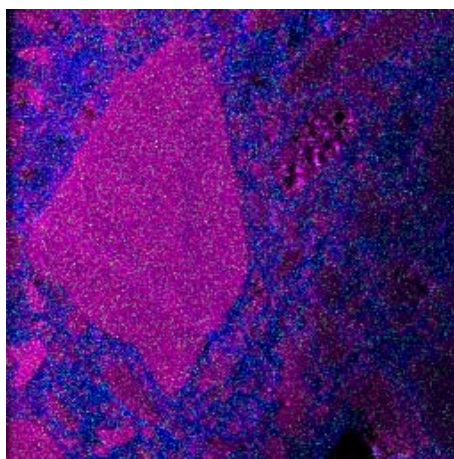
P40 bead

Figure 3.35 249 x 249 μm positive ion ToF-SIMS ion images
of cross-sectioned beads showing the distribution
of paracetamol, spray dried lactose and microcrystalline cellulose

Bead ID	% by ToF-image		
	Red **Drug 152$^+$**	**Green** **(sum of 365$^+$ and** **381$^+$)**	**Blue** **Total Ion**
P40	37.02	9.24	53.74
P25	14.21	12.49	73.29
P10	27.38	11.71	60.91

Bead ID	% by actual bulk composition		
	Paracetamol	**Spray Dried** **Lactose**	**Microcrystalline** **Cellulose**
P40	40	10	50
P25	25	25	50
P10	10	40	50

Figure 3.36 Comparative percentages of bead samples by peak area, ToF-image
and actual make up (bulk composition)
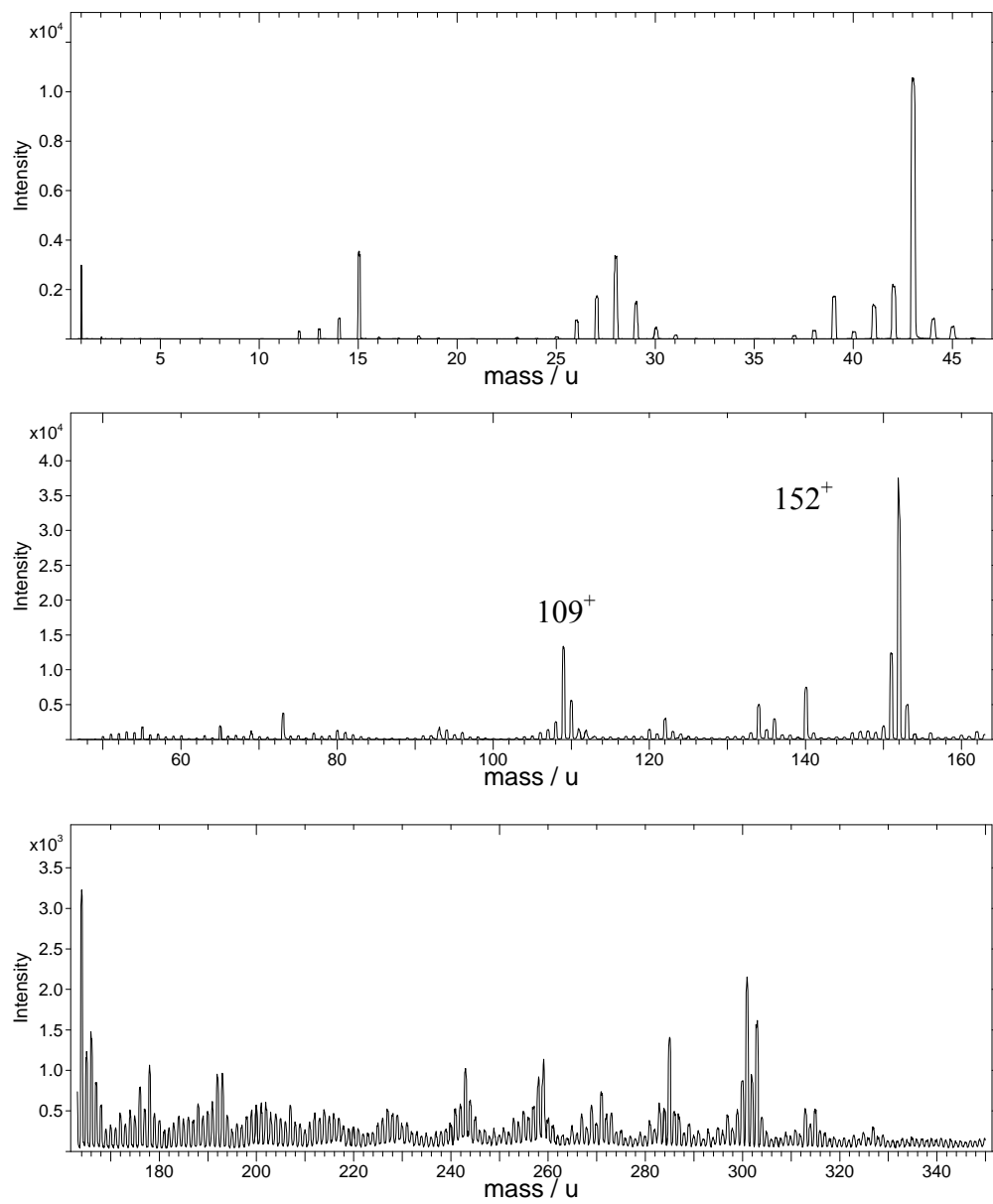
Figure 3.37 Positive ion ToF-SIMS spectra of paracetamol region of interest in cross-sectioned bead sample P40
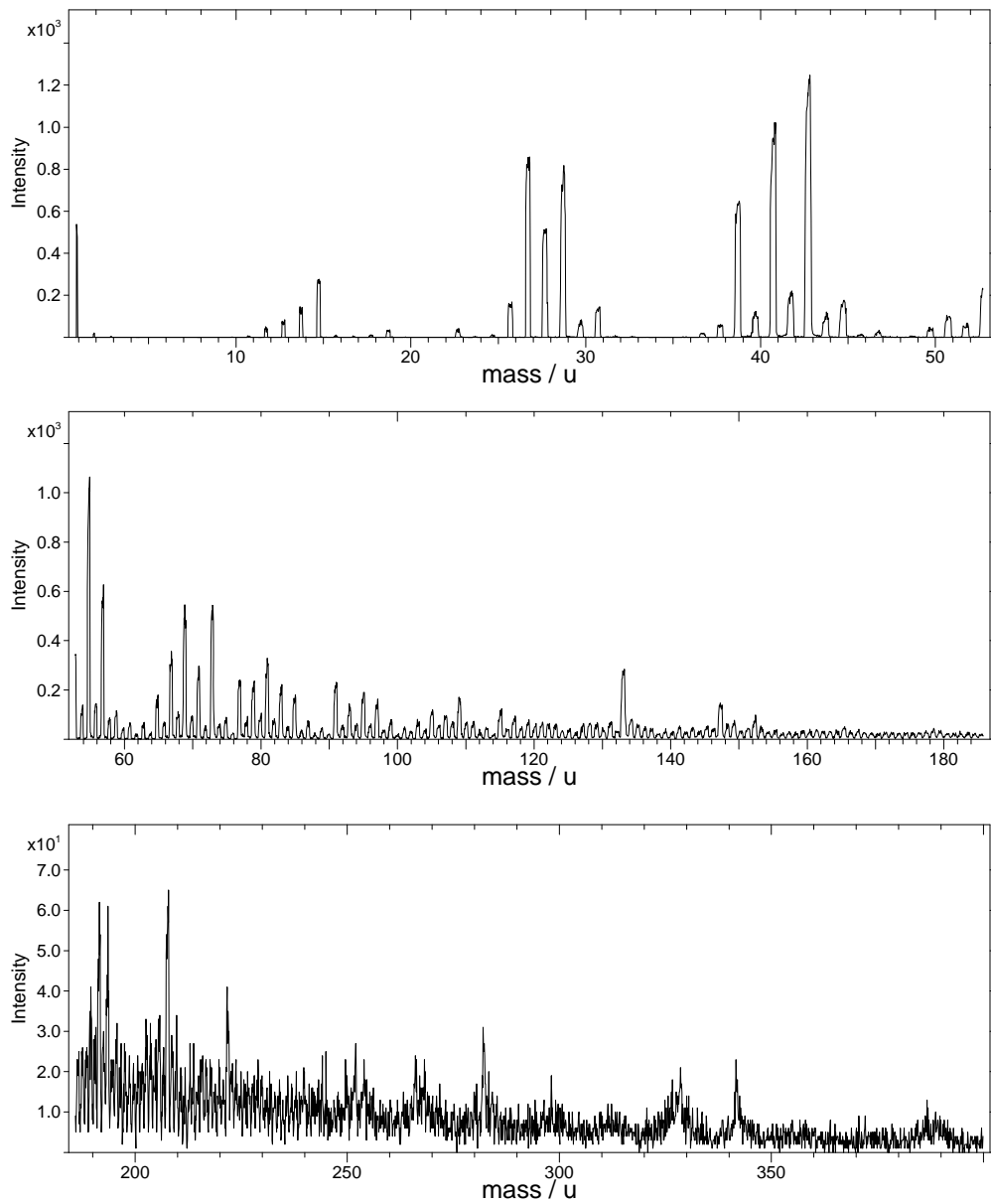
***Figure 3.38 Positive ion ToF-SIMS spectra of blue-green (non-paracetamol)
region of interest in cross-sectioned bead sample P25***

3.4 Conclusions

This chapter looked at the use of ToF-SIMS for the analysis of a number of pharmaceutical systems of paracetamol based tablet and spheroid formulations. The main aims of the chapter were two fold, to assess the ability of ToF-SIMS to evaluate the raw materials and multi-component systems, and to evaluate the use of ToF-SIMS to detect and differentiate between the components used to make the two formulations.

ToF-SIMS was able to provide a qualitative assessment of the surface analysis of the different formulations. In each case, the ability to detect diagnostic secondary ions for the drug and the different excipients allowed an understanding of the chemical composition of the tablet and spheroid systems. The chapter demonstrated that ToF-SIMS can be used to produce spectra of raw materials, tablets and spheroids where in the majority significant diagnostic peaks, that do not suffer from coincidence, can be identified. Peak assignments in this chapter correlated with those produced by Belu in previous work for the active ingredient and a number of the excipients [Belu *et al.*, 2000]. In addition, assignment of the magnesium stearate ions were in agreement with those identified by both Zhou and Pignataro [Zhou *et al.*, 2011; Pignataro *et al.*, 1999].

Chemical mapping was undertaken with ToF-SIMS that showed the chemical distribution of the formulation components across the surface. In line with the work completed by Belu *et al.* in 2000, the drug and the excipients were readily identified within the chemical images. However, their lateral compositions were compared with SEM data to limited success. SEM relies on the identification of topographical and morphological features that distinguish the components within the surface. This work has shown that SEM images of raw materials can prove useful information in regards to the morphology and size distribution of individual components of drug delivery systems. Previous research by Vervaet lists this technique as one of the key methods in assessing the microstructure of pellet surfaces [Vervaet *et al.*, 1995]. The physical change in a raw material due to pharmaceutical processing such as milling, compaction and granulation can render their identification in the SEM images difficult. This was the case for paracetamol at low drug concentrations and excipients such as spray dried lactose. As expected the ToF-SIMS analysis revealed a greater

insight into the chemical distribution of the components in the formulations. The ability to distinguish the drug from the different excipients in the surface was achieved in the ToF-SIMS analysis in a way that was not possible in many of the SEM image data. The lubricant, magnesium stearate, was also shown to exhibit changes in lateral distribution at different drug levels. While the higher resolution data of the SEM provided important correlative morphological and topographical analysis of features within the images, ToF-SIMS complimented this approach with detailed molecularly specific chemical images.

This chapter goes further than the research by Belu *et al*. in 2000 and looked at formulations that possess a range of drug loaded concentrations. Analysis of the ToF-SIMS images showed that the distribution of the drug and components changed as a function of drug level for the different formulations. As expected, there was a corresponding increase in the proportion of drug at the imaged surface as drug loading increased, with a comparable decline in the levels of the excipients. A qualitative visual assessment of the change in levels did not appear to change in line with the bulk formulation compositions.

ToF-SIMS was able to qualitatively detect diagnostic ions for the drug and the excipients in the range of concentrations chosen. A number of approaches were employed to explore the potential quantitative analysis of the drug and excipients in the ToF-SIMS analysis. Different mathematical models using data derived from the high resolution spectra demonstrated that the surface data did not follow the bulk formulations. Bespoke analysis programs were (and can be) written that interrogate the data produced in ToF-SIMS ion images to estimate the quantity of a material at a surface using diagnostic ions. However, this has its own limitations. The program only provides accurate quantification data from the image if key diagnostic ions are available and in the case employed here, can only calculate for a maximum of three components.

The problems associated with the quantitative analysis of data derived from the ToF-SIMS technique are well known, particularly for complex real-life products. The effect environment on ion emission has been extensively documented and this could contribute to the divergence of the surface data from the bulk composition observed within this data on chemically changing formulations across a range of

drug loaded systems. The topography of the different tablet formulations studied in this chapter also changed significantly as a function of drug levels, further complicating the ion generation process and probably impacting on any quantitative approach. The preliminary work on the bead formulations also highlighted that height variance in a sample could have an effect on the data produced. The design of the experiment such as number of areas analysed across a surface and the number of replicates of data analysis will also contribute to the challenges of successful data acquisition. It may very well be that processing and manufacture of pharmaceutical systems themselves such as poor mixing, migration of materials or phase separation of components could lead to differences in surface and bulk formulation.

Clearly a number of factors contribute to problems associated with quantitative analysis of data for complex formulations such as those studied in this analysis. In future chapters we shall move to study model systems that attempt to explore the impact of a number of factors, such as topography, on ion generation to gain a better understanding of the potential of ToF-SIMS in the analysis of complex heterogeneous pharmaceutical formulations.

Chapter 4.

The Role of Roughness in ToF-SIMS Analysis of Non-model Surfaces

4.1 Introduction

In the previous chapter it was concluded that ToF-SIMS enabled qualitative differentiation between the components of pharmaceutical formulations. However, in the complex heterogeneous systems studied, the execution of a quantitative assessment raised challenges for producing reproducible data on the concentrations of drug and excipients on the surface of the formulation. This chapter addresses some of the issues and factors limiting the acquisition of statistically reliable qualitative and quantitative data.

Following the realisation that the tablet data showed high variability, a "back to basics" approach employing model materials was used to further assess the origin of data variability within a ToF-SIMS experiment.

4.1.1 Quantification in ToF-SIMS

Once a drug formulation has been developed, it must be rigorously tested in a quality control laboratory that can approve or reject not only the formulation but also its containers, labelling and packaging materials [Luttrell *et al.*, 2005]. As part of this process, reliable methods are established that allow verification of a products physical and chemical makeup.

An in depth analysis of the chemical and physical nature of a formulation facilitates a better understanding of its behaviour, and in particular may help understand more fully properties such as drug release profiles. Chemical analysis may also be an aid to quality control and help protect against patent infringement.

A great number of analytical techniques have been, and still are, used in dosage form analysis [Aulton, 2002]. This study predominantly looks at ToF-SIMS as an emerging analytical tool. Some of the key methods that are used for quantitative data analysis are discussed.

Quantification in ToF-SIMS is often seen as difficult as large variations in secondary ion yields can occur that are dependent on the chemical environment which is commonly referred to as the 'matrix effect' [Riviere and Myhra, 2009]. These yields can vary by several orders of magnitude and the ion yield for a particular element can vary dramatically, for example, from a metal such as Si and its oxide [Vickerman and Briggs, 2001]. Quantification can also be affected by variation in instrument transmissions, substrate properties or surface contaminants [Grams, 2007].

There are a number of different methods that can be used to gain quantitative data from ToF-SIMS experiments. In 2010, research was conducted to establish the current capability of relative quantification using static SIMS [Green *et al.*, 2010]. This study looked at the variance of ion ratios from standardised Irganox samples using instruments from multiple research laboratories. They found good consistency between the instruments with a standard deviation scatter of around 10%.

One method that is frequently used to exploit ToF-SIMS as a quantitative technique is the calculation of relative sensitivity factors (RSFs), which convert relative ion intensities into concentrations. These are widely used in the microelectronic industry for contamination monitoring of silicon wafers, such as metal contaminants [Schroder-Oeynhausen *et al.*, 1998; De Witte *et al.*, 2000]. However, recently the accuracy of the use of RSFs is questionable as discrepancies, sometimes up to a factor of 10, are observable in existing RSF databases [Veillerot *et al.*, 2011].

Fahey *et al* developed their own algorithms to investigate isotopic ratio measurements for characterising isotopes within small features, such as particles, as they found vendor supplied software was inadequate [Fahey and Messenger, 2001]. Their software applied peak finding and stripping algorithms to the ToF-SIMS data.

A quantitative approach has been used to investigate copolymers and polymer blends [Weng and Chan, 2003]. Although it was found that quantitative analysis could be achieved using diagnostic ions, H-bonding was causing matrix effects. It was concluded that only ions that were not affected by this effect should be selected for analysis.

Multivariate analysis is another common method used in the analysis of ToF-SIMS data [Lee *et al.*, 2008]. Multivariate analysis methods are further discussed in Chapter 6.

4.1.2   Aims of the Chapter

Chapter 3 highlighted the heterogeneous nature of the tablet samples studied, both in terms of distribution of the chemical components across the surface and surface topography. Preliminary attempts were made to assess the use of both spectroscopy and imaging data acquired from the ToF-SIMS to evaluate the concentrations of the different materials at the sample surface. It was concluded that roughness may play a part in ToF-SIMS data providing useful quantitative information.

The main aim of this chapter is to assess the potential effect of roughness on ion yields and hence assess the impact this may have on any quantitative approach.

Initial experiments were performed on the 60% wt% paracetamol tablet analysed in the previous chapter to assess the reliability of results indicating the levels of raw materials in the formulation. Therefore, a model material that exhibits a chemically uniform and flat surface, where the consistency of ratios between diagnostic peaks across the surface could be measured, was required. Polytetrafluoroethylene (PTFE) was selected for this role as it exhibits both of these characteristics. The aims of the PTFE experiment were two fold. The primary focus was to attempt to remove any angle effects that affect sputtering yield by analysing a topographically flat surface. Secondly, the effect of increasing mass number was investigated. Both of these were achieved by looking at the variability of the data acquired.

Following on from this experiment, chemically homogenous samples with varying surface roughness were introduced. The aim of selecting samples with varying roughness, was to investigate the role surface morphology and micro-topography plays in altering the ionisation behaviour of diagnostic ions, and any impact that this may have on a quantitative approach. Magnesium stearate was selected for this experiment as it is a commonly used pharmaceutical material that can be quickly and easily modified. Three different samples of differing degrees of roughness were analysed by ToF-SIMS, primarily looking at the data variability attributed to surface roughness.

Both the PTFE and magnesium stearate used in the initial experiments are chemically homogenous surfaces. Further experiments using glass microscope slides were used to examine if roughness affects different chemical ion yields consistently in a chemically heterogeneous surface.

Finally, the impact of varying the primary ion dose density within the static limit was evaluated to see if this also affected data reproducibility.

4.2 Materials and Methods

4.2.1   Quantification of Tablet Data

In the previous chapter we used the raw count ion yields at m/z 24$^+$ (magnesium stearate), m/z 152$^+$ (paracetamol) and m/z 365$^+$ (spray dried lactose) to initially assess the ability of ToF-SIMS to provide quantitative data for the four tablet samples manufactured. Tablets with varying concentrations of paracetamol and excipients were specifically made for this preliminary analysis within the Laboratory of Biophysics and Surface Analysis at the University of Nottingham (as described in Section 3.2.2). The quality and/or reliability of the actual physical data were not analysed. This chapter will use a method based on standard deviation (σ) calculations to determine how much variation there is in the data sets analysed. Standard deviation is given as:

$$\sigma = \sqrt{\frac{\sum (x_i - \bar{x})^2}{n - 1}}$$

where '$\sum$' is the sum of, 'x_i' is each value in the data set, 'x bar' is the arithmetic mean and 'n' is the number of data points. Standard deviation calculations were applied to six data sets acquired for the 60% paracetamol tablet data, manufactured as per the details in Chapter 3, Section 3.2.2. These data sets were collected over 249 x 249 μm areas, taken 100 μm apart.

4.2.2   PTFE – a Simple Model Surface

The 60% tablet sample consists of three components resulting in a surface topography containing randomised peaks and troughs that was highlighted by the SEM images in Section 3.3.2.1 of Chapter 3. Chapter 3 discusses the potential effect of this surface topography on time-of-flight in Section 3.3.3.1. However, differences in surface topography can have further implications in a ToF-SIMS experiment. For example, Brandon cites a number of factors that influence the sputtering yield of a surface, including the take-off angle of the sputtered ions [Brandon and Kaplan, 2008]. Therefore, a physically non-uniform, but chemically uniform surface will result in differences in take-off angle from any collection point and hence differences in ion yield despite the chemical constancy of the surface. As ion yield is known to be a function of take off angle, a simple experiment was conducted in order to try

and remove this as a contributory factor. PTFE was selected as it is well characterised material with a chemically and physically uniform surface. PTFE is also used as a reference material for ISO 23830 for repeatability and constancy of the relative intensity scale [Lee *et al.*, 2011]. In addition, Lee states that PTFE has excellent area-to-area repeatability with high ion yields in addition to being easy to obtain and use.

4.2.2.1 Atomic Force Microscopy Sample Preparation and Analysis Conditions

Samples were prepared for atomic force microscopy (AFM) by placing the PTFE tape across a glass microscope slide. The roughness of the PTFE surface was measured by AFM. Measurements were carried out in contact mode using a DI Multimode atomic force microscope equipped with a Nanoscope IIIa controller (Veeco, Santa Barbara, CA).

4.2.2.2 ToF-SIMS Sample Preparation and Analysis Conditions

PTFE tape (RS Components, Nottingham, UK) was stretched across a standard ToF-SIMS sample stub. Five runs were completed, each over a 100 x 100 μm area using identical conditions, used to acquire the tablet spectroscopy data detailed in the previous chapter. Ion yields from hydrocarbon fragments in the positive mass range of m/z 0-200 will be analysed using ratio and standard deviation based calculations to look at the variability of the raw data. In addition, the effect of increasing mass number on data variance was also investigated. The implications of these experiments will be discussed in reference to the potential of raw ToF-SIMS data to be used for quantification purposes.

4.2.3 Magnesium Stearate – Varying the Surface Topography

Following the PTFE experiments it seemed that the next natural step would to be to introduce a measurable degree of surface topography to analyse the effect of this on the recorded data. This approach should help to establish to what degree surface topography influences data variance. Magnesium stearate was chosen as its sample surface can easily be changed using mechanical means once it is mounted on a sample stub. Magnesium stearate (Sigma-Aldrich Company Ltd., Dorset, UK) was

prepared using three different methods, detailed below, to produce surfaces of varying roughness.

4.2.3.1   SEM Sample Preparation and Analysis Conditions

Three samples of varying roughness were prepared. Aluminium disks were used for sample mounting. A simple method was devised, described as follows; double-sided sticky tape (3M) was applied to 10 mm diameter machined aluminium disks to provide a surface for the powder to adhere to. The disks were cleaned by ultrasonication in Analar grade acetone prior to sample preparation. In the first sample, the magnesium stearate was sprinkled onto the surface and the excess shaken off. In the second, an additional step of using the back of a spatula to gently smooth the powder was employed. In the final sample, the back of a polystyrene Petri dish was used to apply pressure in order to further smooth the powder surface. These samples will be referred to as "as received" (AR), flattened with spatula (SPAT) and PET Petri dish smoothed (PET) respectively.

SEM micrographs were obtained from a Philips XL30 utilising a lanthanum hexaboride filament operated at 5 keV and a working distance of 15 mm. The samples were gold sputter coated for 3 minutes with an Emscope 500 coater prior to SEM analysis.

4.2.3.2   Laser Profilometry Sample Preparation and Analysis Conditions

Samples were prepared in the same manner as detailed in Section 4.2.3.1. A Laser Profilometer (Scantron Proscan 1000) was used to measure the roughness values of each of the sample surfaces. Analyses were performed over a 2500 μm x 2500 μm area using a 500 x 500 pixel array. Roughness (ISO Ra) values were calculated for 6 lines per sample; three horizontal and three vertical lines were selected using even spacing.

4.2.3.3   ToF-SIMS Sample Preparation and Analysis Conditions

Samples were prepared in the same manner as detailed above in Section 4.2.3.1. Static ToF-SIMS measurements were performed on an ION-TOF ToF-SIMS IV instrument. The flood gun was operated at 30 μA to compensate for sample charging. A gallium pulsed primary ion beam was rastered across the sample. Analyses were

performed in imaging mode over a 384 x 384 µm area with a current of 1.5 pA for 1081 s. The dose was calculated to be 5 x 10^{12} ions cm^{-2}. Charge compensation was achieved by the use of an electron gun operated at 3 keV. The resulting signal is then mass analysed via software calibration using constant mass proportionality and linear regression. For each sample the 384 x 384 µm area analysed was split into a 4 x 4, 16 square grid to investigate the variance of ionisation over the total area.

The corrected intensity value of m/z 24^+ cation was measured in each square. Corrected intensity is defined as the Poisson-corrected summed intensity of the peak area [Malmberg *et al.*, 2011]. These values and the primary ion dose density (PIDD) were then used to calculate a theoretical sensitivity factor (SF) for the magnesium ion in each square with the aim of eliminating any variation in PIDD on ionization from the experimental results. The average and +/-% relative standard deviation (% RSD) of the SF across the grid was then calculated for each analysis area. Triplicate runs were completed for all three samples. The aim of the experiment was to evaluate whether the calculation of SFs, that can potentially be used for quantification purposes, were effected by surface roughness in a chemically uniform surface.

4.2.4   Glass – Introduction of a Second Chemical Component

Glass microscope slides (Scientific Laboratory Slides Ltd., Nottingham, UK) were used as a further model surface as they exhibit minimal roughness in their raw state and contain both silicon and sodium cations. This allows the effect of surface chemistry to be investigated in conjunction with roughness as the slides can easily be modified to introduce topographical features. AFM was used to evaluate the topography of the unmodified slides as they were too smooth for profilometry. Surface roughness was then introduced to the slide during shot peening, which is a cold working process where the surface of a material is bombarded with small spherical particles called shot. Each piece of shot striking the material acts as a tiny peening hammer and results in an indentation of the sample surface [Jeffus, 2004]. The glass slides were bombarded with alumina particles for 1 min. The roughness of these modified surfaces was then analysed using laser profilometry. Both silicon (Si) and sodium (Na) ion yields from the surfaces were analysed using ToF-SIMS.

4.2.4.1 **Atomic Force Microscopy Sample Preparation and Analysis Conditions**

Both unmodified and shot peened glass microscope slides were initially rinsed in acetone (Analar grade), then rinsed in methanol (Analar grade), and dried with nitrogen. (All solvents supplied by Sigma-Aldrich Company Ltd., Dorset, UK). The slides were then submersed in piranha solution (3:1 concentrated sulfuric acid to 30% hydrogen peroxide) for 5 minutes. The slides were then kept in tripled distilled water until required. The roughness of the unmodified slides was measured by AFM. Measurements were carried out in contact mode using a DI Multimode atomic force microscope equipped with a Nanoscope IIIa controller (Veeco, Santa Barbara, CA).

4.2.4.2 **Laser Profilometry Sample Preparation and Analysis Conditions**

The roughness of the slides that had undergone the shot peening process was measured via laser profilometry. Analyses were performed over a 2500 μm x 2500 μm area using a 500 x 500 pixel array using a Scantron Proscan 1000 (Somerset, UK). Roughness (ISO Ra) values were calculated for 6 lines per sample; three horizontal and three vertical lines were selected using even spacing.

4.2.4.3 **ToF-SIMS Sample Preparation and Analysis Conditions**

Samples were prepared in the same manner as detailed in Section 4.2.4.1. Slides were mounted onto standard ToF-SIMS sample stubs using double sided tape. Three analyses per slide were completed. The variance of the silicon and sodium ions was then analysed using the grid method described above in Section 4.2.3.3. The primary aims of this experiment were to look at the effect of having more than one chemical component on the production of SF and any effect that surface topography may have on this.

4.2.5 **The Effect of Altering the Primary Ion Dose on Ion Yield Variance**

The final experiments in this chapter assess the effect of varying the primary ion dose density (PIDD) up to the static limit discussed in Chapter 2. Four runs on an unmodified magnesium stearate powder surface were completed at steadily increasing PIDD values. This was achieved by altering the number of scans from 10

to 20 to 30 to 40. For each run the magnesium ion yield at m/z 24^+ was divided by the PIDD to give a theoretical SF.

4.3 Results and Discussion

4.3.1   Quantification of Tablet Data

The positive ion ToF-SIMS spectrum from a 60% wt/wt% paracetamol tablet is presented in Figure 4.1. Three key diagnostic ions were marked in the spectrum, for magnesium stearate at m/z 24^+, paracetamol at m/z 152^+, and spray dried lactose at m/z 365^+. The corrected area counts for the three key ions in six different areas on the 60 wt/wt% paracetamol tablet surface are presented in Table 4.1.

The table displays percentage values derived from the corrected intensity counts for the three individual key ions that were assigned to the three components. As previously discussed, corrected intensity is defined as the Poisson-corrected summed intensity of the peak area [Malmberg *et al.*, 2011]. For each ion the corrected counts were divided by the total counts for the three ions to elucidate a basic percentage ratio for the key components, magnesium stearate, paracetamol and spray dried lactose. These values were calculated for the six different analysis areas and then the standard deviation of these data sets was determined.

The mean % for magnesium cation at m/z 24^+ was 18.21 with a standard deviation of 3.77. The magnesium Mg^+ ion yield was around five times greater than the spray dried lactose $[M+Na]^+$ ion yield and approximately a fifth of the paracetamol $[M+H]^+$ ion yield. As discussed earlier in the chapter, sputtering yield is known to be affected by both the take-off angle of the sputtered ions and the incident angle of the beam on the surface. As the surface topography of the tablet was known to contain multiple peaks and troughs as highlighted by the SEM images in Chapter 3, Section 3.3.2.1, then it was reasonable to assume some of the variance in the sputter yield could arise from the physical variability of the sample surface. Ion yields are also known to vary due to matrix effects and as this is a multi-component surface then these may also be causing variance. Matrix effects have previously been shown to have varying impacts on key diagnostic ions [Weng and Chan, 2003]. (Matrix effects are introduced in Chapter 1 and will be discussed in more detail later in this work).

The standard deviation (σ) of 3.77 for the magnesium ion was a relatively high value, compared to the percentage value of 18.21. This could partly have been due to the low concentration in the formulation, but also due to its function as a surface

coating over all particles to improve flow and therefore its distribution can change under the compression forces exerted during manufacture. The bulk composition of the tablet was 60 wt% paracetamol, 0.5 wt% magnesium stearate and 39.5 wt% spray dried lactose. However, it could not be assumed that the surface was representative of the bulk composition. The positive ion images of the tables surfaces presented in Chapter 3, (Figure 3.25 to Figure 3.28), highlighted that the coverage of the different materials was typically uneven. As discussed in the previous chapter, magnesium acts as a slip agent and therefore 'spreads' across the surface. This mechanism may allow for a greater concentration of the stearate at the surface, so the actual surface concentration was likely to be higher at the surface than in the bulk as the stearate "coated" larger particles. This process may also have resulted in a large variance in the concentration at the surface and hence the high standard deviation value.

The paracetamol had a more stable ion percentage across the data sets, which more closely correlated with the bulk composition when compared to the other two components. This was reflected in the lower standard deviation (σ) of 3.70 relative to the average percentage value of 80.42. This high percentage value correlated with the SEM images shown in Chapter 3 (Figure 3.20) where paracetamol dominated the images, and appeared to be more evenly distributed than the other two components, particularly in the higher drug concentration formulations.

Spray dried lactose showed the largest variance in the data set presented, with a standard deviation (σ) of 0.55 from an average percentage of 1.37%. The low counts were likely to be attributed to the fact that ionisation tends to decrease as mass number increases [Brandon and Kaplan, 2008]. The positive ion ToF-SIMS image of the 60 wt/wt% tablet in Chapter 3 (Figure 3.27) indicated that the actual percentage at the surface could be far higher than that recorded by the % counts method used in this section. This observation was supported by the RGB analysis results reported in Section 3.3.2.4, where the spray dried lactose percentage for the 60 wt/wt% tablet was measured as 10.37% using this method. However, results from the experiments using PTFE recorded later in this chapter, demonstrated that lower counts do not typically result in greater variance. Therefore, it is most likely that in this case the high variance was primarily a function of the spatial distribution of spray dried lactose across the surface.

Overall, the data demonstrated the value of multiple replicates to gain an understanding of the reproducibility of ion intensity for a data set that included atomic and molecular cations over a range of m/z values.

The production of SF from raw materials could potentially eliminate the effect of ionisation potentials of different ions, which could then be applied to multi component samples. In the past ten years, the use of RSFs has become more common in ToF-SIMS particularly in the field of semi-conductor research [Veillerot *et al.*, 2011; De Witte *et al.*, 2000]. These RSFs allow for variations in secondary ion yield, but can also be matrix dependent [Hart *et al.*, 2011]. The following experiments are designed to assess the factors that may affect the calculation of SF for chemically or physically non uniform materials.
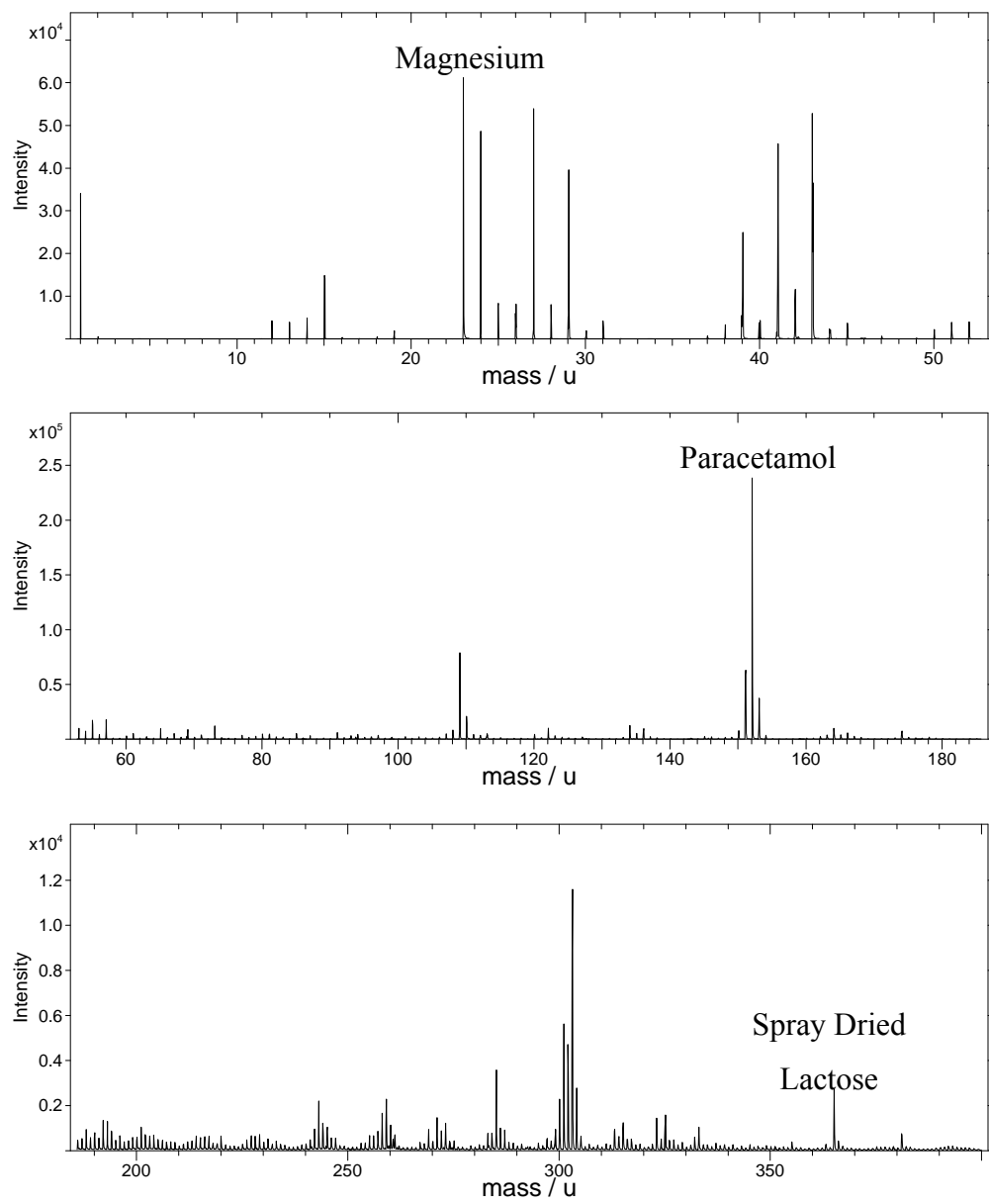
Figure 4.1 Positive ion ToF-SIMS spectrum of 60% paracetamol tablet

149

Area	Corrected Intensity Counts			Percentages		
	m/z 24^+	m/z 152^+	m/z 365^+	m/z 24^+	m/z 152^+	m/z 365^+
1	354963	1270708	33124	21.40	76.60	2.00
2	384532	1461717	22189	20.58	78.23	1.19
3	383519	1341827	18292	22.00	76.96	1.05
4	349724	1785034	13869	16.28	83.08	0.65
5	248967	1733575	41415	12.30	85.65	2.05
6	257249	1264159	20365	16.69	81.99	1.32
Average Percentage (%)				18.21	80.42	1.37
Standard deviation (σ)				3.77	3.70	0.55

Table 4.1 Calculated standard deviations for three key ions from a three component 60 wt% paracetamol tablet

4.3.2 PTFE – a Simple Model Surface

PTFE tape was analysed with AFM and ToF-SIMS to evaluate the effect of roughness on variance in ion yield.

4.3.2.1 Atomic Force Microscopy of PTFE

AFM was used to evaluate the PTFE surface, as its topography was too smooth for laser profilometry measurements to be able to give surface roughness values. The surface roughness values from AFM, over three runs, are presented in Table 4.2. The average ISO Ra value of the PTFE surface as measured by AFM was found to be 11.85 nm.

Ra (nm)			
Run 1	Run 2	Run 3	Ave
11.2	14.7	9.64	11.85

Table 4.2 Atomic force microscopy Ra measurement values of the PTFE surface

4.3.2.2 PTFE ToF-SIMS Measurements

Five sets of ToF-SIMS positive ion data were acquired on different surface areas of a single sample of PTFE. Seven key diagnostic ions were identified and selected for analysis. These seven key diagnostic ions can be observed in the positive ion ToF-SIMS spectrum presented in Figure 4.2, and are in correlation with those previously observed by Gilmore [Gilmore and Seah, 2000]. The corrected area counts for seven key diagnostic ions were measured and the ratio between each of these values and the corrected area count for m/z 169^+ was calculated. The average ion count ratios and the standard deviations of each ratio are presented in Table 4.3.

Ra values measured for this surface confirmed that the roughness values were in the nm scale, with a typical Ra value of just over 10 nm. Therefore, any variance in the data was unlikely to be due to topographical features.

The standard deviation was typically within 10% of the average count value for all the peaks in the range. This was comparable to the work completed by Green, who also cited a standard deviation scatter of around 10% in a flat sample [Green *et al.*, 2010]. In comparison, the standard deviation values for the 60 wt/wt% paracetamol tablet discussed in Section 4.3.1 varied between 5 and 50% of the average value for the three key diagnostic ions over a similar number of analysis areas (six in comparison to five for the PTFE experiments). The key PTFE diagnostic ions showed significant differences across the raw count figures, with the ionization efficiency of m/z 169^+ typically around 10% of that of m/z 31^+. Nevertheless, the standard deviation values did not appear to be effected by the ion intensity levels as they were reasonably consistent across the mass range analysed, i.e. as the mass to charge ratio of the key ions increased, the standard deviation did not appear to vary considerably. However, the greatest variability in the 60 wt/wt% tablet sample was observed in the highest mass diagnostic ion, i.e. the cationised spray dried lactose molecular ion, $[M+Na]^+$ at m/z 365^+. Therefore, it can be concluded that either the chemical and/or physical properties of the surface must have been introducing factors that affected data reproducibility, rather than the lower raw counts values observed in the higher mass ranges of the tablet samples. The 60 wt/wt% sample tablet contained three component organic systems with differing morphologies, chemistries and topographies. Results from multiple runs exhibited varying degrees of consistency in data reproducibility across the ions analysed. The data observed in the PTFE experiment indicated when these chemical and physical features were eliminated, flat and featureless chemically uniform surfaces produced consistent ToF-SIMS data with minimal variability. Therefore, it can be concluded that ToF-SIMS does have the potential for producing reliable quantitative data. However, the extent and subsequent effect of both chemical and physical non uniformity over the analysis area needs to be established, as the tablet data clearly demonstrated that either one, or both, of these factors played a significant role in the collection of reproducible data.
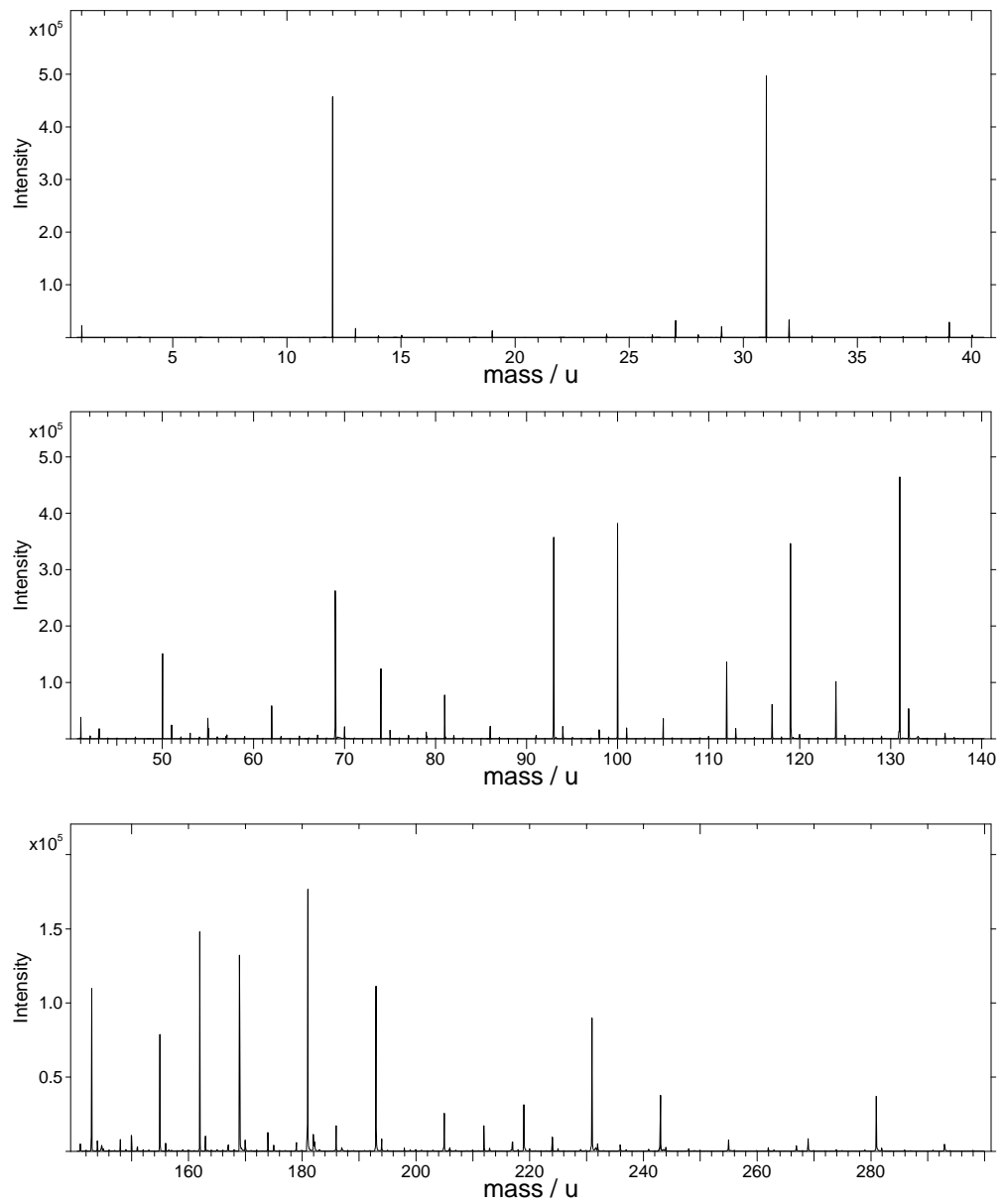
Figure 4.2 Positive ion ToF-SIMS spectrum of PTFE

Corrected area counts for all peaks on 100 x 100 μm areas numbered 1-5							
				m/z			
Area	31	69	93	100	119	131	169
1	2399256	1013811	587682	680921	520326	1226576	230866
2	2322891	1009568	594535	686641	524066	1233965	229451
3	2376139	1107461	635031	716177	596035	1255247	274085
4	2512772	1113228	655459	749955	569757	1329501	252107
5	2272037	1078282	651528	747728	591350	1262539	269948

Ratio of all peaks to m/z 169							
				m/z			
Area	31	69	93	100	119	131	169
1	10.39	4.39	2.55	2.95	2.25	5.31	1
2	10.12	4.40	2.59	2.99	2.28	5.38	1
3	8.67	4.04	2.32	2.61	2.17	4.58	1
4	9.97	4.42	2.60	2.97	2.26	5.27	1
5	8.42	3.99	2.41	2.77	2.19	4.68	1
Average	9.51	4.25	2.49	2.86	2.23	5.04	1.00
Standard Deviation	0.90	0.21	0.12	0.16	0.05	0.38	-

Table 4.3 Standard deviations values for positive peaks in the 0-200 mass range over 5 runs for ToF-SIMS analysis of PTFE

4.3.3 Magnesium Stearate – Varying the Surface Topography

Magnesium stearate powder with three different surface modifications was analysed with SEM, laser profilometry and ToF-SIMS to evaluate the effect of roughness on variance in ion yield.

4.3.3.1 Magnesium Stearate Scanning Electron Microscopy Micrographs

SEM micrographs of the three sample surfaces acquired at appropriate magnifications to be comparable to the 384 x 384 μm region analysed in the ToF-SIMS are presented in Figure 4.3 and Figure 4.4.

The AR sample micrograph is presented in Figure 4.3. Magnesium stearate "plate like" structures of approximately 5 μm can be observed in an open structure that does not appear to be compacted. The SPAT sample micrograph is presented in Figure 4.4. A closer, more 'knitted' together surface with multiple layers in different orientations can be observed. In the final micrograph of the PET sample, Figure 4.5, a further decrease in topography can be observed and the surface appeared to be much smoother. These figures clearly showed a qualitative decrease in surface roughness from Figure 4.3 to Figure 4.5.

4.3.3.2 Magnesium Stearate Laser Profilometry Measurements

Laser profilometry was used to establish quantitative data for comparison to the visually apparent reduction in surface roughness observed in the SEM micrographs. Results from triplicate runs for each sample are presented in Table 4.4.

The Ra values showed an increase in roughness from the PET to the SPAT and AR samples, with average roughness values from 1.75 μm to 7.78 μm. An increase of around 25% in Ra value was observed between the PET sample (1.75 μm) and the SPAT sample (2.16 μm). Results for the AR sample demonstrated an approximately 4-5 fold increase in roughness over the smoothest PET sample, with an average Ra value of 7.78 μm. These values correlated well with visual observations of the surfaces in the SEM micrographs, where the greatest degree of topography was observed in the AR sample, and the SPAT and PET samples exhibited a more consistent surface texture with less height variation in the Z plane.

Figure 4.3 SEM micrograph of magnesium stearate 'as received' (AR)
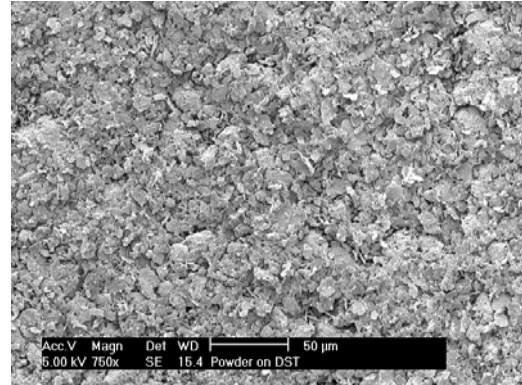
Figure 4.4 SEM micrograph of magnesium stearate smoothed with a spatula (SPAT)
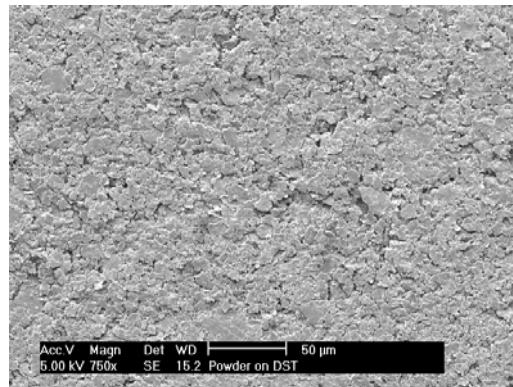
Figure 4.5 SEM micrograph of magnesium stearate flattened with a petri dish (PET)

		X and Y Ra Measurements (µm)							
		X1	Y1	X2	Y2	X3	Y3	Average	σ
	AR	8.61	7.04	6.35	9.19	7.15	8.28	7.78	1.09
Sample	**SPAT**	2.06	3.42	1.28	2.86	1.82	1.54	2.16	0.82
	PET	2.15	1.96	2.08	1.13	1.39	1.77	1.75	0.41

Table 4.4 Laser profilometry Ra measurements for the three magnesium stearate surfaces of decreasing roughness

4.3.3.3 **Magnesium Stearate ToF-SIMS Measurements**

The positive ion ToF-SIMS spectrum of magnesium stearate is presented in Figure 3.14 of Chapter 3 and the peak assignments for this spectrum are discussed in Section 3.3.1.2.

In each of the three samples, the three 384 μm x 384 μm analysis areas were split into 4 x 4 grids. The corrected intensity value of the m/z 24^+ ion was measured for each square in the grid. As described in Section 4.2.3.3, these values and the primary ion dose density (PIDD) were then used to calculate a theoretical SF for the magnesium ion in each square (i.e. the ion yield of the magnesium m/z 24^+ ion was divided by the PIDD). Although, the PIDD was the same for each square in these experiments, the method used could apply to experiments where the PIDD varied, such as the final experiment in this chapter. The average and +/-% relative standard deviation (RSD) of the SF across the grid was then calculated for all three samples. This data is presented in Table 4.5 and the results are discussed in the following paragraphs in conjunction with the roughness values reported in Table 4.4.

The data from Table 4.4 and Table 4.5 was combined to form Figure 4.6; where SF relative standard deviation values were plotted against the Ra values measured by profilometry for the three magnesium stearate samples with varying roughness. A comparative change can be observed between both the SF relative standard deviation and Ra values, as the magnesium stearate surface was compressed to different levels across the series. The greater the degree of compression, the lower the values observed for both data sets. Clearly, the relationship between the two did not appear to be linear. In the smoothest 1.75 μm (PET) sample the average % RSD value was approximately six times the Ra value of the sample at 11.36%, whereas the roughest 7.78 μm (AR) sample, had a corresponding average % RSD value of just over twice the Ra value, at 18.08%. The largest change in both data sets occurred between the AR and SPAT samples, with less subsequent change observed between the SPAT and PET samples. This indicated that surface roughness rapidly introduced data variability in relatively low roughness level (sub 5 μm) surfaces that were chemically homogenous.

		+/- % RSD			
		Run 1	**Run 2**	**Run 3**	**Ave % RSD**
Sample	**AR**	21.75	18.06	14.43	18.08
	SPAT	13.41	9.87	10.79	11.36
	PET	6.45	7.45	9.03	7.64

Table 4.5 Standard deviations of sensitivity factors expressed as +/-% RSD for the three magnesium stearate surfaces of decreasing roughness
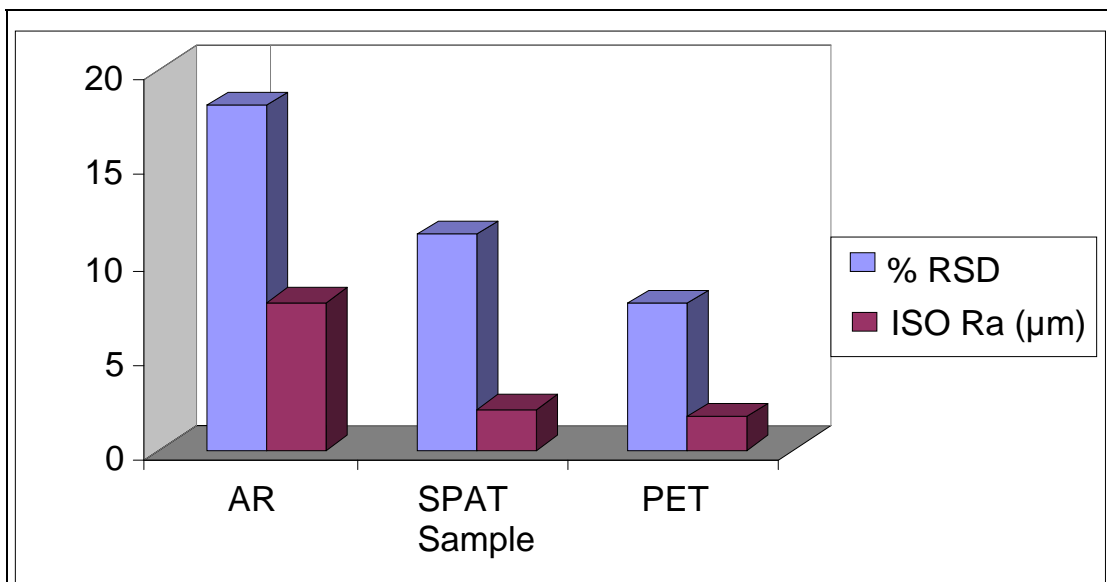
Figure 4.6 % RSD values in relation to Ra values for the three magnesium stearate surfaces of decreasing roughness (data from Tables 4.6 and 4.7)

In summary, Figure 4.6 highlighted that a small change in Ra, of the order of just 1 to 10 microns yielded a large change in % RSD. It also indicated that the calculation of SFs would not be straight forward for samples that exhibit surface topography in the micron range. Even for a chemically homogeneous inorganic surface such as magnesium stearate, the presence of the surface topography over a

few microns influenced the reproducibility of ion yield considerably. The implications of this are considerable in regards to using ToF-SIMS as a quantitative tool. For accurate and reliable quantification data to be gained it is clearly imperative that reproducible data must be acquired. Quantification can only be realistically useful if it is reliable and within an acceptable error limit. For example, 50% +/- 5% may be seen as tolerable, whereas 50% +/- 25% almost certainly would not.

The level of variation within the tablet data was assessed by looking at the standard deviations of the corrected area intensities. When these were expressed as % RSD values of the mean, values of 20%, 5%, and 40% were recorded for the magnesium stearate, paracetamol and spray dried lactose ions, respectively. Although the magnesium stearate and paracetamol % RSD values were similar to the magnesium stearate roughest and smoothest samples respectively, they were not directly comparable as variations in PIDD were not taken into account, and the surfaces were not chemically homogeneous. The spray dried lactose variation cannot be purely attributed to low counts in the higher mass region (m/z 365^+) as the PTFE experiments indicated that lower counts did not appear to directly affect data variation. Whether or not the increased counts that can be achieved through use of a higher initial dose improve data reproducibility will be investigated later in the chapter. Taken together the three previous experiments indicated that roughness effects appeared to be dual faceted, with both the chemistry (seen by variation in the tablet experiments) and degree of roughness (demonstrated by the magnesium stearate experiments) at the surface playing a role.

As ion yield is a function of bombardment angle [Brandon and Kaplan, 2008], these results suggested that the large variance in ion yield, caused by the topographical element, may have been due to shadowing effects. Although a positive correlation was clearly observed between the two data sets, the exact nature of the relationship was unclear. To this end, a larger sample set would need to be assessed; possibly using a material where surface roughness was more easily controllable or consistent. Despite the evidence that these large deviations could be due to localised topographical features, the % RSD value data from the 60 wt/wt% tablet indicated that there was potentially a further factor that may also have caused data variation,

surface chemistry. The following experiments involving unmodified and mechanically altered glass slides sought to assess this as an additional factor.

4.3.4 Glass – Introduction of a Second Chemical Component

Both unmodified and modified glass slides were analysed with AFM, laser profilometry and ToF-SIMS to evaluate the combined effect of surface chemistry and surface roughness on variance in ion yield. Two key atomic ions were selected for analysis, the silicon ion at m/z 28^+, and the magnesium ion at m/z 23^+.

4.3.4.1 AFM of an Unmodified Glass Microscope Slide

AFM was used to evaluate the surface of the slide, as its topography was too smooth for laser profilometry measurements to be able to give surface roughness values. The average ISO Ra value of the unmodified microscope slide measured by AFM was found to be 1.28 nm, with a low standard deviation of 0.06, indicating little variance from the average value across the three runs. These results are presented in Table 4.6.

Ra (nm)				
Run 1	**Run 2**	**Run 3**	**Average**	**σ**
1.22	1.33	1.28	1.28	0.06

Table 4.6 Atomic force microscopy Ra measurement values of
an unmodified glass microscope slide

4.3.4.2 Laser Profilometry of a Shot Peened Microscope Slide

Ra values for the shot peened microscope slides, measured by laser profilometry over three analyses in both the X and Y dimensions, are presented in Table 4.7. The ISO Ra value of the shot peen slide was found to be approximately 5.6 μm with a standard deviation value for the data set of 0.39. This represented a 5000 fold increase in surface roughness from the unmodified slide. The magnesium stearate experiments from Section 4.3.3 analysed the effect of roughness purely on the micron scale. However, roughness measurements on these glass based experiments indicated both nm and μm level roughness, allowing the influence of these different scales on data variability to be investigated.

X and Y Ra Measurements (µm)							
X1	**Y1**	**X2**	**Y2**	**X3**	**Y3**	**Average**	**σ**
5.6	4.9	5.5	5.8	6.2	5.8	5.6	0.39

Table 4.7 Laser profilometry Ra measurement values of a shot peened glass microscope slide

4.3.4.3   Glass ToF-SIMS Measurements

The positive ion ToF-SIMS spectrum of the unmodified glass microscope slide surface highlighting the two key atomic ions, Na^+ and Si^+, is presented in Figure 4.7. These ions were analysed using the grid method, previously described in Section 4.2.3.3, to produce SFs from the data for each square in the grid, % relative standard deviations for these values were then calculated. These % RSD values for unmodified and shot peened glass microscope slide surfaces are presented in Table 4.8.
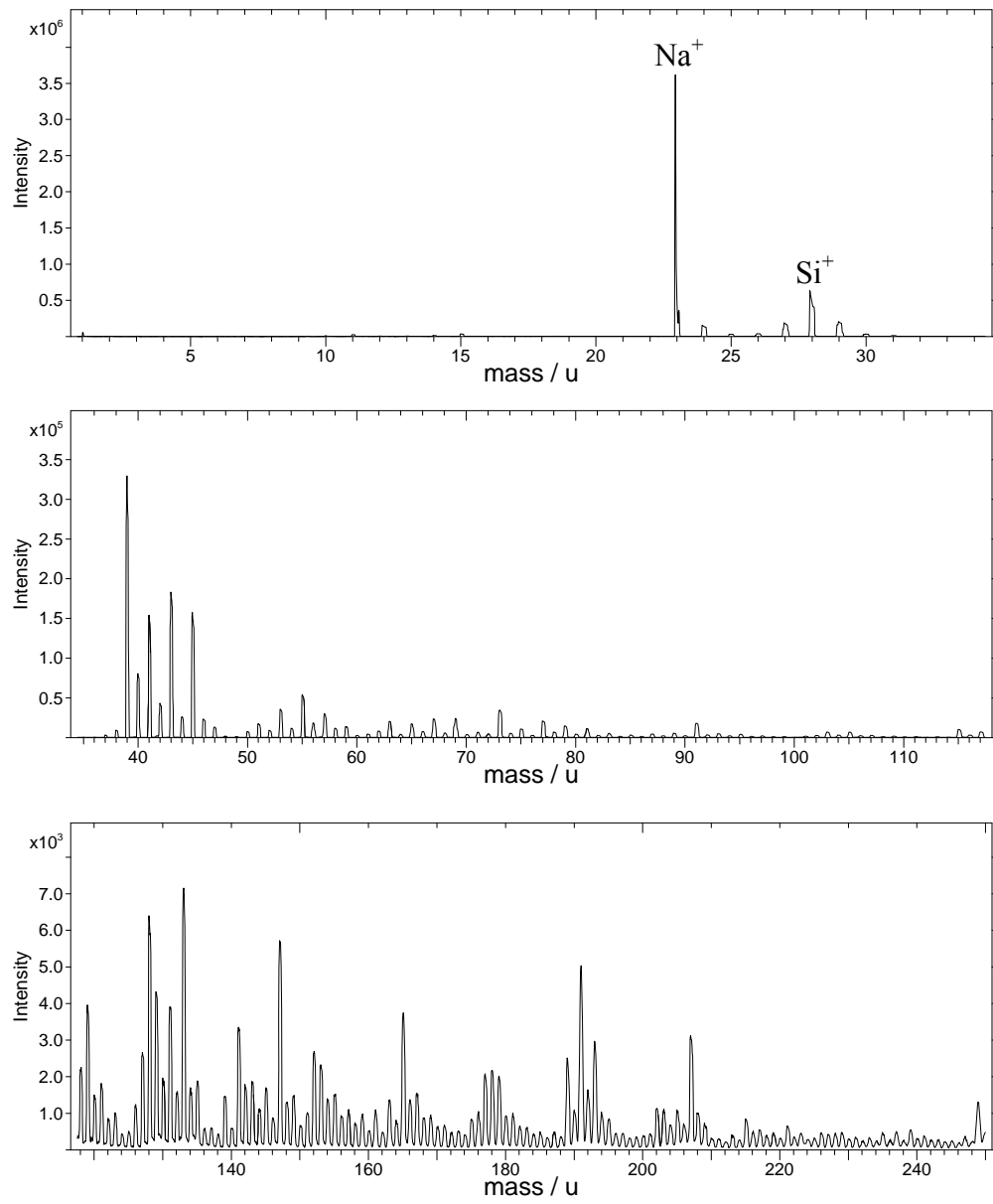
Figure 4.7 Positive ion ToF-SIMS spectrum of an unmodified glass microscope slide

Ion	As Received	Shot Peened
Na$^+$	0.29	58.73
Si$^+$	3.67	11.30

Table 4.8 % RSD values for unmodified and shot peened
glass microscope slide surfaces

Prior to modification, less than 1% RSD was observed in the Si ion at m/z 28$^+$, whereas approximately 3% RSD variance was observed in the Na ion at m/z 23$^+$. These values related to a surface with nanometre level roughness values and indicated that with a near perfectly flat surface at the nanometre scale there was very little variation in the sputtered ions over different areas once any fluctuation in PIDD is taken into account. As discussed earlier in the chapter, ToF-SIMS is often used as a quantification tool in electronics industries to assess doping in silicon wafers through the use of RSFs [Veillerot *et al.*, 2011]. The measurements taken from the glass slide in this experiment indicated that this was a viable and reliable method as very little variance was observed across the surface analysis area, and reproducible data could be obtained.

However, once the sample surface was mechanically altered by shot peening, the variability within the measured SFs increased considerably. From a figure of less than 1% RSD in the SF value for the unmodified surface, the % RSD value for the atomic Na ion increased 200 fold to a value of 58.73%. An increase of the same magnitude was not recorded for the atomic silicon ion, where the % RSD value only increased approximately three fold, from 3.67% to 11.30%.

The influence of the two different scales of surface roughness at the nm (untreated sample) and μm level (modified sample) had very different effects on the two atomic

ions. Initially, less variance was observed in the SF from the sodium ion than the silicon ion when measurements are taken at the nm level roughness scale. However, once roughness was introduced at the micron level scale, the effect of this increase in surface topography on the SF values was several times greater for the sodium ion than the silicon ion. The shot peened roughness level of 5.6 μm fell between the roughness values of the SPAT (2.16 μm) and AR (7.75 μm) magnesium stearate samples analysed in the previous section. The % RSD value for the sodium ion appeared to be comparable to the % RSD values from the SPAT and AR samples. The sodium ion variance at this equivalent roughness level was reported to be 11.30%, whereas the magnesium ion exhibited % RSD values of 11.36 and 18.08 in the SPAT and AR magnesium stearate samples, respectively.

In summary, Table 4.8 highlighted that for surfaces with topographical roughness at the nanometre scale, there were lower levels of data variance than observed for surfaces of the same material with surface roughness at the micron scale. Hence, it was clear that surface topography had a significant role in the reproducibility of ion generation across a surface in ToF-SIMS experiments. However, there was clearly a difference in % RSD values between the sodium and silicon ions for the untreated glass surfaces even when roughness was measured at the nm level. This suggested that there may also be chemical factors influencing the variance for such data sets. In addition, there was a difference in the way the variance of both ions substantially increased, the effect being greater for the sodium ion than the silicon ion once increased surface roughness was introduced. This data again also indicated that data variance was not only altered by surface roughness but that these changes in surface topography may also have affected different ions to a greater or lesser extent. The magnesium stearate experiments highlighted that roughness factors need to be taken into account when conducting SF calculations. The glass experiment added a further caveat, that not only did roughness affect the creation of these calculations, but that the surface chemistry itself could inherently impact the degree to which surface topography affected any SF calculation, and therefore also needed to be taken into account. The influence of the shot peening while intending to change the surface topography may have disrupted or changed the surface chemistry of the glass. For example, the shot peening may have altered the oxide layer which could in turn have had an impact on ion generation. Further insights into this area could be provided by

looking at different sample types and whether ions are affected consistently and across both polarities, e.g. would SiO_3^- show the same trend as the silicon atomic ion? Finally, it is worth commenting that given the significant changes in the variance in the data observed when the roughness values in this experiment moved from the nanometre to the low micron level, then the implications of using ToF-SIMS as a quantitative tool for irregular surfaces of much larger surface topographies in a chemically heterogeneous system seem somewhat limited.

4.3.5 The Effect of Altering the Primary Ion Dose on Ion Yield Variance

The final experiment in this series sought to analyse the effect of altering the primary ion dose density within the static limit. SF values were calculated for the magnesium ion from a magnesium stearate unmodified surface, using the grid method previously described. Sensitivity factors calculated for the magnesium ion over increasing scan periods from this unmodified magnesium stearate powder surface are presented in Table 4.9.

Table 4.9 highlighted that although increasing the PIDD (up to the static limit) appeared to slightly reduce the data variability, that this effect was relatively minimal. For the area analysed, 40 scans represented the static limit. Therefore, 'half' a static dose was used for the 20 scans experiment and a 'quarter' static dose in the 10 scans experiment. The average SF value was reasonably consistent for all experiments, which was expected as this represented the ion yield divided by the PIDD, i.e. as the PIDD increased so did the ion yield. Perhaps surprisingly though this increase in PIDD did not result in statistically improved data. Analysing up to the static limit has always been thought to improve the signal to noise ratio [Vickerman and Briggs, 2001]. However, it seems that even a relatively low PIDD may provide adequate data towards seeking quantitative information for suitable samples, and that current software is excellent at effectively removing noise when calculating peak areas.

Number of Scans	10	20	30	40
Sensitivity Factor (ion yield / PIDD) x 10⁻⁵	9.10	9.18	9.22	9.11
	10.30	10.30	10.40	10.10
	9.91	7.62	7.62	7.47
	4.46	4.47	4.50	4.52
	2.27	2.37	2.45	2.48
	2.97	3.09	3.11	3.01
	4.51	4.60	4.54	4.54
	4.60	4.67	4.67	4.62
Total SF values x 10⁻⁴	4.81	4.63	4.65	4.58
Average SF value x 10⁻⁵	6.02	5.79	5.81	5.73
Standard deviation x 10⁻⁵	3.2	2.9	2.9	2.8
+/- % RSD	53.16	50.09	49.91	48.87

Table 4.9 % RSD values for the magnesium atomic ion, from a magnesium stearate powder surface, presented over increasing time periods

4.4   Conclusions

The initial results in this chapter showed that there was substantial variance in the data acquired for 'real life' samples as highlighted by the standard deviation values seen in the 60% tablet sample. The main aim of this chapter was to assess the potential effect of roughness on ion yields and hence assess the impact this may have on any quantitative approach.

Experiments on a range of different materials were conducted in order to determine to what extent factors, other than differences in bulk composition, caused data variability and to assess whether ToF-SIMS can realistically be employed as a quantitative method for establishing concentrations of different species in the top few layers of a samples surface.

The initial experiments conducted on PTFE demonstrated that for a chemically and physically uniform surface the reproducibility of data was high. The results also demonstrated that this reproducibility was consistent both within the lower and high mass ranges analysed. Although these initial experiments seemed promising in regards to acquiring reliable data, once a homogenous material was modified to introduce roughness it became apparent that any topographical elements significantly influenced the data. This was seen via the variability in the detection of the magnesium atomic ion in magnesium stearate samples with varying roughness characteristics. As primary ion dose density has previously been reported as causing changes in ionisation yield [Brandon and Kaplan, 2008] the potential effects of any variance in the PIDD within the individual areas analysed was removed. This was achieved by dividing the counts for each area by the PIDD to give a SF for subsequent experiments within the chapter. The magnesium stearate experiments clearly showed that introducing roughness resulted in a correlating increase in data variance.

Preliminary investigations into the effect of surface chemistry showed that when two chemical elements were investigated in parallel, as with the unmodified and shot peened microscope slides, the magnitude of the effect of roughness appeared to be ion dependent.

Variation of the PIDD between the static limit and a quarter of the static limit was found to have a minimal effect on data variance.

As a whole the experiments in this chapter indicated that effective and accurate calculation of SFs can be only be achieved if both the influence of surface chemistry and surface topography are accounted for. In summary, there is clear evidence that surface topography has an influence on ion generation from the sample and that variance in data is significantly influenced by changing the surface roughness from the nanometre to the micron scale. It appears that even within the nanometre scale roughness the % RSD varies between ions generated, suggesting a surface chemical effect. Given that the range of surface roughness studied here range from nanometre to up to around the $10\,\mu m$ level, which is lower than one would expect for pharmaceutical formulations such as tablets, the influence of topography on ion variance between data sets could be higher for such samples. In addition, the chemical complexity of multi-component pharmaceutical formulations may also potentially contribute to variance in a data set.

The following chapter aims to use model surfaces to further investigate morphological surface features on data collection and analysis, and whether the geometry of features also has an effect. Previous studies have already shown that varying the matrix material can have a substantial effect on the ionisation behaviour and this will be further investigated in Chapter 6. All of these factors need to be assessed to establish whether ToF-SIMS can be realistically used as a quantitative technique.

Chapter 5.

The Role of Roughness in ToF-SIMS Analysis of Model Surfaces

5.1 Introduction

This chapter seeks to build on the results reported in the previous chapter, through the use of samples with controlled surface topography. Three different types of specimen were used to further investigate the role that the physical state of the surface plays in the potential use of ToF-SIMS as a quantitative technique.

5.1.1 Roughness Effects in ToF-SIMS Data Analysis

There is a large body of research in the literature that examines roughness in the context of ToF-SIMS which relates to dynamic SIMS experiments used for depth profiling and the changes in surface texture that occur during ion bombardment [Gui *et al.*, 2008; Goacher and Gardella, 2010; Garrison and Postawa, 2011]. However, the number of papers reporting the role of roughness on the reproducibility of ToF-SIMS data acquired under a static regimen were few.

In the mid 1990s, Barkshire states that the quantitative surface analysis is not possible due to image artefacts arising from surface topography [Barkshire *et al.*, 1996]. He proposed a method for identifying and removing areas from Auger images that dominated contrast measurements. It was concluded that this method could be directly applicable to other surface sensitive techniques, such as SIMS, for inhomogeneous sample surfaces.

The effects of surface topography on ToF-SIMS ion images have been studied [Lee *et al.*, 2008]. Gold wires of three different diameters were imaged using a bismuth primary ion source. They concluded that samples should be analysed in an orientation that minimises geometrical distortions, be in good contact with a flat conductive substrate, and field effects caused by topography can be reduced by reducing the extractor voltage to a minimum of 500 volts.

Wagner also stated that quantification from ToF-SIMS images can be hindered by topography [Wagner, 2008]. Pixel by pixel normalising methods used to quantify chemical compositions from flat samples were found to be unsuitable for samples with significant topography.

5.1.2   Aims of the Chapter

The aims of this chapter are to build on the results from the previous chapter through the use of materials with pre-defined roughness profiles.

In the first instance, varying grades of abrasive paper were selected as they exhibit roughness profiles that are controlled to achieve their function. The second set of samples show even tighter control of surface topography parameters; these are calibrated precision measurement samples used as precision reference specimens for surface metrology. Four samples of different grades of abrasive paper were selected for analysis and three precision measurement samples. In all cases the samples were gold coated to provide a chemically homogeneous surface and large area analyses of 384 μm x 384 μm were completed.

The data variance across these areas was then measured through the use of SF calculations, allowing for any discrepancies in the primary ion dose density (PIDD). This data was compared to the roughness values recorded for each sample.

A final set of experiments was carried out to specifically assess the impact of varying the distance between the analysis area and the extractor. This experiment effectively mimics the effect of height changes in a sample surface and evaluates whether variance in the normalised total ion counts from diagnostic ions can be attributed to this. This experiment used a gold coated microscope with minimal surface topography.

5.2   Materials and Methods

5.2.1   Gold Coated Abrasive Papers

There are three main systems that are used to grade abrasive papers. They include the FEPA system which prefixes the grade number with the letter 'P' and requires a relatively high tolerance standard in regards to the grit size distribution within the paper [Jewitt, 2004]. Due to the smaller tolerances required during manufacture, this type of abrasive paper was selected for use in this study as a model surface in order to exploit the tighter grit size distribution. Four grades of paper were purchased from P240 to P1200 (RS Components, UK), roughest to smoothest respectively. These samples were gold coated for 3 minutes using an Emscope 500 coater (Emscope, Ashford, UK) operated at 15 µA and laser profilometry was employed to assess surface roughness. The effect of the variance in roughness on ionisation of key gold cations and anions was then measured using ToF- SIMS across the four samples.

5.2.1.1   Laser Profilometry Sample Preparation and Analysis Conditions

Samples were prepared by cutting 10mm x 10mm squares from each of the gold coated abrasive paper grades and mounting these onto aluminium disks. The disks were cleaned by ultrasonication in Analar grade acetone prior to sample preparation. The sample construction is shown in Figure 5.1. A laser profilometer (Scantron Proscan 1000) was used to measure the roughness values of each of the sample surfaces. Analyses were performed over 2500 µm x 2500 µm areas using a 500 x 500 pixel array. Roughness (ISO Ra) values were calculated for three lines per sample, selected using even spacing.

Figure 5.1 Schematic diagram representing laser profilometry sample construction for gold coated abrasive papers
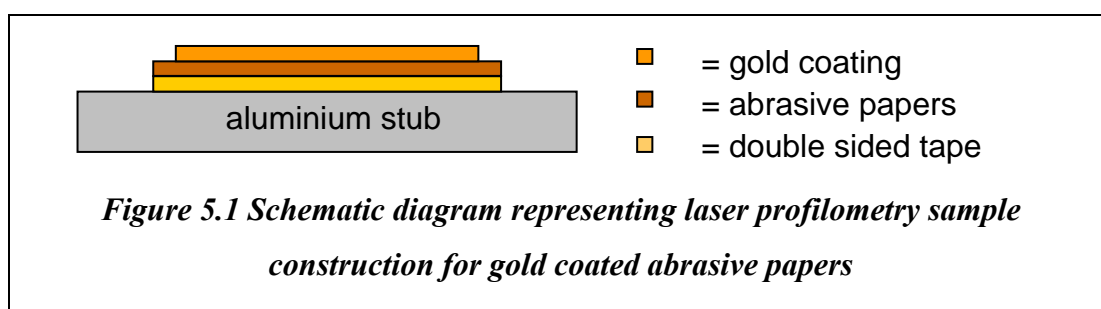
5.2.1.2   SEM Sample Preparation and Analysis Conditions

Samples were prepared as per Section 5.2.1.1. The aluminium stubs were directly mounted onto SEM stubs, using carbon tabs (Agar Scientific Ltd., Essex, UK). SEM micrographs were obtained from a Philips XL30 Scanning Electron Microscope

utilising a lanthanum hexaboride filament operated at 5 keV and a working distance of 15 mm.

5.2.1.3   ToF-SIMS Sample Preparation and Analysis Conditions

Samples were prepared as per Section 5.2.1.1. The same method as used in the previous chapter, and described below, was used to analyse the variance in the sputtered ion counts. Static ToF-SIMS measurements were performed on an ION-TOF ToF-SIMS IV instrument (ION TOF GmbH, Münster, Germany). In all experiments gallium was used as the primary ion. The flood gun was operated at 3 keV, 30 μA to compensate for sample charging. In all cases the analysis dose was kept below the static limit of 1×10^{13} ions cm^{-1}. For each sample a 384 x 384 micron area was analysed. This was then split into a 4 x 4, 16 square grid to investigate the variance of ionisation over the total area. The corrected intensity values of the m/z 197$^-$ (Au) and 591$^-$ (Au$_3$) ions in the negative ion ToF-SIMS spectrum, and 197$^+$ (Au) and 591$^+$ (Au$_3$) ions in the positive ion ToF-SIMS spectrum, were measured in each square. These values were then used in conjunction with the primary ion dose density (PIDD) to calculate a theoretical SF for the individual ions in each square. The average and +/-% relative standard deviation (RSD) of the SFs across the grid was then calculated for all four samples. Positive and negative ToF-SIMS ion images of the samples were also acquired. Triplicate runs from each sample were completed.

5.2.2   Rubert Precision Measurement Samples

Rubert & Co Ltd. (Manchester, UK) specialise in producing comparison specimens for surface roughness control in manufacturing, and precision reference specimens for surface metrology. Their precision reference samples are most often used with stylus-type contacting surface measuring instruments as standardised in ISO 3274, but are increasingly being used for checking optical and non-contacting instruments, especially with regard to roughness parameter evaluation [www.rubert.co.uk]. These samples were selected as they are ideal candidates for model surfaces due to the tight control on the surface texture. Three samples with varying roughness parameters were purchased as summarised in Table 5.1.
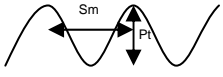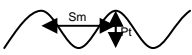
Sample ID	Parameter Values	Roughness Value	Shape	Profile
526	Sm = 100 μm Pt = 10 μm	Ra = 3.15μm	Sine wave	
530	Sm = 100 μm Pt = 3.0 μm	Ra = 1μm	Sine wave	
543	Sm = 2.5 μm Pt = 0.12 μm	Ra = 0.04μm	Sine wave	

Table 5.1 Specifications for Rubert Precision Measurement samples

5.2.2.1 ToF-SIMS Sample Preparation and Analysis Conditions

The precision measurement samples supplied by Rubert were cleaned by ultrasonication in Analar grade acetone prior to sample preparation. The samples were gold sputter coated for 3 minutes with an Emscope 500 coater prior to analysis and mounted onto aluminium stubs (also cleaned in acetone, as per above). ToF-SIMS measurements were completed as per Section 5.2.1.3, i.e. the corrected intensity values of the m/z 197$^-$ (Au) and 591$^-$ (Au$_3$) ions in the negative ion ToF-SIMS spectrum, and 197$^+$ (Au) and 591$^+$ (Au$_3$) ions in the positive ion ToF-SIMS spectrum, were measured in each of the 16 squares within the grid.

5.2.3 Gold Coated Glass Microscope Slides

The previous chapter suggested that the data variance could have been caused by shadowing effects. However, changes in the physical height of the analysis point

may also result in changes in the ion yield. A simple experiment was designed to investigate this potential phenomenon. In the previous chapter the surface topography of glass microscope slides was investigated and found to exhibit minimum roughness, typically in the nanometre region. The previous chapter also demonstrated that flat surfaces typically exhibit minimal variance across a chemically uniform surface. Therefore, a glass microscope slide was selected as the base material due to its minimal surface topography. The slide was then gold coated using the same conditions cited in Section 5.2.1, to provide a homogeneous surface. This sample then underwent analysis in the ToF-SIMS by moving through the optimal height over a 40 micron Z range to investigate the effect of height changes on ionisation yields.

5.2.3.1 ToF-SIMS Sample Preparation and Analysis Conditions

Static ToF-SIMS measurements were carried out using the conditions as described in Section 5.2.1.3. Analyses were performed at five heights over a single 384 x 384 micron area. In each case the duration of the experiment was calculated to be one fifth of the static limit. (The previous chapter has shown that reducing the dose has little effect on data variance.) Therefore, the total dose for the experimental area was kept below the static limit. The optimum height was referred to as zero. The stage was then moved to zero minus 10 microns, zero minus 20 microns, zero plus 10 microns and zero plus 20 microns to obtain the five heights required. The corrected area counts were measured in the ToF-SIMS positive ion spectrum for gold cations at m/z 197^+ and m/z 591^+ and in the ToF-SIMS negative ion spectrum for the respective anions at m/z 197^- and m/z 591^-.

5.3 Results and Discussion

5.3.1   Gold Coated Abrasive Papers

Abrasive papers of four different grades were gold coated and analysed by profilometry and SEM in order to assess the roughness characteristics at each surface. ToF-SIMS analysis was then performed in order to assess the effect of this roughness on variance in ion yield.

5.3.1.1   Laser Profilometry of Gold Coated Abrasive Papers

Ra measurements for the four different grades of abrasive papers, as measured by laser profilometry, are presented in Table 5.2.

Sample	Ra Measurements (μm)				
	Run 1	Run 2	Run 3	Ave	σ
P240	14.4	14.1	13.5	14.0	0.46
P400	8.0	7.9	7.4	7.77	0.32
P800	5.9	5.6	6.1	5.87	0.25
P1200	4.9	4.8	4.9	4.87	0.06

Table 5.2 Laser Profilometry Ra measurements for the four grades of gold coated abrasive papers

Roughness values of 4.87, 5.87, 7.77 and 14.0 μm were recorded for the four samples from P1200 to P240, respectively. The lowest grade of abrasive paper (P240) was approximately three times as rough as the highest grade of abrasive paper (P1200), and approximately twice as rough as the P400 paper. The standard deviation values showed that the results were reasonably consistent, with all exhibiting less than a 5% relative standard deviation to the mean values.

5.3.1.2   SEM of Gold Coated Abrasive Papers

SEM micrographs of each of the four gold coated abrasive paper samples are presented in Figure 5.2. A qualitative decrease in roughness can be observed from the lowest to the highest grade of abrasive paper. These images correlated well with the roughness values reported in the previous table. The two highest grades of abrasive paper visually appeared to be closer together in terms of surface texture than the lower grades, again reflecting the results from the laser profilometry. A significant jump in surface topography from the P400 to the P800 grade can be observed, with the grit in the P800 paper appearing to be larger in size and less tightly packed. There was no directionality within the surface topography and the distribution of the grit appeared to be random.

Sample P240	Sample P400
Sample P800	Sample P1200

Figure 5.2 Scanning Electron Micrographs of the four grades of
gold coated abrasive papers
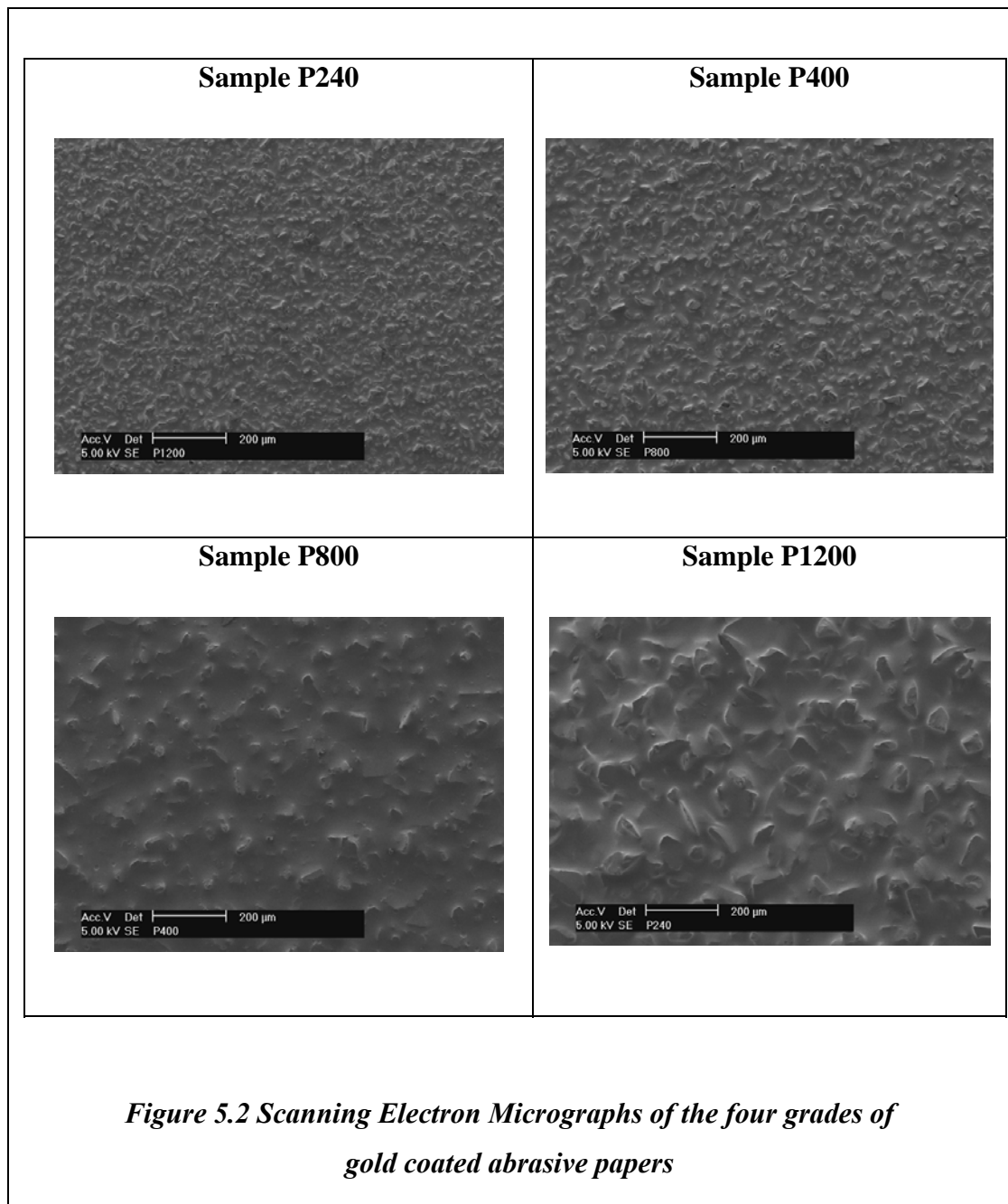
5.3.1.3 ToF-SIMS of Gold Coated Abrasive Papers

The positive and negative ion ToF-SIMS spectra with the key gold ions highlighted are presented in Figure 5.3 and Figure 5.4, respectively. Diagnostic ions at m/z 197 and m/z 591, representing the Au and Au$_3$ ions were clearly observed in both spectra.

Both positive and negative ToF-SIMS ion images were taken for each of the samples from the corresponding mass spectra. Those with the greatest range of roughness

values, the P1200 and P240 samples, are presented in Figure 5.5 and Figure 5.6, respectively.

Burst alignment mode was selected for the ToF-SIMS experiment. As discussed in Chapter 2, this mode allows better spatial resolution which is evident from the images produced from these spectra in Figure 5.5 and Figure 5.6. However, this mode does result in substantially reduced mass resolution, hence the peak broadening that can be observed in both the positive and negative ToF-SIMS ion spectra.

The images in Figure 5.5 and Figure 5.6 correlated well with the SEM images presented in Figure 5.2. In the finer P1200 grade abrasive paper, a smaller grit size was clearly evident, whereas in the P240 sample the grit size was considerably larger. It was notable that the negative ion image appeared to more clearly highlight the "troughs", and the positive image the "peaks", this phenomenon was particularly evident in the finer grade images. Again, no specific directionality was observed within the images.
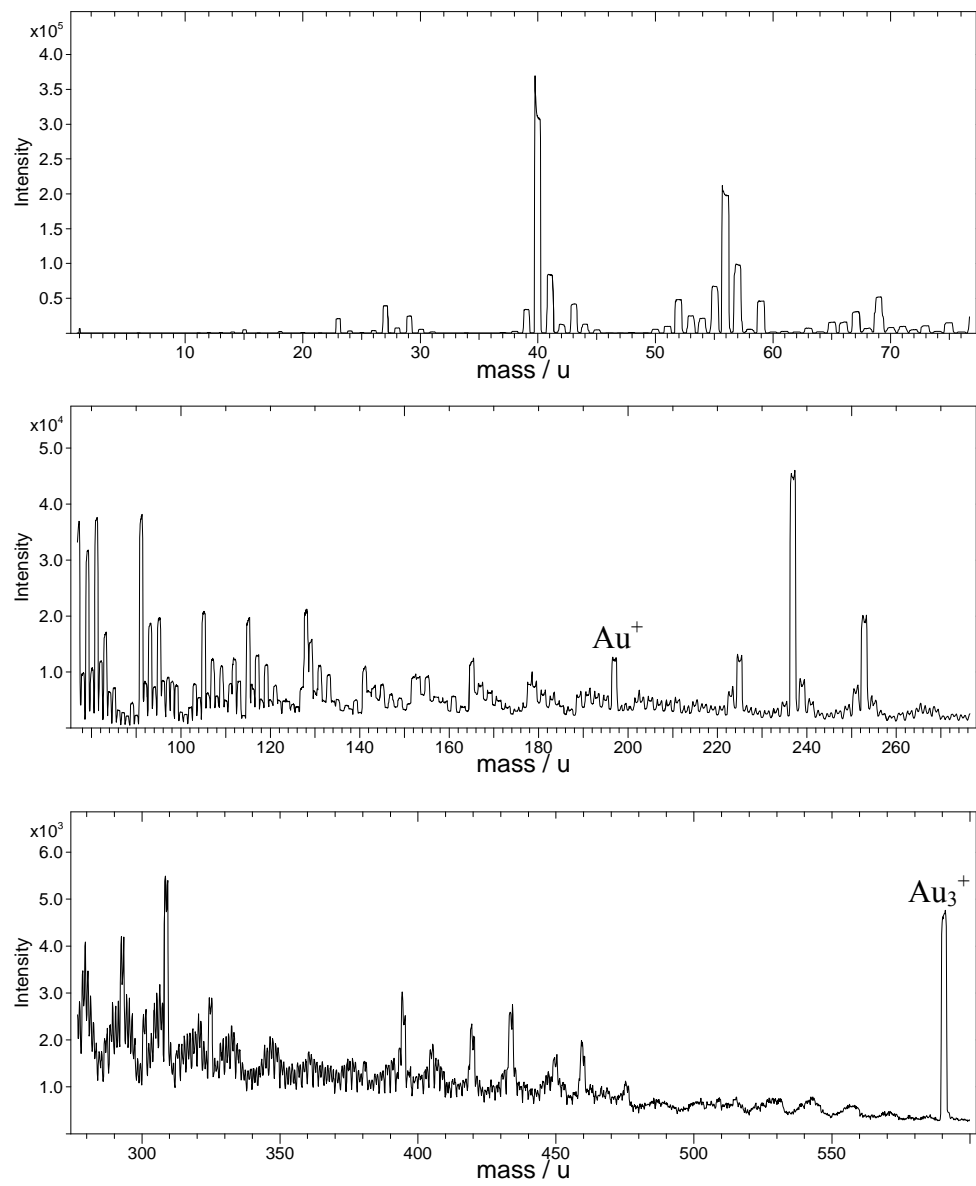
Figure 5.3 Positive ion ToF-SIMS spectrum of P1200 gold coated abrasive paper
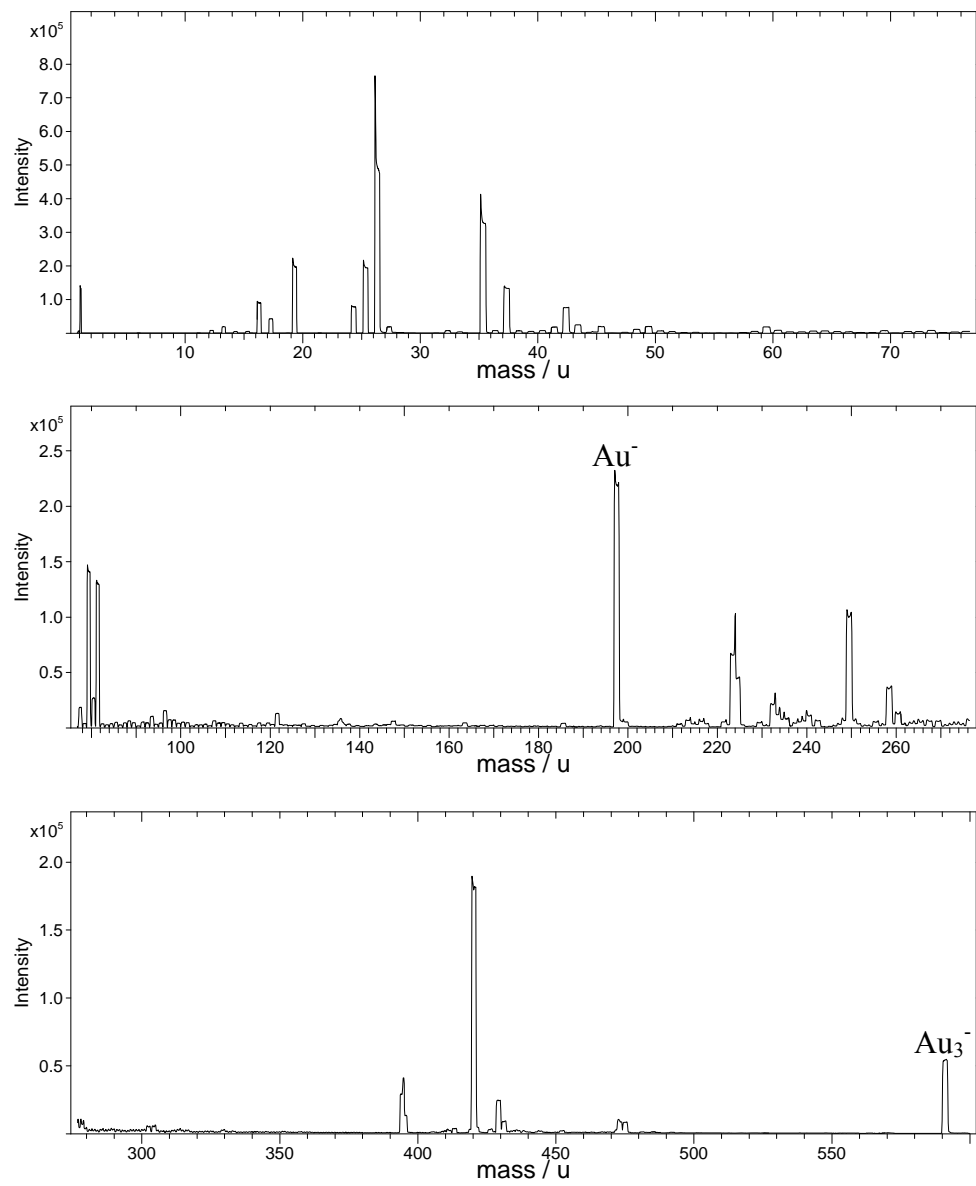
Figure 5.4 Negative ion ToF-SIMS spectrum of P1200 gold coated abrasive paper
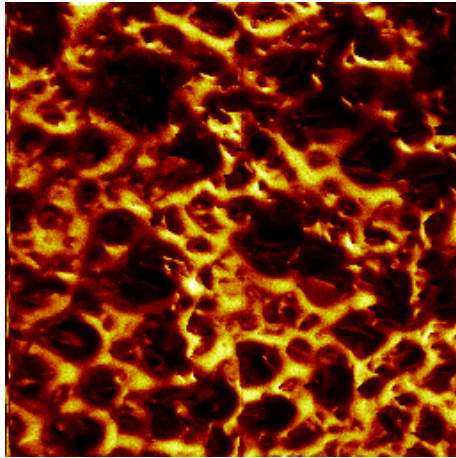
Negative ion Image   **Positive Ion Image**
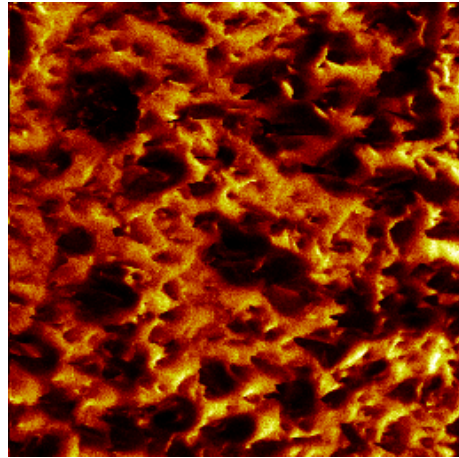
Figure 5.5 ToF-SIMS ion images of the P1200 grade gold coated abrasive paper

(384 x 384 μm)
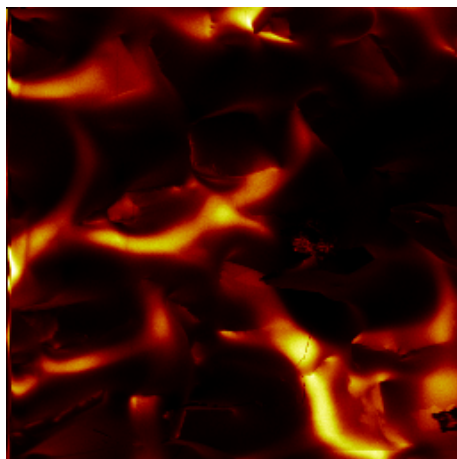
Negative ion Image   **Positive Ion Image**
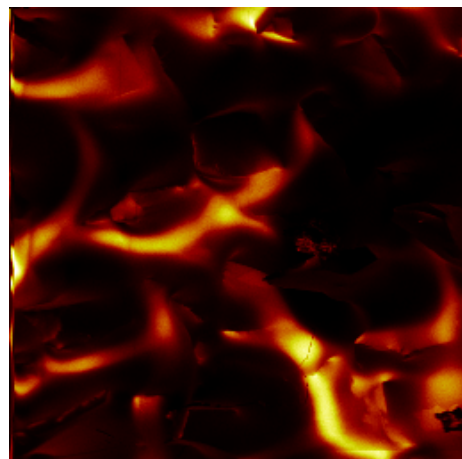
Figure 5.6 ToF-SIMS ion images of the P240 grade gold coated abrasive paper

(384 x 384 μm)

As per the previous chapter SFs were determined for both the gold cations and gold anions, the exact methodology for these samples is described in Section 5.2.1.3. The variance in these values across the analysis area was then calculated by dividing the area into a 4 x 4 grid and measuring the standard deviation across this grid. A bar chart of the average standard deviation values for the Au and Au_3 anions is presented in Figure 5.7. These variance values were then plotted against the Ra values acquired in the laser profilometry experiments. This data is presented for the negative Au and Au_3 ions in the line graph in Figure 5.7. The raw data for these charts and graphs are provided in Appendix 1. The values reported are averaged over three separate sample runs and sought to evaluate data repeatability. Data repeatability is a key factor that Green *et al.* identified as needed as SIMS becomes more widely used in industry to analyse complex samples [Green *et al.*, 2010].

Figure 5.7 Bar Chart and Line Graph of ToF-SIMS negative ion variance in relation to abrasive paper grade and Ra respectively

(Blue = m/z 197⁻ and Pink = m/z 591⁻)
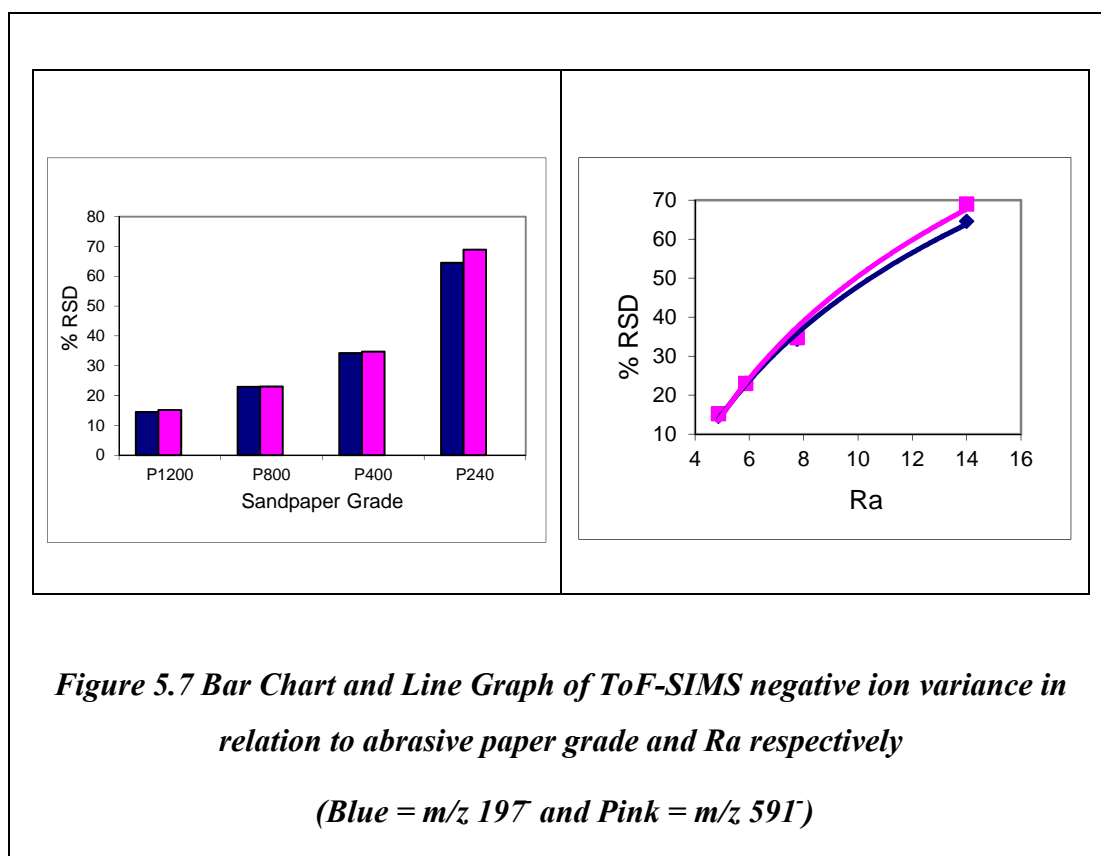
The bar chart in Figure 5.7 highlighted the increase in data variance for the Au and Au_3 anions from the smoothest to the roughest sample, ranging from approximately 15% to 65% for P1200 to P240, respectively. In each case the variance was marginally higher in the lower mass ion (m/z 197⁻) than the higher mass ion (m/z

591⁻), with the largest change occurring between the two lowest grades of abrasive paper and most visible in the P240 abrasive paper. Overall, there was generally good agreement between the two sets of data for the observed trend of increasing roughness resulting in increasing data variance, i.e., as Ra increased % RSD also increased. This correlated well with previous studies reported in Chapter 4. The profilometry results in Figure 5.7 showed that the roughness value for the lowest grade of abrasive paper was approximately three fold that of the highest grade of abrasive paper. The ToF-SIMS results highlighted that the increase in variance caused by this roughness was around four fold. Therefore, it can be concluded that the variance in data does not appear to increase linearly with surface morphology but there is a general trend observed, the rougher the sample, the greater the % RSD.

A bar chart of the average standard deviation values for the Au and Au_3 cations, and corresponding line graph showing these values in comparison to Ra values, is presented in Figure 5.8. Again a positive correlation between the variance in data and the roughness of the sample is observed, with the largest change occurring between the two lowest grades of abrasive paper. The comparative increased level of variance between the lower and higher mass ion is also worthy of note. Although, a greater variance value for the higher mass ion was noted in the anions, this was more pronounced in the cations. Again, this effect appeared to be more significant as the level of surface texture increased, highlighted by the steeper gradient in the line graph that mimicked that observed for the ToF-SIMS negative ion results. In addition, the variance value for each cation was in every case slightly less than that of the respective anion. Therefore, it can be concluded that in the case of gold coated samples roughness played a greater role in data variance on the negative ion ToF-SIMS spectrum than the positive ion ToF-SIMS spectrum for the ions selected.

A 3D bar chart that amalgamates the data above is presented in Figure 5.9. This figure also includes the results for the control sample, a gold coated microscope slide with minimal surface texture at the sub-micron level. The histogram visually reinforces the relationship where with each ion a stepped increase can be observed as roughness increases, and in each case the effect is greater in the negative ion than the positive ion.

These results would indicate that the calculation of a single RSF for any element would be difficult and also be mass dependent. Weng *et al.* have also previously found in their attempts to calculate SFs for styrene-butadiene copolymers that they can only successfully do so for certain diagnostics at specific mass to charge ratios, whereas this cannot be achieved for other ions within the same material [Weng *et al.*, 1995]. Lee also comments that providing quantitative chemical information of surfaces with topography remains a significant challenge due to the lack of systematic and validated measurement methods [Lee *et al.*, 2008].
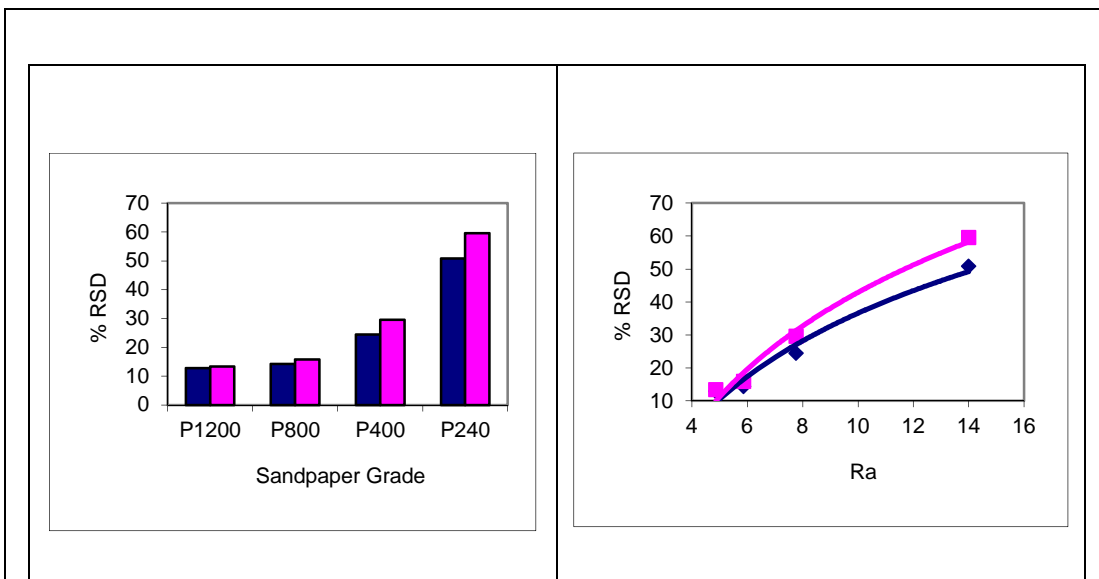
Figure 5.8 Bar Chart and Line Graph of ToF-SIMS positive ion variance in relation to abrasive paper grade and Ra respectively

(Blue = m/z 197$^+$ and Pink = m/z 591$^+$)
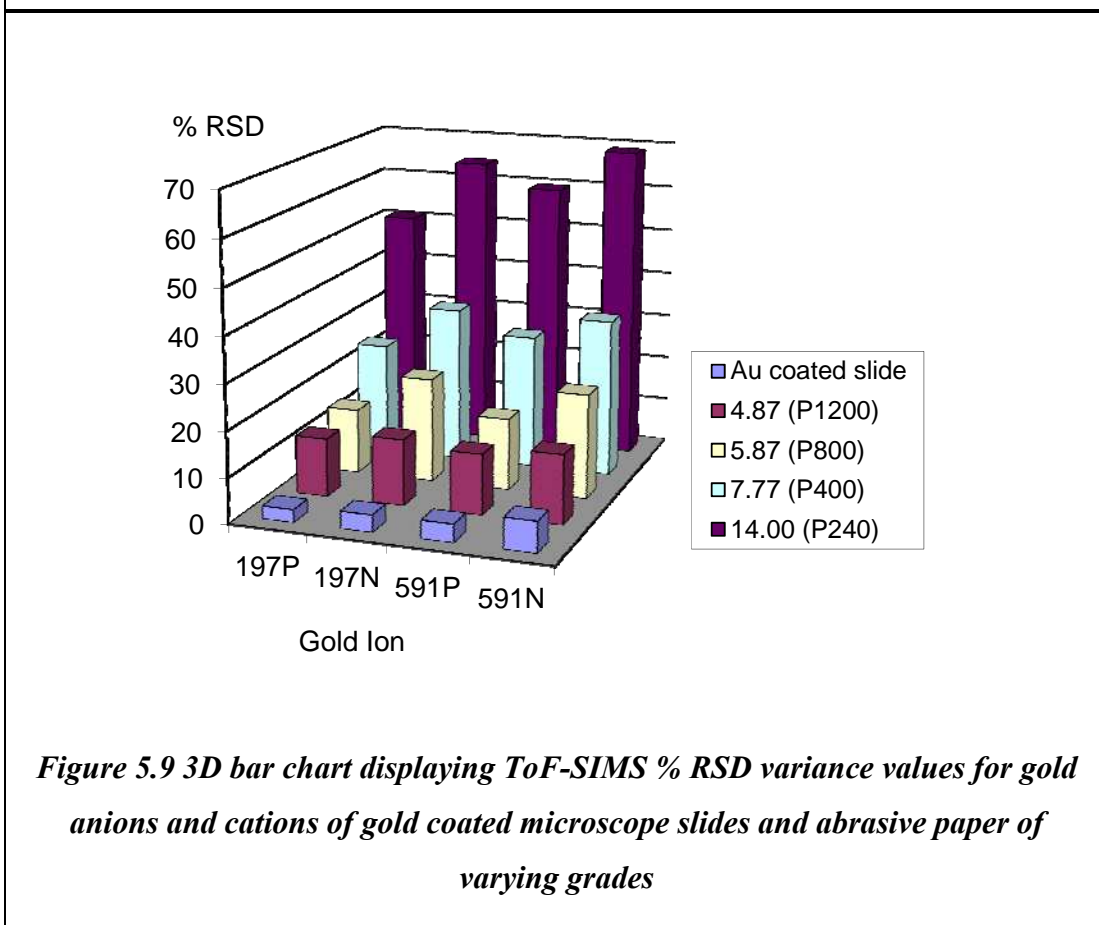
Figure 5.9 3D bar chart displaying ToF-SIMS % RSD variance values for gold anions and cations of gold coated microscope slides and abrasive paper of varying grades

5.3.2   Rubert Precision Measurement Samples

Three varying precision measurement samples were analysed by ToF-SIMS in order to assess the effect of this roughness on variance in ion yield, following gold coating. Ra values for the samples were provided by Rubert and are presented earlier in the chapter in Table 5.1.

5.3.2.1   ToF-SIMS of Rubert Precision Measurement Samples

Sensitivity factors were determined for both gold cations and anions as per the abrasive paper experiments reported above. The variance in these values was then calculated by dividing the area into a 4 x 4 grid and measuring the standard deviation across this grid. A bar chart of the average standard deviation values of ToF-SIMS positive and negative gold (Au and Au_3) ion variance is presented in Figure 5.10. The values reported were averaged over three separate sample runs.

In the anions an increase in variance was observed from the smoothest to the roughest sample, with % RSD values of 16.25%, 23.12% and 27.36% for m/z 197⁻ ion, and 10.03%, 20.20% and 23.99% for the m/z 591⁻ ion for the 543, 530 and 526 samples, respectively. In all three samples, the variance in the anions was greater at m/z 197⁻ than m/z 591⁻. The stepped increased in variance was more pronounced between the 543 and 530 sample, than from the 530 to 526 sample. The respective Ra values for these samples were 543 – 0.04 μm, 530 - 1.0 μm and 526 - 3.15 μm (see Table 5.1). Therefore, the results indicated that the rate of variance increase was greater for sub-micron scale roughness values, the rate of variance tailored off as the roughness exceeded these values, and that the relationship between rate of variance and roughness was not linear.

These results were consistent with the magnesium stearate results reported in the previous chapter i.e., as roughness increased a corresponding increase in variance was also observed. The same methodology was used with three magnesium stearate sample surfaces of varying roughness. % RSD values of 7.64% and 11.36% were recorded for the Mg^+ ion from samples with Ra values of 1.75 μm and 2.16 μm. These rates of variance were lower than the % RSD values from the gold ions recorded for samples with similar Ra measurements of 1.0 μm and 3.15 μm (% RSD values of 23.12% and 27.36% for m/z 197⁻ ion, and 20.20% and 23.99% for the m/z

591⁻ ion, respectively). This indicated that these gold anions from a homogeneous surface were more susceptible to variance than the magnesium cation from a magnesium stearate based chemistry.

The precision measurement results for the gold anions were also consistent with the gold coated abrasive paper results reported earlier in this chapter. In terms of roughness, the gold coated abrasive paper with the lowest Ra value of 4.87 μm, P1200, was most comparable to the precision measurement samples. The average gold anion variance in this P1200 sample was measured at 12.82% and 13.31% for the m/z 197⁻ and m/z 591⁻ ions, respectively. These values were more consistent with the precision measurement sample anion % RSD values from 543 sample with the lowest roughness value of 1.0 μm. This indicated that not only did topography play a part in data variability, but that the directionality / regularity of the surface features may also have influenced the effective calculation of SFs. Lee has also previously observed this phenomenon and recommended that samples with directionality should be analysed in an orientation that minimises geometrical distortions, for example along rather than perpendicular to a fibre [Lee *et al.*, 2008].

In the anions, the increase in the level of variance was more significant in the lower mass anion. However, the relationship between roughness and data variability was not as clear for the positive gold cations. From the smoothest to the roughest sample, % RSD values of 2.98%, 30.40% and 17.10% were recorded for m/z 197⁺ ion, and 5.21%, 23.99% and 16.72% were recorded for the m/z 591⁺ ion, respectively. While in the cations ions, and all previous experiments, there was an increase in the variance between the sample with the lowest and highest Ra values, this direct relationship was not followed when cation variance was compared to roughness for the precision measurement samples. For both m/z 197⁺ and m/z 591⁺ the highest level of variance was observed in the 530 sample, with the "mid" level roughness Ra value of 1.0 μm. % RSD values were observed at 30.4% and 23.99% for the m/z 197⁺ and m/z 591⁺ ions, respectively. Not only were these values far higher than would have been anticipated from the previous experiments based on Ra values, but they also did not follow the previously reported trends in regards to the higher mass gold ion exhibiting greater variance that the lower mass gold ion, i.e. as observed in the abrasive paper experiments. In the sample with the lowest Ra value of 1.0 μm,

substantially less variance was observed in the anions in comparison to the cations. This indicated that in the case of gold Au and Au_3 ions, Ra values of 1 micron appeared to create greater variance in the cations than the anions. In samples with roughness values of greater than 1 micron this differential was reduced.

Figure 5.10 Bar Chart of ToF-SIMS positive and negative gold (Au and Au₃) ion variance from Rubert precision measurement samples
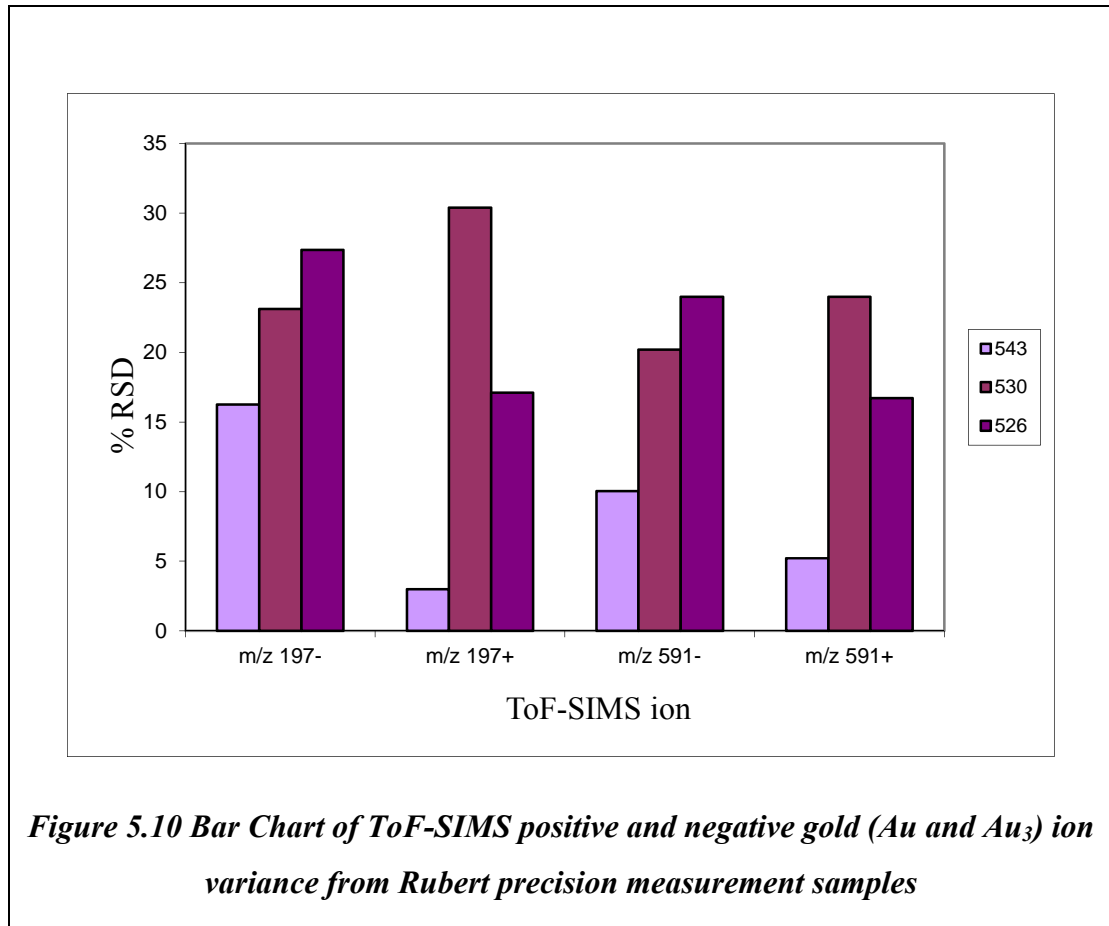
To reiterate, in the abrasive paper experiments roughness affected negative ions more significantly than positive ions. This also appeared to be the case here for both the roughest and smoothest sample, but not the mid-level sample.

The positive and negative gold ion variance from Rubert precision measurement samples in relation to Ra is presented in Figure 5.11. The graph shows a steeper initial increase, as observed in previous samples, over the nanometre range that. However, it should be noted that the data in this graph presents a lower scale of Ra values ranging from 40 nm to 3.15 μm, whereas the abrasive paper Ra values ranged from 4.87 μm to 14 μm. The magnesium stearate samples in Chapter 3 exhibited Ra values of similar levels, and also reflected this rapid increase in % RSD values in the

low figure micron scale. Although, the PTFE experiments in Chapter 2 suggested that the mass to charge ratio may not specifically affect variance, these results have indicated that as roughness increases for the gold surfaces of defined geometry, the rate at which variance was introduced appeared to be mass dependent.
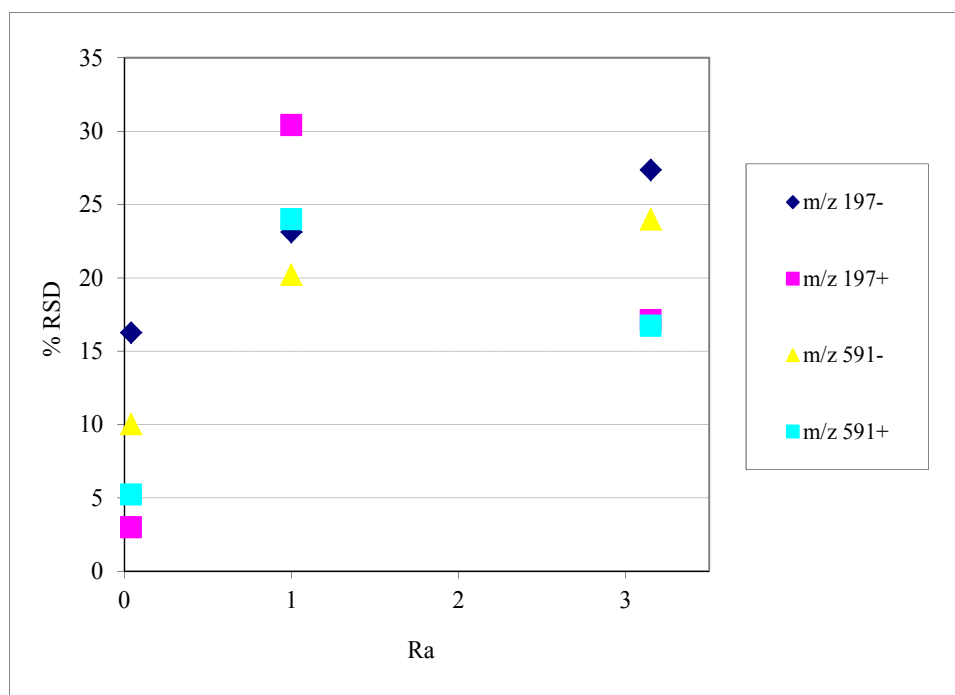
Figure 5.11 Graph of ToF-SIMS positive and negative gold ion variance from Rubert Precision Measurement samples in relation to Ra

The Rubert samples were defined by a number of topographical parameters. The sampling area was a 384 x 384 μm square and for both the 526 and 530 samples the Sm value was constant at 100 μm, i.e. the number of peaks and troughs over the area was constant. (Sm is defined as the distance between two peaks). However, in the sample 543, this Sm value was much smaller, at 2.5 μm. The Pt value in each sample differed (i.e. the distance between peak and trough). In an attempt to account for the different geometries of the samples, a normalising factor was calculated, using the different parameters used to define the sample. This normalising calculation is presented in Table 5.3.

Sample	Area	Sm value (μm)	Pt value (μm)	Normalising factor (Area / Sm*Pt)
526	384	100	10	38.40
530	384	100	3	11.52
543	384	2.5	0.12	18.43

Table 5.3 Normalising factor calculations for Rubert precision measurement samples

When these normalising factors were applied to the positive ion standard deviations the recalculated variance values increased in line with the roughness values (i.e., as roughness increased, data variance followed the same trend). These recalculations are presented in Table 5.4. The validity of this approach can be challenged. However, this approach to interrogate this data must be seen in the context of attempting to provide an explanation for the observed data in the light of the differing sample topographies of defined geometry. The three Rubert precision measurement samples all had different defined geometries and there was no evidence as to why they performed differently to the random surface topographies, other than a specific directionality in the surface features. It was unclear if the nature of the particular geometry of the 530 sample rendered it to have greater variance than the smoother

and rougher samples as defined by their Ra value. The value of such roughness parameters such as Ra in the characterisation of such precision measurement samples can be debated. Ra values were provided by the manufacturer for all of the precision measurement samples. Ra is also known as the arithmetic mean or the centre line average and for a given linear profile represents the area between the roughness profile and the centre line divided by the evaluation length [Bewoor and Kulkarni, 2009]. What this means in practice, is that surfaces with very different profiles can have the same Ra value as Ra is a linear rather than an area measurement, as shown in Figure 5.12. Hence, the geometries of precision machined surfaces with specific directionality, such as Rubert samples, are not well defined by a single value such as Ra but other parameters such as Sm and Pt are required to help characterise the topography. While this work has highlighted that defined surface topography can induce changes in variance that are not simply understood in terms of standard Ra values, there appears to be no clear explanation of why such topographies result in such increased variability in the ToF-SIMS analysis.

		Sample		
		543	**530**	**526**
% RSD for	**m/z 197$^+$**	2.98	30.40	17.10
gold cations	**m/z 591$^+$**	5.21	23.99	16.72
Normalising factor (NF)		18.43	11.52	38.40
Recalculated	**m/z 197$^+$**	54.92	350.21	656.64
Value	**m/z 591$^+$**	96.02	276.36	642.05

Table 5.4 Recalculated standard deviation values following NF (from Table 5.3)
application to gold positive ions for Rubert precision measurement samples

Figure 5.12 Line Representations of surfaces that exhibit the same Ra values
(adapted from Bewoor, 2009)
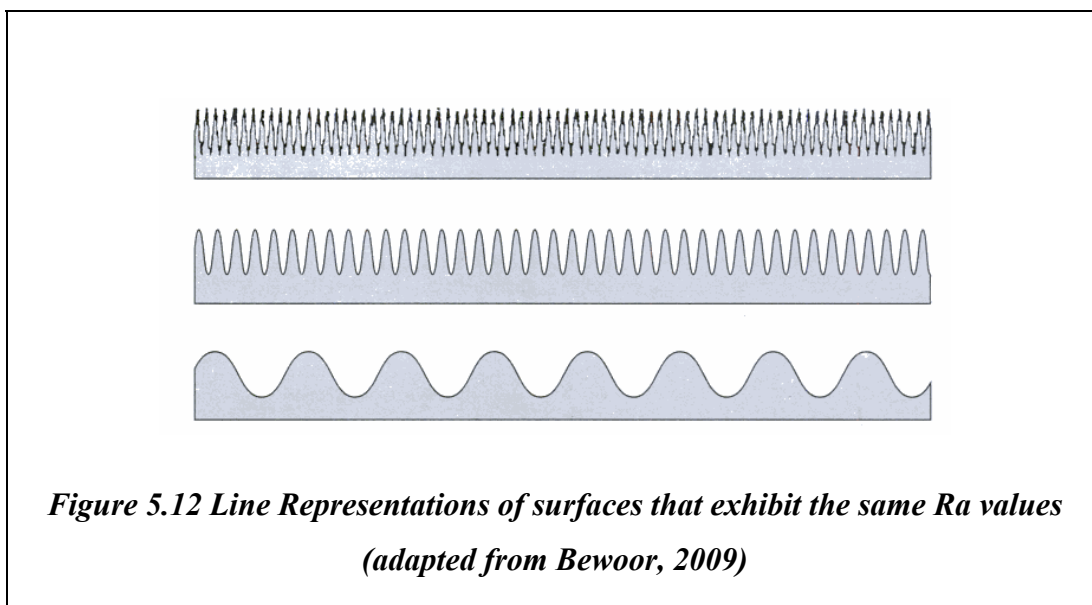
5.3.3 Gold Coated Glass Microscope Slides

Two separate experiments were carried out on the gold coated microscope slides. The first to give a base line of the variance over a given area, and the second to establish how count values potentially influence variance when the sample surface is moved away from the optimum height position (from the extractor cone to the sample surface).

The sample surface was moved towards and away from the analyser in 10 micron steps over a 40 micron range in order to mimic the potential peaks and troughs of a 'real life' sample surface. Measurements were taken at –20 μm, -10 μm, 0 μm, +10 μm and +20 μm relative distance points from the optimum analysis height in relation to the extractor.

Sensitivity factor values of the gold coated microscope slide at the optimum height in relation to the extractor (referred to as 0) are presented in Table 5.5. As in previous experiments, the 384 x 384 micron area was divided into a 4 x 4 sixteen square grid, and the SFs were calculated from the individual ion counts and the PIDD in each square for the gold cations and anions at m/z 197 and 591. In all cases the % relative standard deviation across the grid was below 6%. The gold coated microscope slide surface exhibited no topographical directionality, and was anticipated to have a roughness in the nanometre region similar to a non-coated microscope slide as reported in Table 4.6.

	Sensitivity Factor x10^{-8}			
Area	m/z 197$^-$	m/z 197$^+$	m/z 591$^-$	m/z 591$^+$
a1	5.30	66.51	2.41	7.33
a2	5.31	68.27	2.43	7.67
a3	5.11	69.51	2.34	8.16
a4	5.26	70.13	2.36	8.48
b1	5.23	68.54	2.52	7.55
b2	5.29	71.96	2.43	8.28
b3	5.38	72.10	2.52	8.37
b4	5.56	72.10	2.55	8.22
c1	5.33	71.18	2.54	8.08
c2	5.28	73.55	2.52	8.42
c3	5.45	72.62	2.58	8.24
c4	5.68	73.17	2.65	8.19
d1	5.66	73.33	2.72	8.33
d2	5.62	73.09	2.66	8.25
d3	5.68	73.52	2.71	8.40
d4	5.75	73.4	2.74	8.36
Ave	5.43	71.47	2.54	8.15
% RSD	3.67	3.07	5.02	4.10

Table 5.5 % RSD variance of gold cations and anions from a gold coated microscope slide measured by ToF-SIMS

The % RSD values were low and varied from around 3 to 5% across the ions analysed. The cations and anions exhibited the same two key trends that were evident in the experiments with gold coated abrasive papers:

- variance values for higher mass ions are larger than lower mass ions

- larger % RSD values are seen in the cation that the anion of the same mass

The influence of distance from the extractor cone on normalised counts in the ToF-SIMS experiments was recorded for the four gold ions and the results are presented in Table 5.6. Taking into account variations in PIDD, the results showed that the height variation had a significant impact on the data in all of the ions studied. The greatest % RSD value was obtained for the m/z 197^{+} ion with a % RSD value of 20.97 %, whereas all other ions recorded % RSD values below 10 %.

		Ion Counts			
		m/z 197^{+}	m/z 591^{+}	m/z 197^{-}	m/z 591^{-}
Distance from optimum analysis height (µ)	**+20**	149056	25408	1008171	163582
	+10	173270	27352	1083836	161502
	0	203672	29217	1170191	158680
	-10	133525	25241	980299	172594
	-20	121792	24696	942290	179716
	Average	156263	26382.8	1036957	167214.8
	STDEV	32764.53	1875.585	90760.04	8716.248
	% RSD	**20.97**	**7.11**	**8.75**	**5.21**

Table 5.6 % RSD variance of gold cations and anions from a gold coated microscope slide measured by ToF-SIMS taken at varying "y" positions from the extractor

The normalised total ion counts (NTIC) for each of the ions compared as percentages to the NTIC value at 0, are presented in Figure 5.13. The most obvious pronounced feature in this figure was the apparent reduction or loss in counts for all ions, with the exception of the high mass anion at m/z 591⁻. In the majority of cases, the greatest number of counts for each ion was observed at the optimum 0 position and the ion counts fell away either below or above the optimum position. A loss of up to 40% of signal was observed with a 20 micron change, and this loss appeared to be more pronounced if the sample was too low. The effect was greater in the lower mass ions and greatest in the low mass positive anion. Interestingly, the standard deviation value was also highest in the gold ion m/z 197⁻, indicating that changes in height had a greater effect on this ion than the other ions presented.

Figure 5.13 Bar Chart highlighting ToF-SIMS % NTIC normalised to position 0 for key gold anions and cations
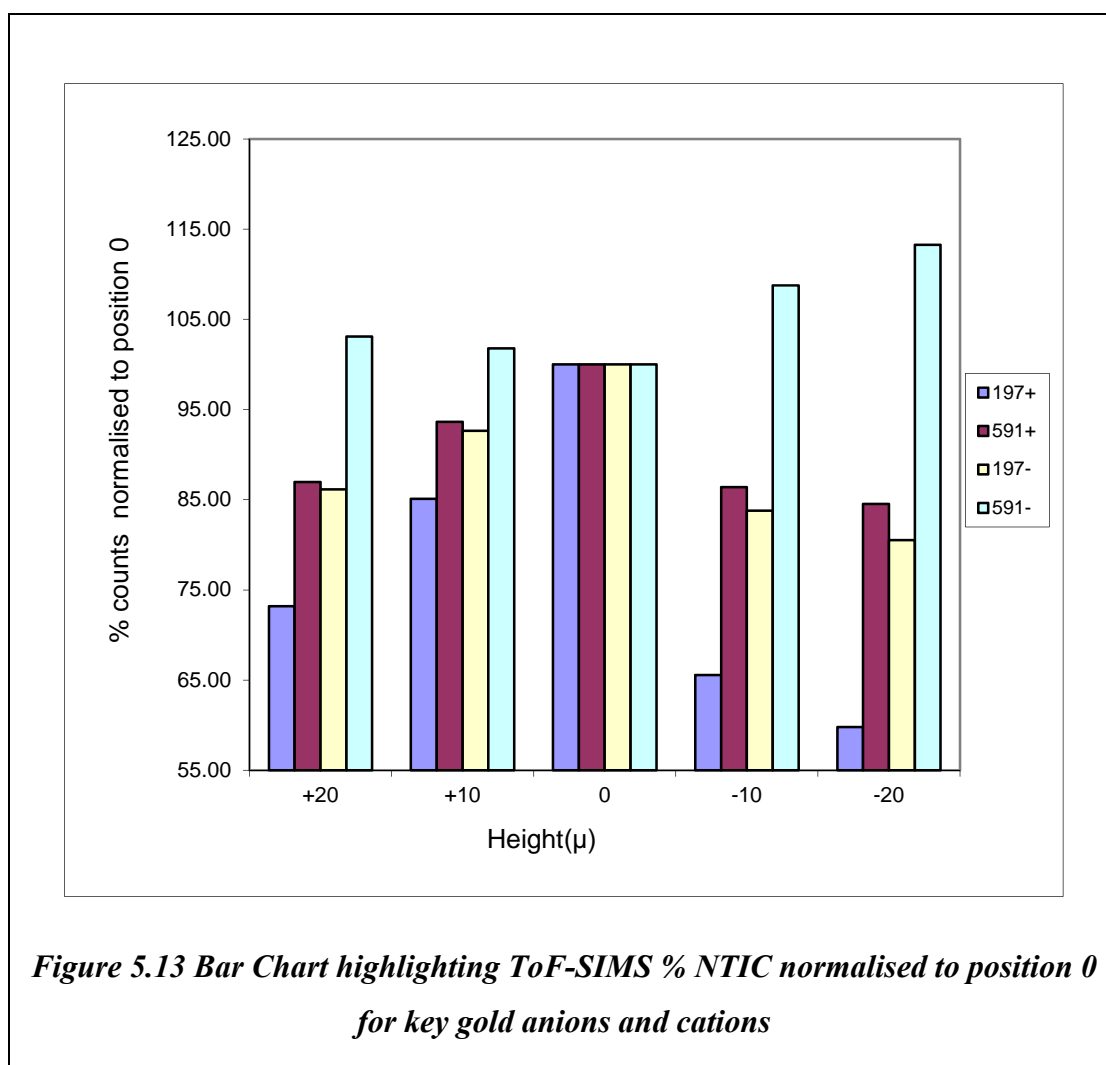
It is possible that the effect of the extraction voltage, applied at the bottom of the tube (as discussed in Chapter 2) alters as the sample is moved toward or away from the extractor cone. Previous work by Lee stated that reducing the extractor voltage may limit field effects caused by topography [Lee *et al.*, 2008]. These changes may also be caused by the way in which the primary ion beam is interacting with the sample surface. The mechanics of ionisation are not well understood [Vickerman and Briggs, 2001] and it would appear that variances in height as well as surface topography also play a role in this mechanism in addition to the more traditionally cited reasons of surface chemistry. Lee cites that the problems of topography introducing artefacts into SIMS spectra and images can arise from both theoretical considerations (e.g. sputtering yields vs. incidence angle) and experimental considerations (e.g. sample mounting and optimal set up) [Lee *et al.*, 2008]. This work mirrors these two observations, through the observations made in the precision measurement samples that exhibit directionality and the observations of the effect of varying the optimal sample height on ion yield.

5.4   Conclusions

This chapter reported on three separate experiments that investigated the effect that roughness had on the calculation of SFs through the use of model systems, and the main aim of this chapter was to build on the results from the previous chapter through the use of these model systems with pre-defined roughness profiles.

The preliminary experiments measured the % relative standard deviation of the ToF-SIMS ion signal across 384 x 384 micron areas of gold coated abrasive papers of various grades. The results showed that for a sample with no directionality in surface topography, as roughness increased there was a correlating increase in variance of the gold ion yields. The rate at which this variance occurred was higher in the negative ions than the positive ions. In addition, the roughness appeared to have a slightly greater effect on the gold cations in comparison to their anion counterparts at the same mass.

The second experiment was performed using the same methodology, but analyses were performed on samples with specific directionality in regards to surface topography. Unlike the random, but reasonably consistent roughness profiles exhibited by the gold coated abrasive papers in both the x and y directions, precision measurement standards with pre-defined profiles were used. These samples have a surface that is patterned in one direction only and are made to exacting standards in order to act as metrology tools. This directionality had a significant effect on the gold ion variance across the analysis area, particularly in the positive ion spectra. The anions no longer followed the trend that increasing Ra had a corresponding variance increase. Ra is a single measurement taken in one direction. With the abrasive papers this value was the same in the x and y direction. However, in the precision measurement samples Ra values only related to the direction of the topographical features (perpendicular measurements would give an Ra value of 0). To allow for this, normalising factors were calculated that incorporated both the Sm and Pt values of the sample. Once these were applied, the anion variance followed a positive trend. This indicated that gold anions are more susceptible to any directionality in a surface than their respective cations.

The final experiment looked at the effect of the distance of the sample in relation to the extractor. Again, gold ions were employed to look at variance. This experiment highlighted that gold anions appeared to be more significantly affected by variations in height than their cation counterparts. Interestingly, in all cases moving away from the optimum height resulted in a loss of signal, with one exception, the high mass gold anion. This experiment, in line with the precision measurement work, indicated that it may be more difficult to produce reliable SFs for anions than cations.

It is clear that the work from Chapters 4 and 5 merits further investigations into this field. These chapters have clearly demonstrated that surface topography can have a significant role in the reproducibility of data in ToF-SIMS analyses. In general, the greater the roughness of the sample, the greater the variance in ToF-SIMS ion yield data. There also appeared to be differences in the susceptibility of the ions within a ToF-SIMS spectrum to this effect and also differences in the effect on cations and anions for certain samples studied. These studies not only informed our understanding of the mechanism of ion generation from these model surfaces, they also helped us to understand some of the factors that make reproducible ToF-SIMS analysis on complex real-life pharmaceutical systems so challenging.

These experiments have been undertaken on model surfaces of defined topography and single chemistry. A further range of different surface topographies could be studied. Model systems which combine a wider range of defined surface topography and also chemistry could be envisaged as future model materials. This work also used a single primary ion source. It would be interesting to see if the same trends are observed in the cations and anions when different primary ion sources are used, and in particular whether polyatomic ion sources that result in an increase in higher mass fragmentation, result in the same effect. Tyler addresses the issue of topography in differentiating between species in the imaging of proteins, and comments that a bismuth primary ion source provides advantages over gallium sources when looking at proteins that are around 10 μm in size [Tyler *et al.*, 2011].

An extensive paper search has found that the majority of papers that look at quantification relate to matrix effects (which are discussed in Chapter 6) or changes in yield that occur during depth profiling (dynamic SIMS) and are based on flat samples, such as silicon wafers. Chapters 3, 4 and 5 would indicate that the level and

type of roughness in a sample surface would warrant further research, particularly in looking at samples that exhibit surface morphology. The effect of the environment surrounding a material on the ionisation yield will be analysed in the next chapter.

Chapter 6.

Principal Component Analysis and Matrix Effects in the ToF-SIMS Process

6.1 Introduction

The two previous chapters examined the effect of roughness on the quantification of ToF-SIMS data through investigating variation in ion yields across the sample surface of non-model and model surfaces. The work in this chapter removes roughness effects from the experiment through the analysis of spun cast samples with minimal topography. The effect of altered surface chemistries, i.e. matrix effects, is investigated through the use of principal component analysis (PCA), a multivariate analysis method. The viability of PCA as a tool to differentiate between samples with complex chemistry is also investigated through applying this tool to the tablets with lowest and highest paracetamol concentrations formulated for Chapter 3.

6.1.1   Selection of Materials for Analysis

Two different drugs and two different polymers were selected for study, and several samples with varying ratios of drug to polymer were formulated. Two drugs with relatively similar chemistry were chosen, flurbiprofen and diflunisal. Flurbiprofen is a non-steroidal anti-inflammatory drug (NSAID) with analgesic and antipyretic properties that is indicated for conditions associated with mild-to-moderate pain [Cefali *et al.*, 1991]. Diflunisal is also a non-steroidal anti-inflammatory drug and is an aspirin derivative. Its long half-life allows for twice daily administration and it is particularly effective in arthritis [Joint Formulary Committee, 1991]. The two polymers that were used as the matrix elements were polyethylene glycol (PEG) and poly(methyl methacrylate) (PMMA). PEG enhances the circulation time and stability of drugs that have low solubility or contain unstable proteins [Ratner, 2004]. PMMA is also used in drug delivery, for example in cholesterol containing microspheres [Elvira *et al.*, 2004].

6.1.2   Matrix Effects in ToF-SIMS

Matrix effects are briefly discussed in Chapter 2 and relate to the dependence of elemental secondary ion yields on the chemical state of the surface [Vickerman and Briggs, 2001]. These yields can vary by several orders of magnitude, and the sensitivity of sputtered ion yields in the matrix composition results in difficulties in the formulation of standards for quantification [Briggs and Seah, 1992].

Jones *et al*. evaluated the effect of different biological compound matrices on the ability of SIMS to provide molecular information [Jones *et al.*, 2006b]. Two similar drug molecules differing by the addition of one ligand (atropine and ipratropium bromide) were mixed with different lipids and the effect of the lipid matrices on the protonated and cationised molecular ions was assessed. They concluded that the lipid matrices had significantly different impacts on the ionisation, and hence detection, of key molecular ions.

The following year, Jones investigated the suppression and enhancement of secondary ion formation due to the chemical environment in SIMS [Jones *et al.*, 2007a]. He concluded that as SIMS is increasingly used for the analysis of more complex systems that the effects of matrix effects must be considered. In addition, he stated that these considerations were particularly important when looking at ion images of molecules within different chemical environments. Analyte/matrix samples were produced by two different methods (solution and powder), with little effect on the protonated ion. Suppression of ions was matrix dependent.

Matrix effects have also been observed in ToF-SIMS analyses of styrene-methyl methacrylate random copolymers [Vanden Eynde and Bertrand, 2000]. The intensities of key ions were measured and compared to increasing styrene content. They observed a correlative relationship between the styrene matrix and the methyl methacrylate ions, where the methyl methacrylate key ions were increasingly suppressed (above that expected in a linear relationship) in comparison to the styrene concentration.

Matrix effects can be reduced in some circumstances by doping the surface with small amounts of metal such as silver [Inoue and Murase, 2005]. Fragmentation of

ions can also be affected by substrate materials causing changes to ionisation yields due to matrix effects [Torrisi *et al.*, 2009].

6.1.3 Multivariate Analysis Methods

Multivariate methods look at reducing large data sets to groups of variables that have correlating features [Vickerman and Briggs, 2001]. It has certain advantages over manual techniques, as it is objective (rather than subjective) and allows for the simultaneous comparison of all the variables in a data set [Lee *et al.*, 2008]. ToF-SIMS is multivariate in nature as each spectrum records intensity values across the entire mass range [Lee *et al.*, 2008]. Multivariate analysis methods are not limited to spectroscopy, but can also be utilised in imaging and depth profiling [Grams, 2007]. Multivariate analysis encompasses a wide range of methods. Principal Component Analysis (PCA) has become more widely used in comparison to other methods such as Partial Least Squares regression (PLS) and Multivariate Curve Resolution (MCR) [Lee *et al.*, 2008].

Multivariate analysis has also been utilised in the analysis of micro arrays, which involve data acquisition from many spots and hence the potential scale of data processing is very high [Scurr *et al.*, 2010]. Both MCR and PLS methods were employed to successfully differentiate secondary ions from regions of the array containing saccharide, linker, salts from the printing buffer, and the background linker chemistry.

In recent years, multivariate analysis has become commonly used in the analysis of large amounts of data, in a wide range of spectroscopic techniques, through the use of automated programs [Lee *et al.*, 2008]. PCA reduces the dimensionality of ToF-SIMS data to a small number of abstract factors that describe the variation in the data, enabling similarities and differences in the samples to become apparent [Graham *et al.*, 2006]. Multivariate methods including PCA have been applied to ToF-SIMS data in both imaging and spectroscopy modes and can also be used as a pre-cursor to additional multivariate methods such as MCR [Scurr *et al.*, 2010]. PCA can be applied to many different samples from the analysis of drug distribution in ocular tissues [Mains *et al.*, 2011] and the structure of lamellar surfaces [Lau *et al.*, 2010].

Wagner *et al*. have successfully used PCA to differentiate between single protein component films absorbed onto mica. They commented that advances in the use of these methods had resulted in the establishment of ToF-SIMS as a premier technique for the characterization of adsorbed protein films [Wagner and Castner, 2004].

PCA has been used to discriminate between the structural conformations of amorphous and flat-on lamellar surfaces of Poly-(bisphenol A-etheralkane) by identifying the ion peaks that contribute to the chemical and structural variations of the folding surfaces [Lau *et al.*, 2010].

6.1.4   Aims of the Chapter

The primary aim of this chapter is to assess the use of PCA for interpretation of ToF-SIMS data, including its value in assessing potential matrix effects in samples with different chemical environments. Several samples with varying ratios of drug to polymer were formulated, and the extent that the different matrices (in this case the polymers) had on the drug ion yields was investigated.

Initially, the ability of ToF-SIMS to identify (through spectroscopy) key ions from the raw materials will be assessed. Secondly, the chapter aims to assess the use of PCA for differentiating between the different sample types containing polymer/drug mixes.

This final experiment in the chapter focuses on using PCA to analyse ToF-SIMS data from the 20 wt% and 80 wt% paracetamol tablets studied in Chapter 3, and assess whether PCA can be used as an effective method to differentiate between the two tablet systems that contained the highest and lowest concentrations of paracetamol.

6.2 Materials and Methods

6.2.1 Raw Materials

The raw materials for the experiments consisted of two active ingredients, two polymers and one solvent.

Name	*RMM*	*Manufacturer*
PEG	$C_{2n}H_{4n+2}O_{n+1}$	Fluka
PMMA	$(C_5O_2H_8)_n$	Rohm Pharma Polymers
Diflunisal	$C_{13}H_8F_2O_3$	Sigma - Aldrich
Flurbiprofen	$C_{15}H_{13}FO_2$	Sigma - Aldrich
Ethanol	C_2H_6O	Sigma - Aldrich

Table 6.1 Details of the raw materials used in the manufacture of samples for ToF-SIMS analysis

6.2.1.1 ToF-SIMS sample preparation and analysis conditions

ToF-SIMS analyses were performed on the raw materials, prior to them being made up into solutions for spin casting. The typical construction of a powder sample prepared for SIMS analysis using a double adhesive layer method is presented in Figure 6.1.

= powder
= sellotape
= double sided tape
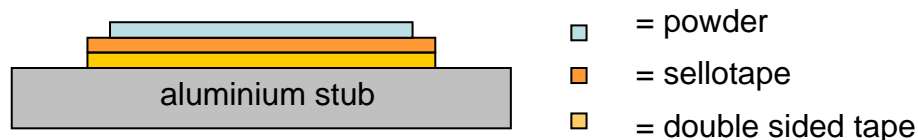
aluminium stub

Figure 6.1 Schematic diagram representing ToF-SIMS sample construction for powder materials

Prior to use, the aluminium discs were cleaned in an ultrasonic bath using a two solvent cleaning process of high purity hexane followed by high purity chloroform. The double sided tape and sellotape layers were then adhered in turn to the disk surface and the powder sprinkled on to this. Excess powder was removed by gently tapping the disk on a hard surface. The powder application procedure was repeated twice to ensure an even and full coverage. The samples were then back mounted into the sample holder, minimising the effect of any tilt that may be present in the discs.

Static ToF-SIMS measurements were performed on an ION-TOF ToF-SIMS IV instrument (ION TOF GmbH, Münster, Germany). In all experiments gallium was used as the primary ion. The flood gun was operated at 3 keV, 30 μA to compensate for sample charging. Random sampling areas of 100 μm x 100 μm were analysed using spectroscopy (high current bunched) mode in order to obtain spectra with high mass resolution. In all cases the analysis dose was kept below the static limit of 1 x 10^{13} ions cm^{-1}.

6.2.2   Drug / Polymer Solutions

Drug / polymer solutions were prepared with ethanol used as the solvent. Two drugs and two polymers were selected, diflunisal and flurbiprofen and PMMA and PEG. In each case the polymer was dissolved in 10ml of ethanol and the drug was added to this solution. Three different concentrations of each active ingredient were studied in each polymer, with 5:1, 10:1 and 100:1 ratios of polymer to active ingredient. The twelve different solutions with relative concentrations and samples IDs are given in Table 6.2.

Sample ID	Level of Drug and Polymer in each solution			
	Diflunisal	*Flurbiprofen*	*PEG*	*PMMA*
DIF1G5	20mg	-	100mg	-
DIF1G10	10mg	-	100mg	-
DIF1G100	1mg	-	100mg	-
DIF1M5	20mg	-	-	100mg
DIF1M10	10mg	-	-	100mg
DIF1M100	1mg	-	-	100mg
FLU1G5	-	20mg	100mg	-
FLU1G10	-	10mg	100mg	-
FLU1G100	-	1mg	100mg	-
FLU1M5	-	20mg	-	100mg
FLU1M10	-	10mg	-	100mg
FLU1M100	-	1mg	-	100mg

Table 6.2 Details of the quantities of raw materials used in the manufacture of samples for ToF-SIMS analysis

6.2.2.1   Spin Casting

Samples in solution were spun cast onto 10mm x 10mm silicon wafers at a spin speed of 300 rpm. Ten drops of each solution were dropped onto the spinning silicon wafers with approximately 10 sec intervals.

6.2.2.2   ToF-SIMS sample preparation and analysis conditions

Samples were prepared in a similar manner as detailed above in Section 6.2.1.1. The double sided tape and sellotape layers were adhered to the aluminium disk surface and the silicon wafer was placed onto the sellotape using tweezers, as shown in Figure 6.2.

Figure 6.2 Schematic diagram representing ToF-SIMS sample construction for silicon wafers
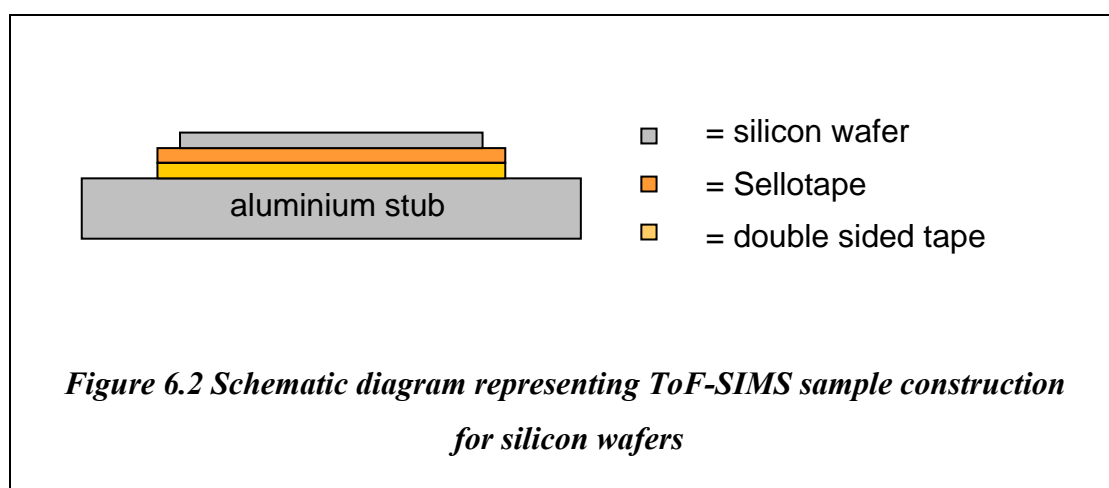
As with the raw materials, static ToF-SIMS measurements were performed on an ION-TOF ToF-SIMS IV instrument (ION TOF GmbH, Münster, Germany). In all experiments gallium was used as the primary ion. The flood gun was operated at 3 keV, 30 µA to compensate for sample charging. Random sampling areas of 100 µm x 100 µm were analysed using spectroscopy (high current bunched) mode in order to obtain spectra with high mass resolution. In all cases the analysis dose was kept below the static limit of 1×10^{13} ions cm^{-1}. Triplicate runs for all samples were completed in both positive and negative polarities.

6.2.3   Principal Component Analysis of Spun Cast Solutions

Prior to analysis the normalised to total ion count intensities of the F$^-$ ion were plotted for each concentration of drug in both polymers. This was to establish the

nature of the relationship between the ion intensities of the F^- ion and the drug concentration in each polymer.

PCA was carried out using the PLS_Toolbox (version 5.2, Eigenvector Research, Manson, WA) for Matlab (Mathsworks, Inc, Natick, MA). Peak lists were generated for both the ToF-SIMS positive and negative ion spectra for all twelve samples. The peak lists were merged (removing overlapping peaks) and the corrected ion intensity data was exported and normalised to the total ion counts. From this data an eigenvalue plot was produced that highlighted the main principal components. A scores plot for the key principal components identified by the eigenvalue plot was plotted in 2 dimensions, i.e., Principal Component 1 (PC1) and Principal Component 2 (PC2). Finally, an analysis of the loadings values for each of the principal components was used to identify the key ions that were causing the variance between the data expressed within the scores plots.

6.2.4 Principal Component Analysis of Tablet Data

PCA was carried out using the Eigenvector PLS_Toolbox described in the previous section. Peak lists were created for the ToF-SIMS positive ion spectra for three analyses of each of the lowest and highest concentrations of paracetamol tablet (20% and 80%). The peak lists were normalised to the total ion count. Eigenvalue and score plots were produced as described in Section 6.2.3. An analysis of the loadings values was also performed.

6.3 Results and Discussion

6.3.1　　　Raw Materials

Four solid raw materials were used in the production of the spun cast solutions. These materials comprised of two active ingredients, diflunisal and flurbiprofen, and two polymers PEG and PMMA. All materials were examined by ToF-SIMS, in both their raw powder state and as spun cast solutions.

6.3.1.1　　　ToF-SIMS Analysis of Raw Materials

The positive and negative ion ToF-SIMS spectra for flurbiprofen are presented in Figure 6.3 and Figure 6.4, respectively. Flurbiprofen has a relative molecular mass of 244.261 with the empirical formula $C_{15}H_{13}FO_2$. An extensive literature review did not result in any reports of SIMS analysis of this material. In the positive ion spectrum a strong and intense peak can be observed at m/z 199^+. Previous gas chromatography–mass spectrometry (GC-MS) work has shown that this peak corresponds to the molecular ion with the loss of the carboxyl group $[M\text{-}COOH]^+$ [Chao *et al.*, 2007]. Although, the protonated molecular ion $[M\text{+}H]^+$ can also be observed in the positive ion ToF-SIMS spectrum at m/z 245^+ it was not as intense as the peak at m/z 199^+. In the negative ion spectrum strong intense peaks can be observed at m/z 60^-, 77^- and 199^-. Fast atom bombardment (FAB) of this material has also reported a peak at m/z 199^- in the negative spectrum. This was assigned to C_6H_5-$C_6H_3F\text{-}CH(CH_3)^-$ corresponding to $[M\text{-}COOH]^-$ [Tsunematsu *et al.*, 1993]. The ions at m/z 199^+ and m/z 199^- were structurally distinct to flurbiprofen, and hence were selected as chemical markers for this material.

The positive and negative ion ToF-SIMS spectra for diflunisal are presented in Figure 6.5 and Figure 6.6, respectively. Diflunisal has a relative molecular mass of 250.198 with the empirical formula $C_{13}H_8F_2O_3$. Again, an extensive literature review did not result in any reports of SIMS of this material. Positive ion peaks were present at m/z 175^+, 184^+, 233^+ and 251^+. Of these, the peak at m/z 251^+ was chemically distinct and represented the protonated molecular ion, $[M\text{+}H]^+$, and as such was selected as a key marker for this material. In the negative ion ToF-SIMS spectrum a strong and intense peaks can be observed at m/z 205^- and m/z 249^-. The MassBank (www.massbank.jp) contains a negative ion spectrum for this material, also showing strong intense peaks at these values. MassBank is the first public repository of mass

spectral data and is intended for use as a data bank for the scientific research community. However, although MassBank does not provide assignments for these peaks, they are most likely [M-H]⁻ and [M-COOH]⁻ The more intense and structurally distinct peak at m/z 249⁻ was used as a molecular marker for this material.

The positive and negative ion ToF-SIMS spectra for PEG are presented in Figure 6.7 and Figure 6.8, respectively. A positive ion ToF-SIMS mass spectrum of PEG shows a characteristic pattern through the PEG monomer unit [Briggs *et al.*, 1989]. This PEG monomer unit, M (CH_2CH_2O), resulted in a recognisable pattern of $[M_x+H]^+$ and $[M_x-H]^+$ which was clearly visible in the positive ion spectrum. Peaks relating to the $[M_x+H]^+$ ions were observed at m/z 45^+, 89^+, 133^+ and 177^+, where x = 1-4. Peaks from the $[M_x-H]^+$ ions were observed at m/z 43^+, 87^+, 131^+ and 175^+, where x = 1-4. This pattern was also evident in the negative ion spectrum, where the PEG monomer unit, M (CH_2CH_2O) again resulted in a clearly recognisable pattern of $[M_x+H]^-$ and $[M_x-H]^-$. Peaks relating to the $[M_x+H]^-$ ions were observed at m/z 45⁻, 89⁻, 133⁻ and 177⁻, where x = 1-4. Peaks from the $[M_x-H]^-$ ions were observed at m/z 43⁻, 87⁻, 131⁻ and 175⁻, where x = 1-4. Peaks relating to $HO(CH_2CH_2O)_x$ were also observed at m/z 61⁻ and m/z 105⁻, where x = 1 and x = 2. These PEG related peaks in the positive and negative ion spectra have previously been observed by Briggs [Briggs *et al.*, 1989].

The positive and negative ion ToF-SIMS spectra for PMMA are presented in Figure 6.9 and Figure 6.10, respectively. PMMA reference spectra for both polarities in the 0 to 200 m/z range identified a number of positive and negative ions that were also observed in this material [Briggs *et al.*, 1989]. These included strong peaks in the positive ion ToF-SIMS spectrum at m/z 59^+ and 69^+ observed in Figure 6.9, which corresponded to CH_3O-CO^+ and $CH_3C(CH_2)CO^+$, respectively. Strong diagnostic ions in the negative ion ToF-SIMS spectra arising from the methacrylate monomer structure were observed at m/z 55⁻ and m/z 85⁻, which corresponded to $[CH_2CH-CO]^-$ and $[CH_3C(CH_2)CO_2]^-$, respectively. In addition, a methoxyl group ion $[CH_3O]^-$ was observed at m/z 31⁻. The clear diagnostic peaks and their assignments that were used for the ToF-SIMS analysis of the drugs and polymers in this chapter are presented in Table 6.3.
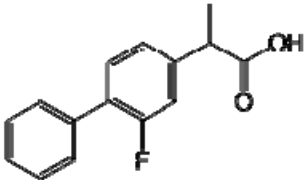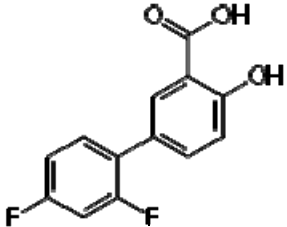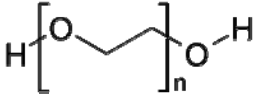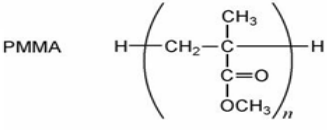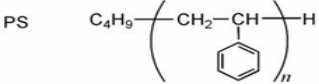
Material	*+ve ions*	*Assignment*	*-ve ions*	*Assignment*
Flurbiprofen	178		60	
	199	[M-COOH]$^+$	77	
	245	[M+H]$^+$	199	[M-COOH]$^-$
Diflunisal	233	[M+H]$^+$	205	[M-H]$^-$
	251		249	
PEG	43,87..	[CH$_2$CH$_2$Ox-H]$^+$	43,87..	[CH$_2$CH$_2$Ox-H]$^-$
	45,89..	[CH$_2$CH$_2$Ox+H]$^+$	45,89..	[CH$_2$CH$_2$Ox+H]$^-$
PMMA	59	[CH$_3$O-CO]$^+$	55	[CH$_2$CH-CO]$^-$
		[CH$_3$C(CH$_2$)CO]$^+$		[CH$_3$C(CH$_2$)CO$_2$]$^+$
	69		85	

Table 6.3 Table summarising the characteristic ToF-SIMS ions identified in the raw materials
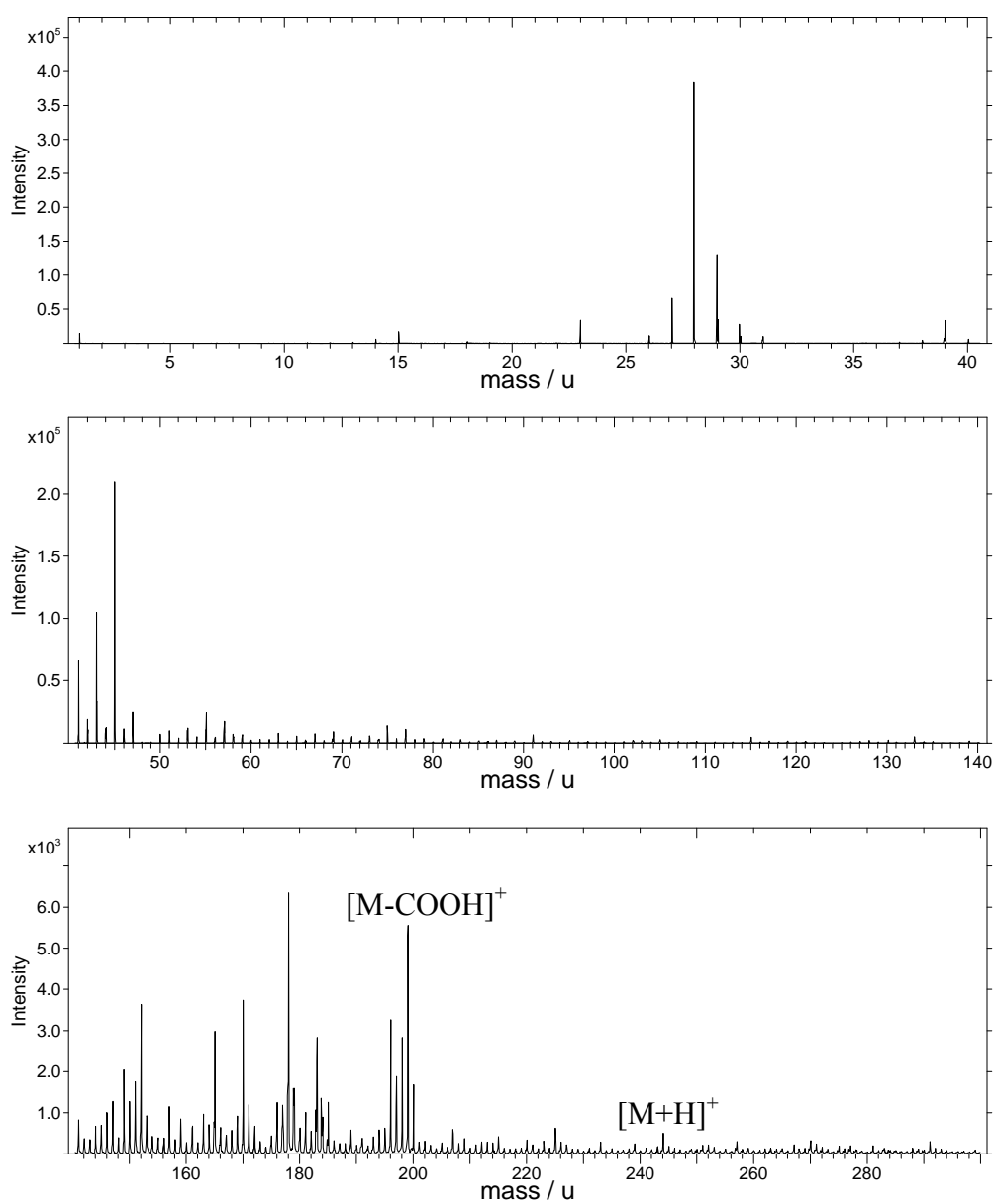
Figure 6.3 Positive ion ToF-SIMS spectrum of flurbiprofen
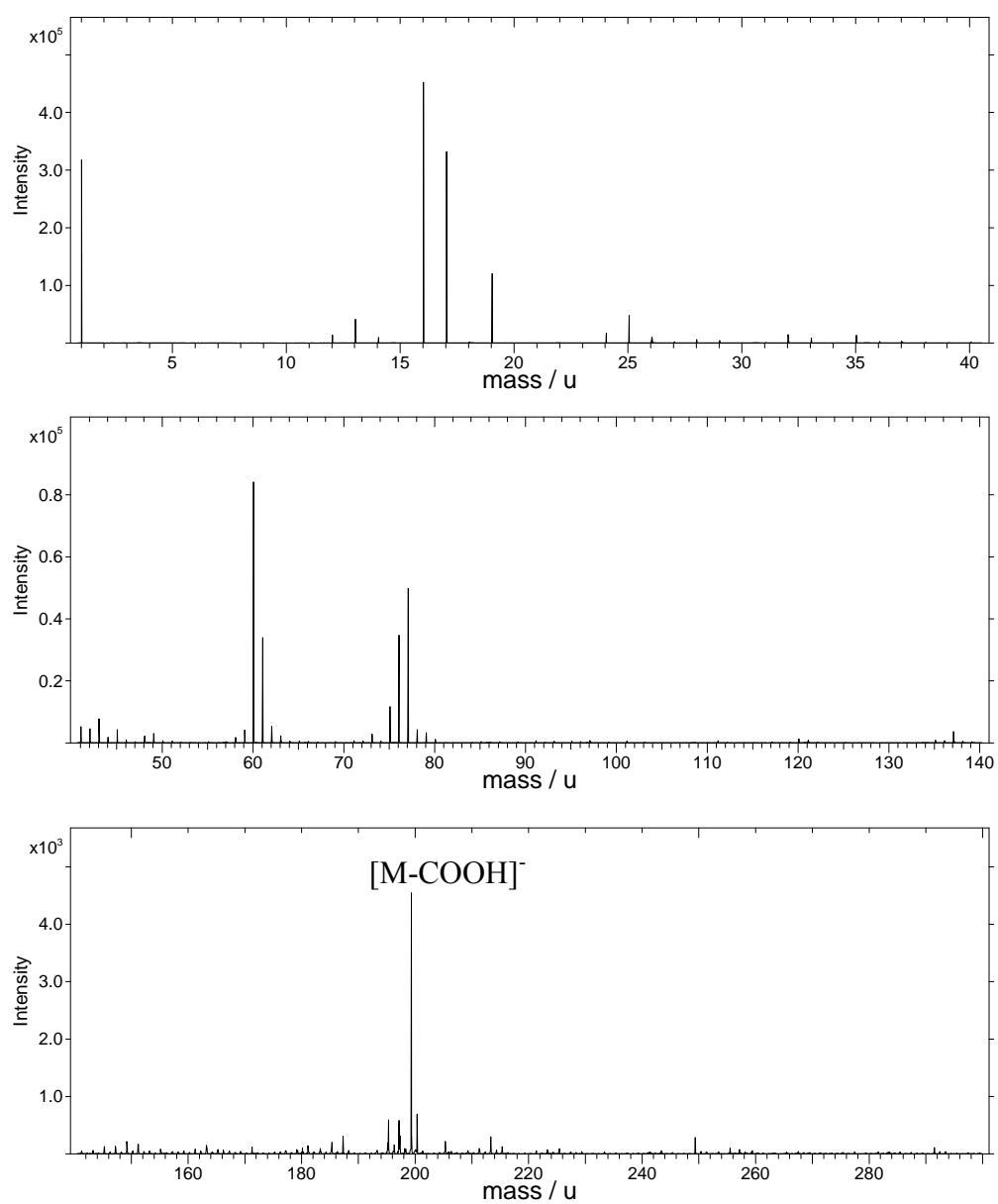
Figure 6.4 Negative ion ToF-SIMS spectrum of flurbiprofen
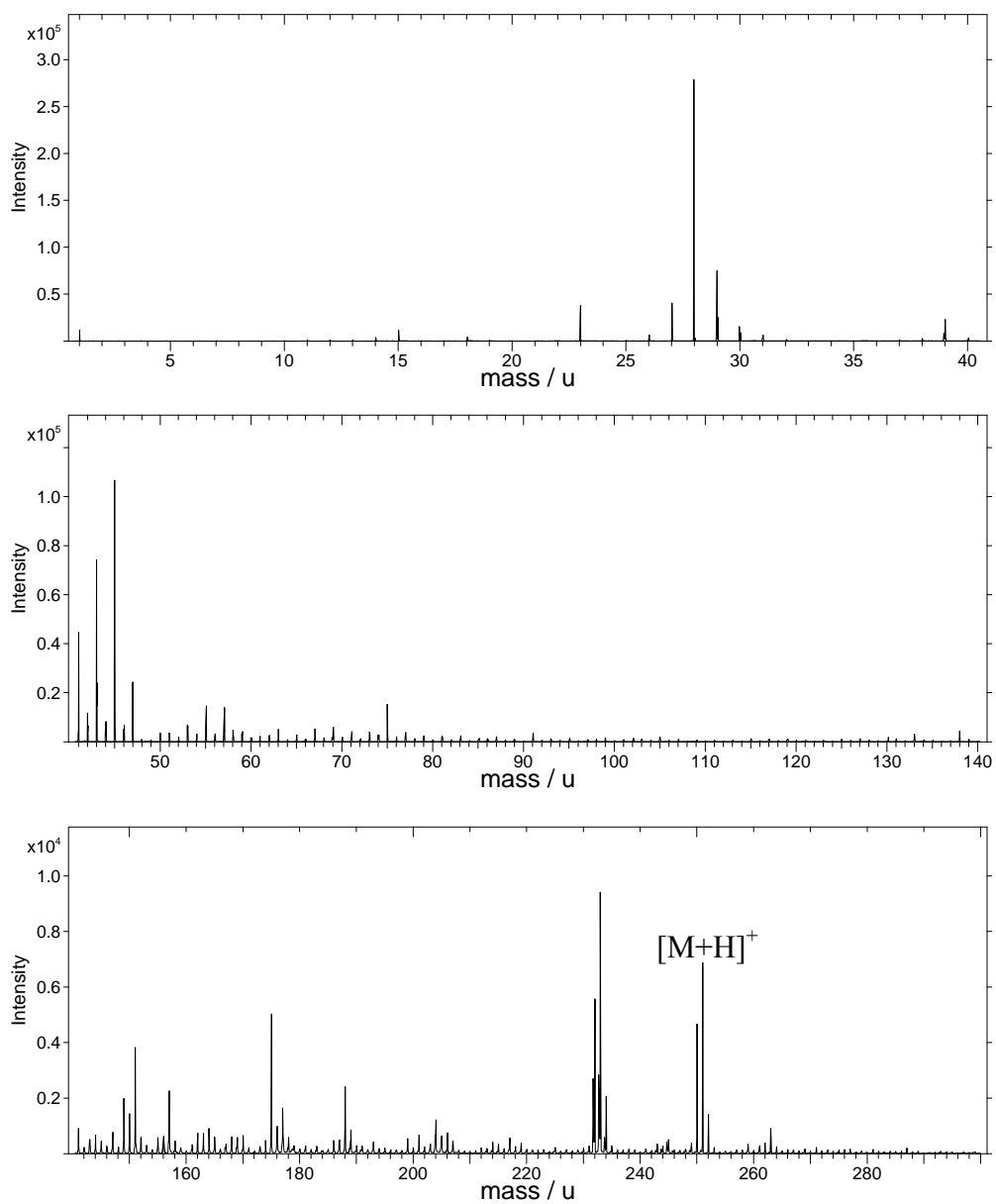
Figure 6.5 Positive ion ToF-SIMS spectrum of diflunisal
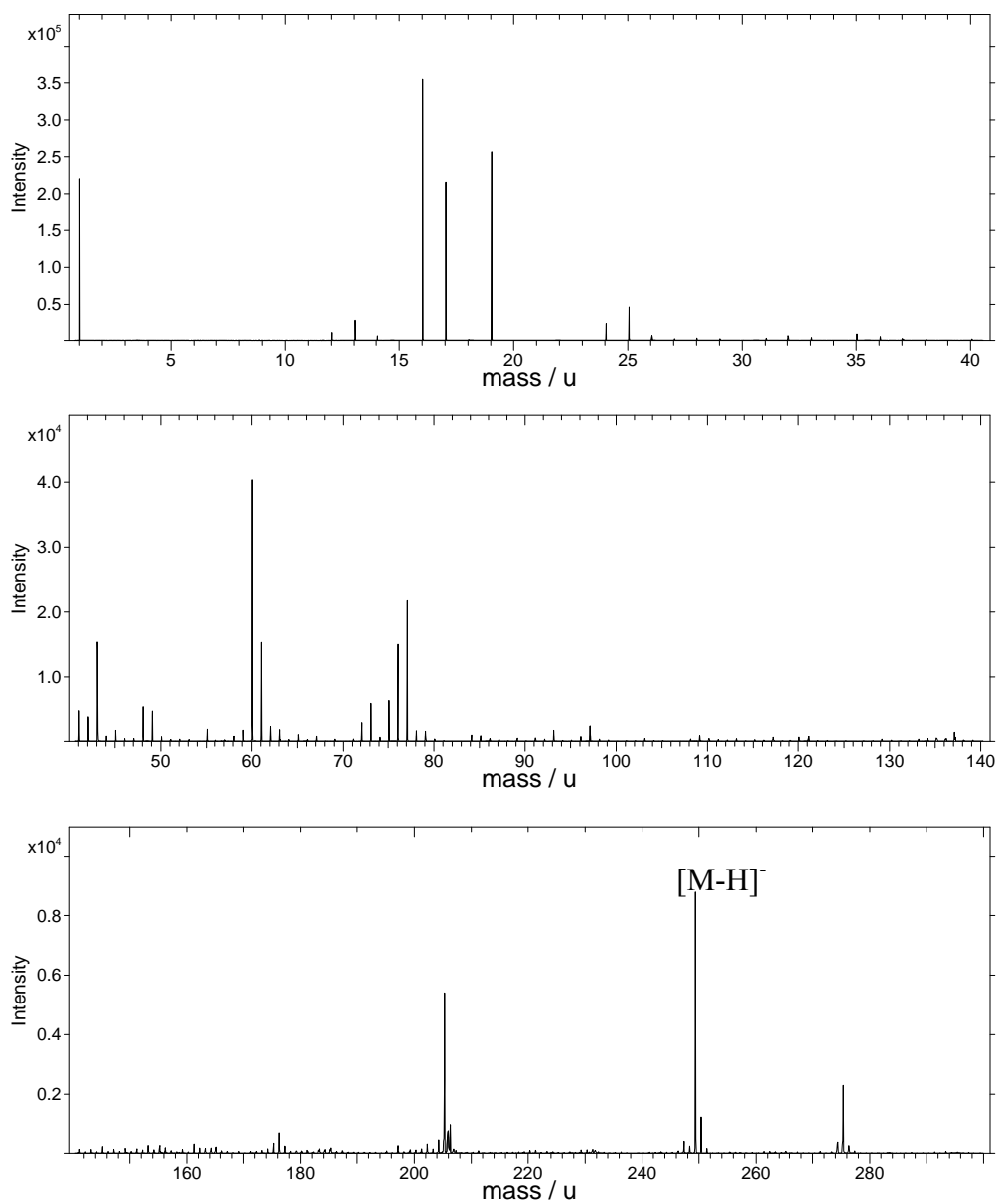
Figure 6.6 Negative ion ToF-SIMS spectrum of diflunisal

Figure 6.7 Positive ion ToF-SIMS spectrum of PEG

(* = repeating monomer unit of CH₂CH₂Ox-H and CH₂CH₂Ox+H)
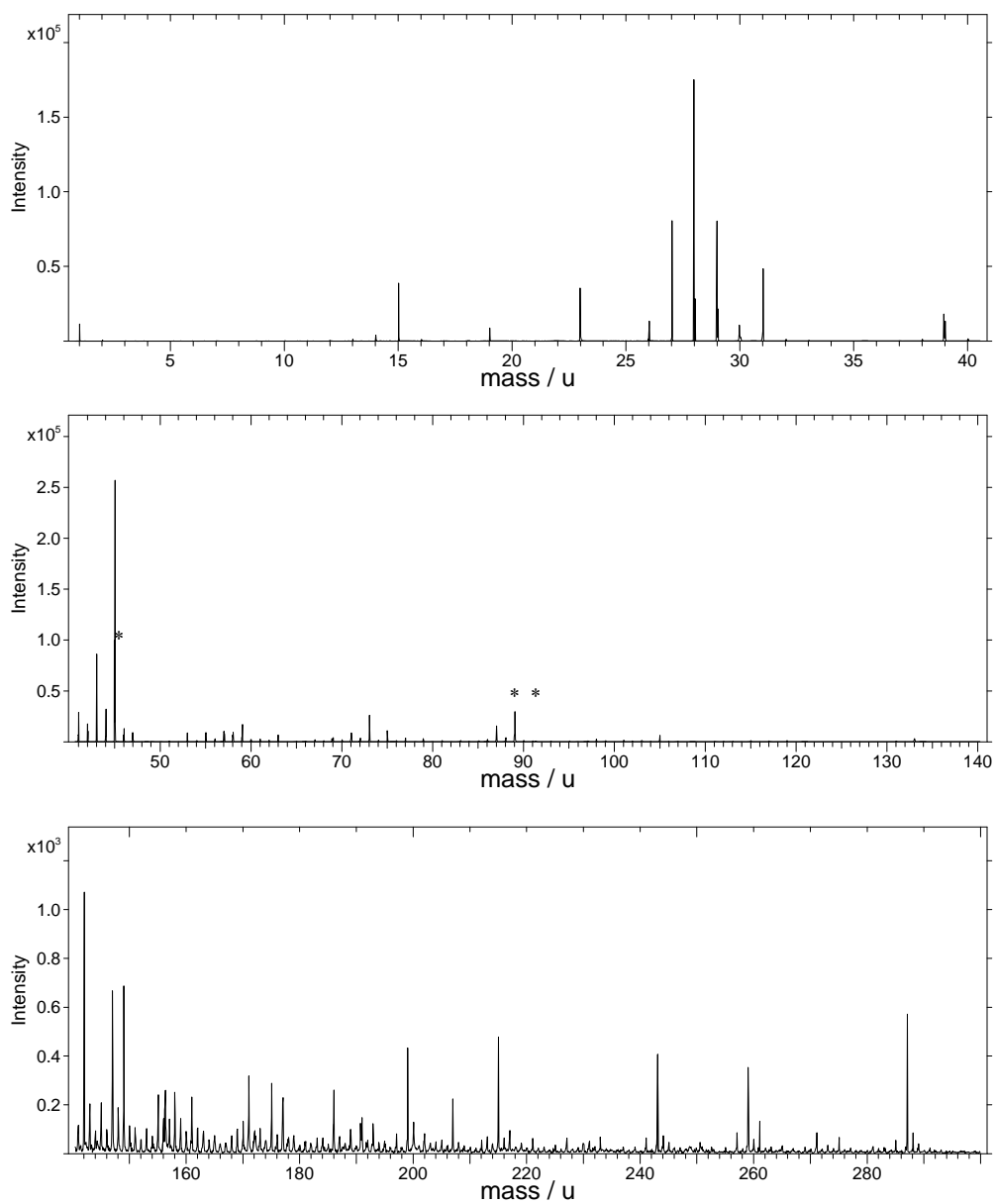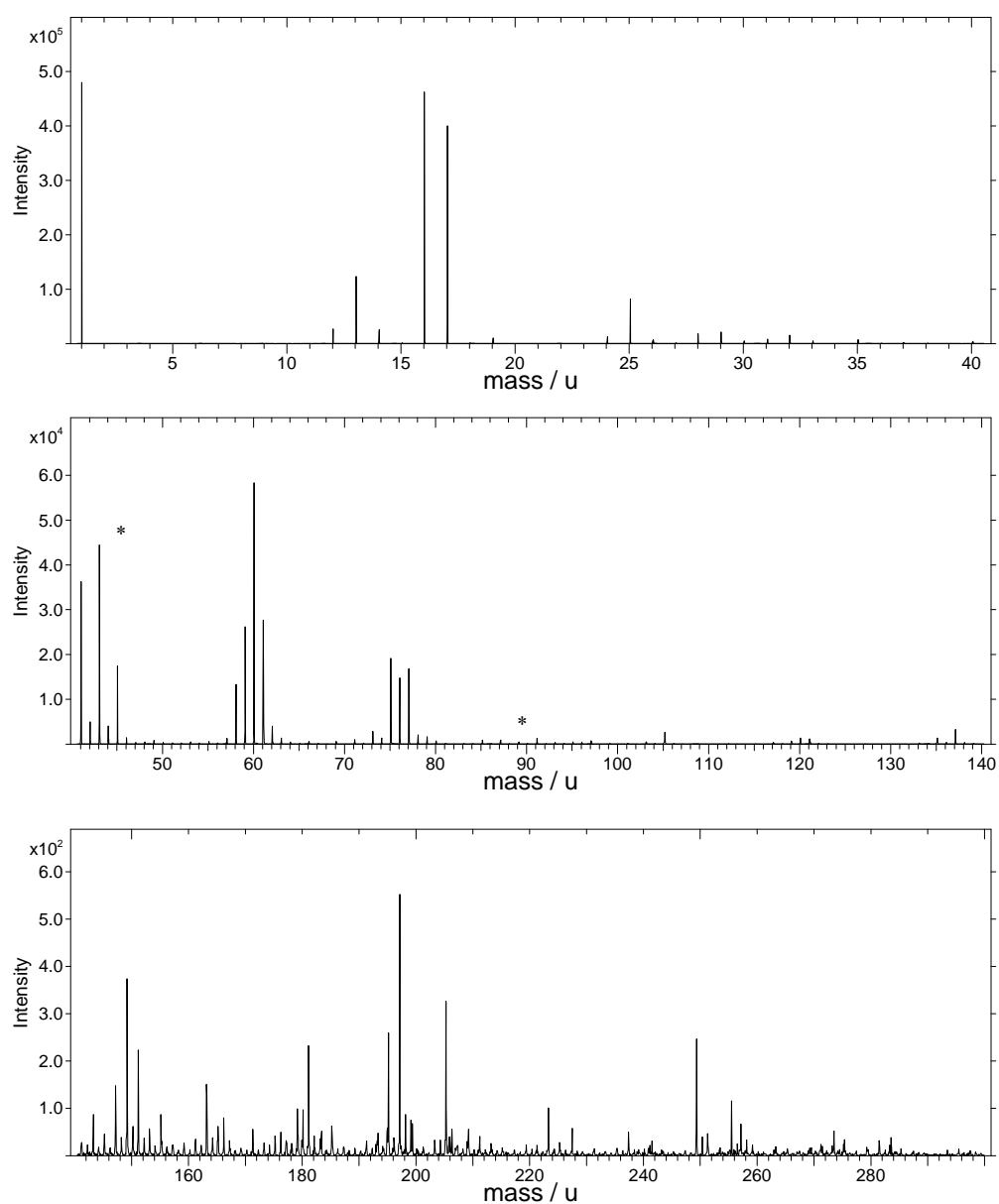
Figure 6.8 Negative ion ToF-SIMS spectrum of PEG

(* = repeating monomer unit of CH₂CH₂Ox-H⁺and CH₂CH₂Ox+H⁺)

m/z 59 = [CH₃O-CO]⁺

m/z 69 = [CH₃C(CH₂)CO]⁺
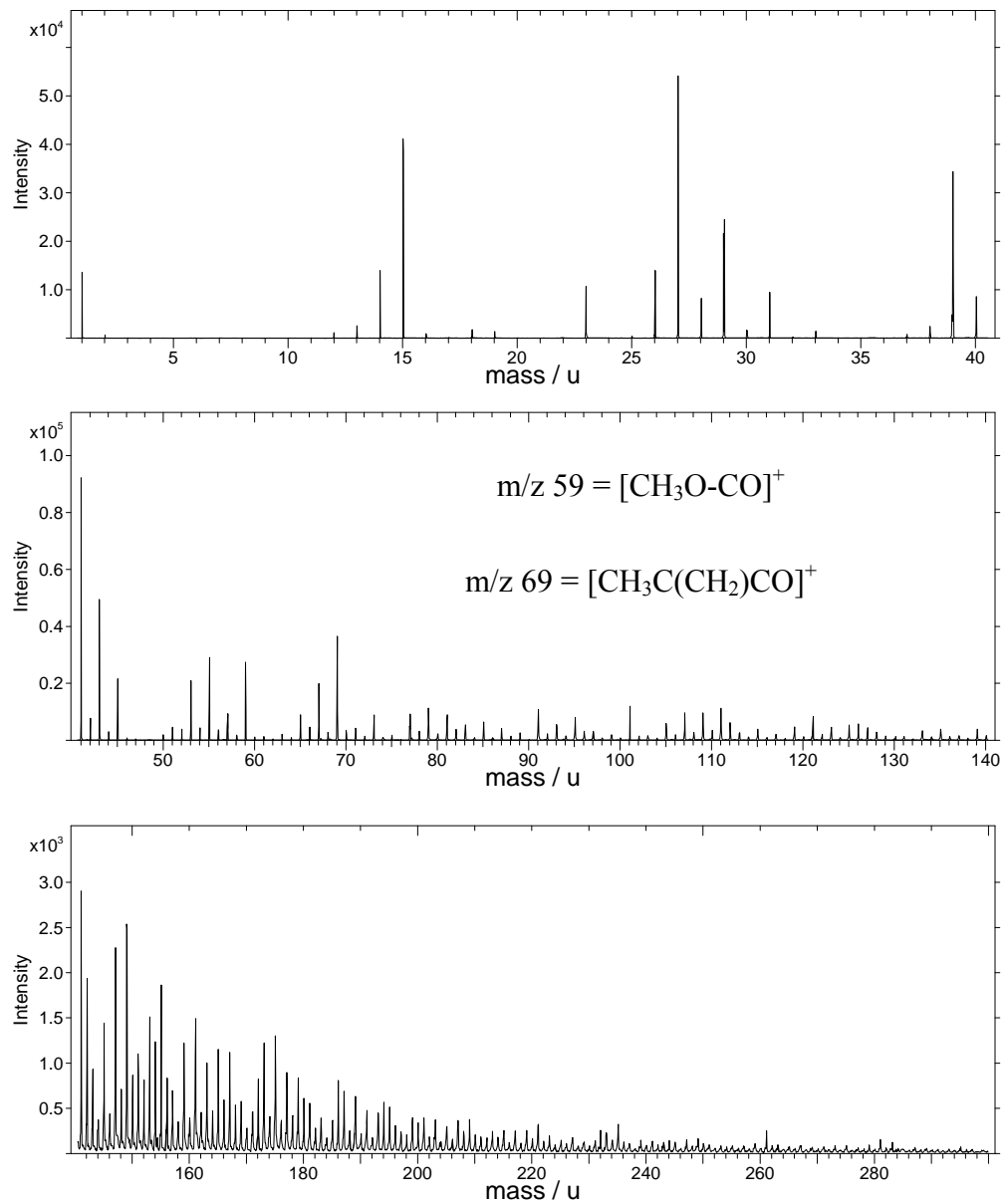
Figure 6.9 Positive ion ToF-SIMS spectrum of PMMA
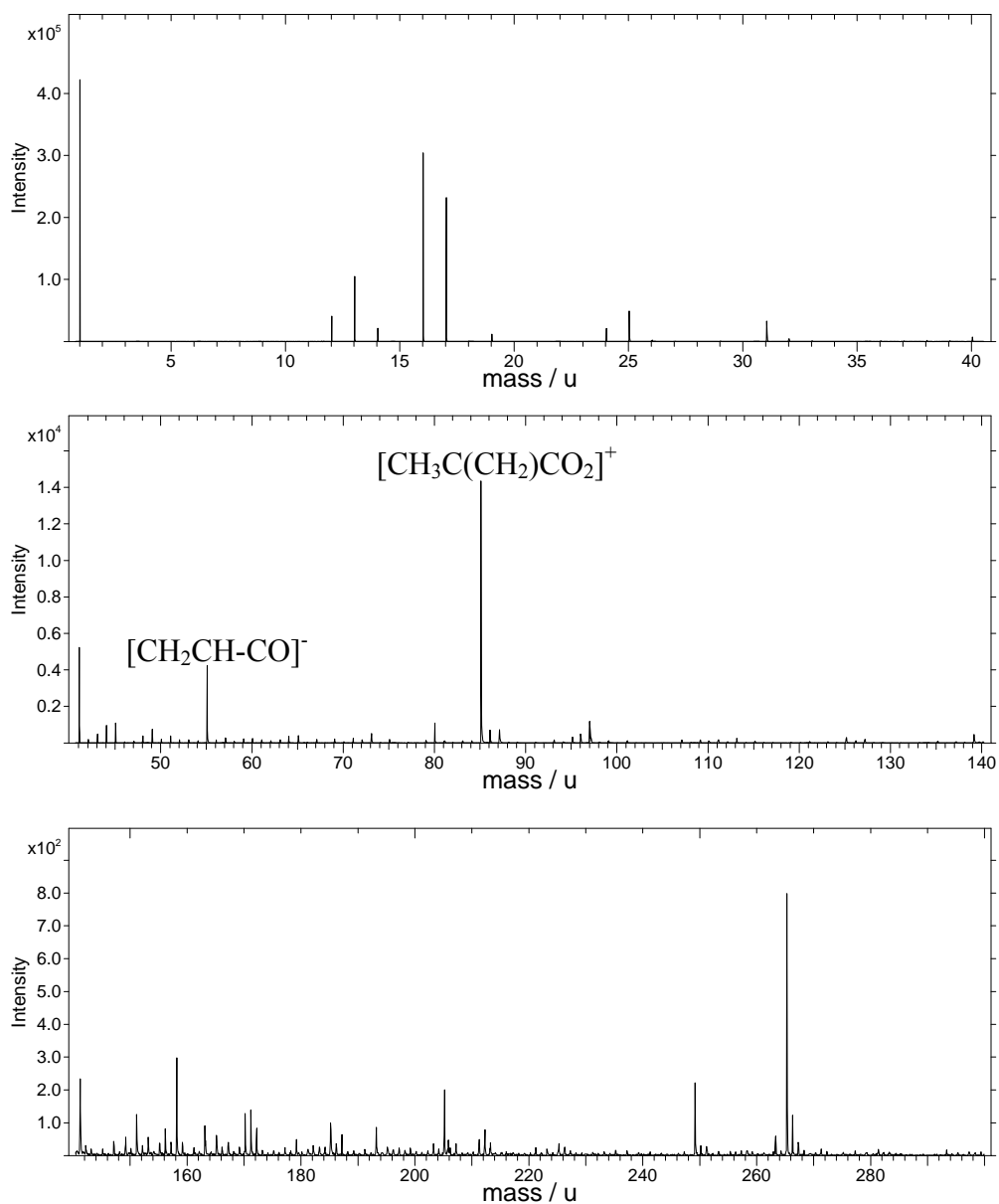
Figure 6.10 Negative ion ToF-SIMS spectrum of PMMA

6.3.2   ToF-SIMS Analysis of Spun Cast Solutions

The drug-polymer solutions were prepared as spun cast films as described in Section 6.2.2.1. Four spectra, representative of the data from the twenty four samples analysed are presented in Figure 6.11 to Figure 6.14.

The positive and negative ion ToF-SIMS spectra representing a ratio of 1:5 diflunisal to polyethylene glycol are shown in Figure 6.11 and Figure 6.12, respectively. The diflunisal protonated molecular ion was not observed in the positive ion spectrum, however the chemically distinct fragment at m/z 233$^+$ was observed. The PEG monomer base repeating pattern of [M$_x$+H]$^+$ and [M$_x$-H]$^+$, where M=CH$_2$CH$_2$O, was clearly observed particularly at low values of x, with visible peaks at m/z 43$^+$, 45$^+$, 87$^+$ and 89$^+$. This suppression effect of the matrix on the key diagnostic ions from the drug has also been previously observed by Vanden Eynde in his work in 2000 [Vanden Eynde and Bertrand, 2000].

The negative ion ToF-SIMS spectrum exhibited more intense diflunisal characteristic peaks than observed in the raw material. [M-H]$^-$ was observed in the spectrum at m/z 249$^-$, and an intense peak at m/z 205$^-$ was also present, previously identified as a chemically diagnostic diflunisal ion, [M-COOH]$^-$. The diagnostic PEG ions were also clearly visible, and were observed at m/z 43$^-$, 45$^-$, 87$^-$ and 89$^-$. These represented the repeating monomer unit described above, in the form [M$_x$+H]$^-$ and [M$_x$-H]$^-$ where x = 1 and 2.

The positive and negative ion ToF-SIMS spectra representing a ratio of 1:5 flurbiprofen to PMMA are presented in Figure 6.13 and Figure 6.14, respectively. Jones concluded that different matrices can have significantly different impacts on the ionisation, and hence detection, of key molecular ions [Jones *et al.*, 2006b]. This effect can be observed when the diflunisal in PEG positive ion ToF-SIMS spectrum is compared to the flurbiprofen in PMMA positive ion ToF-SIMS spectrum. Unlike in the diflunisal/PEG positive ion spectrum, the diagnostic drug ion (flurbiprofen [M-COOH]$^+$) dominated the positive ion ToF-SIMS spectrum in the m/z 150+ range, and was clearly observed at m/z 199$^+$. Unlike the PEG matrix, the PMMA matrix did not suppressed the key diagnostic ions and furthermore a protonated molecular ion at m/z 245$^+$ was also observed. This ion was not seen in the positive ion spectrum for the raw material and indicated that the PMMA matrix may have enhanced ion yields

from the drug. Previously identified PMMA ions were observed at m/z 59^+ and m/z 69^+. The negative ion ToF-SIMS also exhibited more intense characteristic drug peaks than observed in the raw material with a strong and intense peak visible at m/z 199^-. PMMA diagnostic ions were also evident in the negative ion ToF-SIMS spectrum at m/z 55^- and m/z 85^-.

These examples have shown that ion suppression was matrix dependent. This is line with previous work that also observed this phenomenon [Jones *et al.*, 2007a]. The experiments in this thesis used a gallium monoatomic primary ion source. An alternative approach would be to use a polyatomic ion source to increase secondary ion yields in the higher mass regions of the spectra, where diagnostic key ions for the drugs were present. Polyatomic ions have previously been shown to increase the sputter yield [Jones *et al.*, 2006a] without modification to a sample surface using an approach such as surface doping, also cited as an option to increase the weighting of higher mass secondary ion yields [Wiebel *et al.*, 2003].
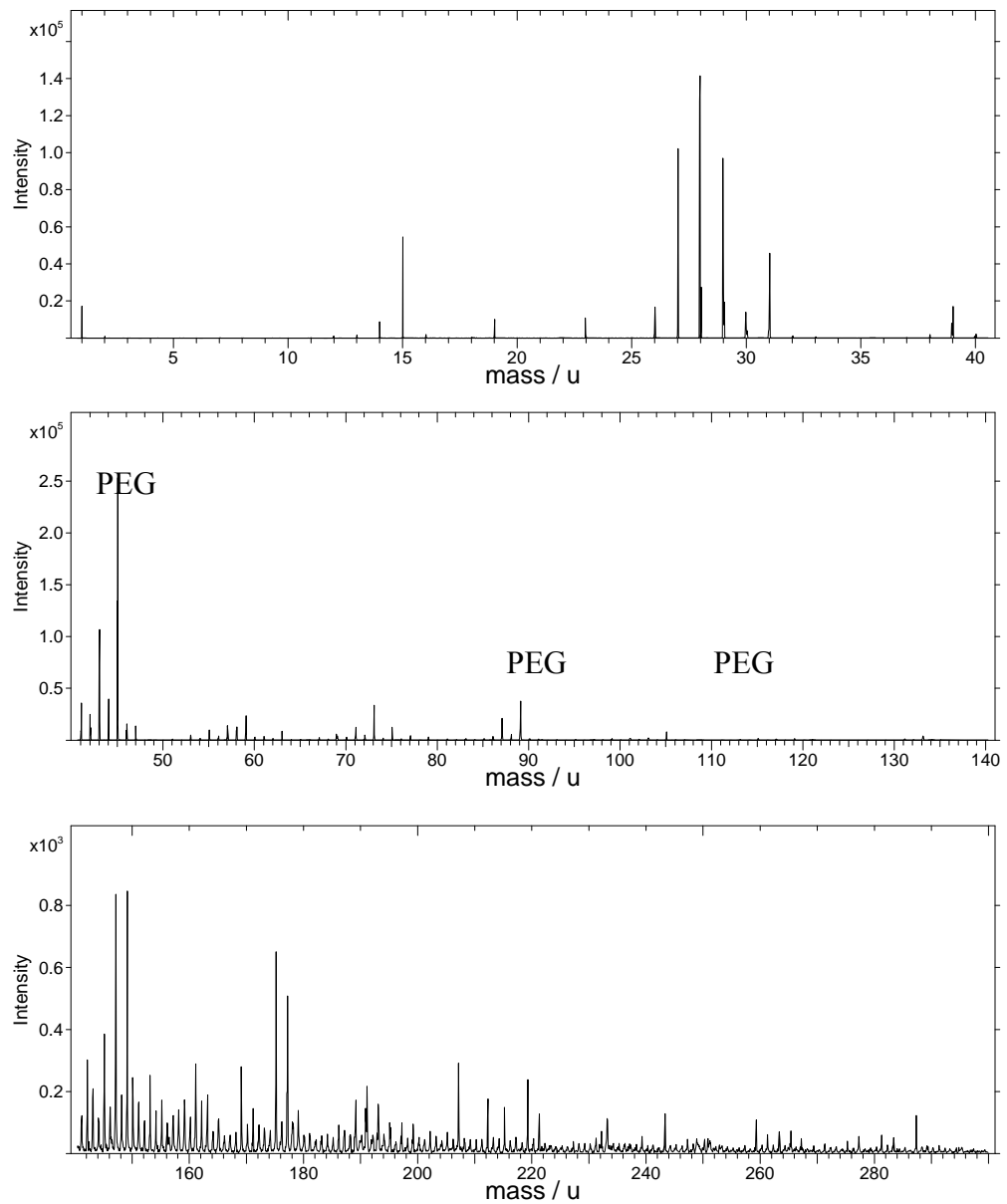
Figure 6.11 Positive ion ToF-SIMS spectrum of DIF1G5
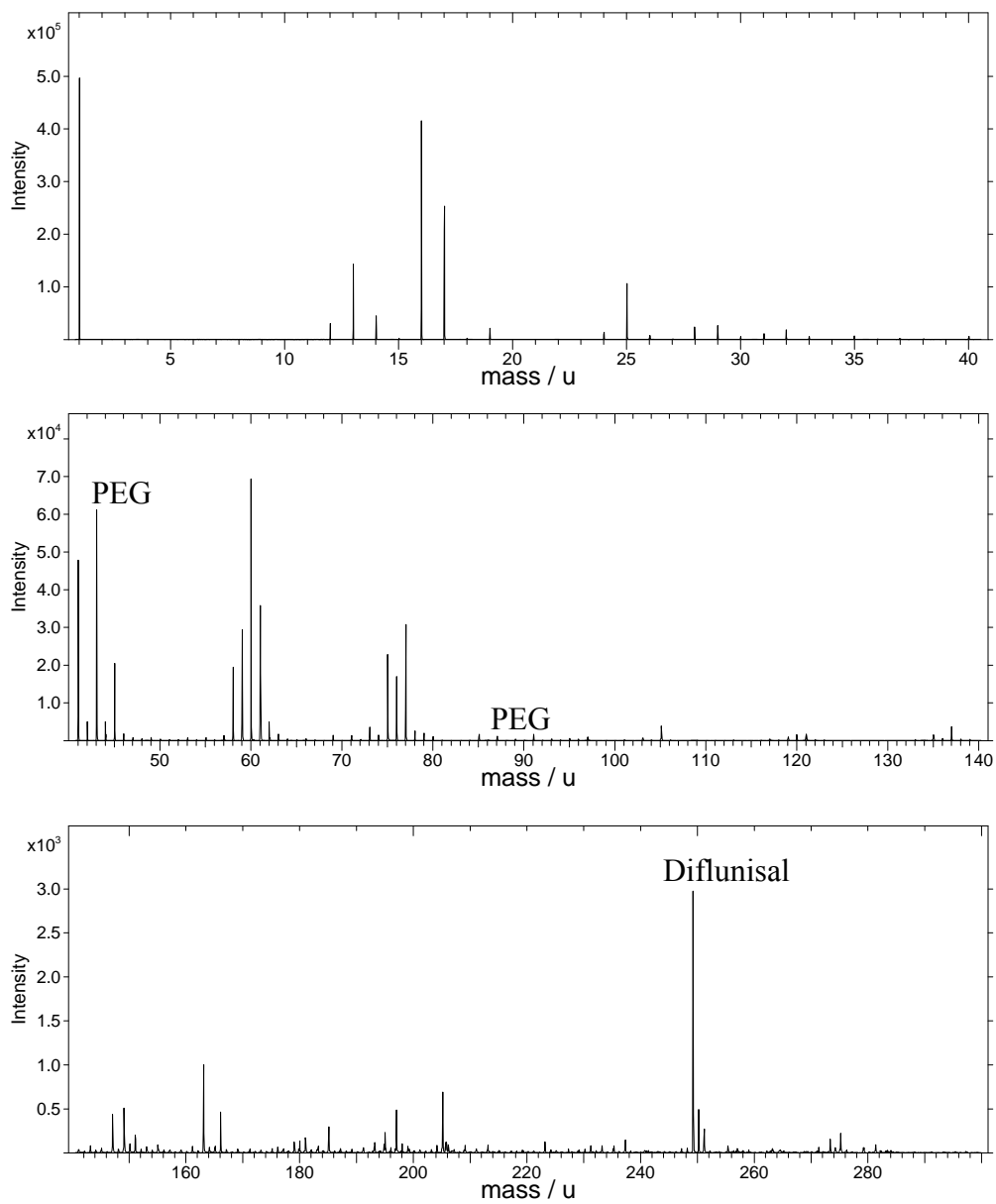
Figure 6.12 Negative ion ToF-SIMS spectrum of DIF1G5
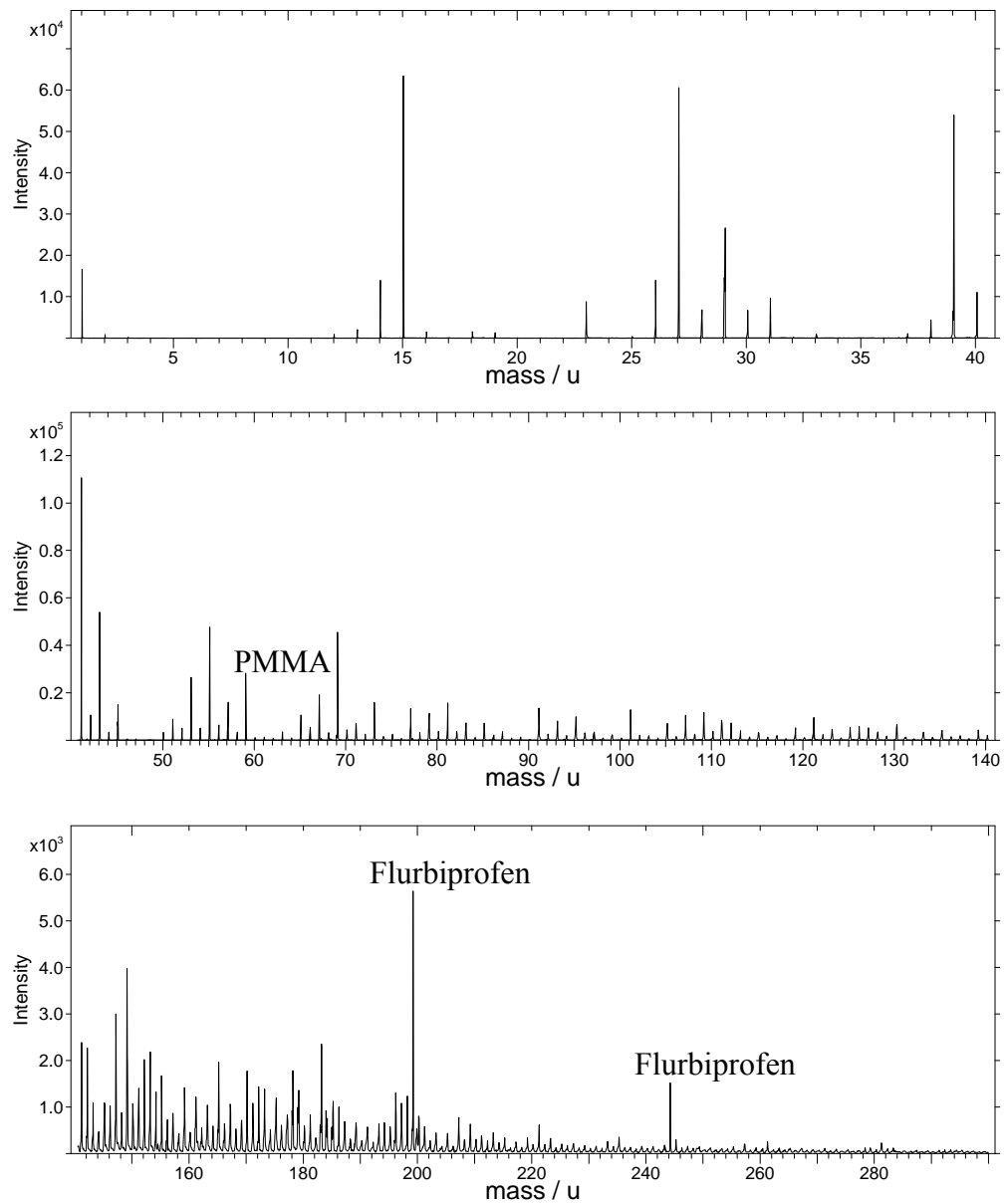
Figure 6.13 Positive ion ToF-SIMS spectrum of FLU1M5
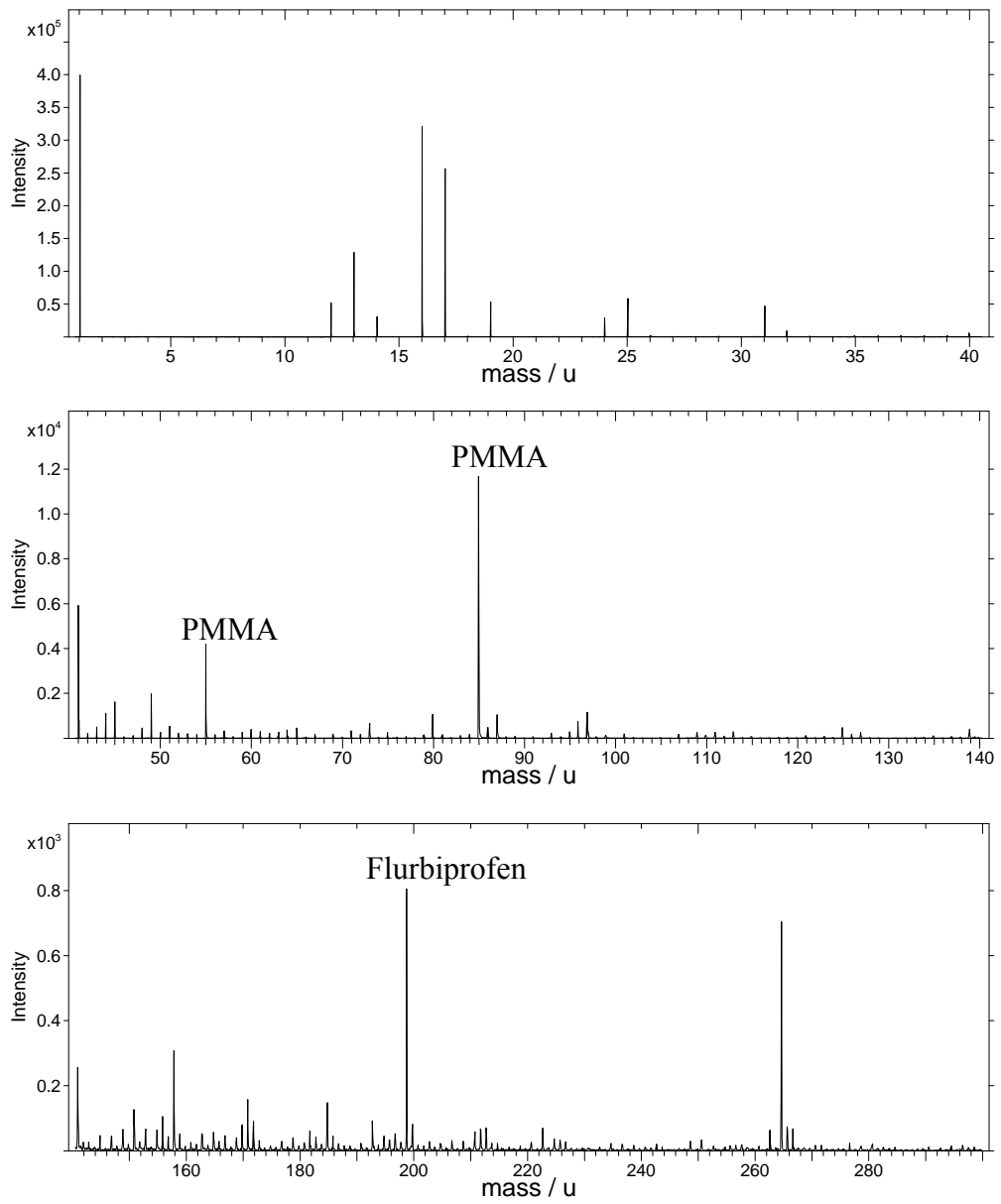
Figure 6.14 Negative ion ToF-SIMS spectrum of FLU1M5

6.3.3   Principal Component Analysis of Drug/Polymer Spun Cast Solutions

Prior to performing PCA of the twelve samples, the level of drug concentration, via the F$^-$ ion was plotted for each concentration of drug in both polymers. This data is presented in Figure 6.15.
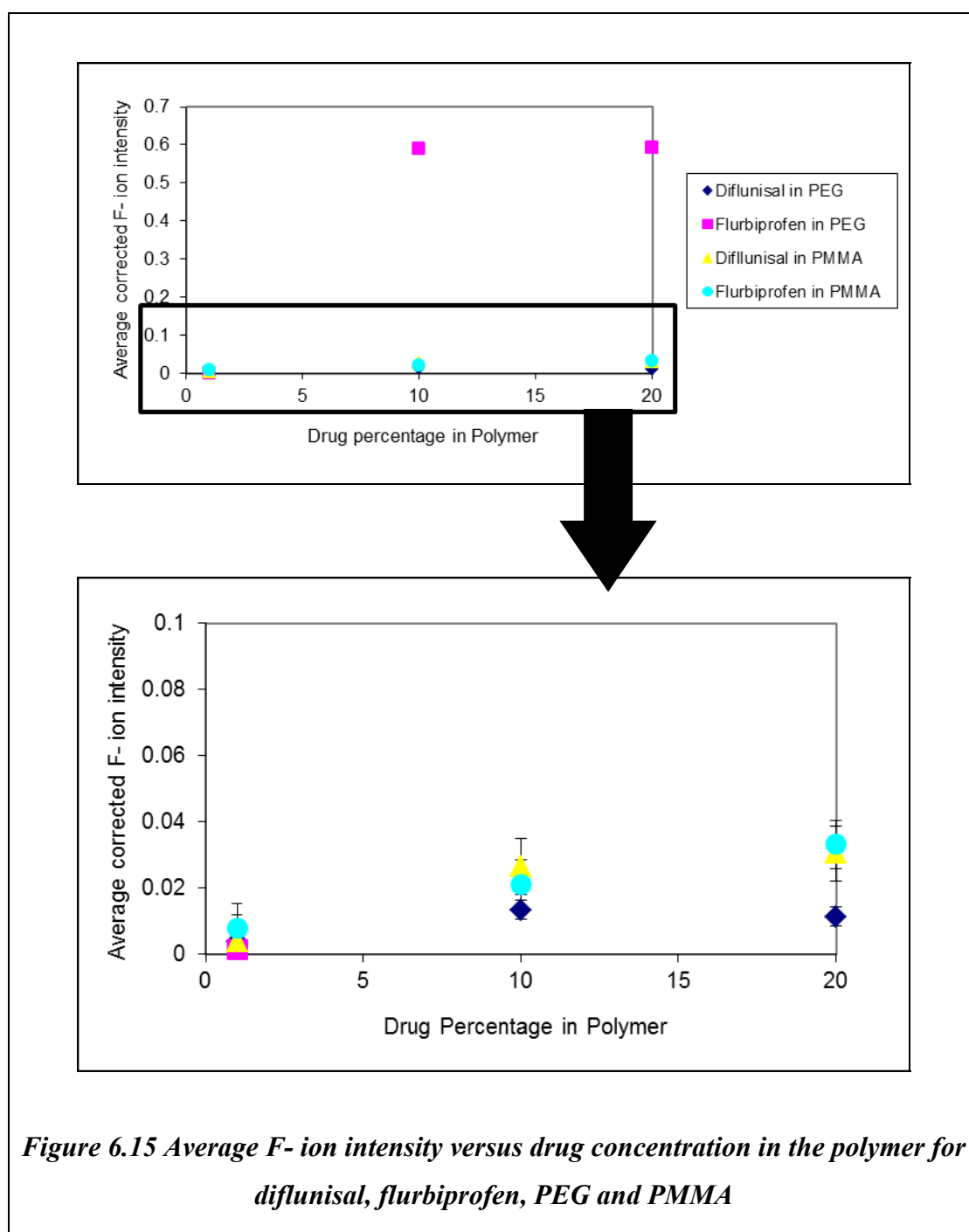
Figure 6.15 Average F- ion intensity versus drug concentration in the polymer for diflunisal, flurbiprofen, PEG and PMMA

226

Figure 6.15 highlighted the non-linear relationship between both the diflunisal and the flurbiprofen in the PEG and the PMMA matrix. Non-linear relationships were also observed for other diagnostic ions for the drugs. Spun cast films exhibit nanometre roughness profiles [Benz *et al.*, 2001]. Therefore, in these samples, roughness cannot be playing a role in the intensity of secondary ion yields, as has been observed in previous chapters. The flurbiprofen in PMMA was the closest to linearity in nature (but extrapolation did not go through the origin) yet a different relationship was observed for the drug in PEG highlighting the impact of chemical environment on ion yields.

PCA was carried out on triplicate positive and negative data sets for all twelve samples. For each sample two separate peak lists were generated, each specific to the positive and negative secondary ion spectra. As a manual process this would have taken several days, if not weeks. However, the use of the automated PCA PLS_Toolbox allowed for rapid processing of the data as reported by Scurr [Scurr *et al.*, 2010]. The corrected peak intensities were normalised to the total ion count thereby accounting for any variation in secondary ion yield between samples. The eigenvalue plot presented in Figure 6.16 indicated that the principal components that exhibited substantial variance, and hence thought to be significant, were PC1 and PC2. The samples could be differentiated on three criteria, which polymer they contained, which drug they contained, and the concentration of these two elements. These will be discussed in terms of the two principal components.

Figure 6.16 Eigenvalue plot from PCA showing principal components 1-5 for the drug polymer solutions of diflunisal / flurbiprofen and PEG / PMMA as described in Table 6.2
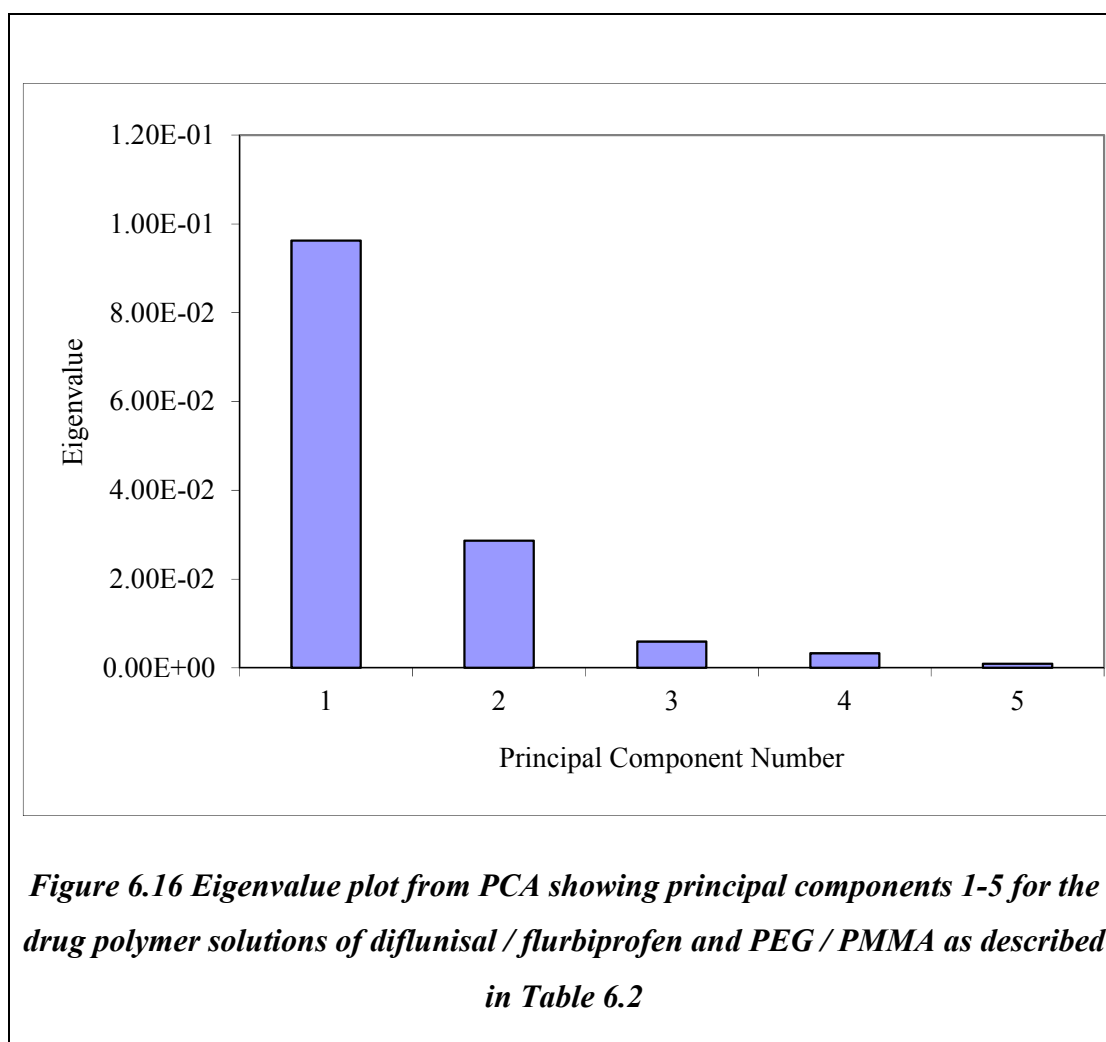
The scores plot derived from the PCA is presented in Figure 6.17. PC1 was plotted on the x-axis and PC2 was plotted on the y-axis. In addition to identifying how samples differentiate or group together, scores plots can add an extra dimension to the analysis by indicating the level of homogeneity within sample sets, i.e. if sample repeats cluster closely or are dispersed in the scores plot, this would suggest that they were homogeneous or heterogeneous, respectively. Three samples were produced for each concentration, from the same batch of solution, using identical preparation and analysis methods for each. Theoretically the samples should therefore have been chemically identical and present in 'tight' clusters of three data points within the scores plots. This was certainly the case for DIF1M5, where the sample data points were located at the same position. In the other samples the data points were also in close proximity, with two exceptions, the two highest concentrations of flurbiprofen in PEG samples. These samples displayed a comparatively wide distribution of data

points, and were observed exhibiting relatively high values in PC1 and PC2. This indicated that the three samples produced for these two concentrations were less chemically homogeneous between sample repeats than the other samples within the analysis data set.

Figure 6.17 Scores plot from PCA data reduction of ToF-SIMS spectra showing principal components 1 and 2 for the drug polymer solutions of diflunisal / flurbiprofen and PEG / PMMA outlined in Table 6.2
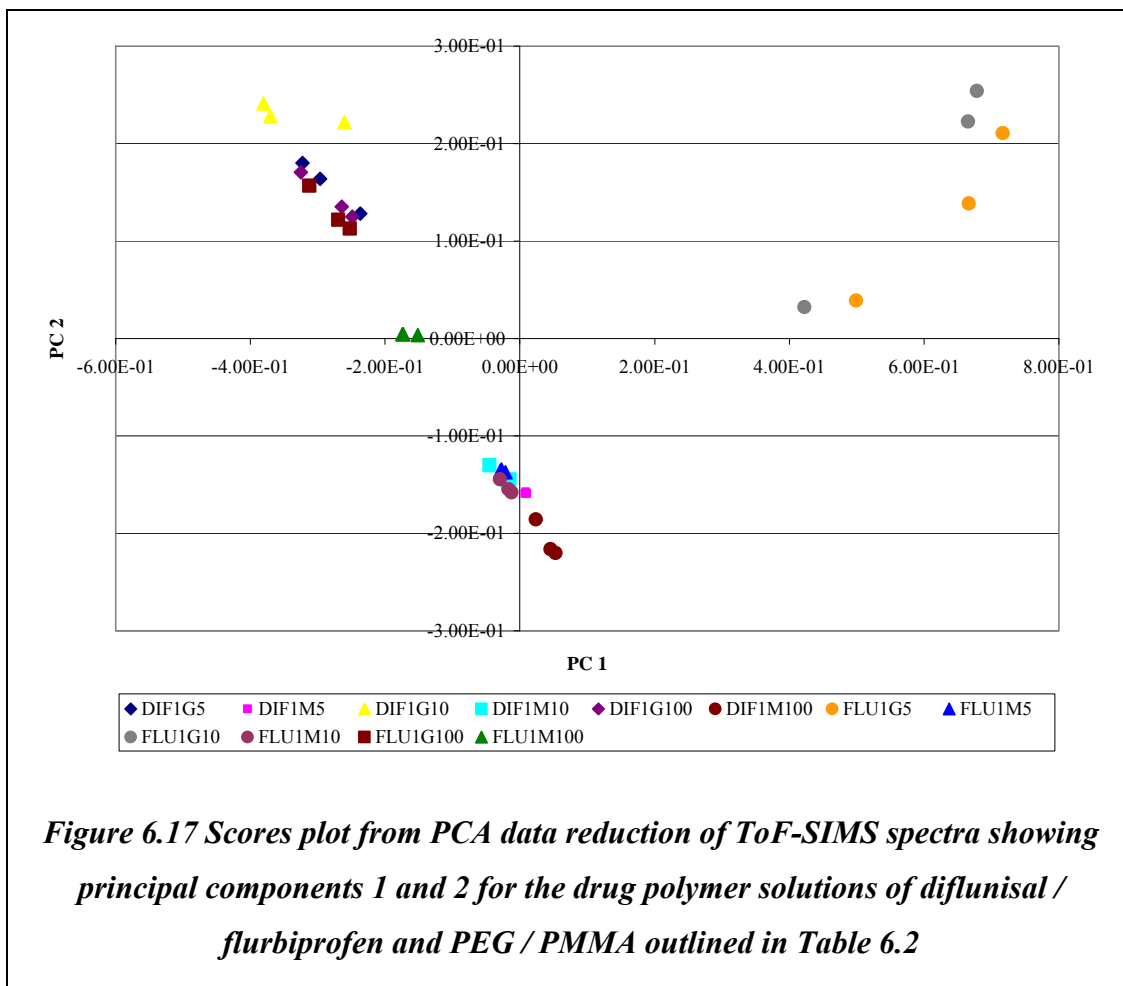
The scores plot in Figure 6.17 clearly highlighted that the sample data points exhibited four distinct groupings. The high concentration flurbiprofen and PEG samples were located together at a higher PC1 value than the other three groupings. These two samples exhibited similar and relatively high PC2 values. A second grouping consisting of four samples was clustered together at a relatively lower value on PC1 than the other groupings. The four samples in this second grouping all contained PEG and comprised of FLU1G100, DIF1G100, DIF1G5 and DIF1G10. FLU100M appeared to be isolated from the other sample data points and was located slightly lower on the PC2 scale than the previous two groupings, and at an

approximate midpoint between them in regards to PC1. The final five samples were clustered together and were located at a similar point on PC1 to the isolated sample. These samples differentiated from the others by their lower PC2 value than the other three groupings. The five samples in this final grouping all contained PMMA and comprised of DIF1M5, DIF1M10, FLU1M5, FLU1M10 and DIF1M100. The distinct clustering that was observed in the scores plot in Figure 6.17 indicated that PCA was able to differentiate between sample types, and exposed differences between them.

6.3.3.1 Principal Component 1

The respective loadings table for PC1 (plotted on the x-axis of the scores plot) is presented in Table 6.4. Origins of each ion were assigned where possible (i.e. if a chemically distinct ion was present at the m/z value). As a general rule, samples that contained higher amounts of the positively loaded ions exhibited higher values in the scores plot on the PC1 (x-axis), whereas samples that contained higher amounts of the negatively loaded ions exhibited lower values in the scores plot on the PC1 x-axis.

All three of the diflunisal and PEG based samples were located at lower values of PC1 in regards to the other samples, whereas the two highest concentrations of flurbiprofen in PEG were plotted at higher values of PC1 relative to the other samples. The two highest concentrations of both drugs in PMMA were located within the five sample cluster discussed above and exhibited intermediate PC1 values relative to the other samples. The position of these data points within the scores plot corresponded to the relative proportions they contained of the significantly loaded ions that made up the individual principal components.

The key ions that contributed to PC1 are presented in Table 6.4, and the respective loadings for PC1 are presented in Figure 6.18. PC1 accounted for 70.74% of the variance in the sample set. Examination of the loadings for PC1 showed that the ions with the greatest positive loadings were m/z 19.00^-, 69.00^+ and 31.00^+ which represented fluorine (found in both drugs), CF_3^+ and CF^+, respectively. The loadings plot in Figure 6.18 clearly showed that these three ions constituted the bulk of the PC1 positive loadings. Although these fluorine related compounds could potentially

arise from both drugs, PCA is not concerned with the intensity level of peaks per se, but the variance across the sample set for any given ion.

Figure 6.18 Loadings as a function of variable from PCA of ToF-SIMS data showing principal component 1 (PC1) for the drug polymer solutions of diflunisal / flurbiprofen and PEG / PMMA as described in Table 6.2

Strongest Positively Loaded Ions			Strongest Negatively Loaded Ions		
Ion	**m/z**	**Origin**	**Ion**	**m/z**	**Origin**
F^-	19.00	Drug	O^-	15.99	Oxygen
CF_3^+	69.00	Drug	OH^-	17.00	Hydroxyl
CF^+	31.00	Drug	Si^+	27.98	substrate
Unknown$^-$	162.99	Drug	$[CH_2CH_2O]+H$	45.04	PEG
SiF^+	46.98	Substrate	SiH^+	28.98	substrate
C^+	12.00	Carbon	CH^-	13.01	HC fragment
$C_3HO_3^-$	84.99	PEG	C_2H^-	25.01	HC fragment
$C_3F_7^+$	169.00	Drug	$C_2H_3^+$	27.02	HC fragment
$C_4HO_3F_2^-$	134.98	Drug	$[CH_2CH_2O]-H$	43.02	PEG
$C_4HO_2F^+$	100.00	Drug	$SiCH_3^+$	43.00	substrate
F_2^-	38.00	Drug	$CH_4CO_2^-$	59.97	PEG

Table 6.4 The Strongest Positively and Negatively Loaded Secondary Ions and Their Corresponding Mass/Charge (m/z) for PC1 as identified by PCA for the drug polymer solutions of diflunisal / flurbiprofen and PEG / PMMA as described in Table 6.2

Further examination of the loadings for PC1 showed that the ions with the most significant negative loadings were m/z 15.99$^-$, 17.00$^-$ and 27.98$^+$, representing oxygen, hydroxyl ions and silicon from the substrate. Again, the loadings plot in Figure 6.18 clearly showed that the first three ions constituted the bulk of the PC1 negative ion loadings. All samples contained O$^-$ and OH$^-$ so can effectively be disregarded in the analysis. This statement applies equally to the silicon ion signal

from the substrate. The next strongest negatively loaded ions that PC1 consisted of were predominantly hydrocarbon fragments and a contribution from the PEG related positive ion peaks at m/z 43$^+$ and m/z 45$^+$. As these were the negatively loaded ions for PC1, samples that exhibited higher count values from these ions were anticipated to exhibit relatively lower scores values for PC1.

Two of the PEG sample sets were located at high PC1 values relative to the other samples, FLU1G10 and FLU1G5. However, it was diflunisal that contained the greatest percentage of fluorine in terms of weight % as diflunisal contains two fluorine atoms. In comparison, the two corresponding high concentration flurbiprofen and PMMA samples were located at intermediate PC1 values in respect of the other samples. From the respective loadings, this indicated that the F$^-$ ion yield was affected by the polymer matrix, with greater secondary ion yields seen from a PEG than a PMMA matrix and greater ion yields from the drug containing the lower quantity of fluorine. This may have arisen for a number of reasons. There may have been a difference in the surface (lateral and surface versus bulk) between the two drugs in the polymer due to preferential surface presence of one of the drugs. In addition, there may have been an influence of the matrix on ion yield through an interaction between the polymer and drug. There may also have been differences in the ion yield of the principle ions between the drugs, and this itself could also have been influenced by environment as a function of the drug to polymer ratio.

However, when lower concentrations of the drug were in the polymer (1 part to 100), this effect seemed to be less significant and potentially reversed as the F100G samples were located at lower PC1 values than the F100M samples. All of the diflunisal / PEG samples were located in a relatively low value PC1 grouping respective to the other samples (D1G5, D1G10 and D1G100) and in particular to the flurbiprofen / PEG indicating that these contained less of the strongest loaded positive fluorine ion, and PCA was able to differentiate between them.

The influence of fluorine in the positively loaded ions was also seen in the flurbiprofen / PMMA samples. In a pattern similar to the flurbiprofen / PEG samples, the two highest concentrations were located at higher PC1 values than the low concentration sample on the scores plot, i.e. the positively loaded ions counteracted the negatively loaded ions for the two highest concentrations. Again, this indicated

that the variance in the fluorine ion dwarfed that of the negatively loaded hydrocarbon fragments. In this respect PC1 differentiated between high and low drug concentrations in both of the polymer matrices. Figure 6.15 indicated that the F^- ion intensity for this sample set was linear, however the other ions that constituted PC1, exhibited enough variance for this linearity not to be observed on the score plot.

The diflunisal containing PMMA samples were all located at intermediate values of PC1 relative to the other samples in the scores plot. The lack of separation between the samples of varying drug level indicated that the fluorine ion was being affected by the matrix.
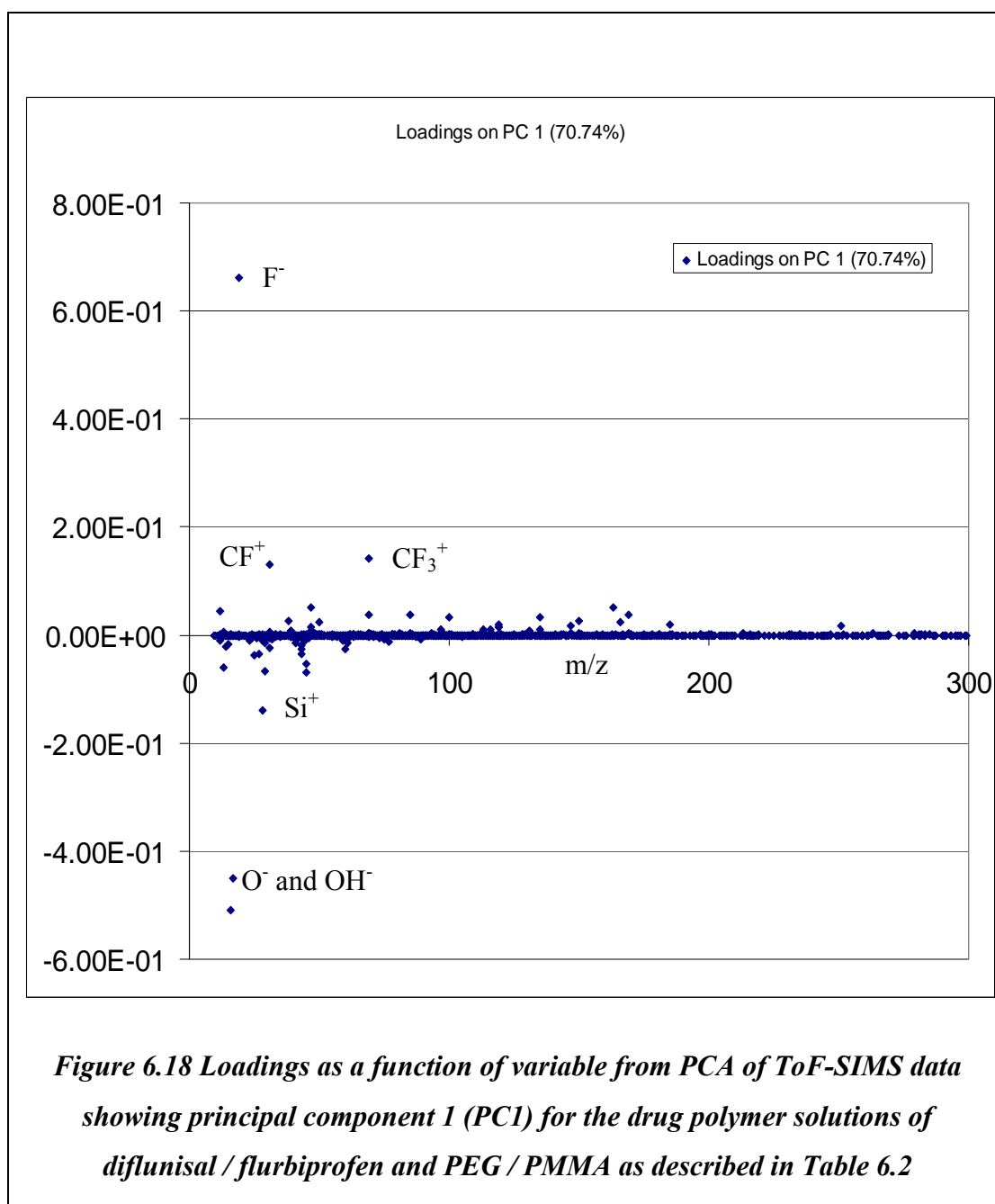
6.3.3.2   Principal Component 2

The respective loadings table for PC2 (plotted on the y-axis of the scores plot) is presented in Table 6.5. Origins of each ion have been assigned where possible (i.e. if a chemically distinct ion is present at the m/z value). The loadings for PC2 indicated where the data points were located within the associated scores plot. As a general rule, samples that contained higher amounts of the positively loaded ions exhibited higher values in the scores plot on the PC2 (y-axis), whereas samples that contained higher amounts of the negatively loaded ions exhibited lower values in the scores plot on the PC2 y-axis.

PC2 appeared to be somewhat easier to interpret than PC1. The sample clustering behaviour exhibited in the scores plot (Figure 6.17) illustrated that the samples were markedly differentiated by their polymer composition with respect to PC2, where PEG containing polymers exhibited higher PC2 values than PMMA containing samples. PCA was therefore able to discriminate between the two polymer containing sample types in regards to PC2. PC2 accounted for 21.06% of the variance in the sample set and the key ions that contributed to PC2 are presented in Table 6.5. Examination of the loadings for PC2 showed that the ions with the greatest positive loadings were m/z 19.00^-, 27.98^+ and 17.00^+ which represented fluorine (found in both drugs), silicon associated ions presumably from the substrate and a hydroxyl group. All of these ions were non-specific in terms of the drugs or polymers. Again, the loadings plot in Figure 6.19 clearly showed that it was the first

three ions that constituted the bulk of the PC2 positive ion loadings. However, the next strongestly loaded ion was the diagnostic PEG ion at m/z 45^+.
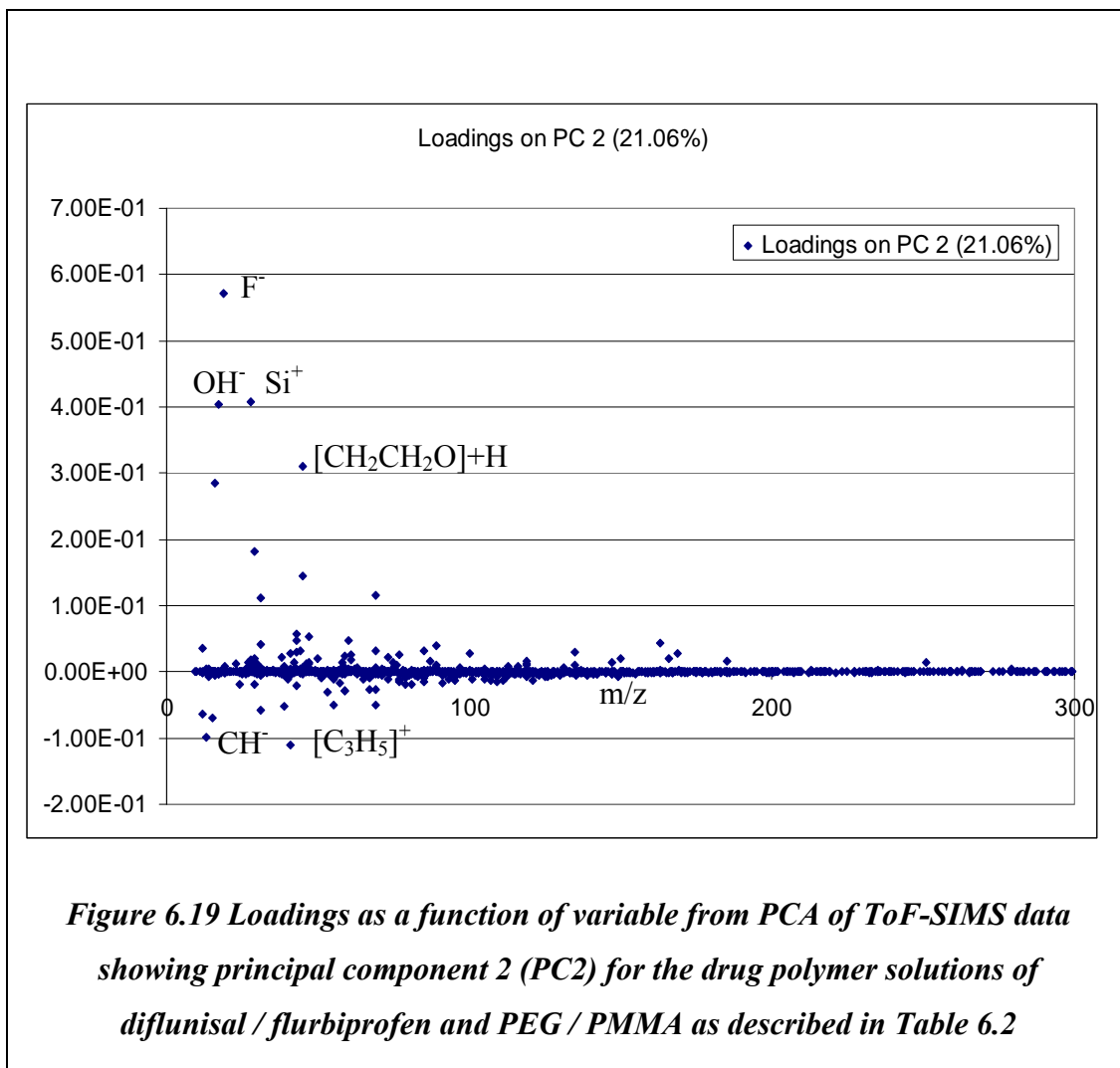
Figure 6.19 Loadings as a function of variable from PCA of ToF-SIMS data showing principal component 2 (PC2) for the drug polymer solutions of diflunisal / flurbiprofen and PEG / PMMA as described in Table 6.2

Strongest Positively Loaded Ions			Strongest Negatively Loaded Ions		
Ion	**m/z**	**Origin**	**Ion**	**m/z**	**Origin**
F^-	19.00	Drug	$C_3H_5^+$	41.04	HC fragment
Si^+	27.98	Substrate	CH^-	13.01	HC fragment
OH^-	17.00	Hydroxyl	CH_3^+	15.02	HC fragment
$[CH_2CH_2O]+H$	45.04	PEG	C^-	12.00	Carbon
O^-	15.99	Oxygen	CH_3O^-	31.02	PMMA
SiH^+	28.98	Substrate	$C_3H_3^+$	39.02	HC fragment
CF_3^+	69.00	Drug	$C_5H_9^+$	69.04	PMMA
SiH_3^+	31.00	Substrate	$C_4H_7^+$	55.06	PMMA
			$C_4H_5^+$	53.04	HC fragment
			$C_2H_3O_2^+$	59.00	PMMA

Table 6.5 The strongest positively and negatively loaded secondary ions and their corresponding mass/charge (m/z) for PC2 as identified by PCA for the drug polymer solutions of diflunisal / flurbiprofen and PEG / PMMA

Further examination of the loadings for PC2 showed that the ions with the most significant negative loadings were m/z 41.04^+, 13.01^- and 15.02^+, which all represented non-specific hydrocarbon fragments. Again, the loadings plot in Figure 6.19 clearly showed that the first three ions constituted the bulk of the PC2 negative ion loadings. The next strongest negatively loaded ions that contributed to PC2 consisted of a mix of hydrocarbon fragments and contributions from the PMMA related positive ion peaks at m/z 69.04^+, m/z 55.06^+ and m/z 59.00^+. As these were

the negatively loaded ions for PC2, samples that exhibited higher count values from these ions were anticipated to appear at relatively low PC2 score values relative to the other samples.

All of the PMMA based samples appeared at lower PC2 values than the PEG based samples. This indicated that PC2 has successfully differentiated between the samples by polymer type. The loadings indicated that the F$^-$ ion yield was affected by the polymer matrix. As the PEG based samples appeared at higher PC2 values than the PMMA based samples in the scores plot, this provided collaborative evidence for the theory that either the PEG matrix in some way enhanced the secondary ion yield of fluorine, or the PMMA matrix suppressed ionisation.

It is interesting, that none of the key diagnostic ions from the drugs, such as [M+H] or [M-COOH] were included in the loadings. This indicated that the variance between these across the samples was less significant than the variance between the ions discussed above.

Although an extensive search of the literature did not find any research that investigated either of these drugs, either in their raw state or as part of a polymer matrix, there were a number of studies that did use PCA to discriminate between different polymers on surfaces. As in the studies reported in this chapter, PCA was found to be an effective tool in the differentiation of samples. For example, PCA has previously been used to look at polymers in PVC-PC polymer blends and specifically to assess the effect of pre-processing data methodologies [Lee and Gilmore, 2009]. They concluded that regardless of these pre-processing methods PCA enabled rapid identification of the polymer blend without any prior knowledge of the system. PCA has also been used to interrogate four different image types, including PEG and PMMA based samples. Again, it was concluded that PCA was very sensitive to the type of pre-processing applied to the data, but can effectively differentiate between polymer species [Tyler *et al.*, 2007]. ToF-SIMS studies of PLLA-PMMA blends have also shown that PCA was able to discriminate from one polymer to another [Cossement *et al.*, 2006].

6.3.4   **Principal Component Analysis of Tablet Data**

PCA was carried out on tablets with the highest and lowest drug concentrations, 80 wt/wt% paracetamol and 20 wt/wt% paracetamol. In each case, three positive ion spectra were used as the raw data. The eigenvalue plot shown in Figure 6.20 clearly highlighted that the majority of the variance in the data arose from PC1. There was also a small, but significant, contribution from PC2. The formation of two distinct clusters from the two different samples was observed when PC1 was plotted versus PC2 in the scores plot shown in Figure 6.21.

The scores plot derived from the PCA showed that there was a clear difference between the two samples in regards of PC1, as all the data points from the 20% sample were on the negative side of the x-axis (PC1) whereas all the data points from the 80% sample were on the right hand side of the x-axis. PCA was therefore able to successfully discriminate between the two sample types in regards to PC1. The analysis of PC2 was not as clear, as although all of the data points from the 80% sample were in the positive x-axis, the 20% sample resulted in data points at both positive and negative values.

The key ions that contributed to PC1 and PC2 are presented in Table 6.6 and Table 6.7, respectively. PC1 accounted for almost 80% of the variance in the sample set. Examination of the loadings for PC1 showed that the ions with the greatest positive loadings were m/z 152.07^+, 151.07^+, 109.0^+5 and 153.08^+, which represented the protonated paracetamol molecular ion $[M+H]^+$, the radical cation of the paracetamol molecular ion, a the paracetamol fragment $C_7H_9O^+$ and the paracetamol $[M+2H]^+$ cation, respectively. As these were the positively loaded ions for PC1, samples that exhibited higher count values from these ions would appear on the positive side of the x-axis. In Figure 6.21 all of the 80% samples were located on the positive x-axis indicating that within the sample set as a whole (i.e. both the low and high paracetamol concentration sample) that the PC1 ions discussed above were more prevalent. This correlated with both the manual analyses for the 80% tablet, reported in Chapter 3, Section 3.3.2.4 where paracetamol was the major ion present. The three points for the 20% concentration tablet all appeared in the negative x-axis indicating that they contained a lower amount of the ions listed in the PC1 positive loadings. Again, this was not unexpected as these contained the lowest concentration of

paracetamol and correlated with the results from Chapter 3 where less paracetamol was seen in both the spectrum and images from this sample. The highest negatively loaded ion for PC1 was Mg^+ at m/z 24. Therefore, samples that were high in magnesium would appear in the negative x-axis and those low in magnesium would appear in the positive axis. Again, a correlation was seen between these and previously reported results, where magnesium stearate was more prevalent in the lower concentration tablets at the surface; all sample points for the 80% tablet in Figure 6.21 appeared in the positive x-axis indicating a relative low concentration of the negatively loaded magnesium ion, whereas all sample points for the 20% tablet appear in the negative x-axis indicating high presence of this ion.

The interpretation of the loadings and scores plot for PC2 was not as straight forward as PC1. PC2 accounted for 15% of the variance in the sample set. Examination of the loadings for PC2 showed that the ions with the greatest positive loadings were m/z 23.98^+, 152.07^+ and 22.99^+, which represented paracetamol $[M+H]^+$, the magnesium cation and the sodium cation. All of the 80% tablet sample points appeared in the positive axis of PC2, indicating that they produced greater amounts of these ions. However, these three ions can be attributed to the three different components; the magnesium cation from magnesium stearate, the protonated paracetamol molecular ion, and the sodium ion that was previously observed in the spray dried lactose positive ion spectrum. However, if the corresponding negatively loaded ions, that the 80% samples contained less of, are analysed then the appearance of the 80% samples in the positive y-axis can be explained. These samples contained relatively few hydrocarbon fragments in comparison to magnesium, paracetamol and sodium which resulted in their appearance on the positive axis of PC2. Two of the 20% sample points appeared in the PC2 negative y-axis, whereas the third was in the positive axis. As stated by Graham, PCA enables differences between samples to become more readily apparent [Graham *et al.*, 2006]. This anomaly clearly demonstrated this advantage of PCA i.e. that as PCA is an automatic process with no manual input, it does not discriminate between samples itself, and can highlight unexpected results. This allows the user to go back and interrogate the original data, in this case the 20% sample observed in the positive axis. When the corrected intensity values of this sample were analysed, the values for the magnesium ion (the ion with the greatest positive loading for PC2) were similar to the other two 20% samples. However, for

the 2nd strongest positively loaded ion (i.e. the protonated paracetamol molecular ion) this anomalous sample exhibited sixty times the intensity of the first 20% sample and three times that of the second 20% sample in raw count values.

In summary, these data have shown that even with a limited sample set PCA was a useful tool in the interrogation and interpretation of ToF-SIMS data, as it successfully differentiated between the two samples and highlighted a potential anomaly in the data. PCA is traditionally used with large data sets [Lee *et al.*, 2008], yet in this work it has added another layer of understanding in regards to assessing the positive ion ToF-SIMS data despite the small sample set.

Figure 6.20 Eigenvalue plot from PCA of ToF-SIMS positive ion spectra showing principal components 1 and 2 for the 20% and 80% paracetamol tablets
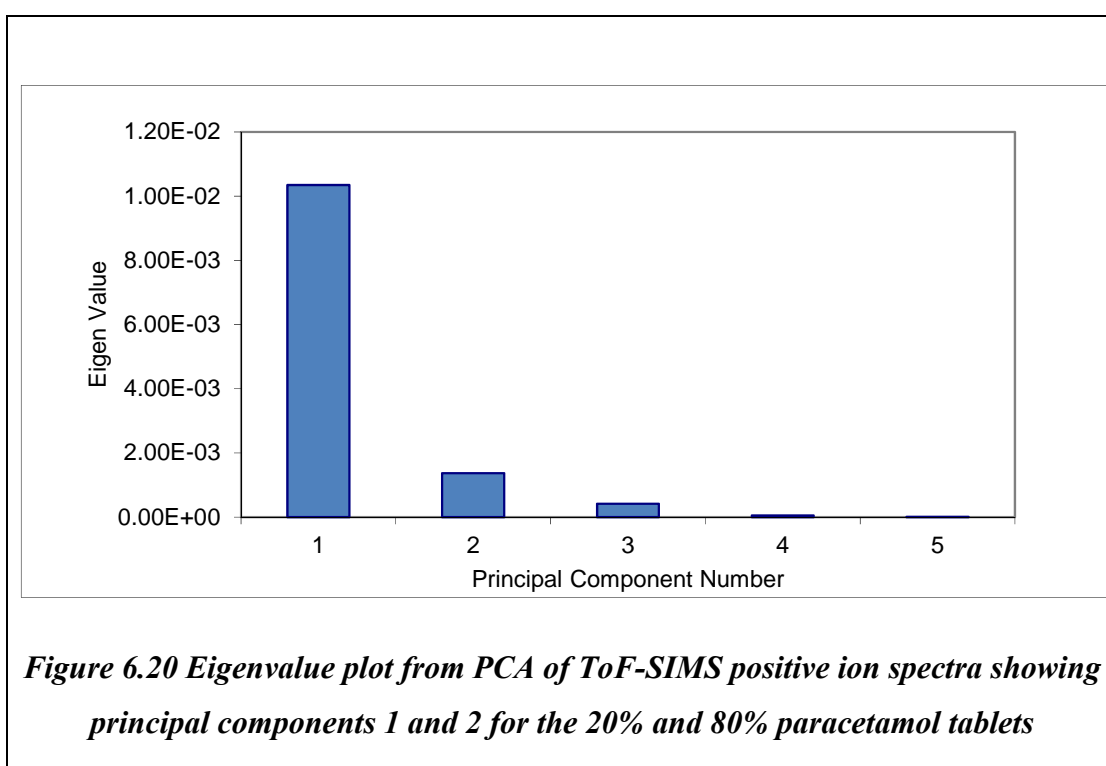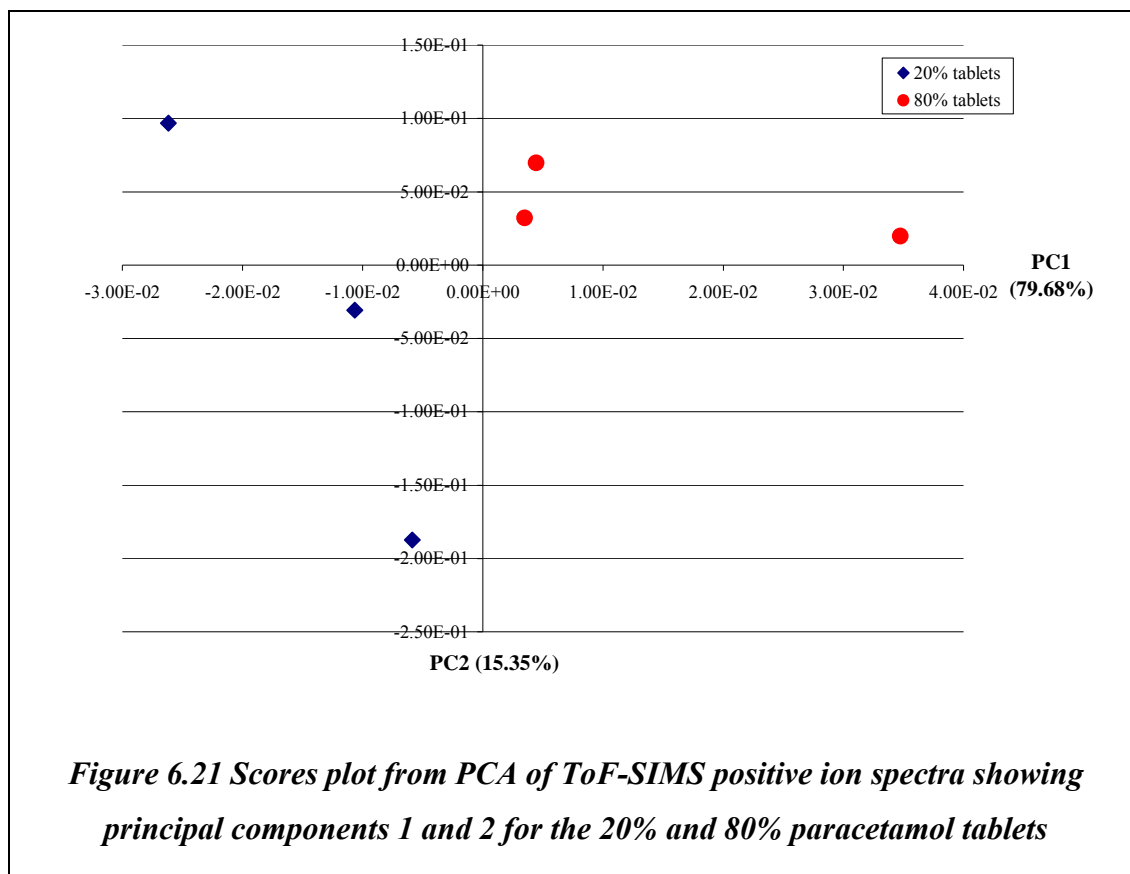
Figure 6.21 Scores plot from PCA of ToF-SIMS positive ion spectra showing
principal components 1 and 2 for the 20% and 80% paracetamol tablets

Strongest Negatively Loaded Ions		Strongest Positively Loaded Ions	
Ion	**m/z**	**Ion**	**m/z**
Mg^+	23.98	Paracetamol [M+H]	152.07
$C_5H_9^+$	68.92	Paracetamol molecular ion	151.07
MgH^+	24.99	Paracetamol Fragment	109.05
C^+	12.00	Paracetamol [M+2H]	153.08

Table 6.6 The 8 strongest negatively and positively loaded secondary ions and
their corresponding mass/charge (m/z) for PC1 as identified by PCA of the 20%
and 80% paracetamol tablets

Strongest Negatively Loaded Ions		Strongest Positively Loaded Ions	
Ion	**m/z**	**Ion**	**m/z**
$C_4H_9O^+$	73.03	Mg^+	23.98
$C_3H_5^+$	41.04	Paracetamol [M+H]	152.07
$C_3H_7^+$	43.06	Na^+	22.99
$C_3H_5O^+$	57.04	$C_5H_9^+$	68.92

Table 6.7 The 8 strongest negatively and positively loaded secondary ions and their corresponding mass/charge (m/z) for PC2 as identified by PCA of the 20% and 80% paracetamol tablets

6.4 Conclusions

The primary aim of this chapter was to assess the use of PCA for interpretation of ToF-SIMS data, including its value in assessing potential matrix effects in samples with different chemical environments. Two different structurally related drugs and two different polymeric materials were investigated, as a prelude to analysing these materials in combination to investigate matrix effects via use of the multivariate technique PCA. The tablets with the highest and lowest concentrations of paracetamol were also analysed with PCA.

ToF-SIMS was used to produce spectra of two different polymers and drugs, where in the majority significant diagnostic peaks that did not suffer from coincidence, were identified. Peak assignments for both polymers correlated well with previous work in this field for both PEG [Keller and Hug, 1999] and PMMA [Briggs *et al.*, 1989]. Verification of peak assignments for the drugs in this chapter proved more difficult as an extensive review of the current literature was unable to identify any work where the key diagnostic ions that are produced by these materials were identified. However, some information was gleaned for the flurbiprofen assignments by an assessment of GC-MS [Chao *et al.*, 2007] and FAB spectra [Tsunematsu *et al.*, 1993]. Assistance with the identification and verification of diflunisal peaks was acquired through the use of a mass spectra database [www.massbank.jp]. Analysis of the spectra from the drug / polymer spun cast solutions showed that the two different polymer matrices had different impacts on the detection of key diagnostic ions from the drugs, and that the polymer matrix had in some cases suppressed ionisation for example in the case of the diflunisal key diagnostic ions ion the PEG matrix. This difference in matrix has previously been observed [Jones *et al.*, 2007a]. The PEG matrix appeared to have a greater suppression effect in the positive ion spectrum in comparison to the negative ion spectrum.

In earlier chapters, conventional methods of analysing the data, such as ratios of intensities to concentrations, have been shown to give little insight into the key differences between samples. Analysis of the distribution of data points on the scores plot created via PCA allowed for comment on the homogeneity of samples that were from the same batch. Analysis of the ions that made up the key principal components and hence the majority of the variance across the sample set, showed that PCA was

an effective method for differentiating between samples and also was able to shed light on how the matrix was affecting secondary ion yields of drug related ions in the polymer matrix. PCA has previously been shown to reduce the dimensionality of data into manageable variables [Tyler *et al.*, 2007].

In summary, this data has shown that PCA was a useful tool in the interrogation and interpretation of ToF-SIMS data and can provide further insight into the ions that cause variance in a data set, both in terms of identifying the key ions that were driving the variance and recognising any anomalies within the data.

The key findings of this chapter indicated that matrix effects can have an influence on secondary ion yields, and hence any approach to producing reliable quantification markers, such as RSFs, would need to allow for these effects.

Chapter 7.
General Conclusions

The work presented in this thesis has centred on the assessment of ToF-SIMS as a surface analytical technique and the factors that control its ability to produce reliable quantitative data.

ToF-SIMS is a surface sensitive technique that is increasingly being used in the pharmaceutical industry for the characterization of formulations during product development to understand the product structure and to troubleshoot problems that emerge in the formulation stability and performance. Drug formulation and the use of ToF-SIMS are briefly introduced in Chapter 1 of this thesis, and the mechanics of the technique are described in Chapter 2.

In Chapter 3 the ability of ToF-SIMS to identify the characteristic peaks off all the different materials in a multi-component system was demonstrated by the analysis of tablet and bead samples containing paracetamol and a range of common excipients. The identification of diagnostic peaks in the spectra allowed for the selection of characteristic ions for the drug and each of the excipients that can be used to produce ToF-SIMS ion images. The spatial distribution of each of the components at the sample surface was successfully mapped and highlighted that the imaging capabilities of ToF-SIMS are excellent. Particular insights were gained into the relationship of the magnesium stearate lubricant in relation to the paracetamol and spray dried lactose in the tablet samples and where the ToF-SIMS images highlighted that the surface distribution and quantity of this material altered according to the bulk composition levels of the other two components.

Further processing of both spectroscopy and imaging data can lead to some useful insights in regards to the distribution of components at the surface. Corrected intensities of diagnostic peaks can be measured and compared to produce information in respect of the quantities of the respective ions at the surface. Although these calculations showed trends that were in keeping with the bulk composition, e.g. increasing concentration was equated by increasing counts, they did not accurately reflect the quantities of raw materials that were used in the manufacture of the

formulations. Bespoke analysis programs were accomplished at interpreting the information within ToF-SIMS ion images and produced semi-quantitative information that was closer to the bulk composition than that observed in the spectroscopy data processing method. Scanning Electron Microscopy was used as a complimentary technique, and provided images that correlated well with their ToF-SIMS counterparts. The combination of these techniques allowed for both the topographical and chemical nature of the surface to be characterised.

Having successfully used ToF-SIMS to provide *qualitative* surface information via spectroscopy, and imaging, preliminary investigations into the reproducibility of any quantitative based data were conducted. Standard deviation calculations of ion yields taken from six tablet samples with the same bulk composition found that high variance was observed between the corrected ion intensities of the diagnostic ions. This lead to further experiments designed to elucidate the factors that contributed to this variance. SEM images of the tablet sample had highlighted that the surface appeared to exhibit significant topography. Investigations into the role of topography as potentially one of the main factors that caused variance drove much of the following work.

Initially, PTFE was selected as a sample surface that is chemically homogeneous and exhibits minimal surface topography. The analysis area was divided into sixteen segments and ToF-SIMS showed that data variance in terms of ion yield across this surface was lower than observed from the complex formulations and in addition that reduced counts in the higher mass range did not appear to cause a rise in the secondary ion yield variance.

The PTFE experiment acted as a building block to further experiments. A substantial body of work that explores the use of ToF-SIMS as a quantitative tool uses the calculation of RSFs derived from pure materials in matrix materials to act as standards. A simple experiment was designed to establish if topography played a role in secondary ion yield generation, and hence impacted on the accurate calculation of RSF values. Magnesium stearate powder samples were mechanically modified to provide three samples with increasing roughness characteristics. Laser profilometry proved an effective tool in measuring the Ra values of these surfaces. Standard deviation calculations applied to these surfaces showed that ion yields were not

consistent, and that as roughness increased so did variance. These experiments exploited one of the key concepts of ToF-SIMS, that essentially every pixel contains its own mass spectrum, and for this reason offline experiments can be completed to provide greater understanding of the sample surface, in this case that ion yields from a chemically homogenous sample were inconsistent.

The magnesium stearate experiment suggested that the physical state of the surface influenced the emission of secondary ion yields from the surface. However, the chemistry of this surface was uniform. Introducing a surface with a more complicated surface chemistry would establish whether surface roughness would impart its effect on secondary ion yield consistently where more than one chemical constituent was present. A microscope glass slide was selected and the ability of Atomic Force Microscopy to successfully establish nanometre scale roughness was demonstrated. Roughness was introduced to the glass slide through a shot peening process. Both the unmodified and modified slide were analysed by ToF-SIMS and the variance in signal from two atomic ions, silicon and sodium, was investigated. The experiment successfully demonstrated that mechanically introduced surface topography has a greater effect on the sodium ion, suggesting that not only did roughness cause inconsistencies in ion yields, but that this effect was not consistent across different chemical species. This would imply that so called matrix effects, where ion yields are influenced by the local chemical environment, could be attenuated in samples that exhibit surface topography in the micron scale.

The final experiment in this series, sought to establish if varying the primary ion dose density within the static limit would influence data reliability. This experiment showed that ToF-SIMS was able to produce reproducible data even at doses of around a quarter of the static dose limit, and that the PIDD did not play a role in the use of ToF-SIMS as a quantitative tool.

The penultimate experimental chapter used model samples to further investigate roughness factors and to establish whether cations and anions of the same chemistry were affected consistently by this phenomenon. Anions typically exhibited greater variance from the same physical area, than their respective cations. Furthermore, the introduction of roughness to a sample surface appeared to have a greater effect on the higher mass ions, which was not observed in flat samples, as demonstrated by the

PTFE experiments. The rate at which data variability occurred appeared to be rapid as Ra values moved from the nanometre scale to the micron scale. Precision measurement samples were also investigated to look at the role of directionality in the surface topography. ToF-SIMS analysis experiments confirmed that the presence of any orientation/directionality in surface features, as well as the level of topography appears to have an effect. Some form of sample rotation, such as that often employed in x-ray diffractometry, may eliminate this factor.

The reasons why roughness induced variability in secondary ion yields was not fully understood. Although they may predominantly have been caused by shadowing effects, the difference in physical height of the analysis point may also have played a role. In order to investigate this, a gold coated glass slide was moved in 10 micron steps towards and away from the optimum height in regards to the extractor cone to simulate height differences that might be present in "real" samples. The effect of this on the normalised total ion count of the gold anions and cations was surprising. The majority of the anions and cations exhibited a loss in counts, of up to 40%. However, the high mass anion counts increased.

The final chapter highlighted the effective use of principal component analysis (PCA) in the interpretation of ToF-SIMS data. PCA was successfully applied to the ToF-SIMS tablet spectroscopy data and was able to clearly discriminate between the highest and lowest concentration tablet samples. This would suggest that PCA is an ideal method for identifying the ions that are causing significant variance within the samples analysed. PCA on these samples also highlighted that one of the sample analysis areas was significantly different to others in the same set. This highlighted that PCA cannot only be used in its traditional form, i.e., a statistical method that pulls out the significant variables within a sample set, but also to assess the homogeneity between samples that should theoretically exhibit the same surface chemistry.

The final chapter also analysed the influence of "matrix effects" in data quantification through the analysis of spun cast polymer / drug samples with minimal topography. PCA successfully established the effect of two different polymer matrices on two chemically similar drugs. Observations of the positions of the sample repeats, also verified the use of PCA to be used as a method establishing

sample repeatability. The use of PCA in ToF-SIMS is an excellent and unbiased method for identifying the key ions that are causing variability in the sample.

The results in this thesis have provided new information on the ability of ToF-SIMS to be used as a quantitative tool in context. They have provided new insights into the role of surface roughness and the effect that this has on secondary ion yields. The experiments as a whole demonstrate that quantitative assessments of pharmaceutical systems through the use of ToF-SIMS may prove very difficult, with physical and chemical factors both influencing the reliability of any data obtained using this technique.

The knowledge that has been gained warrants further investigation into this field to see if a quantitative approach can be devised that fully accounts for these factors. A complete scale of reference specimens that exhibit roughness from a few nanometres to hundreds of microns, with varying engineered topographies, would allow for the exploration of the influence of these surfaces on ion yield variance, both in terms of their overall roughness values and the geometry of the surface features. Following on from this, it is recommended that a number of these specimens are manufactured from different inorganic and organic materials. This would establish whether the different surface chemistries of these materials are more or less prone to fluctuations in ionisation yield as a result of the surface roughness and geometry, and whether these fluctuations are consistent, e.g. for the elemental ion and the oxide. Studies of model organic systems that have the same chemistry but different morphologies are also recommended. For example, active ingredients that are available in crystalline and amorphous forms that are known to exhibit differences in physical and chemical properties or drugs such as Cefdinir, which is patented in several polymorphic forms could be investigated. Since drugs are often present in a crystalline form that may contain a level of amorphous material, known to have significant impact on the surface properties such as water absorption and stability, any differences in the ion yield between the two different phases will also have an impact on any quantitative analysis of the ToF-SIMS data of such systems.

The work in this thesis has exclusively used gallium as the primary ion source. The influence of different primary ion sources on the level of variance in the data, for systems such as the model materials and pharmaceutical formulations that exhibit

different surface chemistries and topographies discussed above, would provide additional information in this territory.

These systematic studies should enable the development of a defined protocol for the quantitative analysis of complex systems, specifying information such as the number of replicates and analysis areas required, and the specific analytical conditions that need to be employed if any form of reliable quantitative results are to be achieved. Until such an understood methodology is advanced, this thesis has demonstrated that quantitative analysis of ToF-SIMS data derived from complex chemically heterogeneous and topographically diverse surfaces of pharmaceutical formulations is not within the grasp of the analytical chemist at this time.

Appendices

Appendix 1: ToF-SIMS positive and negative ion variance in relation to abrasive paper grade and Ra respectively (Raw Data)

Positives	Ra	Run	Av SF 197	+/-RSD%	Av SF 591	+/- RSD%
	4.9	1	3.56E-08	10.29	1.11E-08	10.92
P1200	4.8	2	5.38E-08	12.83	1.41E-08	13.46
	4.9	3	2.42E-08	15.33	7.41E-09	15.55
Averages	4.87		3.79E-08	12.82	1.09E-08	13.31
	5.9	1	8.56E-08	17.45	2.12E-08	19.82
P800	5.6	2	8.48E-08	9.94	2.17E-08	9.74
	6.1	3	7.27E-08	15.47	1.84E-08	18.00
Averages	5.87		8.1E-08	14.29	2.04E-08	15.85
	8	1	6.94E-08	21.84	1.87E-08	26.62
P400	7.9	2	6.20E-08	24.73	1.66E-08	29.95
	7.4	3	5.43E-08	26.72	1.38E-08	31.99
Averages	7.77		6.19E-08	24.43	1.64E-08	29.52
	14.4	1	9.96E-08	53.04	2.63E-08	67.91
P240	14.1	2	1.02E-07	47.85	2.35E-08	56.02
	13.5	3	1.05E-07	51.47	2.37E-08	54.72
Averages	14.00		1.02E-07	50.79	2.45E-08	59.55

Negatives	Ra	Run	Av SF 197	+/-RSD%	Av SF 591	+/- RSD%
	4.9	1	5.97E-07	14.85	6.89E-08	14.24
P1200	4.8	2	6.06E-07	13.39	9.61E-08	13.71
	4.9	3	6.62E-07	15.36	1.31E-07	17.60
Averages	4.87		6.21E-07	14.53	9.86E-08	15.18
	5.9	1	4.86E-07	25.54	6.49E-08	25.34
P800	5.6	2	4.41E-07	20.38	5.96E-08	21.07
	6.1	3	3.98E-07	22.96	5.28E-08	22.58
Averages	5.87		4.41E-07	22.96	5.91E-08	23.00
	8	1	3.90E-07	27.65	5.14E-08	27.27
P400	7.9	2	3.41E-07	34.56	4.35E-08	35.37
	7.4	3	3.58E-07	40.58	4.51E-08	41.44
Averages	7.77		3.63E-07	34.26	4.67E-08	34.69
	14.4	1	4.68E-07	65.53	7.5E-08	70.21
P240	14.1	2	4.32E-07	73.54	6.99E-08	77.59
	13.5	3	4.27E-07	54.46	6.7E-08	59.06
Averages	14.00		4.42E-07	64.51	7.06E-08	68.95

References

ADOVELANDE, J., BOULARD, Y., BERRY, J.P., GALLE, P., SLODZIANC, G. and SCHRÉVEL J. Detection and cartography of the fluorinated antimalarial drug mefloquine in normal and *Plasmodium falciparum* infected red blood cells by scanning ion microscopy and mass spectrometry. *Biology of the Cell,* 1994, 81(2), 185-192.

ADRIAENSEN, L., VANGAEVER, F. and GIJBELS, R. Organic SIMS: the influence of time on the ion yield enhancement by silver and gold deposition. *Applied Surface Science*, 2004, 231-232, 256-260.

ADRIAENSEN, L., VANGAEVER, F., LENAERTS, J. and GIJBELS, R. S-SIMS and MetA-SIMS study of organic additives in thin polymer coatings. *Applied Surface Science*, 2006, 252(19), 6628-6631.

AHADIAN, M.M., IRAJI ZAD, A., NOURI, E., RANJBAR, M. and DOLATI, A. Diffusion and segregation of substrate copper in electrodeposited Ni–Fe thin films. *Journal of Alloys and Compounds,* 2007, 443(1-2), 81-86.

APPELHANS, A. D. and DELMORE, J. E. Comparison of polyatomic and atomic primary beams for secondary ion mass-spectrometry of organics. *Analytical Chemistry*, 1989, 61(10), 1087-1093.

ARIMOTO, M., ICHIKAWA, H. and FUKUMORI, Y. Microencapsulation of water-soluble macromolecules with acrylic terpolymers by the Wurster coating process for colon-specific drug delivery. *Journal of Powder Technology,* 2004, 141(3), 177-186.

AUDINOT, J.-N., SCHNEIDER, S., YEGLES, M., HALLEGOT, P., WENNIG, R. and MIGEON H.-N. Imaging of arsenic traces in human hair by nano-SIMS 50. *Applied Surface Science,* 2004, 231-232, 490-496.

AULTON, M.E. *Pharmaceutics: the science of dosage form design.* 2nd ed. Philadelphia: Churchill Livingstone, 2002.

BARKSHIRE, I.R., KENNY, P.G., FLETCHER, I.W. and PRUTTON M. Quantitative surface microanalysis of samples with extreme topography utilising image interpretation by scatter diagrams and principal component analysis. Ultramicroscopy, 1996, 63(3-4), 193-203.

BARNER-KOWOLLIK, C. (ed.), GRUENDLING, T. (ed.), FALKENHAGEN, J. (ed.) and WEIDNER S. (ed.). *Mass spectrometry in polymer chemistry*. Weinheim: Wiley-VCH, 2011.

BARNES, T.J., KEMPSON, I.M. and PRESTIDGE, C.A. Surface analysis for compositional, chemical and structural imaging in pharmaceutics with mass spectrometry: A ToF-SIMS perspective. *International Journal of Pharmaceutics,* 2011, 417(1-2), 61-69.

BÉCHARD, S.R., QURAISHI, O. and KWONG, E. Film coating: effect of titanium dioxide concentration and film thickness on the photostability of nifedipine. *International Journal of Pharmaceutics,* 1992, 87(1-2), 133-139.

BECKER, J.S. *Inorganic mass spectrometry: principles and applications.* Chichester: Wiley and Sons Ltd., 2007.

BELU, A.M., DAVIES, M.C., NEWTON, J.M. and PATEL, N. ToF-SIMS characterization and imaging of controlled-release drug delivery systems. *Analytical Chemistry,* 2000, 72(22), 5625-5638.

BELU, A.M., GRAHAM, D.J. and CASTNER, D.G. Time-of-flight secondary ion mass spectrometry: techniques and applications for the characterization of biomaterial surfaces. *Biomaterials,* 2003, 24, 3635-3653.

BENNINGHOVEN, A. and SICHTERMANN, W. K. Detection, identification, and structural investigation of biologically important compounds by secondary ion mass spectrometry. *Analytical Chemistry*, 1978, 50(8), 1180-1184.

BENZ, M., EULER, W.B. and GREGORY O.J. The Influence of preparation conditions on the surface morphology of poly(vinylidene fluoride) films. *Langmuir,* 2001, 17(1), 239-243.

BERTRAND, N., GAUTHIER, M.A., BOUVET, C., MOREAU, P., PETITJEAN, A., LEROUX, J.C. and LEBLOND, J. New pharmaceutical applications for macromolecular binders. *Journal of Controlled Release,* 2011, (155(2), 200-210.

BEWOOR, A. and KULKARNI, V. *Metrology and measurement.* New Delhi: Tata McGraw-Hill, 2009.

BIEMANN, K. *Mass spectrometry: organic chemical applications.* New York: McGraw-Hill, 1962.

BOSCH, M.E., SANCHEZ, A.J.R., ROJAS, F.S. and OJEDA, C.B., Determination of Paracetamol: Historical Evolution. *Journal of Pharmaceutical and Biomedical Analysis,* 2006, 42(3) 291-321.

BRAGA, P.C. (ed.), and RICCI, D., (ed.). *Atomic force microscopy: biomedical methods and applications*. Totowa: Humana Press, 2004.

BRANDON, D. and KAPLAN, W. *Microstructural characterization of materials.* Chichester: Wiley and Sons Ltd., 2008.

BRIGGS, D. *Surface analysis of polymers by XPS and static SIMS.* Cambridge: Cambridge University Press, 1998.

BRIGGS D., BROWN A. and VICKERMAN J.C. *Handbook of static secondary ion mass spectrometry.* Chichester: Wiley and Sons Ltd., 1989.

BRIGGS, D., HEARN, M.J. and RATNER, B.D. Analysis of Polymer Surfaces by SIMS. 4-A study of some acrylic homo-polymers and co-polymers. *Surface and Interface Analysis,* 1984, 6(4), 184-192.

BRIGGS, D. and SEAH, M. *Practical surface analysis volume 2 - ion and neutral spectroscopy.* Chichester: Wiley and Sons Ltd., 1992.

BRINDLEY, A., DAVIES, M.C., DAVIS, S.S., HEARN J., LYNN, R.A.P. and WATTS, J.F. The surface characterization of model charged and sterically stabilized polymer colloids by SSIMS and XPS. *Polymer,* 1992, 33(5), 1112-1115.

BRINDLEY, A., DAVIS, S.S., DAVIES, M.C. and WATTS, J.F. Polystyrene colloids with surface-grafted polyethylene oxide as model systems for site-specific drug delivery: I. preparation and surface chemical characterization using SIMS and XPS. *Journal of Colloid and Interface Science,* 1995, 171(1), 150-161.

BRITTAIN, H. *Profiles of drug substances, excipients and related methodology.* New Jersey: Elsevier, 2009. Volume 34.

BRYAN, S.R., BELU, A.M., HOSHI, T. and OIWA, R. Evaluation of a gold LMIG for detecting small molecules in a polymer matrix by ToF-SIMS *Applied Surface Science,* 2004, 231–232, 201–206.

BUGAY, D.E. Characterization of the solid-state: spectroscopic techniques. *Advanced Drug Delivery Reviews,* 2001, 48(1), 43-65.

BURNS, S.A. and GARDELLA Jr., J.A. Quantitative ToF-SIMS studies of protein drug release from biodegradable polymer drug delivery membranes. *Applied Surface Science,* 2008, 255(4), 1170-1173.

CEFALI, E.A., POYNOR, W.J., SICA, D. and COX, S. Pharmacokinetic comparison of flurbiprofen in end-stage renal-disease subjects and subjects with normal renal-function. *Journal of Clinical Pharmacology,* 1991, 31(9), 808-814.

CHAN, J.G.Y., CHAN, H-K., PRESTIDGE, C.A., DENMAN, J.A., YOUNG, P.M. and TRAINI, D. A novel dry powder inhalable formulation incorporating three first-line anti-tubercular antibiotics. *European Journal of Pharmaceutics and Biopharmaceutics,* 2013, 83(2), 285-292.

CHAO, S.H., HO, H.T., CHEN, F.A., LIN, P.Y., YU, Y.C. and WU, A.B. Identification of flurbiprofen and its photoproducts in methanol by gas chromatography-mass spectrometry. *Biomedical Chromatography,* 2007, 21(5), 527-533.

CHAURAND, P. Imaging mass spectrometry of thin tissue sections: A decade of collective efforts. *Journal of Proteomics,* 2012 75(16) 4883-4892.

CLERC, J., FOURRE, C. and FRAGU, P. SIMS microscopy: methodology, problems and perspectives in mapping drugs and nuclear medicine compounds. *Cell Biology International,* 1997, 21(10), 619-633.

COSSEMENT, D., GOUTTEBARON, R., CORNET, V., VIVILLE, P., HECQ, M. and LAZZARONI, R. PLA-PMMA blends: a study by XPS and ToF-SIMS. *Applied Surface Science,* 2006, 252, 6636-6639.

CUN, D., JENSEN, D.K., MALTESEN, M.J., BUNKER, M., WHITESIDE, P., SCURR, D., FOGED, C. and NIELSEN, H.M. High loading efficiency and sustained release of siRNA encapsulated in PLGA nanoparticles: quality by design optimization and characterization. *European Journal of Pharmaceutics and Biopharmaceutics,* 2011, 77(1), 26-35.

CZICHOS, H. (ed.), SAITO, T. (ed.) and SMITH, L. (ed.) *Springer handbook of materials measurement methods.* New York: Springer Science and Business Media, Inc., 2006.

DAVIES, M.C. and LYNN, R.A. A review: secondary ion mass spectrometry (SIMS) of polymeric biomaterials. *Clinical Materials,* 1990, 5(2-4), 97-114.

DAVIES, M.C., LYNN, R.A.P., DAVIS, S.S., HEARN, J., VICKERMAN, J.C. and PAUL, A.J. The application of time-of-flight SIMS for the surface characterization of polymer latex particles prepared with immobilized sugar residues. *Journal of Colloid and Interface Science,* 1993, 161(1), 83-90.

DAVIES, M.C., LYNN, R.A.P., WATTS, J.F., Paul, A.J., VICKERMAN, J.C. and HELLER, J. ToF-SIMS and XPS analysis of the surface chemical structure of some linear poly(orthoesters). *Macromolecules,* 1991, 24(20), 5508-5514.

DESAI, A. and LEE, M. *Gibaldi's drug delivery systems in pharmaceutical care.* Bethesda: American Society of Health-System Pharmacists, 2007.

DE WITTE, H., DE GENDT, S., DOUGLAS, M., CONARD, T., KENIS, K., MERTENS, P.W., VANDERVORST, W. and GIJBEL R. Evaluation of time-of-flight secondary ion mass spectrometry for metal contamination monitoring on Si wafer surfaces. *Journal of The Electrochemical Society,* 2000, 147(5), 1915-1919.

DROUOT, C., ENJALBAL, C., FULERAND, P., MARTINEZ, J., AUBAGNAC, J.L., COMBARIEU, R. and DEPUYDT, Y. ToF-SIMS analysis of polymer bound Fmoc - protected peptides. *Tetrahedron Letters,* 1997, 38(14), 2455-2458.

DUKIC´-OTT, A., THOMMES, M., REMON J.P., KLEINEBUDDE P. and VERVAET, C. Production of pellets via extrusion–spheronisation without the incorporation of microcrystalline cellulose: a critical review. *European Journal of Pharmaceutics and Biopharmaceutics,* 2009, 71(1), 38-46.

DURGIN, J. and HANAN, Z. *Pharmacy practice for technicians*. 3rd ed. New York: Thomson Delmar Learning, 2005.

EDGE, S., BELU, A.M, POTTER, U.J., STEELE, D.F., YOUNG, P.M., PRICE, R. and STANIFORTH, J.N. Chemical characterisation of sodium starch glycolate particles. *International Journal of Pharmaceutics,* 2002, 240(1-2), 67-78.

ELVIRA, C., FANOVICH, A., FERNÁNDEZ, M., FRAILE, J., SAN ROMÁN, J. and DOMINGO, C. Evaluation of drug delivery characteristics of microspheres of PMMA–PCL–cholesterol obtained by supercritical-CO2 impregnation and by dissolution-evaporation techniques. *Journal of Controlled Release,* 2004, 99(2), 231-240.

FAHEY, A.J. and MESSENGER, S. Isotopic ratio measurements by time-of-flight secondary ion mass spectrometry. *International Journal of Mass Spectrometry* 2001, 208(1-3), 227-242.

FELTON, L.A. and MCGINITY, J.W. Adhesion of polymeric films to pharmaceutical solids. European *Journal of Pharmaceutics and Biopharmaceutics,* 1999, 47(1-3), 3-14.

FLETCHER, J.S., LOCKYER, N.P. and VICKERMAN, J.C. C60, Buckminsterfullerene: its impact on biological ToF-SIMS analysis. *Surface and Interface Analysis,* 2006, 38(11), 1393-1400.

FLORENCE, A.T. and ATTWOOD D. *Physicochemical Principles of Pharmacy.* London: Pharmaceutical Press, 2006.

FRAGU, P. and KAHN, E. Secondary ion mass spectrometry (SIMS) microscopy: a new tool for pharmacological studies in humans. *Microscopy Research and. Technique*, 1997, 36(4), 296-300.

FREIRE, C., PODCZECK, F., VEIGA, F. and SOUSA, J. Starch-based coatings for colon-specific delivery. Part II: Physicochemical properties and in vitro drug release from high amylose maize starch films *European Journal of Pharmaceutics and Biopharmaceutics*, 2009, 72(3), 587-594.

GANDERTON, D., JONES, T. and MCGINITY, J. *Advances in Pharmaceutical Sciences Volume 7.* London: Academic Press Ltd., 1995.

GARRISON, B.J. and POSTAWA, Z. Effect of sample rotation on surface roughness with keV C_{60} bombardment in secondary ion mass spectrometry (SIMS) experiments. *Chemical Physics Letters,* 2011, 506(4), 129-134.

GASPAR, D.J., LASKIN, A., WANG, W., HUNT, S.W. and FINLAYSON-PITTS B.J. TOF-SIMS analysis of sea salt particles: imaging and depth profiling in the discovery of an unrecognized mechanism for pH buffering. *Applied Surface Science,* 2004, 231–232, 520-523.

GAZI, E., LOCKYER, N.P., VICKERMAN, J.C., GARDNER, P., DWYER, J., HART, C.A., BROWN, M.D., CLARKE, N.W. and MIYAN, J. Imaging ToF-SIMS and synchrotron-based FT-IR microspectroscopic studies of prostate cancer cell lines. *Applied Surface Science,* 2004, 231–232, 452-456.

GETTINGS, M. and COAD, J.P. A preliminary study of pure metal surfaces using Auger Electron Spectroscopy (AES), X-ray Photoelectron Spectroscopy (XPS) and Secondary Ion Mass Spectroscopy (SIMS). *Surface Science,* 1975, 53(1), 636-648.

GILLEN, G., FAHEY, A., WAGNER, M. and MAHONEY, C. 3D molecular imaging SIMS. *Applied Surface Science,* 2006, 252(19), 6537-6541.

GILMORE, I.S. and SEAH, M.P. Static SIMS: metastable decay and peak intensities. *Applied Surface Science,* 1999, 144-145, 26-30.

GILMORE, I.S. and SEAH, M.P. Static SIMS: towards unfragmented mass spectra - the G-SIMS procedure. *Applied Surface Science,* 2000, 161(3-4), 465-480.

GILMORE, I.S. and SEAH, M.P. Electron flood gun damage in the analysis of polymers and organics in time-of-flight SIMS. *Applied Surface Science,* 2002, 187(1-2), 89-100.

GOACHER, R.E. and GARDELLA Jr., J.A. Analysis of C_{60}^{+} and Cs^{+} sputtering ions for depth profiling gold/silicon and GaAs multilayer samples by time of flight secondary ion mass spectrometry. *Applied Surface Science,* 2010, 256(7), 2044-2051.

GODDARD, J.M. and HOTCHKISS, J.H. Polymer surface modification for the attachment of bioactive compounds. *Progress in Polymer Science,* 2007, 32(7), 698-725.

GORNER, T., GREF, R., MICHENOT, D., SOMMER, F., TRAN, M.N. and DELLACHERIE, E. Lidocaine-loaded biodegradeable nanospheres: Optimisation of the drug incorporation into the polymer matrix. *Journal of Controlled Release,* 1999, 57(3), 259-268.

GRAHAM D.J. WAGNER M.S. and CASTNER D.G. Information from complexity: Challenges of TOF-SIMS data interpretation. *Applied Surface Science,* 2006, 252(19), 6860-6868.

GRAMS, J. *New trends and potentialities of ToF-SIMS in surface studies.* New York: Nova Science Publishers, Inc., 2007.

GREEN, F. M., GILMORE, I. S., LEE, J. L. S., SPENCER S. J. and SEAH M. P. Static SIMS-VAMAS interlaboratory study for intensity repeatability, mass scale

accuracy and relative quantification. *Surface Interface Analysis,* 2010, 42(3), 129-138.

GUAD, R. S., SURANA, S. J., TALELE, G. S. TALELE, S. G. and GOKHALE S. B. *Natural excipients.* Pune: Nirali Prakashan, 2006.

GUI, D., XING, Z.X., HUANG, Y.H., MO, Z.Q., HUA, Y.N., ZHAO, S.P. and CHA L.Z. Roughness development in the depth profiling with 500 eV O_2^+ beam with the combination of oxygen flooding and sample rotation. *Applied Surface Science,* 2008, 255, 1433-1436.

HA, C. S. and GARDELLA Jr., J.A. Jnr. Surface chemistry of biodegradable polymers for drug delivery systems. *Chemical Reviews,* 2005 105(11), 4205-4232.

HALE, P.S., KAPPEN, P., BRACK, N., PRISSANAROON, W., PIGRAM, P.J. and LIESEGANG, J. Micropatterning of fluoropolymers. *Applied Surface Science,* 2006, 252(6), 2217-2228.

HART B.R., DIMOV S.S. and SMART R.S.C. Development of a TOF-SIMS technology as a predictive tool for the needs of the mineral processing industry. *Surface and Interface Analysis,* 2011, 43(1-2), 449-451.

HELLSING, M., FOKINE, M., CLAESSON, Å., NILSSON, L.-E. and MARGULIS W. ToF-SIMS imaging of dopant diffusion in optical fibers. *Applied Surface Science*, 2003, 203-204, 648-651.

HERSH, E.V., MOORE, P.A. and ROSS, G.L. Over-the-counter analgesics and antipyretics: a critical assessment. *Clinical Therapeutic,* 2000, 22(5), 500-548.

HIRSCH, S., BINDER, V., SCHEHLMANN, V., KOLTER, K. and Bauer, K.H. Lauroyldextran and crosslinked galactomannan as coating materials for site-specific drug delivery to the colon. *European Journal of Pharmaceutics and Biopharmaceutics,* 1999, 47(1), 61-71.

HOLLYHEAD, L. *Nanometre scale surface characterisation of engineered biomimetic materials.* Ph.D. thesis, University of Nottingham, 2006.

HUSSAIN M.S.H., YORK P., TIMMINS P. and HUMPHREY P. Secondary ion mass spectrometry (SIMS) evaluation of magnesium stearate distribution and its effects on the physio-technical properties of sodium chloride tablets. *Powder Technology,* 1990, 60(1), 39-45.

INGRAM, P., SHELBURNE, J.D., ROGGLI, V.L. and LEFURGEY, A. *Biomedical applications of microprobe analysis.* San Diego: Academic Press, 1999.

INOUE, M. and MURASE A. Reduction of matrix effects in TOF-SIMS analysis by metal-assisted SIMS (MetA-SIMS). *Surface and Interface Analysis,* 2005, 37(12), 1111-1114.

ISANBOR, C. and O'HAGAN, D. Fluorine in medicinal chemistry: A review of anti-cancer agents. *Journal of Fluorine Chemistry,* 2006, 127(3), 303-319.

JARVIS, K.L., BARNES, T.J. and PRESTIDGE, C.A. Surface chemistry of porous silicon and implications for drug encapsulation and delivery applications. *Advances in Colloid and Interface Science,* 2012, 175, 25-38.

JEFFUS, L.F. *Welding: principles and applications.* New York: Thomson Delmar Learning, 2004.

JEWITT, J. *Taunton's complete illustrated guide to finishing.* Newton: The Taunton Press, 2004.

JOHN, C.M., ODOM, R.W., SALVATI, L., ANNAPRAGADA, A. and LU, M.Y.F. XPS and ToF-SIMS microanalysis of a peptide/polymer drug delivery device. *Analytical Chemistry,* 1995, 67(21), 3871-3878.

JOINT FORMULARY COMMITTEE. *British National Formulary*, British Medical Journal Publishing Group and Pharmaceutical Press, 1990.

JOHN, C.M. and ODOM, R.W. Static secondary ion mass spectrometry (SSIMS) of biological compounds in tissue and tissue-like matrices. *International Journal of Mass Spectroscopy and Ion Processes,* 1997, 161(1-3), 47-67.

JONES, D. *Pharmaceutics - dosage form and design.* London: Pharmaceutical Press, 2006a.

JONES, D. *Pharmaceutical applications of polymers for drug delivery.* Shrewsbury: Rapra Technology Limited, 2009.

JONES, E.A., FLETCHER, J. S., THOMPSON, C.E., JACKSON, D. A., LOCKYER, N. P. and VICKERMAN, J. C. ToF-SIMS analysis of bio-systems: Are polyatomic primary ions the solution? *Applied Surface Science,* 2006a, 252(19), 6844-6854.

JONES, E.A., LOCKYER, N.P and VICKERMAN, J.C. Suppression and enhancement of non-native molecules within biological systems. *Applied Surface Science,* 2006b, 252(19), 6727-6730.

JONES, E., LOCKYER, N., KORDYS, J. and VICKERMAN, J. Suppression and enhancement of secondary ion formation due to the chemical environment in static-secondary ion mass spectrometry. *Journal of the American Society for Mass Spectrometry,* 2007a, 18(8), 1559-1567.

JONES, E., LOCKYER, N. and VICKERMAN, J. Mass spectral analysis and imaging of tissue by ToF-SIMS—the role of buckminsterfullerene, C_{60}^{+}, primary ions. *International Journal of Mass Spectrometry,* 2007b, 260(2-3), 146-157.

KACHRIMANIS, K. and MALAMATARIS, S. Compact size and mechanical strength of pharmaceutical diluents. *European Journal of Pharmaceutical Sciences,* 2005, 24(2-3), 169-177.

KATDARE, A. (ed.), and CHAUBAL, M.V. (ed.) *Excipient development for pharmaceutical, biotechnology, and drug delivery.* New York: Informa Healthcare, 2006.

KELLER, B.A. and HUG, P. Time-of-flight secondary ion mass spectrometry of industrial materials. *Analytica Chimica Acta,* 1999, 393, 201-212.

KEMPSON, I.M., BARNES, T.J. and PRESTIDGE, C.A. Use of TOF-SIMS to study adsorption and loading behavior of methylene blue and papain in a nano-porous silicon layer. *Journal of the American Society for Mass Spectrometry,* 2010, 21(2), 254-260.

KINGSHOTT, P., WEI, J., BAGGE-RAVN, D., GADEGAARD, N. and GRAM, L. Covalent attachment of poly(ethylene glycol) to surfaces, critical for reducing bacterial adhesion. *Langmuir,* 2003, 19(17), 6912-6921.

KOLLMER, F. Cluster primary ion bombardment of organic materials. *Applied Surface Science,* 2004, 231-232, 153-158.

KOTTER, F. and BENNINGHOVEN, A. Secondary ion emission from polymer surfaces under Ar^+, Xe^+ and SF_5^+ ion bombardment. *Applied Surface Science,* 1998, 133(1-2), 45-57.

KREUTZWALD, P., MALINOVSKAJA, K. and VESKI, P. Effect of diluents and disintegrants on the release of poorly soluble drugs from hard gelatine capsules. *European Journal of Pharmaceutical Sciences,* 2007, 32(1), 49-50.

KUO, J. (ed.) *Electron microscopy: methods and protocols.* Totowa: Humana Press, 2007.

LANG, F.R., LEONARD, D., MATHIEU H.J., MOSER, E.M. and BERTRAND, P. Bulk and surface quantification of a biodegradable and -medical copolyester. *Macromolecules,* 1998, 31(18), 6177-6183.

LARRAS-REGARD, E. and MONY, M.C. Scanning ion images; analysis of pharmaceutical drugs at organelle levels. *International Journal of Mass Spectrometry and Ion Processes,* 1995, 143, 147-160.

LAU, Y.T.R., WENG, L.T., NG, K.M. and CHAN, C.M. Lamellar orientation on the surface of a polymer determined by ToF-SIMS and AFM. *Applied Surface Science,* 2008, 255(4), 1001-1005.

LAU, Y.T.R., WENG, L.T., NG, K.M. and CHAN, C.M. Time-of-flight-secondary ion mass spectrometry and principal component analysis: determination of structures of lamellar surfaces. *Analytical Chemistry,* 2010, 82(7), 2661-2667.

LEADLEY, S.R., DAVIES, M.C., DOMB, A., NUDELMAN, R., PAUL, A.J. and BEAMSON, G. Analysis of the surface chemical structure of copolymers of poly(sebacic anhydride) with ricinoleic acid maleate using XPS and ToF-SIMS. *Macromolecules,* 1998(b), 31(25), 8957-8965.

LEADLEY, S.R., DAVIES, M.C., VERT, M., BRAUD, C., PAUL, A.J., SHARD, A.G. and WATTS, J.F. Probing the surface chemical structure of the novel biodegradeable polymer poly(β-malic acid) and its ester derivatives using ToF-SIMS and XPS. *Macromolecules,* 1997, 30(22), 6920-6928.

LEADLEY, S.R., SHAKESHEFF, K.M., DAVIES, M.C., HELLER, J., FRANSON, N.M., PAUL, A.J., BROWN, A.M. and WATTS, J.F. The use of SIMS, XPS and in situ AFM to probe the acid catalysed hydrolysis of poly(orthoesters). *Biomaterials* 1998(a), 19(15), 1353-1360.

LEE, J.W. and GARDELLA Jr., J.A. Simultaneous determination of drug surface concentration and polymer degradation kinetics in biodegradable polymer/drug membranes: a model drug delivery system. *Applied Surface Science,* 2004, 231–232, 442-446.

LEE, J.L.S., GILMORE I.S, FLETCHER I. and SEAH M.P. Topography and field effects in the quantitative analysis of conductive surfaces using ToF-SIMS. *Applied Surface Science,* 2008, 255(4), 1560-1563.

LEE, J.L.S. (ed.) and GILMORE, I. S. (ed.) *The application of multivariate data analysis techniques in surface analysis: the principal techniques.* 2nd ed. Chichester: Wiley and Sons Ltd., 2009.

LEE, J.L.S., GILMORE, I. S. and SEAH, M.P. Linearity of the instrumental intensity scale in TOF-SIMS – a VAMAS interlaboratory study. *Surface and Interface Analysis,* 2011, 44(1), 1-14.

LEGGETT, G.J. and VICKERMAN, J.C. Sample charging during static SIMS studies of polymers. *Applied Surface Science,* 1995, 84(3), 253-266.

LINTON, R.W. and GOLDSMITH, J.G. The role of secondary ion mass spectrometry (SIMS) in biological microanalysis: technique comparisons and prospects. *Biology of the Cell,* 1992, 74, 147-160.

LIU, H. and WEBSTER, T.J. Nanomedicine for implants: A review of studies and necessary experimental tools. *Biomaterials* 2007, 28(2), 354-369.

LUTTRELL, A., FARB, D. and KIRSCH, R. *Pharmaceutical Quality Control Lab Guidebook.* Los Angeles: UniversityOfHealthCare, 2005.

MAHONEY, C. M. Cluster secondary ion mass spectrometry of polymers and related materials. *Mass Spectrometry Reviews,* 2010, 29(2), 247-293.

MAHONEY, C. and FAHEY, A. Three-dimensional compositional analysis of drug eluting stent coatings using cluster secondary ion mass spectrometry. *Analytical Chemistry,* 2008, 80(3), 624-632.

MAHONEY, C.M., PATWARDHAN, D.V. and MCDERMOTT, M.D. Characterization of drug-eluting stent (DES) materials with cluster secondary ion mass spectrometry (SIMS). *Applied Surface Science,* 2006a, 252(19), 6554-6557.

MAHONEY, C.M., ROBERSON, S.V. and GILLEN, G. Depth profiling of 4-acetamindophenol-doped poly(lactic acid) films using cluster secondary ion mass spectrometry. *Analytical Chemistry,* 2004, 76 (11), 3199-3207.

MAHONEY, C.M., YU, J., FAHEY, A. and GARDELLA Jr., J.A. SIMS depth profiling of polymer blends with protein based drugs. *Applied Surface Science*, 2006b, 252(19), 6609-6614.

MAINS, J., WILSON, C. and URQUHART, A. ToF-SIMS analysis of ocular tissues reveals biochemical differentiation and drug distribution. *European Journal of Pharmaceutics and Biopharmaceutics,* 2011, 79(2), 328-333.

MAISTO, S.A., GALIZIO, M. and CONNORS G. J. *Drug use and abuse.* 6th ed. Belmont: Wadsworth, 2011.

MALMBERG, P., JENNISCHE, E., NILSSON, D. and NYGREN, H. High-resolution, imaging TOF-SIMS: novel applications in medical research. *Analytical and Bioanalytical Chemistry,* 2011, 399(8) 2711-2718.

MARVOLA, M., NYKÄNEN, P., RAUTIO, S., ISONEN, N. and AUTERE A.-M. Enteric polymers as binders and coating materials in multiple-unit site-specific drug delivery systems. *European Journal of Pharmaceutical Sciences,* 1999, 7(3), 259-267.

MASHKOVSKII, M.D. Naming and classification of drugs. *Pharmaceutical Chemistry Journal,* 1993, 27(10), 667-670.

MCPHAIL, D.S. Some applications of SIMS in conservation science, archaeometry and cosmochemistry. *Applied Surface Science,* 2006, 252(19), 7102-7112.

MEYER, K. and ZIMMERMANN, I. Effects of glidants in binary powder mixtures. *Journal of Powder Technology,* 2004, 139(1), 40-54.

MILOJEVIC, S., NEWTON, J.M., CUMMINGS, J.H., GIBSON, G.R., BOTHAM, R.L., RING, S.G., STOCKHAM, M. and ALLWOOD, C. Amylose as a coating for drug delivery to the colon: Preparation and in vitro evaluation using 5-aminosalicylic acid pellets. *Journal of Controlled Release,* 1996, 38(1), 75-84.

MOINI, J. *Cardiopulmonary pharmacology for respiratory care.* Sudbury: Jones and Bartlett Learning, 2012.

MORA-HUERTAS, C.E., FESSI, H. and ELAISSARI, A. Polymer-based nanocapsules for drug delivery. *International Journal of Pharmaceutics,* 2010, 385(1-2), 113-142.

MURAMBIWA, P., MASOLA, B., GOVENDER, T., MUKARATIRWA, S. and MUSABAYANE, C.T. Anti-malarial drug formulations and novel delivery systems. *Acta Tropica,* 2011, 18(2), 71-79.

NGUYEN, S., ALUND, S.J., HIORTH, M., KJONIKSEN, A.L. and SMISTAD, G. Studies on pectin coating of liposomes for drug delivery. *Colloids and Surfaces B – Biointerfaces,* 2011, 88(2), 664-673.

O'CONNOR, D.J., (ed.) SEXTON, B.A. (ed.) and SMART R.S.C. (ed.) *Surface analysis methods in materials science.* 2nd ed. Berlin: Springer-Verlag, 2003.

OHMAE, N., MORI, S. and MARTIN, J.M. *Micro and nanotribology.* New York: The American Society of Mechanical Engineers, 2005.

PACHOLSKI, M. L. and WINOGRAD, N. Imaging with mass spectrometry. *Chemical Reviews,* 1999, 99(10), 2977-3006.

PAJANDER, J., HAUGSHOJ, K.B., BJORNEBOE, K., WAHLBERG, P. and RANTANEN, J. Foreign matter identification from solid dosage forms. *Journal of Pharmaceutical and Biomedical Analysis,* 2013, 80, 116-125.

PASSARELLI, M.K. and WINOGRAD, N. Lipid imaging with time-of-flight secondary ion mass spectrometry (ToF-SIMS). *Biochimica et Biophysica Acta (BBA) - Molecular and Cell Biology of Lipids,* 2011, 1811(11), 976-990.

PASSCHIER, C.W. and TROUW, R.A.J. *Microtectonics, Volume 1.* Berlin: Springer-Verlag, 2005.

PAUL, A.J. Organic and molecular imaging by ToF-SIMS – at the cutting edge. *Spectroscopy Europe,* 2005, 17(5), 25-27.

PERKINS, M.C., BELL, G., BRIGGS, D., DAVIES, M.C., FRIEDMAN, A., HART, C.A., ROBERTS, C.J. and RUTTEN F.J.M. The application of ToF-SIMS to the analysis of herbicide formulation penetration into and through leaf cuticles. *Colloids and Surfaces B: Biointerfaces,* 2008, 67(1), 1-13.

PIGNATARO, B., PANEBIANCO, S., CONSALVO, C. and LICCIARDELLO, A. Study of aged Langmuir-Blodgett monolayers by AFM and ToF-SIMS mapping. *Surface and Interface Analysis,* 1999, 27(5-6), 396-400.

PILCER, G. and AMIGHI, K. Formulation strategy and use of excipients in pulmonary drug delivery. *International Journal of Pharmaceutics,* 2010, 392(1-2), 1-19.

PRESTIDGE C.A., BARNES T.J. and SKINNER W. Time-of-flight secondary-ion mass spectrometry for the surface characterization of solid-state pharmaceuticals. *Journal of Pharmacy and Pharmacology,* 2007, 59(2), 251-259.

RAFATI, A., BOUSSAHEL, A., SHAKESHEFF, K.M., SHARD, A.G., ROBERTS, C.J., CHEN, X., SCURR, D.J., RIGBY-SINGLETON, S., WHITESIDE, P., ALEXANDER, M.R. and DAVIES M.C. Chemical and spatial analysis of protein loaded PLGA microspheres for drug delivery applications. *Journal of Controlled Release*, 2012, 162(2), 321-329.

RATNER, B.D. *Biomaterials science: an introduction to materials in medicine.* 2nd ed. Amsterdam: Elsevier Academic Press, 2004.

REALDON, N., RAGAZZI, E., DAL ZOTTO, M. and DALLA FINI, G. Layered excipient suppositories: The possibility of modulating drug availability. *International Journal of Pharmaceutics,* 1997, 148(2), 155-163.

RIVIÉRE, J.C. (ed.) and MYHRA, S. (ed.) *Handbook of surface and interface analysis: methods for problem-solving.* 2nd ed. Boca Raton: CRC Press, 2009.

RUBAKHIN, S.S., JURCHEN, J.C., MONROE, E.B. and SWEEDLER, J.V. Imaging mass spectrometry: fundamentals and applications to drug discovery. *Drug Discovery Today,* 2005, 10(12), 823-837.

SAKAMOTO, T., KOIZUMI, M., KAWASAKI, J. and YAMAGUCHI, J. Development of a high lateral resolution ToF-SIMS apparatus for single particle analysis. *Applied Surface Science,* 2008, 255(4), 1617-1620.

SALDI, F., SCHNEIDER, S., WENNIG, R. and MIGEON, H.N. *Detection and quantification of drugs using ToF-SIMS.* 6th International Conference on Secondary Ion Mass Spectrometry and Related Topics (SIMS VI), 1997, p.209-12.

SARANTOPOULOS, P.D. Manufacturing in the pharmaceutical industry. *Journal of Manufacturing Systems,* 1995, 14(6), 452-467.

SCHRODER-OEYNHAUSEN, F., BURKHARDT, B., FLADUNG, T., KOTTER, F., SCHNIEDERS, M., WIEDMANN, L. and BENNINGHOVEN A. Quantification of metal contaminants on GaAs with time-of-flight secondary ion mass spectrometry. *Journal of Vacuum Science and Technology B,* 1998, 16(3), 1002-1006.

SCURR, D.J., HORLACHER, T., OBERLI, M.A., WERZ, D.B., KROECK, L., BUFALI, S., SEEBERGER, P.H., SHARD, A.G. and ALEXANDER M.R. Surface characterization of carbohydrate microarrays. *Langmuir,* 2010, 26(22), 17143-17155.

SETOU, M. (ed.) *Imaging mass spectrometry: protocols for mass microscopy.* New York: Springer, 2008.

SHOKRI, J., AHMADI, P., RASHIDI, P., SHAHSAVARI, M., RAJABI-SIAHBOOMI, A. and NOKHODCHI, A. Swellable elementary osmotic pump (SEOP): an effective device for delivery of poorly water-soluble drugs. *European Journal of Pharmaceutics and Biopharmaceutics,* 2008, 68(2), 289-297.

SIEPMANN, F., SIEPMANN, J., WALTHER, M., MACRAE, R.J. and BODMEIER, R. Polymer blends for controlled release coatings. *Journal of Controlled Release,* 2008, 125(1), 1-15.

SIMCHI, A., TAMJID, E., PISHBIN, F. and BOCCACCINI A.R. Recent progress in inorganic and composite coatings with bactericidal capability for orthopaedic applications. *Nanomedicine: Nanotechnology, Biology and Medicine,* 2011, 7(1), 22-39.

STOREY, R.A. (ed.) and YMEN, I. (ed.) *Solid state characterization of pharmaceuticals.* Chichester: Blackwell Publishing, 2011.

SUTCLIFFE, M., COMBARIEU, R., REPOUX, M. and MONTMITONNET, P. Tribology of plane strain compression tests on aluminium strip using ToF-SIMS analysis of transfer films. *Wear,* 2003, 254, 65-79.

TAN, M.X.L. and HAPGOOD, K.P. Foam granulation: Binder dispersion and nucleation in mixer-granulators. *Chemical Engineering Research and Design,* 2011, 89(5), 526-536.

TEODORO, O.M.N.D. and MOUTINHO, A.M.C. Characterization of a barium surface by AES, XPS and SIMS. *Vacuum,* 2002, 64(3-4), 431-437.

TORRISI, A., TUCCITTO, N., AUDINOT, J.N., ZHAVNERKO, G. MIGEON, H.N. and LICCIARDELLO, A., Nano- and microstructured polymer LB layers: A combined AFM/SIMS study. *Applied Surface Science,* 2008, 255(4), 1006-1010.

TORRISI, A., TUCCITTO, N. and LICCIARDELLO, A., Effects of the substrate on ToF-SIMS spectra of thin films of some fluorinated compounds deposited on calcarenite. *International Journal of Mass Spectrometry,* 2009, 281(1), 157-166.

TOUBOUL, D., KOLLMER, F., NIEHUIS, E., A., BRUNELLE A. and LAPRÉVOTE, O. Improvement of biological time-of-flight-secondary ion mass spectrometry imaging with a bismuth cluster ion source. *Journal of the American Society for Mass Spectrometry,* 2005, 16(10), 1608-1618.

TOUBOUL, D., ROY, S., GERMAIN, D.P., CHAMINADE, P., BRUNELLE, A. and LAPRÉVOTE, O. MALDI-TOF and cluster-TOF-SIMS imaging of Fabry disease biomarkers. *International Journal of Mass Spectrometry,* 2007, 260(2-3), 158-165.

TRAPP, M. and STAHL, H. Distribution analyses of pharmacologically relevant high molecular compounds using secondary ion mass spectrometry (SIMS). *Journal of Molecular Structure,* 1995, 348, 397-399.

TSUNEMATSU, H., HANAZONO, H. and YAMAMOTO, M. Fragmentations of flurbiprofen-L-arginine diastereomers in negative ion fast-atom-bombardment mass spectrometry. *Biological Mass Spectrometry* 1993, 22(12), 703-706.

TYLER, B.J., BRUENING, C., RANGARANJAN, S. and ARLINGHAUS, H.F. TOF-SIMS imaging of adsorbed proteins on topographically complex surfaces with Bi_3^+ primary ions. *Biointerphases,* 2011, 6(3), 135.

TYLER, B.J., RAYAL, G. and CASTNER, D.G. Multivariate analysis strategies for processing ToF-SIMS images of biomaterials. *Biomaterials,* 2007, 28, 2412-2423.

UCHEGBU, I.F. and SCHÄTZLEIN, A.G. *Polymers in drug delivery.* Boca Raton: CRC Press, 2006.

VAIDYA, M.P. and AVACHAT, A.M. Investigation of the impact of insoluble diluents on the compression and release properties of matrix based sustained release tablets. *Journal of Powder Technology,* 2011, 214(3), 275-381.

VANDEN EYNDE, X. and BERTRAND, P. "Matrix" effects in ToF-SIMS analyses of styrene-methyl methacrylate random copolymers. *Macromolecules,* 2000, 33(15), 5624-5633.

VARHEGYI, E.B., JONDA, S., PERCZEL, I.V. and MEIXNER, H. AES, SIMS, XPS analysis and electrical conductance of Ta-doped SrTiO3 thin films. *Sensors and Actuators B: Chemical,* 1998, 47(1–3), 164-170.

VEILLEROT, M., BARNES, J.P. and DANEL, A. Trace metal contamination quantification on silicon wafers using ToF-SIMS: RSF determination from deposited droplet standards. *Surface and Interface Analysis,* 2011, 43(1-2), 569-572.

VERVAET, C., BAERT, L. and REMON, J. Extrusion-spheronisation: A literature review. *International Journal of Pharmaceutics,* 1995, 116(2), 131-146.

VICKERMAN, J.C. (ed.) and BRIGGS, D. (ed.) *ToF-SIMS: Surface analysis by mass spectrometry.* Chichester and Manchester: IM Publications and SurfaceSpectra Limited, 2001.

VICKERMAN, J. C. and GILMORE, I. S. *Surface analysis: the principal techniques.* Chichester: Wiley and Sons Ltd., 2009.

VILLANOVA, J.C.O., AYRES, E. and ORÉFICE, R.L. Design of prolonged release tablets using new solid acrylic excipients for direct compression. *European Journal of Pharmaceutics and Biopharmaceutics,* 2011, 79(3), 664-673.

WAGNER, M.S. Towards quantitative chemical imaging with ToF-SIMS. *Applied Surface Science,* 2008, 255(4), 992-996.

WAGNER, M.S. and CASTNER, D.G. Analysis of adsorbed proteins by static time-of-flight secondary ion mass spectrometry. *Applied Surface Science,* 2004, (231-232), 366-376.

WATTS, J.F. *An introduction to surface analysis by electron spectroscopy.* New York: Oxford University Press, 1990.

WEIBEL, D., WONG, S., LOCKYER, N., BLENKINSOPP, P., HILL, R. and VICKERMAN, J. C. A C_{60} primary ion beam system for time of flight secondary ion mass spectrometry: its development and secondary ion yield characteristics. *Analytical Chemistry,* 2003, 75(7), 1754-1764.

WENG, L. T., BERTRAND, P., LAUER, W., ZIMMER, R. and BUSETTI, S. Quantitative surface analysis of styrene-butadiene copolymers using time-of-flight secondary ion mass spectrometry. *Surface and Interface Analysis,* 1995, 23(13), 879-886.

WENG, L.T. and CHAN, C.-M. ToF-SIMS quantitative approaches in copolymers and polymer blends. *Applied Surface Science,* 2003, (203–204), 532-537.

WESTBROOK, C., KAUT ROTH, C. and TALBOT, J. *MRI in practice.* Chichester: Blackwell Science, 1998.

YORK, P. The use of glidants to improve the flowability of fine lactose powder. *Journal of Powder Technology,* 1975, 11(2), 197-198.

ZHENG, J. *Formulation and analytical development for low-dose oral drug products.* Chichester: Wiley and Sons Ltd., 2009.

ZHOU, Q., DENMAN, J., GENGENBACH, T., DAS, S., QU, L., ZHANG, H., LARSON, I., STEWART, P. and MORTON, D. Characterization of the surface properties of a model pharmaceutical fine powder modified with a pharmaceutical lubricant to improve flow via a mechanical dry coating approach. *Journal of Pharmaceutical Sciences,* 2011, 100(8), 3421-3430.